Sliding-Rolling Ratio during Deep Squat with Regard to Different Knee Prostheses

Gusztáv Fekete[1], Patrick De Baets[1], Magd Abdel Wahab[1], Béla Csizmadia[2], Gábor Katona[2], Libardo V. Vanegas-Useche[3], José Alfredo Solanilla[3]

[1] Ghent University, Laboratory Soete, Department of Mechanical Construction and Production, Ghent, Belgium, gusztav.fekete@ugent.be, patrick.debaets@ugent.be, magd.abdelwahab@ugent.be

[2] Szent István University, Institute of Mechanics and Machinery, Department of Mechanics and Technical Drawing, Gödöllő, Hungary, csizmadia.bela@gek.szie.hu, katona.gabor@gek.szie.hu

[3] Technological University of Pereira, Faculty of Mechanical Engineering, Pereira, Colombia, lvanegas@utp.edu.co, joseing@utp.edu.co

Abstract: The sliding-rolling ratio between the femoral and tibial condyles throughout the active functional arc of the knee (20-120º of flexion angle) is currently unknown. Since wear is the most determining lifetime factor of the current total knee replacements, the presence of sliding-rolling cannot be neglected. The reason lies in the fact that this phenomenon causes different material abrasion compared to pure sliding or rolling alone. Only a limited amount of studies have dealt with this question related to the condyles of the knee prostheses, most of them by means of experimental tests and only in the segment where the motion begins (0 to 20-30º). The primary aim of this paper is to investigate how the sliding-rolling ratio changes between the condyles of five different knee prostheses in the functional arc of the knee (20-120º) as a function of flexion angle. For the analysis, five prosthesis models with identical boundary conditions have been constituted and numerical simulations were carried out using the MSC.ADAMS program system. Beside the sliding-rolling ratio, the normal and friction force between the connecting surfaces has also been calculated as a function of flexion angle.

Keywords: sliding-rolling ratio; contact forces; deep squat; knee prostheses

1 Introduction

In the case of normal flexion or extension of the human knee joint, the local kinematics of the patellofemoral joint can be characterized as partial rolling and sliding. This particular movement is under the control of the connecting femoral-

tibial surfaces and the connecting ligaments. The precise ratio of the sliding-rolling phenomenon throughout the active functional arc of the knee is currently unknown, although it is commonly accepted by the early works of Zuppinger [32] and Braune et al. [2] that up to 20-30˚ of flexion angle rolling is dominant, while beyond these angles the roles invert, and sliding becomes prevailing.

The combination of this complex motion, in addition to the incongruence of the connecting femoral and tibial condyles, raises the most difficult questions in the development of total knee replacements (later on TKRs). The relevance of the subject is undisputed, since during the knee or hip [17] prosthesis design, wear as an upcoming problem will appear in time. Only in the US, 350,000 total knee arthroplasty procedures are carried out annually [5], and it is shown in another study that for over the half of the retrieved prostheses failure is possibly due to wear or fatigue cracking [1].

Wear is the most determining lifetime factor in the current TKRs, and for this reason the presence of sliding-rolling cannot be neglected. The reason lies in the fact that this phenomenon causes different material abrasion compared to pure sliding or rolling alone [30]. Several test set-ups and techniques are available [14, 25, 29] to quantify the wear on the prosthesis surfaces, but it is only partially known what forces appear on the surface or how much sliding-rolling ratio should be applied during standard tests.

Besides the actual load, the sliding-rolling ratio is one of the most important parameters of the wear tests, since if it is set incorrectly high or low, then the wear will be over- or underestimated. There are only limited appearances in literature of numerical or analytical modeling of the sliding-rolling phenomenon, while experimental tests are slightly more frequent.

In regard to the experimental approaches, McGloughlin and Kavanagh [16] designed and built a three-station wear testing rig in order to assess the influence of kinematic conditions on the quantitative wear on the basis of TKR materials. In their study, they used a flat plate and a cylinder to measure how the wear rate is influenced by different sliding-rolling conditions. According to their results, above 50º of flexion angle at 0.95-0.99 sliding-rolling ratio, the wear rate reached the maximum. Reinholz et al. [24] developed a revolving simulator which allowed setting the sliding-rolling ratio between 0 to 1 (which means between 0 and 100% of sliding). In their experiments they investigated the alteration of the coefficient of friction up to 70% of sliding. Van Citters et al. [28] designed a six-station tribotester that is able to test six specimens simultaneously.

In their tests, the sliding-rolling ratio was set to a maximum 0.4 by means of creating 40% of sliding and 60% of rolling [27]. In other tests, Sukumaran et al. [26] applied a maximum of 0.3 sliding-rolling ratio.

In a comprehensive study, Hollman et al. [10] investigated the sliding-rolling behavior on 11 subjects without knee pathology and 7 subjects with injured

anterior cruciate ligaments. They proved with electromyographic signals and a mathematical model based on the concept of the path of instantaneous center of rotation (PICR) that the sliding-rolling coefficient varies between 0.3 and 0.46 in the early flexion angles (between 0 and 30º).

According to these studies, in the case of experimental testing of prosthesis materials, the sliding-rolling ratios are widely applied between 0.3-0.4 in the range of 0 to 30º flexion angle. Above this certain angle, only McGloughlin and Kavanagh [16] carried out experiments and proved that the sliding-rolling ratio reaches higher values, although they did not use real prosthesis components but rather a cylinder and a flat plate.

As for the numerical modeling side, one of the earliest models that investigated the sliding-rolling phenomenon is credited to Chittajallu and Kohrt [3]. In essence, their model is more like a stiffness model that considers all the major ligaments, but it can also calculate the sliding-rolling ratio. The ratio was defined as follows: a value of one represents pure rolling; infinite represents pure sliding; while intermediate values represent the combinations of the two phenomena. The major disadvantage in this model, besides the oversimplified surfaces (the femur is a circle, and the tibia plateau is a flat plate), is that the physical interpretation of the values between one and infinite is not clear.

On the basis of experiments carried out by Iwaki et al. [13] and Pinskerova et al. [22] on loaded, unloaded and cadaver knees, Nägerl et al. [21] re-investigated the question of the sliding-rolling ratio by analytical and numerical techniques and found new results in the higher range of flexion angle (Table 1).

Table 1
Various sliding-rolling ratios reported by Nägerl et al [21] based on the data of Pinskerova et al. [22]

Sliding-Rolling ratio	**Range of flexion**	**Medial compartment**			**Lateral compartment**		
		Loaded	Unloaded	Cadaver	Loaded	Unloaded	Cadaver
χ	0-20˚	0.04	0.2	0.37	-0.24	0.83	0.63
χ	45-90˚	0.9	0.91	0.92	0.8	0.57	0.57

It becomes apparent from Table 1 that the sliding-rolling ratio is slightly higher on the medial compartment than on the lateral compartment, and the loading condition alters the sliding-rolling ratio.

By summarizing the findings of the experimental and mathematical (numerical) literature, in the case of the experimental testing of prosthesis materials, the sliding-rolling ratios are widely applied between 0.3-0.46 [10, 26, 27, 28] but only in the range of 0 to 30º flexion angle due to the firm belief that in the beginning of the motion rolling is dominant. At higher flexion angles, presumably, the sliding-rolling ratio changes significantly [13, 16, 22], but the results related to the sliding-rolling ratio above 30º of flexion angle are rather limited.

Since the pattern of the sliding-rolling phenomenon has not been thoroughly investigated in full extension, the aims of this paper are:

I To determine the pattern and magnitude of sliding-rolling ratio between 20-120˚ of flexion angle for several prosthesis geometries. This segment is considered as the fundamental active arc (see Figure 1) which is totally under muscular control and involves most of our daily activities [6]. For this reason, in this study the arcs between 0-20˚ and 120-160˚ are not considered.

II To investigate how the sliding-rolling ratio changes depending on the different commercial and prototype prostheses. This should help to find the lower and upper limits of the sliding-rolling ratio between the condyles.

III To investigate how the friction force and the normal force alter as a function of flexion angle with respect to realistic frictional condition. By knowing these forces in the active functional arc, the actual load during the wear test could be correctly set.

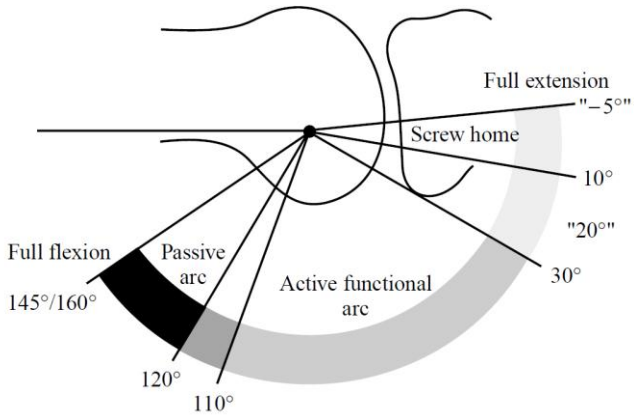

Figure 1
Major segments of human arc of flexion [21]

2 The Models

As a basis for the multibody models, several commercial prostheses and one prototype prosthesis were used. These prostheses are namely:

- Prosthesis 1: Prototype from the SZIU, non-commercial,
- Prosthesis 2: BioTech TP Primary knee [12],
- Prosthesis 3: BioTech TP P/S Primary knee [12],

- Prosthesis 4: BioMet Oxford Partial knee [11],
- Prosthesis 5: DePruy PFC [7].

The prostheses geometries were 3D scanned (Prost. 1-4) or received in STL files (Prost. 5). After correcting the disclosing errors of the surfaces by genetic algorithm [9] the geometries were converted into PARASOLID solid bodies.

2.1 Description of the Multibody Model

After creating the geometrical models, a multibody model was built in the MSC.ADAMS [20] program system. The following boundary conditions were applied on each model identically:

- The bones, such as the tibia, patella and femur, were assumed as rigid bodies, since the influence of deformation in this study is neglected.
- Only the patellar ligament and the quadriceps muscle were considered in the numerical model. The quadriceps muscle and the patellar ligament were modeled as simple linear springs (SPRING element see Figure 2). The stiffness coefficient was set to 130 N/mm and the damping coefficient to 0.15 Ns/mm for both springs, which correspond to the measured values in the literature [15, 18].
- A FORCE VECTOR was applied on the femur distalis (see Figure 2), which represented the load of the body weight (BW). The magnitude was set to 800 N (1 BW).
- The femur distalis was constrained by a GENERAL POINT MOTION, where all the coordinates can be prescribed (see Figure 2). Only one prescription was set: the endpoint of the femur (distalis) can only perform translational motion along the *y* axis.
- The ankle part of the model was constrained by a SPHERICAL JOINT, which allows rotation about all axes, but no translational motions are permitted at that point (see Figure 2). By applying this constraint, the tibia can perform a natural rotation and a kinematic analysis can be carried out in a further study.
- Between the femur, tibia and patella, CONTACT constraints were set according to Coulomb's law with respect to the very low static and dynamic friction coefficients (μ_s = 0.003 μ_d = 0.001) similarly to real joints [19, 23] (see Figure 2). The kinetic relationship between the normal and friction forces ($\boldsymbol{F}_n$, $\boldsymbol{F}_s$) and the flexion angle can be analyzed.

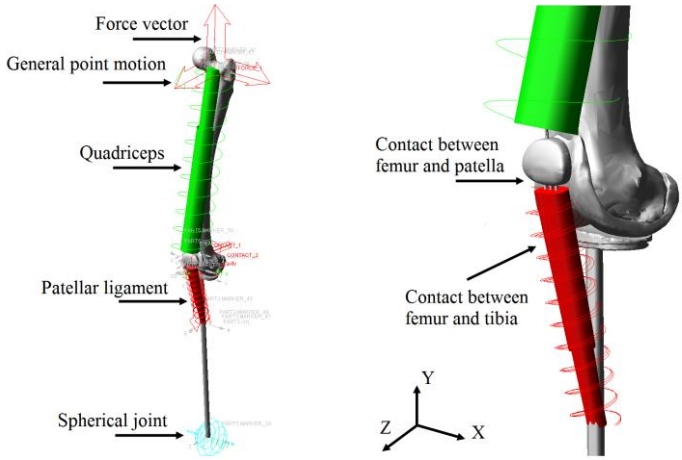

Figure 2
Multibody model

Since the MSC.ADAMS is a multibody dynamic program, it creates and solves simultaneously linear or non-linear Ordinary Differential Equations (ODE) and non-linear Differential-Algebraic Equations (DAE).

GSTIFF type integrator [8] was used in MSC.ADAMS for solving the ODE and DAE of the motion. The solver routine was set to work at a maximum 10^{-3} tolerance of error, while the maximum order of the polynomial was defined as 12. The solution converged very quickly with these parameters; the model in different positions during simulation is presented in Figure 3.

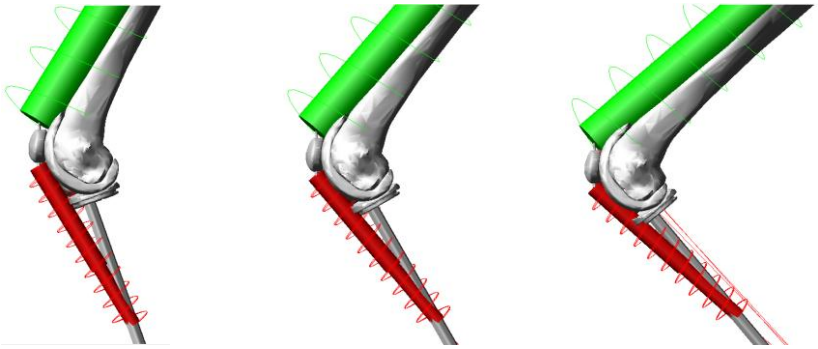

Figure 3
Multibody model in different positions during simulation

The post-processing was carried out in MSC.ADAMS and partly in Excel. The MSC.ADAMS software can directly compute forces, velocities and accelerations, but not rotations.

2.2 The Calculation Method

The following kinematic quantities can be directly calculated by MSC.ADAMS during the simulation of the motion as a function of time:

- $\bar{r}_{Ci}(t)$ vector-scalar function, which determines the instantaneous position of the connecting points of the two bodies defined in the absolute coordinate system (see Figure 4). If i = 1, contact between femur and tibia, if i = 2, contact between femur and patella.
- $\bar{r}_{CMF}(t)$, $\bar{r}_{CMT}(t)$, $\bar{v}_{CMF}(t)$, $\bar{v}_{CMT}(t)$, $\bar{\omega}_{CMF}(t)$ and $\bar{\omega}_{CMT}(t)$ vector-scalar functions, which determine the instantaneous position of the center of mass (CM_i), velocity and angular velocity of the femur (F) and the tibia (T) defined in the absolute coordinate system (see Figure 4).
- $\bar{e}_{Ci}(t)$ vector-scalar function (unit-vector), which determines the instantaneous tangent vector respectively to the contact path defined in the absolute coordinate system (see Figure 5).

Besides the kinematic quantities, the MSC.ADAMS software can calculate kinetic quantities as well, for example:

- Contact forces between the articular surfaces, reaction forces and moments in the applied constrains or forces in the springs.

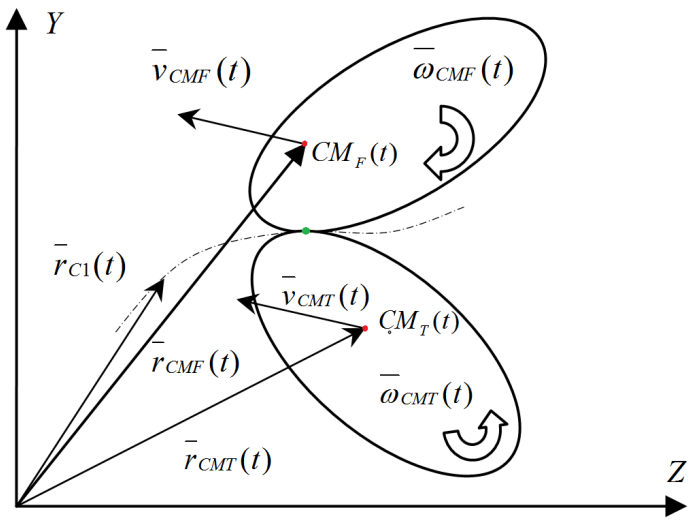

Figure 4
Kinematic quantities between the femur and tibia

In order to calculate the sliding-rolling ratio, additional kinematic quantities have to be determined as well (these quantities cannot be calculated directly with MSC.ADAMS):

– $\bar{r}_{CF}(t)$, $\bar{r}_{CT}(t)$, $\bar{v}_{CF}(t)$ and $\bar{v}_{CT}(t)$ are vector-scalar functions, which determine the instantaneous position and velocity in the contact point (C) of the connecting femoral or tibial surfaces respectively (see Figure 5).

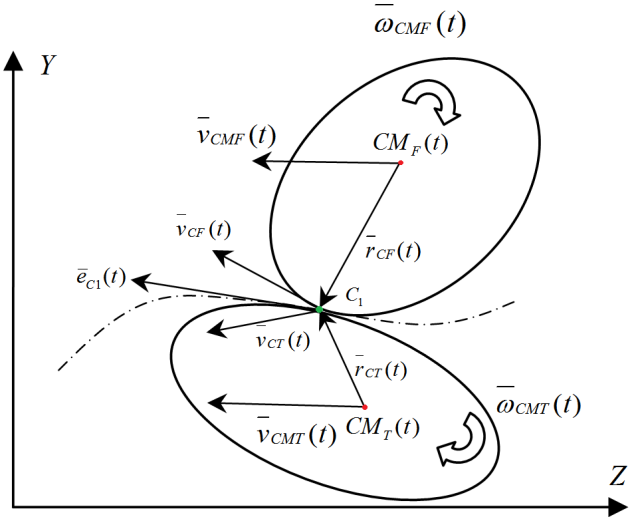

Figure 5
Kinematic quantities between the femur and tibia

Since the multibody model is considered rigid, the rigid body kinematics is applicable. To obtain the velocity of a point – in our case point C – the following calculation algorithm is as follows [4]:

$$\bar{v}_{CF}(t) = \bar{v}_{CMF}(t) + \bar{\omega}_{CMF}(t) \times \bar{r}_{CF}(t) \tag{1}$$

$$\bar{v}_{CT}(t) = \bar{v}_{CMT}(t) + \bar{\omega}_{CMT}(t) \times \bar{r}_{CT}(t) \tag{2}$$

where,

$$\bar{r}_{C1}(t) = \bar{r}_{CMF}(t) + \bar{r}_{CF}(t) \rightarrow \bar{r}_{CF}(t) = \bar{r}_{C1}(t) - \bar{r}_{CMF}(t) \tag{3}$$

$$\bar{r}_{C1}(t) = \bar{r}_{CMT}(t) + \bar{r}_{CT}(t) \rightarrow \bar{r}_{CT}(t) = \bar{r}_{C1}(t) - \bar{r}_{CMT}(t) \tag{4}$$

by substituting equation (3) and (4) into (1) and (2) we obtain,

$$\bar{v}_{CF}(t) = \bar{v}_{CMF}(t) + \bar{\omega}_{CMF}(t) \times \left(\bar{r}_{C1}(t) - \bar{r}_{CMF}(t)\right) \tag{5}$$

$$\bar{v}_{CT}(t) = \bar{v}_{CMT}(t) + \bar{\omega}_{CMT}(t) \times \left(\bar{r}_{C1}(t) - \bar{r}_{CMT}(t)\right) \tag{6}$$

Now, the velocities with respect to the femur and tibia are determined in the contact point, in the absolute coordinate system (see Figure 6).

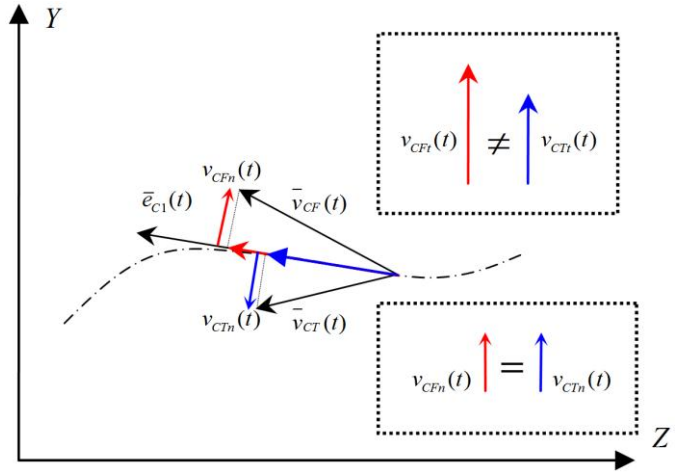

Figure 6
Velocities of the femur and tibia in the contact point

By multiplying equation (5) and (6) with the $\bar{e}_{C1}(t)$ unit vector, we can derive the tangential scalar component of the femoral and tibial contact velocities with respect to the contact path:

$$v_{CFt}(t) = \left[\bar{v}_{CMF}(t) + \bar{\omega}_{CMF}(t) \times \left(\bar{r}_{C1}(t) - \bar{r}_{CMF}(t)\right)\right] \cdot \bar{e}_{C1}(t) \tag{7}$$

$$v_{CTt}(t) = \left[\bar{v}_{CMT}(t) + \bar{\omega}_{CMT}(t) \times \left(\bar{r}_{C1}(t) - \bar{r}_{CMT}(t)\right)\right] \cdot \bar{e}_{C1}(t) \tag{8}$$

The tangential scalar components are only valid, if the following condition is satisfied:

$$v_{CFn}(t) = v_{CTn}(t) \tag{9}$$

This means that the normal scalar components of the femoral and tibial contact velocities must be equal; otherwise the two surfaces would be either crushed into each other or would be separated.

Since scalar contact velocities are available, by integrating them over time the connecting arc lengths with respect to the femur and tibia can be calculated as:

$$S_{femur}(t) = \int v_{CFt}(t) \cdot dt = \int \left[\bar{v}_{CMF}(t) + \bar{\omega}_{CMF}(t) \times \left(\bar{r}_{C1}(t) - \bar{r}_{CMF}(t)\right)\right] \cdot \bar{e}_{C1}(t) \cdot dt \tag{10}$$

$$S_{tibia}(t) = \int v_{CTt}(t) \cdot dt = \int \left[\bar{v}_{CMT}(t) + \bar{\omega}_{CMT}(t) \times \left(\bar{r}_{C1}(t) - \bar{r}_{CMT}(t)\right)\right] \cdot \bar{e}_{C1}(t) \cdot dt \tag{11}$$

By having the arc lengths on both connecting bodies, the sliding-rolling ratio can be introduced, and denoted by χ:

$$\chi(t) = \frac{\Delta S_{tibiaN}(t) - \Delta S_{femurN}(t)}{\Delta S_{tibiaN}(t)} \tag{12}$$

where,

$$\Delta S_{femurN}(t) = S_{femurN}(t) - S_{femurN-1}(t) \tag{13}$$

$$\Delta S_{tibiaN}(t) = S_{tibiaN}(t) - S_{tibiaN-1}(t) \tag{14}$$

are the corresponding incremental differences of the connecting arc lengths.

The χ function – or sliding-rolling function – is defined as the ratio of the distance travelled by the contact point on the tibia to the distance travelled by the contact point on the femur over a specified increment of movement. By this function, exact conclusions can be drawn about the sliding and rolling features of the motion. A sliding-rolling ratio (χ) of zero indicates pure rolling, while one describes pure sliding. If the ratio is between zero and one, the movement is characterized as partial rolling and sliding. For example a sliding-rolling ratio of 0.4 means 40% of sliding and 60% of rolling. A positive ratio shows the slip of the femur compared to the tibia. If the sign is negative, then the tibia has higher slip compared to the femur.

It is desirable to determine the sliding-rolling ratio as a function of flexion angle rather than the time; thus the flexion angle (α) was derived by integrating the angular velocities of the femur and tibia about the *x* axis over time, and taking this into account, the model was set in an initial 20 degree of squat at the beginning of the motion.

$$\alpha(t) = \int \omega_{CMFx} \cdot dt + \int \omega_{CMTx} \cdot dt + 20 \tag{15}$$

Since the $\alpha(t)$ function has been determined, the time can be exchanged to flexion angle and the sliding-rolling function (χ) can be plotted as a function of flexion angle:

$$\chi(\alpha) = \frac{\Delta S_{tibiaN}(\alpha) - \Delta S_{femurN}(\alpha)}{\Delta S_{tibiaN}(\alpha)} \tag{16}$$

3 Results

After all of the simulations were carried out on all the five prostheses, the following results related to the sliding-rolling ratio and the connecting forces were obtained:

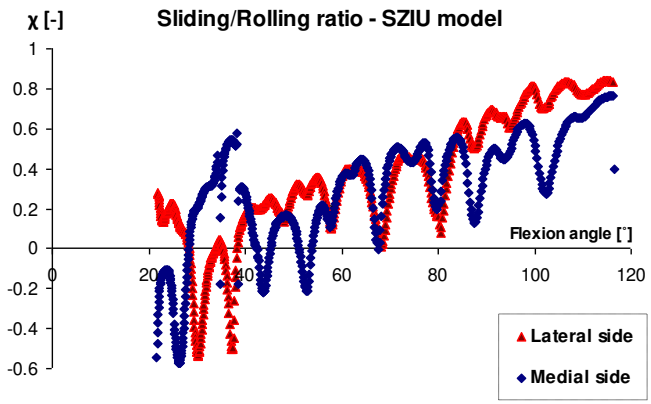

Figure 7
Sliding-rolling function of the SZIE model

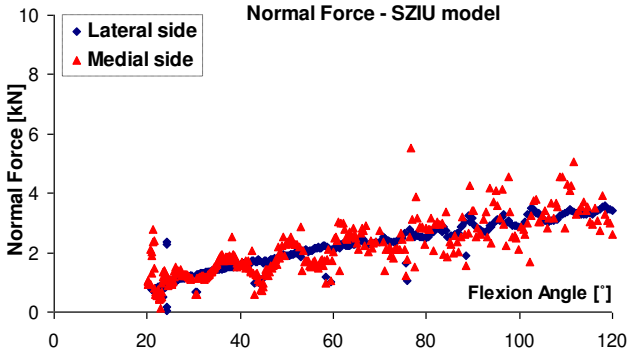

Figure 8
Normal force function of the SZIE model

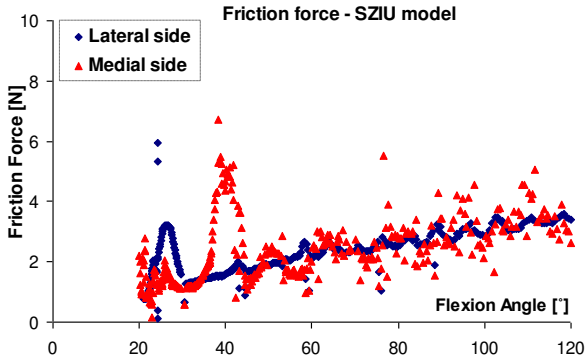

Figure 9
Friction force function of the SZIE model

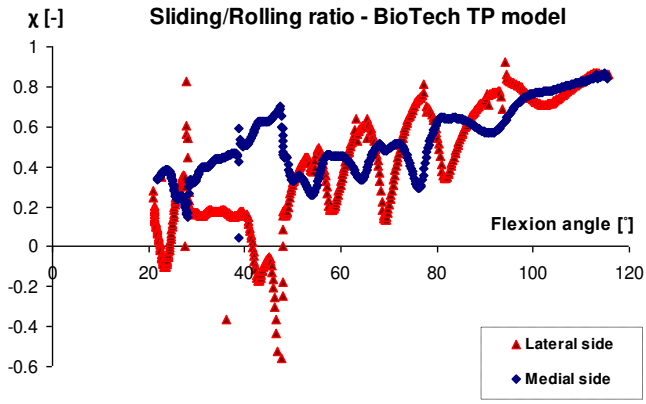

Figure 10
Sliding-rolling function of the BioTech TP model

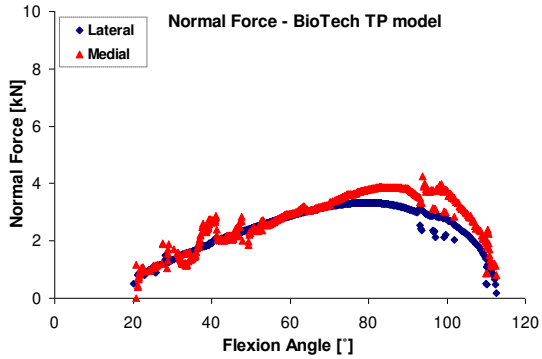

Figure 11
Normal force function of the BioTech TP model

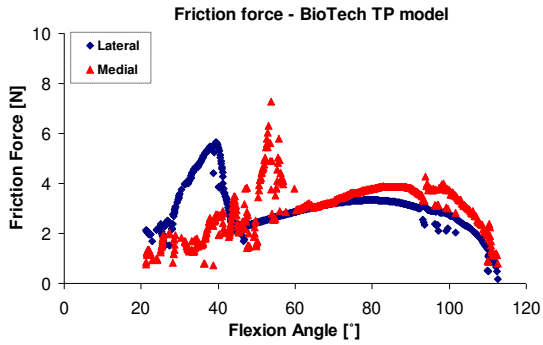

Figure 12
Friction force function of the BioTech TP model

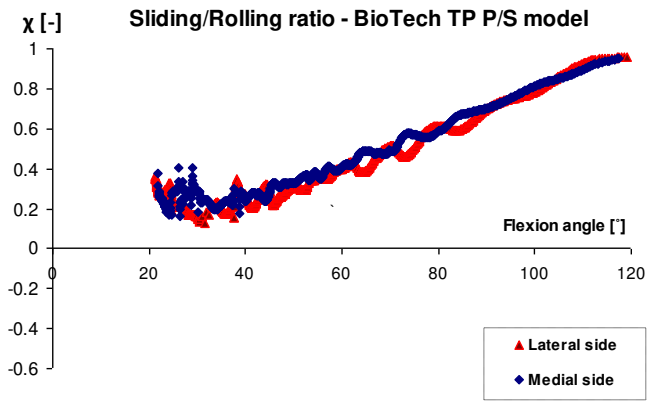

Figure 13
Sliding-rolling function of the BioTech TP P/S model

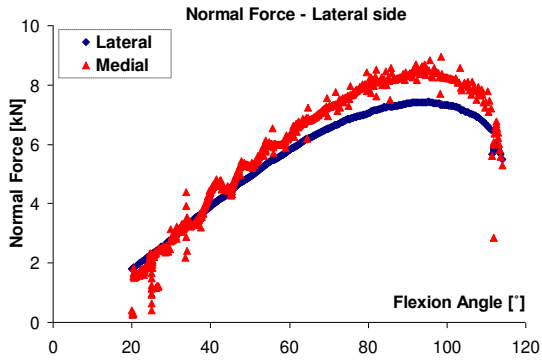

Figure 14
Normal force function of the BioTech TP P/S model

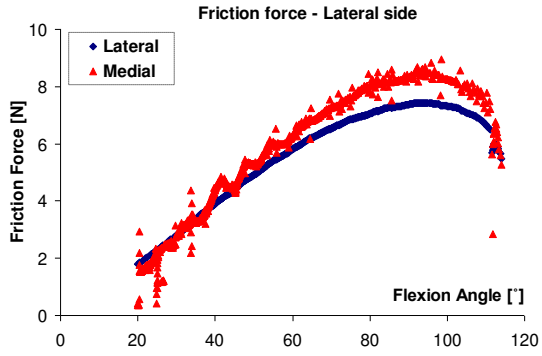

Figure 15
Friction force function of the BioTech TP P/S model

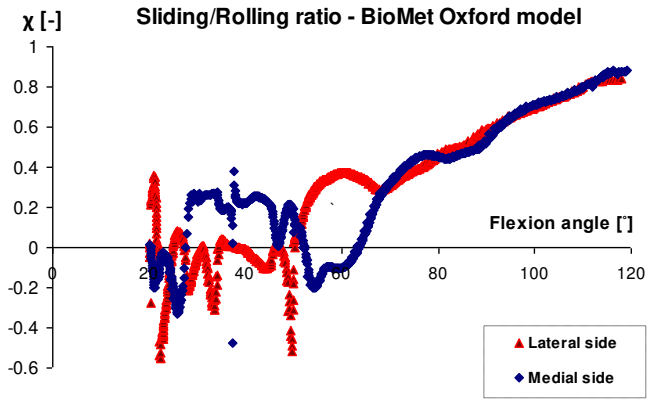

Figure 16
Sliding-rolling function of the BioMet Oxford model

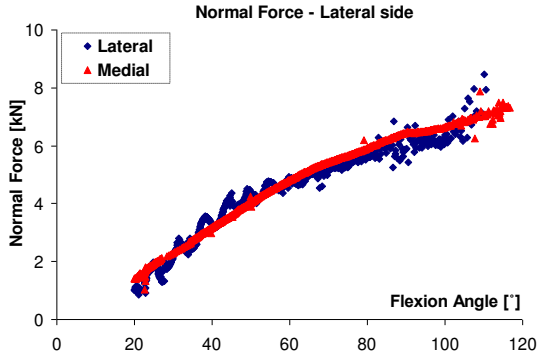

Figure 17
Normal force function of the BioMet Oxford model

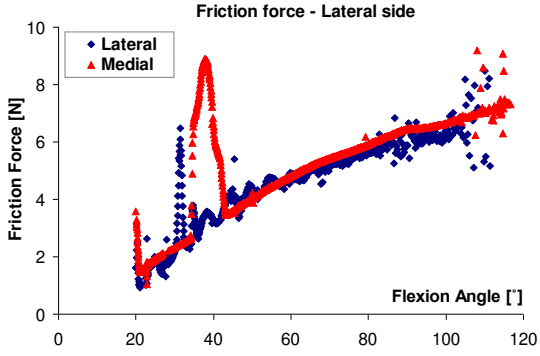

Figure 18
Friction force function of the BioMet Oxford model

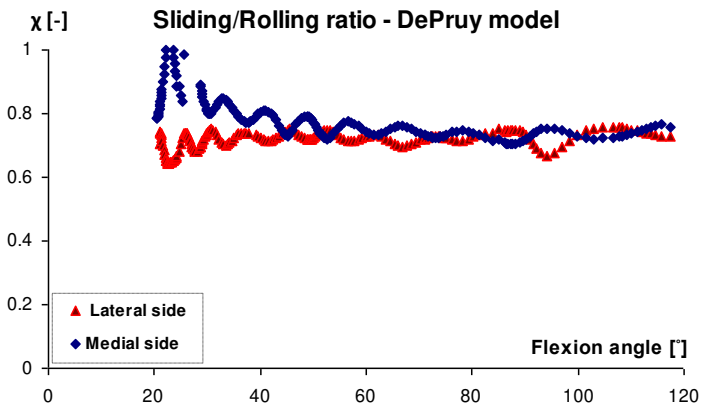

Figure 19
Sliding-rolling function of the DePruy model

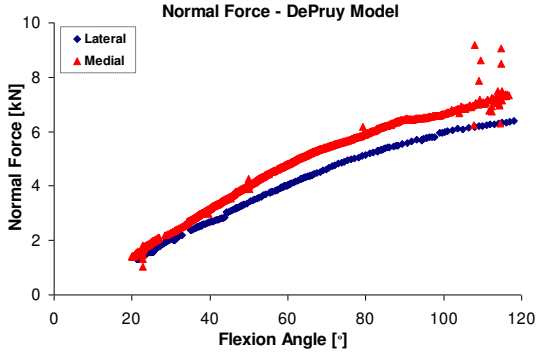

Figure 20
Normal force function of the DePruy model

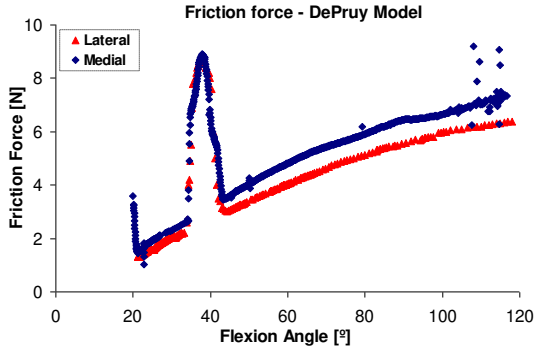

Figure 21
Friction force function of the DePruy model

Let us first look at the magnitude and the pattern of the sliding-rolling ratio of the different prostheses and then at the normal and friction forces.

In the case of the SZIU prototype model (Figure 7), the lateral side starts from a positive sliding-rolling ratio of 0.2, while the medial side starts between -0.25 and -0.6. Starting from 45˚ of flexion angle, the ratio increases with occasional irregularity to 0.86 in the lateral side and 0.76 in the medial side. If we neglect the occasional irregularity, the increment shows closely linear growth. With regard to the kinetics – namely the normal and friction force (Figures 8 and 9) – between the condyles, the evolution of the forces can be described as linearly increasing, with a maximum of 3.58 kN and 3.58 N with respect to the normal and the friction force. Generally more scatter is observed at the medial side.

The BioTech TP and the TP P/S models (Figures 10 and 13) are from the same manufacturer, although they have different characteristics both in their kinematics and kinetics. While the TP P/S model has a very smooth sliding-rolling evolution along the complete segment (0 to 120˚), the normal and friction forces (see Figures 11 and 12) are twice as great compared to forces of the TP model (see Figures 14 and 15), where the sliding-rolling function is more hectic. The sliding-rolling curves of the TP start approximately from 0.4, while the TP P/S from 0.3. From 45-50˚ degree of flexion angle, both TP and TP P/S functions begin to increase, the TP P/S with much less irregularity. The maximum sliding-rolling ratio reaches 0.86 in the case of the TP model and 0.95 in case of the TP P/S on both medial and lateral side, which gives the TP P/S model the highest sliding-rolling value among the tested prostheses.

The BioMet Oxford model (Figure 16) has a very low sliding attribute between 20-60˚ of flexion angle at the medial side (it jumps to a higher value only for a very limited period), and beyond 60˚ it follows also a closely linear growth to 0.88 on the lateral side and 0.85 on the medial side. In contrast with the BioTech TP and the SZIU models, the curve is very smooth after 60˚ of flexion angle.

As for the kinetics, the forces have the same magnitude as the BioTech TP P/S, although here more scatter appears at the lateral side (see Figures 17 and 18).

While the evolutions of the sliding-rolling functions are somewhat similar regarding the SZIU, BioTech TP- TP P/S or BioMet Oxford models, the DePruy prosthesis (Figure 19) follows a completely different and unusual pattern. The curve is practically constant, with less than 5% of periodic deviation. The maximum value of the curve is registered at 23˚ of flexion angle at the medial side where it reaches for a short interval the value of one, which means complete sliding, then the function decreases to 0.75. The contact forces (see Figures 20 and 21) are similar to the Biomet Oxford model.

If we compare the magnitude of the lateral and medial sliding-rolling ratio, a slightly higher percentage of sliding can always be credited to the medial compartment. This difference is quite visible for the DePruy prosthesis while it is less obvious concerning the SZIU, BioTech and BioMet models.

This difference was also confirmed by the study of Wilson et al. [31]. From 0˚ to 5˚ of flexion angle the sliding-rolling ratio at the medial side was significantly higher (approximately 1.5-2 times) compared to the lateral side; between 5˚ and 10˚ was about 1-0.5 times and from 20˚ of flexion angle the difference stays in the range of 5-8%. Since in general the sliding-rolling ratio is slightly (5-8%) higher on the medial side, the medial results were plotted on the following Figures 22 and 23.

By fitting a second-order function on each medial sliding-rolling curve, and summarizing them in one graph, the following results are obtained (see Figure 22).

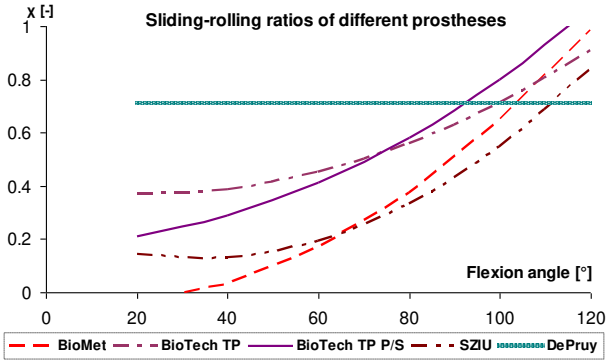

Figure 22
Summarized sliding-rolling ratios of the different models on the medial side

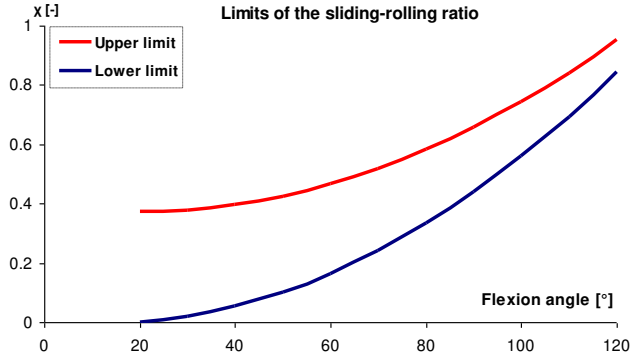

Figure 23
Limits of the sliding-rolling ratio on the medial side

From Figure 22, a well-visible trend appears along the flexion angle for the SZIU, BioTech TP, BioTech TP P/S and the BioMet Oxford models. In addition, upper and lower limit have been drawn where most of the functions are located (see Figure 23).

Conclusions

In this paper the evolution of the sliding-rolling ratio curves has been introduced in the active functional arc of the knee in the case of several commercial and one prototype prostheses. By these curves it becomes possible to estimate the applicable sliding-rolling ratio with respect to the flexion angle.

As was concluded by McGloughlin and Kavanagh [16], a higher sliding-rolling ratio generates a higher wear rate as well; thus, depending on the testing angle, a proper ratio has to be applied during tribological tests. Up to 50° of flexion angle 0.4-0.45 sliding-rolling ratio is adequate, as has been presented by earlier authors [10, 26, 27, 28]; above this specific angle, the currently determined sliding-rolling ratios are more prevalent, since at 120° of flexion angle the ratio can easily reach 0.85-0.95.

As a summary, the currently determined pattern (see Figures 22-23) – obtained by the five different prosthesis geometries – can provide a future limit for experimental tests related to the applicable sliding-rolling ratio with the actual normal and friction load. These applicable loads are represented in this study as normal and friction forces.

Acknowledgement

This work was supported by the FWO (project number: G022506), the Ghent University – Labo Soete, and the Szent István University – Faculty of Mechanical Engineering and Mechanical Engineering PhD School.

We would like to thank the useful comments of Prof. Gábor Krakovits in questions related to anatomy and prostheses.

References

[1] Blunn G. W, Joshi A. B, Minns R. J.: Wear in Retrieved Condylar Knee Arthroplasties. *Journal of Arhtroplasty*, **12** (1997), pp. 281-290

[2] Braune W, Fischer O.: Bewegungen des Kniegelenkes, nach einer neuen Methode am lebenden Menschen gemessen. S. Hirtzel, Leipzig, Germany, 1891

[3] Chittajallu S. K, Kohrt K. G.: FORM 2D – A Mathematical Model of the Knee. *Mathematical and Computer Modelling*, **24** (1999), pp. 91-101

[4] Csizmadia B, Nádori E.: Mozgástan (Dynamics), Nemzeti Tankönyvkiadó, Budapest, Hungary, 1997

[5] Flannery M, McGloughlin T, Jones E, Birkinshaw C.: Analysis of Wear and Friction of Total Knee Replacements. Part I. Wear Assessment on a Three Station Wear Simulator. *Wear*, **265** (2008), pp. 999-1008

[6] Freeman M. A. R.: How the Knee Moves. *Current Orthopaedics*, **15** (2001), pp. 444-450

[7] Fregly B. J, Besier T. F, Lloyd D. G, Delp S. L, Banks S. A, Pandy M. G, D'Lima D. D.: Grand Challenge Competition to Predict in Vivo Knee Loads. *Journal of Orthopaedic Research*, **30** (2012), pp. 503-513

[8] Gear C. W.: Simultaneous Solution of Differential-Algebraic Equations. *IEEE Transactions on Circuit Theory*, **18** (l971), pp. 89-115

[9] Gyurecz Gy, Renner G.: Correcting Fine Structure of Surfaces by Genetic Algorithm. *Acta Polytechnica Hungarica*, **8** (2011), pp. 181-190

[10] Hollman J. H, Deusinger R. H, Van Dillen L. R, Matava M. J.: Knee Joint Movements in Subjects without Knee Pathology and Subjects with Injured Anterior Cruciate Ligaments. *Physical Therapy*, **82** (2002), pp. 960-972

[11] http://www.biomet.hu, Accessed: 03.04.2012

[12] http://www.biotech-medical.com, Accessed: 02.28.2012

[13] Iwaki A, Pinskerova V, Freeman M. A. R.: The Shapes and Relative Movements of the Femur and Tibia in the Unloaded Cadaver Knee. *Journal of Bone and Joint Surgery*, **82-B** (2000), pp. 1189-1195

[14] Lauren M. P, Johnson T. S, Yao J. Q, Blanchard C. R, Crowninshield R. D.: In Vitro Lateral versus Medial Wear of a Knee Prosthesis. *Wear*, **255** (2003), pp. 1101-1106

[15] Ling Z-K, Guo H-Q, Boersma S.: Analytical Study on the Kinematic and Dynamic Behaviors of the Knee Joint. *Medical Engineering and Physics*, **19** (1997), pp. 29-36

[16] McGloughlin T, Kavanagh A.: The Influence of Slip Ratios in Contemporary TKR on the Wear of Ultra-High Molecular Weight Polyethylene (UHMWPE): An Experimental View. *Journal of Biomechanics*, **31** (1998), p. 8

[17] Michalíková M, Bednarčíková L, Petrík M, Živčák J, Raši R.: The Digital Pre-Operative Planning of Total Hip Arthroplasty. *Acta Polytechnica Hungarica*, **7** (2010), pp. 137-152

[18] Momersteeg T. J. A, Blankevoort L, Huiskes R, Kooloos J. G. M, Kauer J. M. G, Hendriks J. C. M.: The Effect of Variable Relative Insertion Orientation of Human Knee Bone-Ligament-Bone Complexes on the Tensile Stiffness. *Journal of Biomechanics*, **28** (1995), pp. 745-752

[19] Mow V. C, Soslowsky L. J.: Lubrication and Wear of Joints. In: Mow V. C, Hayes W. C.: Basic Orthopaedic Biomechanics. Raven Press, New York, USA (1991), pp. 245-292

[20] MSC.ADAMS Basic Full Simulation Package: Training Guide. Santa Ana, USA, 2005

[21] Nägerl H, Frosch K. H, Wachowski M. M, Dumont C, Abicht Ch, Adam P, Kubein-Meesenburg D.: A Novel Total Knee Replacement by Rolling Articulating Surfaces. *In Vivo* Functional Measurements and Tests. *Acta of Bioengineering and Biomechanics*, **10** (2008), pp. 55-60

[22] Pinskerova V, Johal P, Nakagawa S, Sosna A, Williams A, Gedroyc W, Freeman M. A. R.: Does the Femur Roll-Back with Flexion? *Journal of Bone and Joint Surgery*, **86-B** (2004), pp. 925-931

[23] Quian S. H, Ge S. R, Wang Q. L.: The Frictional Coefficient of Bovine Knee Articular Cartilage. *Journal of Bionic Engineering*, **32** (2006), pp. 79-85

[24] Reinholz A, Wimmer M. A, Morlock M. M, Schnelder E.: Analysis of the Coefficient of Friction as Function of Slide-Roll Ratio in Total Knee Replacement. *Journal of Biomechanics*, **31** (1998), p. 8

[25] Saikko V, Calonius O.: Simulation of Wear Rates and Mechanisms in Total Knee Prostheses by Ball-On-Flat Contact in a Five-Station, Three Axis Rig. *Wear*, **253** (2002), pp. 424-429

[26] Sukumaran J, Ando M, De Baets P, Rodriguez V, Szabadi L, Kalacska G, Paepegem V.: Modelling Gear Contact with Twin-Disc Setup. *Tribology International*, **49** (2012), pp. 1-7

[27] Van Citters D. W, Kennedy F. E, Collier J. P.: Rolling Sliding Wear of UHMWPE for Knee Bearing Applications. *Wear*, **263** (2007), pp. 1087-1094

[28] Van Citters D. W, Kennedy F. E, Currier J. H, Collier J. P, Nichols T. D.: A Multi-Station Rolling/Sliding Tribotester for Knee Bearing Materials. *Journal of Tribology*, **126** (2004), pp. 380-385

[29] Van Ijsseldijk E. A, Valstar E. R, Stoel B. C, Nelissen R. G. H. H, Reiber J. H. C, Kaptein B. L.: The Robustness and Accuracy of in Vivo Linear Wear Measurements for Knee Prostheses Based on Model-based RSA. *Journal of Biomechanics*, **44** (2011), pp. 2724-2727

[30] Wimmer M. A.: Wear of Polyethylene Component Created by Rolling Motion of the Artificial Knee Joint, Aachen, Shaker Verlag, Germany, 1999

[31] Wilson D. R, Feikes J. D, O'Connor J. J.: Ligaments and Articular Contact Guide Passive Knee Flexion. *Journal of Biomechanics*, **31** (1998), pp. 1127-1136

[32] Zuppinger H.: Die aktive im unbelasteten Kniegelenk. Wiesbaden, Germany, 1904

Nomenclature

$\chi(\alpha)$: Sliding-rolling ratio (-).

α : Flexion angle of the knee (°).

$\bar{r}_{Ci}(t)$: Vector describing the path of the contact points (m).

$\bar{r}_{CMF}(t)$ and $\bar{r}_{CMT}(t)$: Displacement vectors of the center of masses (m).

$\bar{v}_{CMF}(t)$ and $\bar{v}_{CMT}(t)$: Velocity vectors of the center of masses (m/s).

$\bar{\omega}_{CMF}(t)$ and $\bar{\omega}_{CMT}(t)$: Angular velocity vectors of the center of masses (1/s).

$\bar{e}_{Ci}(t)$: Tangential unit-vector of the contact path (-).

$\bar{r}_{CF}(t)$ and $\bar{r}_{CT}(t)$: Displacement vectors determining the contact point with respect to the center of masses (m).

$\bar{v}_{CF}(t)$ and $\bar{v}_{CT}(t)$: Velocity vectors determining the velocities in the contact point with respect to the center of masses (m/s).

$v_{CFt}(t)$ and $v_{CTt}(t)$: Tangential velocity components in the contact point (m/s).

$v_{CFn}(t)$ and $v_{CTn}(t)$: Normal velocity components in the contact point (m/s).

$S_{femur}(t)$ and $S_{tibia}(t)$: Arc lengths of femur and tibia (m).

Review of Competitiveness Indices that Use Knowledge as a Criterion

Andrea Katić[(1)], Ilija Ćosić[(2)], Goran Anđelić[(3)], Saša Raletić[(4)]

[(1)] University EDUCONS, FABUS, Serbia, katicandrea@fabus.edu.rs

[(2)] University of Novi Sad, Faculty of Technical Sciences, Serbia, ftndean@uns.ac.rs

[(3)] University EDUCONS, FABUS, Serbia, andjelic@fabus.edu.rs

[(4)] University of Novi Sad, Faculty of Economics, Serbia, raletic@mpk.edu.rs

Abstract: Orientation towards a knowledge economy is visible in all development strategies of both the EU and Serbia. This article first shows the classification and systematization of the most relevant competitiveness indices, along with the participation assessment of components measuring the knowledge competitiveness within them. Secondly, the article examines and demonstrates the position of Serbia. The basic hypothesis confirmed in the article is that the position of Serbia, as a transition country, was not sufficiently analyzed, especially in terms of knowledge indicators. This developed a second hypothesis, also confirmed in this article, that the existing indicator models are not adequate for transition countries such as Serbia, and that there is a need for setting up a new revised model.

Keywords: competitiveness indices; knowledge society; knowledge as a criterion for competitiveness; Serbia

1 Introduction

In March 2010, The European Commission created a new strategy entitled "Europe 2020 – EU Strategy for Smart, Sustainable and Inclusive Growth", which points out the most important elements of the new program [1]. The top three priorities are:

- **Smart growth***:* economic development based on knowledge and innovation;
- **Sustainable growth**: promoting a resource efficient, greener and more competitive economy;
- **Inclusive growth***:* providing a high-employment economy delivering economic, social and territorial cohesion.

Seven key initiatives have been set for achieving these priorities, three of which are related to knowledge [2] [3] [4]. They are grouped within the first priority and are concerned with upgrading European performances in education, research and development and the digital society [5]. A number of indicators were established for monitoring the success of both Lisbon Strategy and Europe 2020, dealing with the competitiveness of European countries – the Competitiveness Indices [6]. Various organizations all over the world perform similar monitoring of global competitiveness. It is estimated that there are over 100 such indicators presented in different forms. The best known one is the Global Competitiveness Index (GCI), annually issued in a detailed report by the World Economic Forum (WEF), which includes 142 countries worldwide [7].

Following the latest round of EU enlargement that took place at the beginning of 2007, with Bulgaria and Romania becoming the 26th and 27th EU member states, the next prospective members appear to be the West Balkans region countries [8]. It is an open question, however, as to what extent the accession countries will be able to benefit from an increase in the quality of FDI that they receive due to EU membership [9]. The competitiveness dimension is especially significant in transition countries, considering that these countries experience dynamic changes in their socio-economic systems and are constantly challenged to be successfully involved in the global market race. Serbia and the countries of the West Balkans are particularly important, with their European (EU) perspective, their education tradition, their developed scientific research infrastructure and their prominent scientific results.

This article has two dimensions – descriptive and quantitative. The aim of the descriptive dimension is to conduct a systematization and a classification of these indices using knowledge as a criterion. It will present the ones related to knowledge, innovation and improvement of the citizens' education, which have their share in the overall competitiveness of one system, along with the level that a certain society has reached on its way to the "knowledge society", as the most competitive society to which the EU strives. These indices, also called knowledge society indices, will be specially analyzed from the aspect of Serbia and other transition countries, with critical assessment of their improvement. The aim of the quantitative dimension is to assess the role and participation of knowledge in competitiveness indices and the position of Serbia according to them. The results of the study of the European Competitiveness Index of Serbia, with the evaluation of the role that knowledge has in the overall ranking of Serbia, will be presented for this purpose [10] [11].

The main hypothesis of the article (H0) is that Serbia, as a transition country in the process of European integration, has not been well analyzed as regards knowledge competitiveness. The existing competitiveness indices do not provide enough information for detecting the so-called development bottlenecks. According to these indices, Serbia ranks very low, the lowest of all European countries, which results in a negative image of the country and unfavourable starting positions. The

main hypothesis generates the next one, (H1), which claims that there is a need to create a new knowledge society competitiveness index model for Serbia, which could be used for all transition countries. In this sense, the findings of this article may contribute to the development of further research of competitiveness.

2 Theoretical Background

2.1 Knowledge Society as a Development Strategy in Europe and Serbia

The term "knowledge society" was first used by Peter Drucker in 1969, while its current meaning originates from the 1990s [12]. It is grounded on knowledge – a resource different from all the others, because it is enlarged by use and share. The knowledge society is a society of mobility and has been the most competitive society in the history of mankind [13].

The knowledge society needs to have a high percentage of academically educated citizens, huge investments in education, science and research, encouraging learning through the whole life, quality and available information and communication infrastructures and services, a propulsive and competitive economy, available information and easy access to it. Many recent studies maintain that regional characteristics influence innovative performance, innovation processes and the innovation patterns of firms [14]. A knowledge society is not just a society based on applying information and communication technologies, where knowledge is the most expensive product, but a society that enforces new ways of organization, gives new roles to known systems (with the education system being one of them), and redefines and revalues human and other resources, such as space and time [15]. In short, national economies are becoming more knowledge-based economies, where productivity and growth have become more dependent on knowledge [16].

Economic development has always been knowledge-based. However, the scope and significance of knowledge to economic processes has fundamentally changed over the past number of years [17]. The ever-accelerating creation and dissemination of knowledge has led to the modern rapid and efficient production techniques, plus the increased probability of leapfrogging, which has consequently resulted in the world economy becoming increasingly more competitive. Responding to the latter situation in the transforming engines of economic development, the European Commission launched the Europe 2020 Strategy in March 2010, to exit the crisis and prepare the EU economy for the challenges of the next decade. The agreement to launch the new EU strategy creates a need for research initiatives to develop a new concept of competitiveness, with much of the research focusing on how the knowledge society and competitiveness interact [18].

Strategy Europe 2020 defines “Smart growth” as strengthening knowledge and innovation as drivers of our future growth. This requires improving the quality of education, strengthening research performance, promoting innovation and knowledge transfer, making full use of information and communication technologies, and ensuring that innovative ideas can be turned into new products and services that create growth and quality jobs and can help address European and global societal challenges [1].

As a European Union candidate country preparing for accession, Serbia must foster the competitiveness of its economy [19]. The “Serbia 2020” strategy also focuses on knowledge as the key factor of development. According to current investments in science of 0.3% of Gross Domestic Product (GDP), Serbia is far behind in comparison to Europe and developed countries of the world [20]. The vision of the scientific and technological development of Serbia is that Serbia should become an innovative country where scientists can reach European standards, contribute to the overall level of social knowledge, and improve the technological development of the economy [21] [22] [23].

2.2 The Role of Knowledge in Raising National and Regional Competitiveness

Many policy makers express serious concerns about national competitiveness [24]. In the modern-day globalised world, competitiveness has become a milestone of both advanced and developing countries [25]. Thus, if the competitiveness of a nation is properly managed, enhanced human welfare should be a key expected outcome [26]. National competitiveness is a complex concept. It involves many aspects in measurement and requires much effort in data collection [35]. National competitiveness was first defined in the research of Porter (1990) [29] as a result of a nation’s ability to generate innovation in order to accomplish or keep an advantage over other nations in the key industrial branches. Competitive regions and cities are places where both companies and people want to invest and be located [28]. Competitiveness is the ability of one economy to attract and keep firms active with stable and growing market share, managing to hold and raise the standard of living to all the participants [31].

The Organization for Economic Co-operation and Development (OECD) suggested that competitiveness should be understood as "the ability of companies, industries, regions, nations or supranational regions to generate, while being and remaining exposed to international competition, a relatively high factor of income and a factor of employment levels on a sustainable basis" [32]. The World Economic Forum (WEF) defines competitiveness as "the set of institutions, policies, and factors that determine the level of productivity of a country. The level of productivity, in turn, sets the sustainable level of prosperity that can be earned by an economy" [33].

Further research by Thurow (1993) emphasizes that in knowledge-based economies nations first need to develop specialization in order to reach a world-class standard of living for its citizens [30]. In order to advance effectively towards the knowledge-based economy, countries need to invest in both the creation and the diffusion of new knowledge [27]. Also, the individual states and regions must cope with impacts of globalization process due to create conditions for their higher productivity and competitiveness [34].

In many cases, neither Serbia nor its autonomous province were included in forming the competitiveness index. In the review given in tables 1-4, it is evident that only a part of indices shown includes Serbia, but none of them include its Autonomous Province of Vojvodina. This points to the requirement that European criteria and principles are to be applied internally, so that European competitiveness indicators of Serbia and Vojvodina respectively are achieved.

The first efforts towards reaching this goal were made in 2006, when the calculation of composite parameters was performed along with the comparison of obtained results within the study of "The Competitiveness Index of AP Vojvodina", where the obtained index of Vojvodina is regarded in relation to the matching index for EU countries (EU-25). A methodology devised by Huggins and Izushi (2002) was used for calculating Vojvodina's competitiveness index, which was also applied to ranking regions in Great Britain, as well as the regions and countries of the EU and metropolitan areas worldwide [36]. 2004 data was used in determining this index [37]. The results indicate that AP Vojvodina was ranked at the last place, the 26th place, out of the 25 EU countries and Vojvodina, with the index value of 62.55.

In a repeated study, completed in 2009, the comparison was based on 2007 data [10] pertaining to 27 EU countries, and this time Serbia was included in the ranking as well as AP Vojvodina (as a region). According to these results, the position of AP Vojvodina was not changed. It still held the last, i.e. 29th place, below the 27 EU countries and the Republic of Serbia.

The above study was repeated once again in 2009, this time for EU-27 and Serbia proper, in order to determine the position of Serbia [11]. The same methodology was used, but with more recent data (year 2008). The composite index of competitiveness of European countries and Serbia shows that Serbia was still positioned at the last place, i.e. the 28th place.

However, the composite index of competitiveness of Serbia in the field of education ranks Serbia at the 19th place [11]. It is obvious that Serbia is placed in the lower half according to the level of competitiveness in the field of education, but on a par with most countries of the European Union. The average value of the composite index of competitiveness in the field of education for the 27 European Union countries amounted to 100.31, while the value for Serbia was 91.3. This positions Serbia at 91% of the EU average, which can be considered a very good result. The composite index of competitiveness in the field of creativity ranks

Serbia at the 27th place, just above Romania. It is interesting to note that according to the number of patent requests per million Serbian citizens, Serbia is ranked in the tenth place, which again confirms in practice the assumption that the population of Serbia is very innovative. Despite this fact, Serbia is at the last place, the 28th place, according to the number of employees in research and development per 100 economically active citizens. This means that innovators and inventors in Serbia have not found their place in the real sector, and knowledge is not sufficiently used or patented, although it is generally known that investment in research and development is one of the basic requirements for creating and raising competitiveness.

3 Methodology

The presented methodology of work is related to its descriptive and quantitative dimension. Methods of synthesis and analysis were applied in the descriptive dimension of research. Theoretical research includes scientific description, classification, explanations and prediction, and methods appropriate to these segments of scientific research, e.g. compilation, classification, comparison and similar methods. The research results are presented in the analytical tables and charts, but also in the actual existing examples. Secondary data was used, mainly official studies and reports of various indices of competitiveness, available on the Internet. The position of Serbia, according to these indices, is highlighted.

The quantitative dimension of research relates to assessment of the role and participation of knowledge in competitiveness indices. Estimates which are made in paragraph 4.2 are based on percentage share of the parameters of knowledge in composite indicators.

As the first competitiveness research in Serbia and Vojvodina, the presentation of the methodology and results of studies on European Competitiveness Index of Serbia and AP Vojvodina are presented [37] [30].

In order to obtain comparable data, a conversion of all variables (input data) has been made to obtain the average for all that equal 100:

$$s_{ij} = \frac{x_{ij}}{\overline{x}_j} \cdot 100 \tag{1}$$

where the symbols are:

i	ordinal number of the region/country
j	ordinal number of indicators
x_{ij}	value of the j-indicator of the i-indicator of the region/country
s_{ij}	standardized value of the j- indicator, indicators of the i-region, country
$\overline{x}_j$	average value of j-indicator

A factor analysis was performed over the set of converted variables, where the choice of the number of factors is done on the basis of this Catell's test according to the linear diagram of distinctive values. The actual orientation of factors in the factor space is arbitrary, so it is reasonable to make a rotation of factor values to obtain the most appropriate structure for the practical interpretation [30].

The study used a standard computer varimax rotation technology. Based on the rotated factors, the dimensions obtained indicate a link between factors and original indicators. It also provides sub-composite indicators f_{ik} (for i-region/country and k-factor), the points that belong to individual cases; in this case the regions, according to various factors.

The formation of the composite index methodology was carried out by Huggins-Izushi, using Data Envelopment analysis, which is a special application of linear programming methods that maximize the weighted sum of factor points f_{ik} for individual regions with weight p_{ik} :

$$p_{i1}f_{i1} + ... + p_{iq}f_{iq} = z_i \rightarrow \max \tag{2}$$

where the total number of factors, k=1 ,..., q at limitations

$$\begin{aligned} p_{i1}f_{i1} + ... + p_{iq}f_{iq} = z_{ii} \le 1, \quad \forall i \\ p_{ik} > 0, \quad \forall k \end{aligned} \tag{3}$$

The procedure returns the value of weights that gives the maximized weighted sum of factor points z_{ii} for a given region, and for the same set of weights the weighted sum of factors for all other regions is calculated.

In this manner, a set of weighted factor sums is obtained from which the geometric average value is calculated as a composite indicator, i.e. a general competitiveness index for a given region or country. Due to the standardization of the obtained DEA indicators, the geometric average of deviation is multiplied by the converted indicators (square root of variance), more precisely

$$\sigma_j = \sqrt{\frac{\sum_{i=1}^{m}(x_{ij} - \overline{x}_j)}{n}} \tag{4}$$

and then 100 is added. The final result represents the index with an average of 100, with reverberation of real deviations between regions/countries [30].

4 Data and Results

As this article involves two dimensions of research, this section will primarily present results and discussion about the descriptive part. Afterwards, we can see the quantitative dimension of the research, which demonstrates the role and participation of knowledge component within competitiveness indices and position of Serbia according to these.

4.1 Analysis of Existing Competitiveness Indices with Participation of the Knowledge Component

The knowledge-based economy has become a major trend in international society in the 21st Century [38]. This article deals with 17 indices that define the competitiveness of a certain economy and involve the knowledge parameters. The authors propose that they can be classified into the following four categories:

1) Competitiveness Indices
2) Knowledge Competitiveness Indices
3) Innovation Competitiveness Indices
4) Information Technology Competitiveness Indices

In tables 1-4 below, the key indices are displayed according to the above categories and basic characteristics: the name of the index; the name of the institution which issues it; the beginning year of publication; the frequency of publishing; the highest ranked countries in the latest report; the number of countries ranked; the number of variables (the relationship between quantitative and qualitative data); the relationship of the weight coefficient, the number and name of sub-indices (the number of spaces/the number of parameters); and the position of Serbia and the percentage ratio to other countries.

The Competitiveness Indices, as the most general category, including the analyzed IMD World Competitiveness Index (Yearbook), Global Competitiveness Index – GCI [7] [40], Index of Economic Freedom and European Competitiveness Index, contains a small portion of knowledge components, except The European Competitiveness Index in which 3 out of 5 elements are related to the role of knowledge. The Index of Economic Freedom [53] does not contain any knowledge component. The highest ranked countries according to these indices are Switzerland, Singapore, Hong Kong, the USA and Scandinavian countries. Serbia is not ranked according to the IMD World Competitiveness Index (Yearbook) and the European Competitiveness Index [41], whereas according to the Global Competitiveness Index – GCI and the Index of Economic Freedom, it is ranked in the third quarter of countries. Thus, it is clear that Serbia is not analyzed adequately when it comes to knowledge components.

Economic activities associated with the production and utilization of information and knowledge has become an engine of economic growth [42]. The Knowledge Competitiveness Indices, as a narrower category that includes the analyzed Knowledge-based Economy Index (former New Economy Index) [43], the Metropolitan New Economy Index [43], the Knowledge Economy Index (KEI) and Knowledge Index (KI) and the World Knowledge Competitiveness Index (WKCI) [54], contain a great portion of knowledge components. The highest ranked countries and regions according to these indices are the USA and Scandinavian countries. It is typical for these types of studies not to be published regularly, but rather periodically. Also they analyze not only the Knowledge

Economy Index (KEI) and the Knowledge Index (KI), but the regional knowledge competitiveness as well. Out of the above mentioned indices, Serbia is ranked only according to the Knowledge Economy index (KEI) and Knowledge Index (KI), and is placed in the second quarter of countries [55]. Due to the fact that the mentioned index is published periodically (1995, 2000, 2008), we can again conclude that Serbia is inadequately analyzed in terms of the knowledge component.

The Innovativeness Competitiveness Indices refer to the ability of a single economy to introduce innovation and innovative changes into the environment [45] [46]. Innovative capacity is the capacity to generate new knowledge and transform it into new products, processes and forms of organization [47] [48]. The Innovativeness Competitiveness Indices, with the analyzed Global Innovation Index [56], the Innovation Union Scoreboard [57], the Atlantic Century Benchmarking EU & US Innovation and competitiveness [49], the BCG Report entitled "The Innovation Imperative in Manufacturing" [50], and Report: Innovation: Transforming the way business creates [58] are oriented towards innovativeness as one of knowledge components, while other knowledge components are less analyzed. Today, many developing countries around the world are oriented towards innovation as a means of spurring regional economic development and wealth creation while preserving national competitiveness [59]. The highest ranking countries and regions appearing among these indices are Singapore, Japan, South Korea and Scandinavian countries. Out of the mentioned surveys, Serbia is ranked in 3 out of 5 of these indices, one of which is a single study. This means that Serbia is inadequately analyzed in terms of the innovation component.

The Information technology Competitiveness indices, as a specialized category, involving the Global Information Technology Report – Networked Readiness Index [51] [52], the Information Society Index [60] and Measuring the Information Society – The ICT Development Index [61], are committed to the usage of information technologies as one of the knowledge components, while other components are less analyzed. The highest ranked countries and regions are Scandinavian countries, South Korea and the USA. Serbia is ranked only according to the Global Information Technology Report – Networked Readiness Index and by the ICT Development Index. This means that Serbia is inadequately analyzed in terms of the usage of information technologies.

Based on the analysis of different groups of indices that include parameters of knowledge, one can observe a very poor ranking of Serbia, and its absence in case of several studies. The main hypothesis (H0), that Serbia as a transition country in the process of European integration is insufficiently analyzed in terms of knowledge competitiveness, has been evaluated as correct. The existing competitiveness indices do not provide enough information to help detect the so-called development bottlenecks. It is evident that the ranking of Serbia is very low according to the knowledge indices.

Table 1

Indices of competitiveness

Index name	Name of the institution releasing the index and the start year of the release	Frequency of publication	Best ranked countries in the latest report	Number of countries ranked	Number of variables (quantitative / qualitative data ratio)	Ratio of weighted coefficients	Sub-composite indices and number of fields/number of parameters	Serbia's rank and % rank among other countries
IMD World Competitiveness Index (Yearbook)	International Institute for Management Development – IMD, since 1989.	Annually	1. Hong Kong 2. USA 3. Switzerland 4. Singapore 5. Sweden Report: 2012	59	329 (219/110)	quantitative - 1 qualitative – 0,64	1. Economic performance (5/76) 2. Government Efficiency (5/71) 3. Business Efficiency (5/67) 4. Infrastructure (5/113)	Serbia is not ranked
Global Competitiveness Index (formerly: Global Competitiveness Report)	World Economic Forum since 1979. (upgraded in 2004)	Annually	1. Switzerland 2. Singapore 3. Sweden 4. Finland 5. USA Report: 2011/2012	142	111 (35/76)	Not same for all countries – dependent on the level of development	1. Basic requirements (4 fields/46) 2. Efficiency enhancers (6 fields/49) 3. Innovation and sophistication factors (2 fields/16)	95/142 (2011/2012) (66.9%, in the 3rd quarter among states)
Index of Economic Freedom	The Heritage Foundation and The Wall Street Journal since 1995.	Annually	1. Hong Kong 2. Singapore 3. Australia 4. New Zealand 5. Switzerland Report: 2012	179	Each sub-composite index uses a different methodology for its formation	Each sub-composite index is weighted equally	1. Business freedom 2. Trade freedom 3. Fiscal freedom 4. Government size 5. Monetary freedom 6. Investment size 7. Financial freedom 8. Property rights 9. Freedom from corruption 10. Labour freedom	98/179 (2012) (54.7%, in the 3rd quarter among states)

European Competitiveness Index	Robert Huggins Association	Periodically (2004, 2006.)	1. Finland 2. Luxembourg 3. Switzerland 4. Norway 5. Denmark Report: 2006	27 states and 118 regions	36 quantitative data	Each sub-composite index is weighted equally	Creativity Economic Performance Infrastructure and Accessibility Knowledge Employment Education	Serbia is not ranked

Source: the authors

Table 2

Knowledge indices of competitiveness

Index name	**Name of the institution releasing the index and the start year of the release**	**Frequency of publication**	**Best ranked countries**	**Number of countries ranked**	**Number of variables (quantitative/qualitative data ratio)**	**Ratio of weighted coefficients**	**Sub-composite indices and number of fields/number of parameters**	**Serbia's rank and % rank among other countries**
Knowledge-based Economy Index (formerly: New Economy Index) **since 2001.**	Milken Institute, University of California	Two times study	n/a	n/a	12	n/a	n/a	Serbia and Europe are not ranked
The Metropolitan New Economy Index 2001.	Progressive Policy Institute (PPI)	Single study	1. San Francisco 2. Austin 3. Seattle 4. Gainesville 5. San Diego Report: 2001.	All the states of the USA	21 (total)	2/1,5/3/4/4 (each field has different weight)	1. Knowledge jobs 2. Globalization 3. Economic dynamism and competition 4. Transformation into digital economy 5. Innovation capacity	Serbia and Europe are not ranked

Knowledge Economy Index (KEI) and Knowledge Index (KI)	The World Bank Institute's Knowledge for Development Program (K4D) Since 1995.	Periodically (1995, 2000, 2008)	1. Denmark 2. Sweden 3. Finland 4. Netherlands 5. Norway Report: 2008.	146	83 (total)	Equal weight	1. Economic and institutional regime 2. Education and skills 3. Information and communication infrastructure 4. Innovation system	53/146 (0.36% in the second quarter)
World Knowledge Competitiveness Index (WKCI)	Centre for International Competitiveness	Periodically (five releases), Latest: 2008.	1.San Jose-Sunnyvale-Santa Clara, US 2.Boston-Cambridge-Quincy, US 3.Hartford, US 4.Bridgeport-Stamford-Norwalk, US 5.San Francisco-Oakland-Fremont, US Report: 2008.	145 world regions	19 quantitative	Equal weight	1. Capital components 2. Knowledge economy production 3. Regional economy outputs (including economic knowledge outputs) 4. Sustainability	Serbia is not ranked

Source: the authors

Table 3

Innovativeness indices of competitiveness

Index name	**Name of the institution releasing the index and the start year of the release**	**Frequency of publication**	**Best ranked countries**	**Number of countries ranked**	**Number of variables (quantitative/qualitative data ratio)**	**Ratio of weighted coefficients**	**Sub-composite indices and number of fields/number of parameters**	**Serbia's rank and % rank among other countries**
Global Innovation Index	Confederation of Indian Industry along with	Annually	1. Switzerland 2. Sweden 3. Singapore	125	60 (36/24) (divided into input and output	Equal weight	Inputs: 1. Institutions, 2. Human Capacity	55/125 (0.44 in the 4th quarter

	INSEAD (The Business School for the World) Since 2008.		4. Hong Kong 5. Finland Report: 2011.		parameters)		3. General and ICT 4. Infrastructure, Market Sophistication 5. Business Sophistication Outputs: 1. Scientific Outputs 2. Creative Outputs and Well-Being.	among states)
Innovation Union Scoreboard since 2010, (formerly European Innovation Scoreboard)	Maastricht Economic and social Research and training centre on Innovation and Technology (UNU-MERIT)	Annually	1. Sweden 2. Denmark 3. Finland 4. Germany 5. UK Report: 2011.	34 European countries and 6 world countries	25 (quantitative data, divided into input parameters, firm activities and output parameters)	unweighted average of the re-scaled scores for all indicators	Inputs: 1. Human resources Human resources 2. Open research systems 3. Finance and support 4. Firm activities 5. Firm investments 6. Linkages & entrepreneurship 7. Intellectual assets Outputs: 1. Innovators 2. Economic effects	29/34 (0.85 in the 4th quarter among states)
The Atlantic Century Benchmarking EU & US Innovation and Competitiveness	The Information Technology and Innovation Foundation	Annually	1. Singapore 2. Finland 3. Sweden 4. USA 5. S. Korea Report: 2011.	40	16 (quantitative data)	10/20/12/20/13/25 (each field has different weight)	1. Human capital 2. Innovation capacity 3. Entrepreneurship 4. Information technology (IT) infrastructure 5. Economic policy 6. Economic performance	Serbia is not ranked
The BCG Report: The Innovation Imperative in Manufacturing	Boston Consulting Group, National Association of Manufactures, and the US-based Manufacturing Institute	Single study 2009.	1. Singapore 2. S. Korea 3. Switzerland 4. Iceland 5. Ireland	110 world countries + 50 USA states	n/a	n/a	Inputs: 1. Fiscal policy 2. Business performance 3. Other policies Outputs: 1. R&D results 2. Innovation environment 3. Public impact of innovation	Serbia is not ranked
Report: Innovation:	Economist Intelligence Unit	Single study	1. Japan 2. Switzerland	82	18 (6/12)	7/3 (each field has	1. Direct innovation inputs 2. Innovation environment	67/81 (in the 4th

Transforming the way business creates		2007.	3. USA 4. Sweden 5. Finland			different weight)		quarter among states)

Source: the authors

Table 4

Information technology indices of competitiveness

Index name	Name of the institution releasing the index and the start year of the release	Frequency of publication	Best ranked countries	Number of countries ranked	Number of variables (hard/qualitative data ratio)	Ratio of weighted coefficients	Sub-composite indices and number of fields/number of parameters	Serbia's rank and % ratio among other countries
The Global Information Technology Report - Networked Readiness Index (using their methodology)	World Economic Forum since 2001. Centre for International Development (CID) at Harvard University	Annually	1. Sweden 2. Singapore 3. Finland 3. Denmark 4. Switzerland Report: 2012.	142	53 (25/28)	Equal weight	1. Environment 2. Readiness 3. Usage 4. Impact	85/133 (in the 3rd quarter among states)
Information Society Index - payable	n/a	n/a	n/a	53	15	n/a	n/a	n/a
Measuring the Information Society – The ICT Development Index	Market Information and Statistics Division within the Telecommunication Development Bureau of ITU	Annually	1. S. Korea 2. Sweden 3. Island 4. Denmark 5. Finland Report: 2011 (data for 2010.)	154	11 (quantitative data)	40/40/20	1. ICT access 2. ICT use 3. ICT skills	50/152 (in the 2nd quarter)

Source: the authors

4.2 The Role and Participation of Knowledge in the Competitiveness Indices and the Position of Serbia

It can be seen from the above mentioned division of indices which include the parameters of knowledge that they can be treated differently in the case of the Competitiveness Index. 60% of overall indicators appear in the case of European Competitiveness Index; in the case of Global Competitiveness Index they are present in 25%, while they are not mentioned at all in the case of the Index of Economic Freedom. By the analysis of a group of indices treated as Knowledge Competitiveness Indices, one can see that the results are not updated enough and that they are mainly focused on the area of the USA.

The data presented in this article show that education is one of the few development opportunities of Serbia, and that it can be a real source of increased competitiveness of its economy. However, in addition to education, the knowledge society also requires a willingness to develop entrepreneurial spirit, promotes innovation and encourages creativity. It is therefore necessary to invest more in this area as well as to recognize their importance by public and private initiatives.

In most cases, Serbia is ranked in the third quarter of the world's states, while this is even worse if compared with the countries of Europe, where it is always placed almost at the bottom. However, very few studies analyze the ranked countries according to individual factors, and it is difficult to determine the specific reasons for the poor positioning. Also, most of the presented indices are made for the developed countries and do not reflect enough the real situation in Serbia as a country in transition. Hence, the great importance of a few national studies that analyze the position of Serbia is recognized. In the European Competitiveness Index [11], Serbia is placed in the second half according to the level of competitiveness in the field of education, and on a par with most countries of the European Union. This suggests not only a good position of Serbia in this segment, but also that Serbia's competitiveness would be far better if the knowledge and education aspects were valued more. Given that education is a key factor in the knowledge society, it can be concluded that in order to monitor the progress of Serbia and other transition countries, it is necessary to redefine the weighting factors for calculation of competitiveness indices, i.e. to redefine the share of certain areas, but also the number of input parameters in this field. The second hypothesis (H1), which claims that there is a compelling need for the formation of a new competitiveness index of the knowledge society for Serbia, and which could also be a model for all countries in transition, is accepted. In this sense, the findings of this article may contribute to developing further research on competitiveness.

Conclusions

Commitment to knowledge economy and the development of technological and scientific capacity are evident in all basic development strategies in the European Union and Serbia. Due to the development of the information revolution and the increasing availability of information, the further progress of social community is not entirely dependent on purely economic factors. Knowledge, innovativeness, enterprise, adoption of new technologies etc. also become the key requirements for the growth of national competitiveness. Numerous indices reflecting the competitiveness of both national and regional economies are defined for the purpose of following the progress in this area.

In order to conduct comprehensive research, this article reviewed two dimensions – descriptive and quantitative. In this context, the object of the research of the descriptive part of the study was the analysis of the most relevant indices of competitiveness available, while the evaluation of the proportion of components measuring the knowledge competitiveness within the indices was presented in the quantitative part. Another object of research was the evaluation of the position of Serbia as a potential candidate country for the EU membership according to all indices analyzed.

It can be concluded from the set hypotheses that Serbia is inadequately analyzed regarding knowledge competitiveness, that the existing indices in which Serbia is analyzed do not offer enough information on knowledge development in Serbia, and also that Serbia is at the very bottom in comparison to European and world countries.

Also, the analysis implies that existing models of knowledge are not appropriate for countries in transition, such as Serbia. In order to achieve the set goals, it is necessary to make a new revised model to better indicate specific problems, for example the development bottlenecks in the development towards the achievement of a knowledge society. The key parameters of this new model would be knowledge, innovation, education, use of IT technology and development of knowledge jobs.

References

[1] European Commission: EUROPE 2020: A Strategy for Smart, Sustainable and Inclusive Growth, Brussels, 2010

[2] The European Economic and Social Committee and the Committee of the Regions: Europe 2020 Flagship Initiative, Innovation Union, Brussels, 2010

[3] The European Economic and Social Committee and the Committee of the Regions: A Digital Agenda for Europe, Brussels, 2010

[4] The European Economic and Social Committee and the Committee of the Regions: Youth on the Move, An initiative to unleash the potential of

young people to achieve smart, sustainable and inclusive growth in the European Union, Brussels, 2010

[5] Publications Office of the European Union: Europe's Digital Competitiveness Report, Luxembourg: Publications Office of the European Union, http://ec.europa.eu/digital-agenda, 2010

[6] ESIB: The Lisbon agenda, ESIB—the National Unions of Students in Europe, Belgium, 2006

[7] World Economic Forum: The Global Competitiveness Report 2011–2012, World Economic Forum, Geneva, 2011

[8] Lejour A, Mervar A, Verweij G: The Economic Effects of Croatia's Accession to the European Union, Eastern European Economics, 47(6), 2009, pp. 60–83

[9] Narula R, Bellak C: EU enlargement and consequences for FDI assisted industrial development, Transnational Corporations, United Nations, 18(2), 2008, pp. 69-90

[10] Ćosić I, et al: The Competitiveness of AP Vojvodine as a European region, Study for Provincial Secretariat for Science and Technological Development of AP Vojvodina and Provincial Secretariat for Regional and International Cooperation of AP Vojvodina, Faculty of Technical Sciences and Faculty of Economics, Novi Sad-Subotica, (In Serbian), 2009

[11] Ćosić I, et al: The European Competitiveness index, Study for Ministry for Science and Technological Development of Republic of Serbia and Provincial Secretariat for Science and Technological Development of AP Vojvodina, Faculty of Technical Sciences, Novi Sad, (In Serbian), 2009

[12] Drucker P: The Age of Discontinuity, Guidelines to Our Changing Society, Harper & Row: New York, 1969

[13] Drucker P: My view of management - ideas that have improved management, Novi Sad: Adizes, (In Serbian), 2006

[14] Isaksen A, Onsager K: Regions, networks and innovative performance: The case of knowledge-intensive industries in Norway, European Urban and Regional Studies, 17(3), 2010, pp. 227–243

[15] Jelinčić J: The Europeization of Serbia – Knowledge Society, Open Society fond, Belgrade, 2007

[16] Asian Development Bank: Moving Toward Knowledge-Based Economies: Asian Experiences, Asian Development Bank, 2007

[17] Nijkamp P, Siedschlag I: Innovation, Growth and Competitiveness, Dynamic Regions in the Knowledge-Based World Economy, Advances in Spatial Science, 2011

[18] Balkyte A, Tvaronavičiene M: Perception of competitiveness in the context of sustainable development: Facets of "Sustainable Competitiveness",

Journal of Business Economics and Management, 11(2), 2010, pp. 341 – 365

[19] Farrugia N: Constructing an Index of International Competitiveness for Malta, Bank of Valletta Review, 26, 2002, pp. 20-37

[20] General Secretariat of the President of the Republic: Serbia 2020: The Concept of Development of Serbia up to the Year 2020, General Secretariat of the President of the Republic, www.predsednik.rs, (In Serbian), 2010

[21] European Integration Office of Republic of Serbia: European Orientation of Serbian Citizens, Trends, European Integration Office of Republic of Serbia (In Serbian), 2010

[22] European Commission: Annual Growth Survey, Annex 1. Progress Report on Europe 2020, Brussels, 2011

[23] European Commission: Annual Growth Survey, Annex 3. Draft Joint Employment Report, European Commission, Brussels, 2011

[24] Lall S: Competitiveness Indices and Developing Countries: An Economic Evaluation of the Global Competitiveness Report, World Development, 29(9), 2001, pp. 1501-1525

[25] Önsela S, Ülengina F, Ulusoyb G, Aktaşc E, Kabakc O, Topcuc Y: A new perspective on the competitiveness of nations, Socio-Economic Planning Sciences, 42(4), 2008, pp. 221-246

[26] Ülengina F, Kabakb O, Önsela S, Aktasb E, Parkerc B: The Competitiveness of Nations and Implications for Human Development, Socio-Economic Planning Sciences, 45(1/3), 2011, pp. 16-27

[27] Saisana M, Saltelli A, Schulze N, Tarantola S: Uncertainty and Sensitivity Analysis for the Knowledge-Based Economy Index, Conference on Medium-Term Economic Assessment (CMTEA), Sofia, Bulgaria, 2005

[28] Kitson M, Martin R, Tyler P: The Regional Competitiveness: An Elusive yet Key Concept?, Regional Studies 38(9), 2004, pp. 991-999

[29] Porter M: The Competitive Advantage of Nations, Harvard Business Review, 1990

[30] Huggins R: Designing A European Competitiveness Index: Measuring The Performance and Capacity of Europe's Regions and Nations, European Regional Economic Forum, Nova Gorica, Slovenia, 2005

[31] Storper M: The regional world: territorial development in a global economy, Guilford Press, New York, 1997

[32] Hatzichronoglou T: Globalization and Competitiveness: Relevant Indicators, OECD Science, Technology and Industry Working Papers, 5, 1996, pp. 62

[33] Schwab K: The Global Competitiveness Report 2009-2010, Geneva: World Economic Forum, 2009, pp. 492

[34] Lesáková L: The Process of Forming the Regional Innovation Strategy, Acta Polytechnica Hungarica, 8(1), 2011, pp. 5-22

[35] Kaoa C, Wub W, Hsiehc W, Wanga T, Lina C, Chena L: Measuring the national competitiveness of Southeast Asian countries, European Journal of Operational Research, 187(2), 2008, pp. 613-628

[36] Huggins R, Izushi H: World Knowledge Competitiveness Index 2002: Benchmarking the Globe's High-Performing Regions", Robert Huggins Associates, Cardiff, http://www.cforic.org, 2002

[37] Ćosić I, et al: The Competitiveness index of AP Vojvodine, Study for Provincial Secretariat for Science and Technological Development of AP Vojvodina, Faculty of Technical Sciences, Novi Sad, (In Serbian), 2006

[38] Hsua G, Linb Y, Wei Z: Competition policy for technological innovation in an era of knowledge-based economy, Knowledge-Based Systems, 21(8/12), 2008, pp. 826-832

[39] Sala-i-Martin X, Blanke J, Hanouz MD, Geiger T, Mia I: The Global Competitiveness Index 2010–2011: Looking Beyond the Global Economic Crisis, World Economic Forum, Geneva, 2010, pp. 3-49

[40] Browne C, Geiger T: The Executive Opinion Survey: The Business Executives' Insight into their Operating Environment, World Economic Forum, Geneva, 2010, pp. 75-83

[41] Rosselet-McCauley S: What is the World Competitiveness Yearbook? www.imd.ch/wcy, 2012

[42] Kriščiūnas K, Daugėlienė R: The Assessment Models of Knowledge-Based Economy Penetration, Engineering Economics, 5(50), 2006, pp. 36-46

[43] Milken Institute: Knowledge-based Economy Index, https://www.milkeninstitute.org, 2001

[44] Atkinson R, Gottlieb P: The Metropolitan New Economy Index, Benchmarking Economic Transformation in the Nation's Metropolitan Areas, 2001

[45] Furman JL, Porter ME, Stern S: The determinants of national innovative capacity, Research Policy, 31, 2002, pp. 899–933

[46] National Endowment for Science: The Innovation Index Measuring the UK's Investment in Innovation and Its Effects, National Endowment for Science, Technology and the Arts, www.nesta.org.uk, 2009

[47] Krätke S: Regional Knowledge Networks, A Network Analysis Approach to the Interlinking of Knowledge Resources, European Urban and Regional Studies, 17(1), 2010, pp. 83-97

[48] Wonglimpiyarat J: Innovation index and the innovative capacity of nations, Futures, 42(3), 2010, pp. 247-253

[49] Atkinson R, Andes S: The Atlantic Century Benchmarking EU & U.S, Innovation and Competitiveness, The Information Technology and Innovation Foundation (ITIF), www.itif.org, 2009

[50] Andrew J, DeRocco E, Taylor A: The Innovation Imperative in Manufacturing, How the United States Can Restore Its Edge, www.bcg.com/publications, 2009

[51] Dutta S, Bilbao-Osorio B: The Global Information Technology Report 2012, Living in a Hyperconnected World, World Economic Forum and INSEAD, www.weforum.org/gitr, 2012

[52] Dutta S, Mia I, Geiger T: The Networked Readiness Index 2010–2011: Celebrating 10 Years of Assessing Networked Readiness, 2011

[53] The Heritage Foundation: Index of Economic Freedom, The Heritage Foundation, www.heritage.org/Index/about, 2012

[54] Huggins R, Izushi H, Davies W, Shougui L: World Knowledge Competitiveness Index, Centre for International Competitiveness, University of Wales Institute, Cardiff, http://www.cforic.org, 2008

[55] The World Bank Institute's Knowledge for Development Program (K4D), Knowledge for Development Program in the World's Economies Measuring Knowledge, Knowledge Assessment Methodology and Knowledge Economy Index, The World Bank Institute's Knowledge for Development Program (K4D) www.worldbank.org/kam, 2008

[56] INSEAD: Global Innovation Index 2010/11, INSEAD, http://www.globalinnovationindex.org, 2011

[57] UNU-MERIT: Innovation Union Scoreboard, The Innovation Union's performance scoreboard for Research and Innovation, Maastricht Economic and social Research and training centre on Innovation and Technology (UNU-MERIT), www.proinno-europe.eu/metrics, 2010

[58] Valery N, Kekic L: Innovation: Transforming the way business creates includes a global ranking of countries, An Economist Intelligence Unit, 2007

[59] Gibson D, Naquin H: Investing in Innovation to Enable Global Competitiveness: The Case of Portugal, Technological Forecasting and Social Change, 2011, pp. 1299–1309

[60] IDC: IDC's Information Society Index, www.idc.com/offices, 2010

[61] International Telecommunication Union: Measuring the Information Society, The ICT Development Index, International Telecommunication Union, 2011

Historical Origin of the Fine Structure Constant[1]

Part IV: Coronatio: Explicandi et Applicandi Subtilita(ti)s Structurae Constantis Sephano Rege[2]

Péter Várlaki[1,2], Imre J. Rudas[3]

[1]Széchenyi István University
Egyetem tér 1, H-9026 Győr, Hungary, varlaki@sze.hu

[2]Budapest University of Technology and Economics

[3]Óbuda University
Bécsi út 96/B, H-1034 Budapest, Hungary, rudas@uni-obuda.hu

Abstract: Part IV of our paper on the historical (archetypal) background of the "fine structure constant" deals with the general physical and psychic world views, concealing the dynamic isomorphic meaning systems, related to Saint Stephen (Sephanus Rex) found in works of 1000 years old. Following the comparison of the representations (pre-figurations of the dynamic models) of the demonstrated background languages, we present that the author devoted himself to create a common background language of different religious courses. We intend to show that the background language (considered in general as a mapping of primordial images for "system and control" problems), was centred on his assumed proto-Cabbala, the Book of Bahir and its concealed meaning system, in close relation with the numeric archetype of 137 and the 137-type of "fine structures" within the decimal sephirotic world "controlling system" of the pleroma (the hypothesised "transcendent cyber space").

Keywords: Number archetype137; Fine structure constant; King Stephanus

[1] The paper is dedicated to the memory of C. G. Jung (1875-1961) on the occasion of his 137th birthday.

[2] Some possible 'interpretations' of the Latin subtitle *"Summary (Crowning): The interpretation and the application stable built by King Sephanus", "Interpretations and applications of the fine structure constant by King Sephanus," "Interpretations and applications of the stable built 'exactness' by King Sephanus."* Sephanus *(SEPHANVS)* Rex *(REX)* (King Sephan or Sephen) is a "mystical" name (meaning 'The Hidden' or 'The Concealing') given by himself St Stephen of Hungary on his Royal Robe.

1 Introduction

In the closing part of our paper, first of all we deal with the methodical questions of the revealing poetic hermeneutic systems of works containing the central role of the number 137, and particularly with the creative deformational "techniques", which generate new semiotic systems and hidden meanings. We evince the common similitude of the structures of the pictorial depiction forms and the letter or language mystic patterns of meaning of the works of fine arts and mystic literature alike. Then we show angel Yophiel representing and impersonating the number 137 and the two (merging) cherub systems' "structure" of likewise 137 on the Pala d'Oro and the Coronation Mantle, together with the exploration and analysis of the concealed (and concealing) name of the author, the great king, and its representative and significant meaning content. Thereafter, we deal in detail with the identification of the concealed naming of the great king, his peoples and his kingdom in the Bahir and in the Royal Mirror, tightly related to the number 137, as a number archetype of directing-controlling mediating-medium. We pay attention even to the exploration of the decimal sephirotic system's language mystic invariant, as well, to the basis of their isomorphic renderings. Furthermore, we attempt to identify the meaning systems of the patterns related to the origin, foundation and genealogic myth of the author's kingdom hidden in the Bahir's Hebrew-Aramaic text. We touch upon the close correlations of the cosmic language mystic and the astronomical and astrological "background theories". We also deal with the particular rendering forms of the decimal sephirotic system through the representation of the 3-4 transformations, demonstrating the way these patterns "form" the pre-figuration of the representations of the straight and inverse dynamic input and output systems. We intend to display some particularly fascinating examples of the 3-4 transformations' tight correlation with the number 137, or its directing and controlling force, judged as important and "viewed as objective" by Jung and Pauli. We discuss briefly at the end the questions of the representations of the proto-Cabbalistic "Eucharist" in the Bahir. We plan to deal with their detailed explication in our subsequent studies [32].

2 About the Methodological Foundation of the Structural and Hermeneutical Approach

As well as on the superscription of the Coronation Mantle (the Casula), in the Latin and Greek lettering system of the Pala d'Oro (the back panel of the altar) and the Holy Crown, we find a trilingual reference system that is based on the quotations of the Old Testament. In this, behind the Greek and Latin text, a complex system of Hebrew names and meanings can often be detected [14, 30].

In this section, in addition to the interpretation of the special and unlikely visual representations, we intend to discuss the system of superscriptions, based on their seemingly rule-violating patterns, especially the productive deformation and anomalies of the quotes and lettering types.

Assuming that the creator of such an extremely expensive and significant work of art faced not only the traditional artistic (poetic and hermeneutic) criteria, but also such inherited religious traditions and theological ideas, along with artistic forms and aesthetic principles as well that had reached an elevated level of optimization between reality and abstraction in an earlier artistic and liturgical culture. (This complexity can be observed in the well-known works of the 10th century Byzantine artists.)

In such a situation, the creative author (originator), the creator of something new, who perhaps, wishing to conceal a radical new world view, attempts to terminate the highly optimized unity (based on the given religious traditions and theological ideas, and specific to the artistic reality) of concrete and abstract. But it is not done merely for annihilation. As Anthony Storr writes *"Works of art similarly (to the religious rituals) concerned order. Although the great creators are often distinguished by their propensity to break rules, there are always rules for them to break. A work of art without any order or arrangement is inconceivable"* [3]. Based on form, the Pala d'Oro, the Casula and the Holy Crown can be seen as the artistic bearers of "holiness" (as in traditional religious opus) if we avoid recognising some unrealistic forms of depiction. How can one still comprehend that a system is "annulled" yet it is still there unharmed? This means on the one hand that the earlier religious tradition, the theological routine and the representations used before are not the highest level of organising forces ruling the material, but rather themselves become material ("prima materia"), a material for other, new ordering principles and theories. On the other hand, this means that these higher level theories in the end follow the same idea: these too are in accordance with the given era's religious and artistic world of ideas, and try to build a bridge between the abstract and the concrete, the ideal and the sensual.

It is safe to assume that the Casula, the Pala d'Oro and the Holy Crown should all be viewed as this type of novelty artistic creations. Notably, ones with concrete theurgic, mystic theosophic, political-theological and historical interpretational aims, in which, in accordance with the traditions of the era, these aims appear hidden in those forms of the representational systems that deviate from tradition: E.g. in the transposition of the typical traditional depiction of faces that carry a

[3] Storr, A.: Dynamics of Creation (1972). See also Bonyhai, G.: Collected Works, Budapest, 2000, pp. 201-205. Although a smaller legend states but Stephen was permeated with *ars grammatica* from an early childhood (J. Szűts, 1988) "*... If we accept ... and based on the bigger legend we have to accept that this work was written by St Stephen himself"* (Guoth 1943) (Regalis eduxtus – "*Big Legend*" (Vita) 5, and *Scientia grammaticae artis Ingutus* – Little Legend (Vita) 2. Hartwick 4)

meaning; and also in the productively deformed depictions of the superscriptions and the quotations. In this case, the material of the motif pattern of the code breaking is not the portrayed figures' well-known depiction or the formation of the traditional transcription of letters but the system of improbable deformations, or transformations, which provides such new material bearing intentional attributes with which the outlines of the meanings of quasi-conclusions could appear. So, in theory the "transformed depiction of face types" and the patterns of letters create such a world of meanings, the rules of which concur with the traditional forms of portrayal and of the rules and laws of the world of writing. However, their improbable pattern of formation generates a text and code system, therefore types of pictures with signifying attributes can emerge, the symbols. This applies to the striking and form breaking systems of depiction of the apostles, prophets, etc. (see Bonyhai 2000)

How is it possible to fulfil the requirement of the improbable order; what could the unusual distribution of the elements be applied to?[4] The regulation of reference is not other than our experience (as undetached observer's) with the given era's writing and forms of portrayal, the system of knowledge harvested from the statistical distinctness (averages, dispersion). In this way, because of the improbabilities, the re-interpretable order can become symbolic material, and thus the work not only contains simple elements, but it becomes a whole – variant piece of work. Based on the creative interpretation of time and space, causality, the usual traditional forms, the improbabilities and the probabilities, the possibilities and impossibilities (because of the traditional familiarity of space and the productive deformity of causality) the new symbols and values can apply. All of this, in our case, bears a political-theological and concrete historical message that rests on a concrete, new, mystic-theosophical and theurgic base, in which the mythical genealogic legitimisation of the new (St Stephen's) "Roman Kingdom's" royal house plays a great role [14, 30].

Observe now some important examples, patterns that will play a role in our later analysis in order to illustrate the ideas mentioned above. On the left side of the circular inscription of the Crowning Mantle (Fig. 1) we can see the special joint letters ***TA*** and the abbreviation of the word *"est"*, where the wave of both letters, both joining and abbreviation and their double point can surely be interpreted as

[4] *"...We can refer to the unforgotten history of hermeneutics. Before it was self-evident that the task of hermeneutics is the alignment of the meaning of the text to the concrete situation in which the text is interpreted. The original model of this the interpretation of the divine will, who can understand the language of the oracle ... The philological hermeneutics along with the juristic and theological hermeneutics were originally connected by application, that is a basis of all understanding." "...The religious holy text should not be regarded as a mere historical document but it should be understood that it could practice its impact of salvation ... then it has to be understood again and differently in every moment, every concrete situation. Understanding here is always application."* (Gadamer, H-G.: Truth and Method, 2004) Thus, we can summarize roughly the credo of the art of St Stephen.

the sign for the twin-motif. This is also reinforced by the round and square letter pairing ***CE*** in the word ***ECCLESIAE*** (Fig. 2), with which we can get the reference to ***ECCE ELIAS*** *(above the name of "Iohannes"!)*. This, based on the book of Malachias, refers to the rising sun, the rebirth of the Messiah, and according to the Strabo interpretation [7, 14], Phares and Zara's rebirth. This motif is continued in the expression ***SANCTA(E) MARIAE,*** where the author leaves the letter ***E*** from the end of the genitive of the Latin word in order to make the strings of letters over the name of Thomas (meaning twin in Hebrew) appear for the reader as ***TAMAR*** (Fig. 1). The consolidation after the productive deformation in the ambivalent form of depiction is brought by the author by the double stroke of the right side of the letter ***A***. He thus indirectly refers to the missing letter E and at the same time notes that in the ambivalent "order of semiotics" after all there is no spelling mistake. Tamar here, according to the traditions of the Middle Ages, is not only the impersonator of the Jews but of the one and whole, Ecclesia "consisting of twins" and of the "*Ecclesia de gentibus et judaeorum"* (see Green 1979 [7]).

Figure 1
Particular lettering on the Crowning Mantle's circular inscription

The Tamar (Thamar) motif, as we have already mentioned and as will also be shown later several times, has a great presence on the Mantle. It is possible that the signifying of God's two hands with the sun symbol and the words "opening" and "gap" (in Hebrew it's Peretz –or Phares) refer to the meaning of the names of the Messiah twins (Phares – opening and Zara – rising sun) and of the proto-Kabbalistic interpretation of right and left hand. In Fig. 1 we can observe the creative deformation in the superscription ***Sancta***(***e*** - missing) ***Mariae*** that reminded us of the name Tamar. As has already been mentioned, the symbolic

presence of Thamar is also reinforced by the double (!) lines of letters above the name of the prophet Thomas, whose name means "twin" in Hebrew, and also, the finely scribed symbolic form of the letter ***M*** that reminds us of a tree of a date palm. As we have mentioned on several occasions in the *Hortus Deliciarum*, Thamar is the embodiment of the Church, the Ecclesia and the Holy Virgin. This provides a firm basis to be able to signify symbolically as the Holy Virgin the Church and the God-Mother both, and as an antitype. All these can be interpreted as the allusion of the rebirth of Christ as the "Divine twin", as in God and Human, where the not so hidden appearance of the possible reading of "***ECCE ELIAS***" from Ecclesia can also point to the advent of the Messiah. "Elias" (as St John the Baptist), Tamar with the Christ-figure of "Pricipium et Finis" constitute a Deesis[5].

Figure 2
The meaning identification of "Ecce Elias" from the "Ecclesiae"

[5] "Trinity formulas" are usually "representations" of the dynamics of the Ten Sefiroth in the Book Bahir. This kind of "Deesis" (Prayer) is manifested in addition to the three Tetragrammaton and the Trishagion by the three Crowns of Israel as well (§152). In this picture the "female" crown is the crown of Kingdom and the "male" crown is related to the Priestly crown, while the crown of Torah is related to the "God-image" according to the symbolic structure of the Holy Crown. In this passage the threefold crown of Israel is equalled a parabola of the threefold interpretation of Tefillin (**תפילין,תפילה**), which can be interpreted as "Prayer", i.e. Deesis (Δεησις) in Greek. On the Royal Robe, thus the Messiah (Father and Son) represents the potential world structure and archetypes, while the Heavenly Mother figure represents the 3rd along with the 10th Sefirah. They can be considered as an input-output of a hypothetical dynamic (control) system. Between the double Sophia, or Shekina (as input-output), the six unified Sefirot in one "person" represents the straight and inverse transformation of the Sephirotic system dynamics. The classical Deesis on the Robe, the heavenly God mother, Christ (in the center) and the Summus Rex "also" represents Saint John the Baptist, and can be identified (as a hidden manifestation of this potential Trinity) in the real time (reappearing regularly in the history) in the inscription around the Christ figure of Principium et Finis by the above discussed creative deformation (see Figs. 1 and 2). Here the Lord manifested in the time is naturally the Principium et Finis as a Messiah for a given period of time "between" "the Beginning and the End". On the right side of the Lord, in the inscription, we can decode the fragment "Ecce Elias" from the "Ecclessiae". Similarly, on the left side of the Lord's figure in the inscription, the name of Tamar can be decoded. Naturally, prophet Elijah from the Christian view can be concerned in the real time as Saint John the Baptist. Consequently, this "concealed Deesis" is entirely isomorphic with the potential "great" Deesis of the Robe and through the Mother Tamar, it is a symbol of the rebirth of Christ in the ("actual") historical time, here and now in the "Ecclesia Sanctae Mariae" and in the name "Sephanvs Rex" as (anagram) Phares Xenvs (see in verse Math 25:35 Christ as ξενος).

3 The Union of the Crowning (Incarnation) and the Two-Cherub System on the Pala d'Oro

The two cherubs and the Yophiel motif most probably can be identified most clearly in the portrayal system of the Pala d'Oro. Descriptions of Yophiel (יופיאל=137) in the Antiquity and in the Middle Ages are connected to three works. The oldest is in the *Sar ha Torah* book, which is part of the Hekhaloth literature, where Yophiel, the angel of the Torah, interpreter of the secrets of the Torah, who brought down (or drew down) Gods presence into this world, the Shekina (in the Christian sense the Celestial Queen Sophia or Mary) into Gods ever building Sanctuary, amongst the two Cherubs (drawing down theurgy [9]). In the Medieval Hebrew writing of Gedulath Moshe, who also follows the antique traditions, the angel Yophiel appears as the seventh celestial angel, whose other name is Dina [5]. The latter can be interpreted as the word that in Hebrew and Aramaic means law, or following the law. Here, in addition to his being the law and the angel of the Tora, he is also the teacher of souls, a speaker of 70 languages, who is God's linguist and interpreter in one.[6] In this way, the numerical value of the expressions

[6] The text referring to it in Gaster's translation is the following: *"And after that Moses saw an angel in the heaven called Araboth, i.e. the seventh heaven, and this angel was teaching the souls which were created by God at the time of the Creation and have been placed in paradise. The name of the angel was X. He teaches them in seventy languages in the college on high, and they answer: "Thus is the law of Moses given by tradition from Mount Sinai [as it is said Dina was set and the books were opened and Dina is none other than this angel, who is the guardian angel of the Law and of wisdom." He has also another name, they call him Jefefiyah, for the name of the guardian angel of the Law is* ***Iofiel"*** [5]. In the Christian tradition (where neither the tradition's origin nor its time can be established) they correspond to the cherubs or cherub guarding the tree of Eden. Another tradition views him as the teacher of Noah's sons. "*In Christian tradition, it is Yophiel who drove Adam and Eve from the Garden of Eden, which would make him the first Angel to appear in the Bible. In this case he would also be the Angel guarding the Tree of Life with a flaming sword"* [15]. The third literature that has been mentioned is the so called Hai Gaon text, which is part of the Eleazar fragments, as we have mentioned in the first part, possibly comes, as we reckon, from the court of St Stephen. This is where we can see the emphasis on the numerical value of 137 of the name Yophiel, which coincides with the number 137 of the wheel of the Ezekiel vision, the ophanim. This, as we could observe, is the archetype of the Crown, which is why the author identifies Yophiel with the two words of the Crown: the expressions Atarah and Keter, the Hebrew words of crown [3, 4]. Here he appears as the leader of the 7 heavens' 7 angels, which is in symmetry with the contents of the other two literatures. His task is the crowning of God and the ten, and the tenth kingdom, furthermore, the drawing of the Sekhina into the tenth kingdom. The crown, by the way, is depicted at the end of the writing as a dual masculine and feminine unity. The Crown is a god-name consisting of 42 letters. Yophiel, as a result of a transformational sequence, creates a unity with subsequent three angels [4]. The crown of the god-name, which consists of 42 letters, belongs to them. Since Scholem connects the text to the Bahir authorial circles [20], it is most natural that the top-most three archangels Michael, Gabriel and Uriel can be identified with the Bahir's 72 charactered (and joint) name of God. Thus, the lower 7 sephirot or attributes represent a 72+42=114 lettered God-name. In sections 141-143 of the Bahir, the first sephira is the Aleph

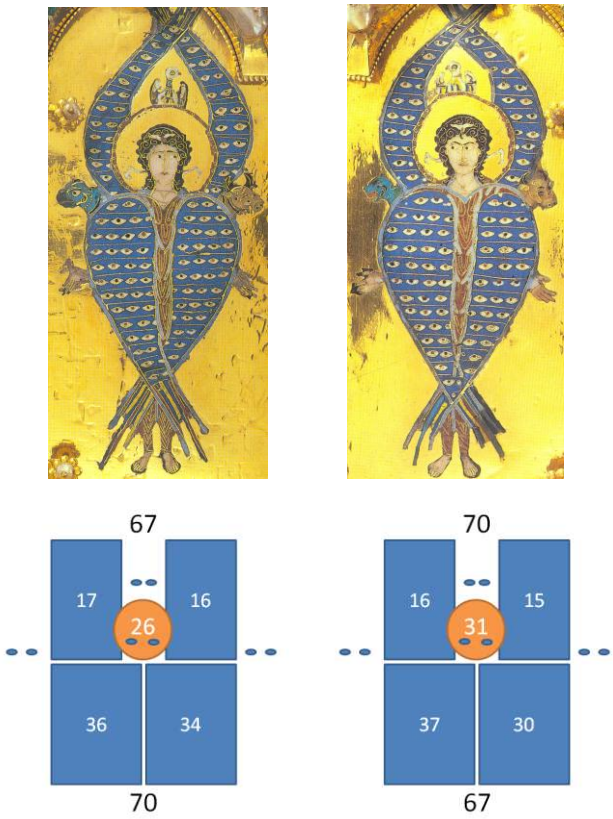

Figure 3
The "Double Cherub" system and the representation of the 137 "fines tructure"

"*Chessed Dina*" or "Law and Mercy" or "Dina's (Yophiel's) mercy is 137. The mythologem of the Pala d'Oro's Yophiel and the two cherubs uses the well-known ancient and Medieval writings concerned with the two cherubs and their Hieros Gamos. Of these there is a very important text, connected to the earliest Philo, Origenes and Tadshe Midrash, in which the two cherubs represent the two names of God (YHVH and ELOHIM, 112=**אלהים יהוה**)[7]. These, along with the masculine

and Kether Elion is the top Crown, while the second and the third sephira is identified 'partly' with the 22 letters of the Hebrew alphabet and their interpretations. These originate from the ancient Aleph and represent the Tora and its interpretations (see section 70). Thus most probably, intentionally, in the joint interpretation of the Bahir and the Eleazar fragment, the 1+22+72+42=137, the divine letters and the appearance of the God-name in the 10 sephirot, is a conscious construction.

7 The kind reader can follow the semiotic interpretations of the discussed "symbolic mathematics" of the meaning transformations and symbolic meaning-systems, without any knowledge of the Hebrew letters and words, by the next not usual simple transliterations of the Hebrew letters

and feminine interpretation of the cherubs, highlight God's androgynous aspect. With the uniting of the cherubs, the two God-names unite as well, *"their sexual relationship is projected onto a higher metapsychical level: that of a pair of angels"*[9]. Considering the tradition of the Tadshe, the union of two God-names and the cherubs symbolizes the balancing of the two attributes, Mercy and Judgement. The very same ideas appear in the writings of Eleazar of Worms [3,4], which we can view as the peculiar summary of the preceding traditions in the same form, and these were most probably formulated in the court of the great king. The Eleazar summary and the separate Yophiel mythologem together make the poetic-hermeneutic implementation of the 'plot' of the Pala d'Oro possible. In other words, the 'plot' of the Pala d'Oro more or less uses all the traditions mentioned so far, and from these it composes a unique crowning ceremony in God's eternal church's (Sophia's) Sanctuary, along with the creation of a dynamic 'background system" belonging to the 137 numeral archetype.

Let us have a look at the possible number-based interpretations of the portrayal system of the two cherubs. On the gloria of the right cherub (on the left side of the picture) there are 26 ornaments that correspond to the iris of the eye. This clearly refers to a Tetragammaton. The cherub, as we have mentioned several times, as a unique depiction, has 4 heads and 4 faces in accordance with Ezekiel's beings with a soul, despite the fact that these cherubs are the ones facing each other on the left and right hand side of the Ark of the Covenant and the Sanctuary of the Temple of Solomon. The 4 faces obviously mean 8 more eyes (of which 6 are visible). We can count 33 eyes on the upper part of the wing. In Fig. 3 we can observe that the gloriole, the eyes of the 4 cherub faces and the upper part of the wing create a unity similar to the bottom two wings. The number and sum of the ornaments is thus 33+26+8=67. The number of eyes on the bottom two wings is 36 and 34, which is altogether 70. Pay attention to the fact that the portrayal of the cherub's four wings corresponds to the vision portrayal of Ezekiel. The two cherubs of the Ark of Covenant and the sanctuary are almost always depicted with 6 (less frequently with 2) wings according to the number of wings of the seraphs. Thus, altogether we get the number 137. Here the interpretation is 67, the number of the Hebrew word Binah (**בינה**), while the 70 can also mean the Tamar motif of 70 (Ex 15:27), the 70 languages and the 70 nations. Thus, the composition refers to the understanding of all the world's languages, and within it the number 137, which is solely the attribute of Yophiel, the universal interpreter. If the two hidden eyes are counted with the bottom part, we get the usual 65+72=137 composition. The other natural composition of the depiction could be when we take the ornaments of the eyes and the gloriole separately. The number of the eyes is obviously 36+34+33+8=111 while the gloriole, the ornament of the

(along with their numbers) into Latin (based upon the Kaplan's renderings [2]): א-A=1, ב-B=2, ג-G=3, ד-D=4, ה-H=5, ו-V or W=6, ז-Z=7, ח-Ch=8, ט-T'=9, י-I or Y=10, כ ך -K=20, ל-L=30, מ ם–M=40, נ ן -N=50, ס-S'=60, ע-E=70, פ ף-P or F=80, צ ץ-Tz=90, ק-Q=100, ר-R=200, ש -S or Sh=300, ת-T or Th=400.

Tetragammaton, is 26. We can observe that the 111 corresponds to the word Aleph, while the 26 to the YHVH (**יהוה**) or the YVY (**יוי**), the frequently discussed names of God. From these letters we directly get the name Yophiel. The 137 is of course the number of the Hebrew word for wheel (137=**אופן**); thus this number supplements the missing wheel of the cherubs of the Ezekiel vision in the 'outer' portrayal. In the case of the left cherub (the one on the right viewing the picture) we can count 31 ornaments on the gloriole. This corresponds to the Hebrew word AL (אל) God-word which is the basis of the word Elohim. In this way, it is true that the two cherubs represent the two names of God, the Tetragammaton and the Elohim with the AL God-word, in accordance with the tradition in which the right hand side represent God's masculine aspect and the left hand side represents the feminine one. The number of the eyes of the upper two wings is 31; the number of entities of the upper part – similarly to the structure of the right hand side one – is 31+31+8=70. The bottom two wings of the cherub show 37 and 30 eyes. Thus, the number of the entities in the bottom part is 67. So vertically, mirror-symmetrically, the cherub on the left hand side represents the same 137 composition as the right hand side cherub. On the two bottom wings of the cherub on the left there are two eyes, with one black and one burgundy-coloured iris (the other irises are similarly coloured) without the white of the eye, that is, only given with the iris. Here, counting these special eyes as part of the upper section, we also get the 72+65 = 137 composition. The mirror symmetry is the symbol of unity and the holy union. Thus, based on numerology, we can safely talk about, the Hieros Gamos of the two cherubs and the two God-names, the representative of which is the angel of the crown, Yophiel. This is confirmed by the composition of the ornaments of the eyes and the gloriole on the angel on the left hand side. Since the number of eyes altogether is 37+30+31+8=106, we have the numerical value of the Hebrew word Yophi, or 'nice'. In this way the 106+31=137 composition, although in a different form, still gives us the name Yophiel. In the interpretation of the right side, the name Yophiel comes from the letters of Aleph (**אלף**) and God YVY (**יוי**), while in the case of the left cherub, it was composed from the words interpreted from 106 and 31, the God-names of YVFY (**יופי**) and AL (**אל**), respectively.

On the Pala d'Oro, under the two cherubs there is the picture of the prince and the princess waiting for their coronation and their Hieros Gamos. It proves that the picture is about the renewal of the kingdom by the royal heir's coronation and symbolic wedding ceremony, where the Divine presence, the Shekina (or Sophia), has arrived – based on the unity of the two cherubs and the two God-names courtesy of Yophiel – which is in the Christian interpretation the Godmother, who would proceed with the coronation in the spirit of the Solomon royal crowning. On behalf of the Godmother, it is Yophiel who represents the crown and the crowning itself, too. At the side of the royal pair waiting to be crowned we can see King Solomon and King David, as they are speaking to them. King Solomon is the only one who looks at the prince sideways, and it seems that under the archangelic arch (amongst the prophets he is the only one portrayed with one) with his angelic

face as the seventh angel in the centre Yophiel represents him. The admonition written on his book suggests this too. The book is about the temple of Sophia, its seven pillars or the Shekina and the seven heavens and their seven archangels. On the Pala d'Oro, the arch of King Solomon, the gloriole and the decorating system also gives the number 137, indicating the possible identification of him with the Archangel Yophiel.[8] As is well-known, God gave Solomon wisdom in a way that in Solomon's Judgement and Justice God is himself manifested. Bahir here identifies just judgement with the word Din. The numerical value of Din Chokhmah (**דין חכמה**=137) from the Bahir, or Solomon's wise judgement, is 137, which again refers to the name of the archangel Yophiel, since his other name is Dina, which can be written in Hebrew with the Letter He instead of the Aleph: DINH ChKM (**דינה חכם**=137). So Chokam's Dina, with the retaining of the 137 numerical value, can be interpreted that the Wise, in our case Solomon, is Dina himself, or in other names the Archangel Yophiel. To summarize, King Solomon appears on the Pala d'Oro as the royal representation of the crowning archangel Yophiel. (We can see the very same in the depiction of Constantine on the Crown, where the joint portrayal of Great Constantine, the liberator, King Solomon permeated by Wisdom and Archangel Yophiel appear as a joint personality on the Crown.) In the sephirotic system of the Kabbalah, in the position of Tifereth as the reconciliator of the attributes of Mercy and Judgement (the archangels Michel and Gabriel), he is the son and Sophia or the Holy Ghost impersonated by Yophiel. Also, he is the king as well, to whom Peace belongs, and thus (just as Kaplan discusses this sample of the Bahir – section 65) he has his wedding with his bride, the kingdom named Peace (Malkuth) at the same time of the crowing by the Mother. Jung recognises this proto-Kabbalistic image when he talks about the Christian (pleromatic) idea of divine incarnation in the Kabbalah, as we explained in the conclusion of the second part (see also the 13 footnote in the II. part)

We find the other form that is connected to the number 137 of the incarnation of the royal pair in the lower centre of the Pala d'Oro. Above the royal couple we can see the evangelists Matthew and Luke, who signify the dual paternal and maternal incarnation genealogy of Christ. The latter proves that the number of the characters of the two Greek-named prophet images (creating a centre the on the right hand side of the royal pair) is 62, while on the other side we can count 75 characters (and the sum of all the letters is 137). As we have already explained, the number 62 (61) corresponds to the genealogy of the Gospel of Matthew from Adam to Christ [14]. The genealogy of 76 from Adam to Christ comes from the Gospel of Luke, according to the Vulgate; counting the shared Christ we get 137 here as well. Therefore, the other major motif of the crowning of the prince and the princess is the union of the feminine and masculine genealogy of Christ's incarnation, which is represent by the number137. Thus, we can draw the

[8] The arch is 30, the gloriole is 33+8, the crown is 42+10+6=58 plus the 8 lock of hair attached to the crown, thus similarly 71+66 to the already discussed composition of 137=66+71 of the „Table- Temple" [8].

conclusion that that both the Divine wedding in the heavens and the royal crowning and wedding on Earth is represented in the given kingdom by the number 137, in the centre of which there is Yophiel, who gives the crown, and who also administers, personifies and represents the crowning. Apart from the eyes on the 4 wings, there are 4 on one of the half wings, two on three half wings, and there are 3 all white patchy pattern on four half wings. The number 22 can mean (probably) the 22 holy letters of the Hebrew alphabet, which, as is known, can be interpreted as seraphs. This momentum carries the symbol of the union of the two cherubs and signifies Yophiel, who in both the Judaist and the Christian traditions is interpreted as a cherub.[9]

In connection with this, we can also highlight the already discussed Hieros Gamos of the two cherubs that are approaching each other on the Pala d'Oro. Considering the emphasised role of the prophet Habakkuk both on the Pala d'Oro and on the Crowning Mantle it seems evident – as we have discussed several times – that the depicted image of two Chaioth-Cherubs is based on verse 3.2 of Habakkuk. One of the main passages in the Bahir is where Habakkuk appears as the main prophet of the Kabbalah and the cherub-chariot mysticism. The call for God that his work should be between the two Chaioth-Cherubs is given based on the translation of the LXX. It is visible on the Pala d'Oro that the year of 1105, probably in the structure of the centre following an older design the two Chaioth-Cherubs are situated almost exactly in the centre, more centrally from the two upper, static, original cherubs. Touching the two upper Evangelists, quasi linking the two original one faced Cherubs of the Sanctuary (Ark of Covenant, Temple of Solomon) with the 4 cherubs of the Ezekiel vision, who obviously correspond to the Ezekiel vision's 4 Chaioth-Cherubs. (Since the 4 cherubs are the symbol of the 4 Evangelists, the 4 Evangelists are personifications of the 4 Chaioth-Cherubs.) Because in the text of verse 3.2 of Habakkuk the word QRB (קרב) could mean approaching something, near or in the transferred sense it could also mean the Hieros Gamos, so the unique depicting system (and the above discussed union mysticism's number-symbol system) makes it unequivocal that here we talk about the Chaioth-Cherubs of Habakkuk, which joins the original two cherubs with the 4 Chaioth-Cherubs of the throne chariot. In this sense, the author describes an evolutionary motif in connection with the evolution of the cherubs, which stretches from the original two cherubs of the Ark of the Covenant and the Temple of Solomon through the two cherub system of Habakkuk, along the Ezekiel vision to the 36 true, 4 centred cherubs. However, this means that here on the Pala d'Oro, in the Sanctuary, on the throne of God, on the crown, in addition to the reigning Divinity and Mary (who is obviously the Shekina), there are 8 cherubs, since the 4 Evangelists symbolize 4 cherubs. With the union of Habakkuk's two Chaioth (which is proven by the 70th passage of the Bahir), which is also meant as the

[9] For accuracy's sake we have to mention that on the two lower wings of the cherub on the left hand side there are two eyes visible, a black and a burgundy (the other eyes are also like this) without the white, well separated from the above mentioned white patchy pattern.

union of the two God-names, the angel Yophiel emerges with his dual cherub aspect. Thus, in accordance with our previous discussion (in connection with the Bahir), in the transferred sense, the 7 cherub-angel led by Yophiel personifies the 7 sephirot, while the upper 3 sephirot are represented by the throne-crown, the Christ Pantocrator and the God-mother. Yophiel, with the paternal guidance of King Solomon, leads the young royal couple waiting to be crowned to this Sanctuary.

4 The Two Cherubs and Habakkuk in the Bahir and on the Mantle

In our hermeneutic circles, the interpretation of Habakkuk's verse 3.2, which plays a central role in the Book of Bahir, is also important. The first part of verse 3.2 refers to the first three sephirot of the 10, based on the expression: *"LORD, I have heard the report about You and I fear."* The first, the hearing, is identified with the sephira of understanding or comprehension. The news, the good news, the Torah, or in the Christian interpretation the Gospel, is the second sephira. Fear of God here refers to the third and the last sephira [22]. In the interpretation of the rest of the verse, the possible ambivalent interpretation of the original Hebrew text and the unique translation of the Septuagint play an important role. A usual contemporary translation would be thus: *"O LORD, revive Your work in the midst of the years"*. The Hebrew original ***BQRB SNIM (בקרב שנים)*** makes the *BQR BSNIM (**בקר בשנים**)* interpretation possible: Lord, your work 'morning', the rebirth (by the twins) happen throughout the years. The 'Boqer' (morning) interpretation is clear in the 73. The passage of the Bahir and passages 62-72 as a whole deal with the mystical interpretation of verse 3.2. However, the question arises as to why the author in the Book of Bahir identifies the prophet Habakkuk with the vision of the throne-chariot of God, with the cherubs and also with the vision of the 10 sephirot. Furthermore, in the latter case, it is identified also with the 10 sephira, the kingdom, the daughter of the king and the imperative of her presence in this world. The answer comes, in addition to the self-evident verse 3.8, from the utterly unique, and in its own way surprising, Greek translation of Hab 3.2, in the *Septuagint.* Here we find the first instance of the expression ***BQRB SNIM ChIIV***, literally, the Greek translation of 'inside the years', ***ΕΝ ΜΕΣΩ ΔΥΟ ΖΩΩΝ*** or between the two soulful (living) creatures, or in other words, 'between the two cherubs' (Fig. 4). The writer of the Septuagint could have been influenced by the four cherubs of the Ezekiel vision, or the two cherubs of the Ark of Covenant or the Temple of Solomon. At any rate, for a mystic "proto-Kabbalist", the Greek translation offers a great opportunity for the joint interpretation of the Merkabah vision and the temple's two cherubs, which connects them while also treating them as separate places of symbols. It is so because the whole Greek partial text

from verse 3.2 expresses the following: (Habakkuk 3.2) "*κυριε εισακηκοα την ακοην σου και εφοβηθην κατενοησα τα εργα σου και εξεστην* **εν μεσω δυο ζωων** *γνωσθηση εν τω εγγιζειν τα ετη επιγνωσθηση εν τω παρειναι τον καιρον αναδειχθηση εν τω ταραχθηναι την ψυχην μου εν οργη ελεους μνησθηση."* The English translation is the following: *3.2: "O Lord, I have heard thy report, and was afraid: I considered thy works, and was amazed:* ***thou shalt be known between the two living creatures,*** *thou shalt be acknowledged when the years draw nigh; thou shalt be manifested when the time is come."* From the original Greek text and the English translation one can sense the prioritized status of Habakkuk in connection with the Throne-chariot vision.

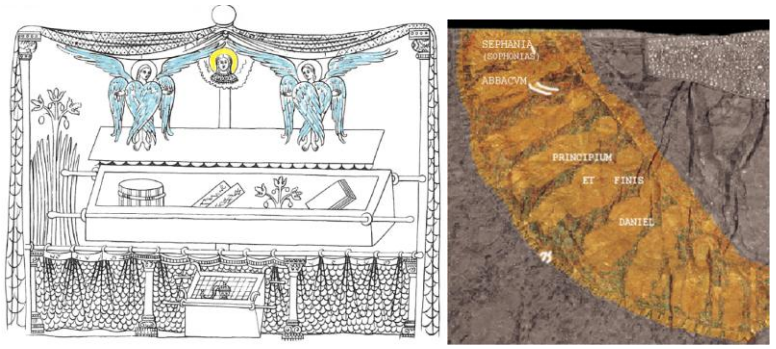

Figure 4

(a) Christ appearing between the two cherubs, as God, symbol of the rising sun. (Hortus D. Fol. 46r)

(b) Habakkuk, Sephania and the prophet Daniel and Christ as principium et finis at the Royal Robe

All these mean that it is not only about the Merkabah vision, the incorporation of Kabbalah, and the two cherubs, but about the so called Drawing Down theurgy that was known in Antiquity. It most probably happened because of the Hellenic influence (Idel 1988 [9]). The essence of this theurgic activity, along with the prayer and the vision, is that the presence of God in this world, in Hebrew the Shekina, is drawn to our world, into our kingdom based on the traditions, in between the two cherubs of the Temple of Solomon. The early and well-discussed du-parcufim and the kabbalistic-theurgic theories in connection with this, the divine face, the ha-Panim and Angel Yophiel were discussed in detail by Idel in his book titled Kabbalah (Idel 1988 [9]) He reveals the connection between the early hermetic mysticism and the Drawing Down. The prayer is for the two angels from earlier, who arrive in the company of Shekina, or who accompany Sekhina to God's (King Solomon's) temple in between the two cherubs.

5 Archangel Yophiel and Saint Stephen on the Mantle

Let us have a look at the appearance of the motifs in connection with Yophiel in other important parts of the Coronation Mantle, bearing in mind the system found on the Pala d'Oro. We have discussed in detail before the allusions resulting from the whole structure [30]. We should note also that the 137 composition found on the four Mandorla can be given as the traditional 72+65 and, taking into account the 31 letters of the Mandorla of the uppermost king (Summus rex), it can also be given in the "Yophiel composition" of 106+31=137. We can also observe the possible interpretations of 112+25+1, which connects the symbolism of the Yophiel crown and the crown mysticism with the Triple Crown made up of the letters of the Hebrew word *man (AIS-***איש**) from the Book of Bahir [32]. This obviously corresponds to the uniformed Atara Echod (ET'RH AChD-**עטרה אחד**) crown united from the three God-names [32] Naturally, Yophiel is, as we have mentioned, the Atara himself, and the crown is the eternal crown of the number 137, where the Greek translation of the Atara is, of course, Stephanos.

The twin motif of the whole system of symbols can be applied here and is strengthened by the dual (twin) depiction of Christ (the "A ω" on the right and "Principium et Finis" on the left). Underneath, in the row of the Apostles, there are the twins of Judah and Thomas and Taddeus (separately), coming from creative deformation. Similarly as on the Pala d'Oro, it is realised in the pairing of the king and the queen, in the lowermost circle (from the 7 heaven of the Mantle). Between them there is the picture of Saint Emmerich (Emericus) under the Mandorla of Christ on the throne [32]. Additionally, we will see it also in the dual symbolism of Sephanus and Stephanus, which is unique in religions and in the history of arts (Fig. 5). This was anticipated by the hidden importance of prophet Sephania's (**צפניה**) never written but extremely important, highlighted name. "Sephanus" means hidden, or rather the hider. Since its Greek version is Sephanos (**Σεφανος** = 1026), with a numerical value of 1000+26, it can be written as the Hebrew word Aleph (ALF **אלף**), meaning 1000, and the number 26; therefore, we get to the 137 composition based on the numerical value of 111 of the word Aleph as 111+26=137, which can be interpreted as the name of Yophiel. Thus, the name of the great king whose name otherwise means crown, symbolically hides the priest angel Yophiel, the angel of the crown and crowning, which is not at all surprising seeing that he is one of the main characters of his son's coronation.

Figure 5
"SEPHANVS REX": Sephanus Rex ("King Sephen") with the Disk, Asterisk and Aerion as well as Stephanus (Protomartyr) with pointy beard on the Royal Robe

Next to him Stephanus, under Levi Matthew (!), as "Levita Stephanus", also portrays the ecclesiastical equivalent of Yophiel, and does so in an astonishing way; as we have mentioned, a unique way in the history of arts: with a goatee or a pointy beard (Fig 5). (He is followed by Pope Clement with the inscription 'Clemens'.) The expression '*facie angeli'* is well known from the Acts of the Apostles, based on which, portrayal can only happen without a beard. The pointy beard, as a creative deformation in the given hermeneutic circle induces a strong surplus meaning if we carry out interpretations in all three languages of the Bible. One of the possible interpretations can originate in Greek and Hebrew, in which the triangular, vertex beard can be called Κορυφη, which has the connotation of Crown (as the Στεφανος), as well as 'kodkod bazakan' (BZKN KDKVD **קדקוד בזקן**). This word, like the korufe, literally means that there is a triangular peak in the beard. In this case we see the triangle upside down (since the 'kodkod' also means peak of the roof). Thus, with the 'grammar-dikduk' writing, we get the following anagram: *ZaKaN BaDiKDUK* (ZKN BDKDVK **זקן בדקדוק**). The latter means that the "Person" is prestigious and well-practiced in grammar or linguistics. The basis of the wordplay is that the word 'zakan' means 'beard' and 'old prestigious man' at the same time. While the word 'kodkod', without the letter Vav, is the mirror-symmetric equivalent of 'dikduk' (grammar). Thus, in this interpretation, the goatee beard of Stephanus primus diaconus (Levite), whose Hebrew name according to this expression **,לוי כליל א** gives the number 137, means the representation of the man prestigious in grammar, and in a medieval sense in maths and logic. The other interesting aspect of the wordplay is that with the joining of the two Dalet letters we get the Hebrew name (**בדקדוק חבקוק**) of the prophet Habakkuk. In this hermeneutic circle, the prophet, along with Saint Stephen, is the main cultivator of grammar, the letters, the numeric-archetypes and symbolic mathematics.

The other Hebrew interpretation originating from the depiction of the man with the goatee beard is none other than in Hebrew AIS TIS ZKN (**איש תיש זקן**), or the

'is tis zakan'. The anagram of this is 'is zain keset' or AIS ZIN QST (**איש זין קשת**), which could mean the men of the seven colours of the rainbow. This draws our attention to the fact that Stephanus here represents the ten sephirot, since in the context of the Bahir, the AYS partly symbolises the crown, and partly the crown of the trinity, the symbol of the first three sephirot just as the Aleph (141 §), while the 'Zain' through the seven colours of the rainbow (QST) characterises the lower seven sephirot. This representation corresponds exactly to the crown-angel Yophiel who represents all the 7 heavens, whose name, as we have already pointed out, originated from the crown of the AYS. Similarly, it also corresponds to Stephanus, as the representation of the *7 deacons*, since in the expression, through AYS (which is the 'Atara Echod', or Stephanos in the Bahir), the word crown lays indirectly – or rather the name of the Proto-martyr. Otherwise, the symbolism of the 7 colours of the rainbow means the personification of the 7 activities of the Holy Spirit, both in the case of Yophiel and of Stephen. To Yophiel, based on his name, Sophia is attached as the personification of the first three sephirot, and likewise, Mary, the Celestial Queen to Stephen. As we have shown in the representational system of the Pala d'Oro, Solomon with his own three "crowns" and the 7 columns of the temple of Sophia built by him are connected to both of them [14]. Thus, the king bearing Wisdom, referring to the house of Sophia and the 7 columns on the picture of the Pala d'Oro, appears as the angel Yophiel before us, as we have discussed. We also showed that Emperor Constantine, the builder of the Christian version of the Sophia temple by Solomon, the Liberator of the Church, appears both as King Solomon and as the angel Yophiel on the Holy Crown in the peculiarity of the representational system. [10]

The special grammatical abilities of Saint Stephen were noted even in his childhood, as we have mentioned before. As a scholar of grammar, his presence can be felt in the 6th chapter of his famous Royal Mirror. [28] In the 8th chapter he appears before us rather as an interpreter, a hermeneutic king. The two dreams, most probably coming from the personal traditional circles of the king, written in his canonization documents in the second half of the 11th century, were probably not a coincidence. The two dreams foretell his birth and his role in history and the history of salvation; one in his father's dream, the other in his mother's dream. In the former case, a handsome boy appears as a divine apparition, a messenger of God or an angel, and suggests that his son will receive the first worldly and eternal

[10] We showed this in the picture of St Stephen of the Pala d'Oro [14]. From the mystical interpretation of the name 'Levi' and the celebration of its 360th day, we can infer a connection to the 36-ers. It is an old tradition with King Solomon too, that the 36 deans (**Στοιχεια**) appear before him; therefore he is the master of the 36 or the 72 temporal and linguistic systems because of Wisdom too [1]. We have proven of Yophiel as well that, based on the Antique writings and traditions, he is the teacher of the 70 or in the context of the Bahir, the 72 languages. That is, the sending of Sophia, the main Divine interpreter in the Christian interpretation, as the Holy Spirit to the apostles, is realised in the knowing of the 70 or 72 languages, which is portrayed in an exactly 2x36 structure in the picture of the Pala d'Oro concerned with this.

crown[11] of their people. The handsome boy (the beautiful angel sent by God) and the central role of the crown clearly refer to the crown-angel of Yophiel, whose name means Beauty of God. This is reinforced in his mother's dream where the Protomartyr Levite Stephanus appears in clerical robes (vestment Levitici and not Levitae), and in addition to telling about the birth of the boy and him being given a crown, he also tells her to give his name to the boy. On the Coronation Mantle, as we can observe, the pairing of Sephanus and Stephanus next to each other shows the exact sameness of the meaning of the Beauty of God crown-angel Yophiel and the saint angel-faced, crown-named Protomartyr in the spirit of a unique twin symbolism.

In connection with the pointy beard, we must also mention the Latin and Greek interpretations of the goatee. In Latin, goatee is 'aruncus', and the person wearing it is the 'aruncius' (ARVNCIVS). The latter is a well-known Roman family name. Amongst its ancient variations we can find the expression 'arungus', which corresponds perfectly to the Greek original. The anagram of 'aruncius' is ARCVS VNI, which means the arch of a unit or the rainbow of it; that is, in the given hermeneutic circle, it carries an equivalent meaning with the Hebrew word of goatee, since the word 'uni' (unus) can signify the unity of the upper three sephirot, while the 7 colours of the 'arcus' or its number 7 signifies the lower 7 sephirot together. Thus even the Latin expression can point to the angelic activity of the identification of Saint Stephen and the angel Yophiel, as well as the realisation of the crown in the living Church. The other anagram of 'Arungus' corresponds to the word anagram that comes from Greek. 'Arungus' in another form is VNGARVS, while the Greek 'Aruggos' (ο Αρυγγος) can also be replaced by the VNGAROS or Ουγγαρος anagram. The peculiarity of the Greek word for goatee is that its numerical value is 777=7x111. In both forms its symbolic potential can refer to the fact that it can show the 3+7 compositional sephirotic

[11] This Divine revelation happens to Stephen's father rex Geysa, who is already infused by the new direction; this is aptly paralleled by David and Solomon's legend from the Old Testament: "*cumque nimium esset solicitus — Geysa — de rebellibus domandis et ritibus sacrilegis destruendis ... mirabili visione noctu consolatus eum dominus, fecit astare sibi* ***iuvenem delectabilem aspectu****, qui dixit ei: pax tibi christi electe, iubeo te de sollicitudine tua fore securum, non tibi concessum est perficere quod meditaris, quia manus pollutas humano sanguine gestas, de te filius nasciturus egredictur, cui haec omnia disponenda divinae providentiae consilio dominus commendabit, hic unus erit de regibus electis a domino, coronam vitae secularis commutaturus aeterna"*. (Hartvic. v. s. Steph. 3. and leg. maj. 3) It happens again before the birth of Stephen and the centre of the promise is the new symbol of power, the crown: *"uxorem eius (Sarolt) — Geysae — iam apropinguantem partui tali voluit visione divina gratia consolari, apparuit namque illi beatus* ***Levita*** *et prothomartyr* ***Stephanus levitici habitus ornatus insignibus****, qui eam alloqui taliter cepit: confide in domino mulier, et certa esto, quia filium paries, cui primo in hac gente corona debetur et regnum*". That is why Stephanus is a visio, as the legend says: "*Stephanus quippe graece, coronatus sonat latine*." Hartvic. 4-5; We may see, it is a remarkable allusion for the joint Greek-Latin crown in the background with the Kelil, the Hebrew-Aramaic known version of Stephanus' name and the number 137 together with the participation of "Levita" (priest) angel Yophiel for the mystical interpreter.

system. Thus, it carries an equal numerical meaning with the Latin (and the Hebrew) version, based on an obviously random or perhaps a synchronistic coincidence. So, besides the eternal angelic role interpreted archetypically or on a metaphysical plan, as the unity of the twins of Sephanus and Stephanus, the great king both on the planes of concrete temporality and personality appears as a prestigious linguist, a symbolic mathematician and as 'ungarus Stephanus' or 'rex ungarorum', personifying archangel Yophiel too, or at least in the Mantle's interpretative system of the deep structure of portrayal.

To summarise regarding the pointy beard:[12] On the Coronation Mantle Saint Stephan's portrayal with the pointy beard (Spitzbart) as we explained in the methodical section, is apparently a very powerful deformation being as it is a severe breaking of the order of portrayal. On the other hand the peculiarity of the depiction is that here the action of reconstruction also happens. Here it is also valid that for the sake of breaking the rules, there are rules to break. Here the construction is ensured by the fact that the peak of the pointy beard can be expressed with the Greek word of **Κορυφη** (korufe), as well. This, however, in the LXX may mean the word crown along the top of the head, in the same way as the Greek word of **Στεφανος** (Stephanos). Thus, the angel-faced Saint Stephan's pointy beard breaks the usual order of portrayal; on the other hand it is reconstructed on the level of abstraction by the significant emphasising of the word and name for crown. The word korufe corresponds exactly to the already discussed word "kodkod" (**קדקד**), which equally means the top of the head and the peak of the triangle. As we can see, reading it in a reverse order exactly corresponds with the peculiar and unique Hebrew word of dikduk, which equally means grammar, accuracy and perfection. The scope of its meaning covers Philology, as well. In this way, along with the Greek and Latin words for goatee beard, it is about the ungarus philologist king, named Crown, who is fond of accuracy and order (the system in a general meaning), i.e. it is also in our case about Saint Stephen. Next to him the inscription of **Sephanus** rex corresponds well to the above expounded hidden meaning content, as it is about the hidden king concealing the essential meaning, which is expressed in a plasticized way by the Latin-Hebrew wordplay of Sephanus (Sephania). The "triangular beard" in the given context seems to be a suitable symbol for the cognitive "mediation" or "transformation" between the beardless, angelic face and the natural "amorphous" beard, i.e. between the celestial and earthly sphere. A mirror symmetric representation of St. Stephen (of angelic face) can be seen in the Hortus' Incarnation picture (see Fig. 1 in part II) with an apex crown in a most distinguished and singular position directly behind the apostles on a joint axis with the angel (Yophiel). On the other side with the same apex crown (but entirely covered directly behind the other group of the apostles) St. Lawrance (Lavrentius)

[12] It is worth to note that the dreamfigure „Pointy beard" plays a crucial „similar" role in Pauli's famous dream-series interpreted in Jung's Psychology and Alchemy.

can be found, whose name also has the connotation of wreath or crown. There are 137 days between their feast days. The two "Levites" with angelic faces could be an allusion to the incarnation (137) between the two cherubs and the "triad" crown or the unified three crowns, as well, connected to the Virgin Mother, also composing a 3-4 transformation (see later in detail).

6 Yophiel, the Sephirotic Tree and Stephanus Concealed in Bahir

6.1 The Issue of Name Concealment (First Approach Interpretation)

If we, contrary to Scholem, agree with Neumark's assumption about the Book Bahir being in its hidden way an indeed consciously planned and enciphered opus[13], then we rightfully assume that the author hid his name in a part of pivotal importance of this late artificial Midrash in accordance with the customs of the era. Evidently, it is within the most important and surprising section in the book of Bahir, in a well-known Midrash passage (Beresith Rabbah 3:8) quoted in Bahir, dealing with the creation of the angels, where there unexpectedly appears the inverse tree of God in its well-known archetypal, dynamic and less likely matching to the Judaism picture, identifying it with the 10 attributes of the Gnostic pleroma, which would appear in the form of the 10 angels/cherubs or 10 kings in the later sections of the opus (as in the Admonitions [28]). It is even verified by the coincidence that the numeric values of the Hebrew words angel (Malak **מלאך**) and tree (Ailen **אילן**) are the same. Apparently, into such a text section it is worth incorporating a "message" containing a hidden meaning of quintessential importance, a message unexpected and essentially offensive to the tradition moulded with creative strain. Naturally the semblance of an insignificant completion of the tradition is maintained in the end. It might have been a particularly excellent opportunity for the author amidst the possible numerous passages of the Talmud or Midras, the one in which Rabbi Luliani bar Tabri (**לוליאני בר טבראי**) expounded his opinion on the relationship of creation and angels after Rabbi Chanina (his name corresponds to the Latin Clemens!)[14]. The Hebrew

---

13 „*Neumark's thesis (is) that an author with a theoretical or speculative tendency clothed his ideas, very artificially and conciously, in the form of a midrash, which really did not suit these ideas at all."(Scholem* [20])

14 It is characteristic of the thoughtful editing of the Bahir, with recognising the synchronistic attributes, that following the letter Gimel symbolising the sephirotic Eucharist, the quoted Midrash passage contains the name Chanina, which on one hand denotes clemensy (Clementia), and on the other hand refers to the letter Chet (§34), while it is the abbreviation of the Hebrew

name, Luliani bar Tabri as Scholem and others denote it axiomatically, is equivalent with ***the (Latin-Greek based!) Hebrew form of Julianus the son of Tiberius (Rabbi Julian, der sohn des Tiberius*** [22]) from the Bereshith Rabba.[15] Evidently, the name from the point of view of hidden symbolic interpretation could indicate a probable Roman monarch, as well, belonging to Gens Iulia, who wished to express his ancient doctrines here in a concealed way. The other possibility of this Midrash'part is to relate the name of R. Yochannan to the "angelhood", which in our context could be a hint to the known angelic representation of St John the Baptist with its potential hermeneutic relationship through the proto-martyr St Stephen to King St Stephen, which is one of the main hidden meanings throughout the Book. This important but sophisticated issue will be discussed in another papers (see e.g. [32]).

Another splendid possibility comes from the Hebrew form of Luliani or Lulayni **לוליאני**. The significance of its value of 137 cannot be over-estimated. Its natural anagram is the LVI AILN **אילן לוי**, i.e. it is about a tree of a person of the Levite order within the Iulianus or Lulianus name, which might indicate a depiction of the "world tree" of a probable Levite author in Beresith Rabba. Namely, it came embedded in the text of Rabbi Luliani or Iulianus on the pretext of his name or preferably on the basis of taking into consideration "the synchronistic potential" of this name. As the result of this obviously conscious "planning" just the Levites appears in the text of Bahir superseding the Luliani, which on the basis of "Temurah (anagram) theorem" allows us to interpret the tree of Levi i.e. the tree of the ten sephiroth and the 36 just men (deans). In passage 95 of the Bahir, also considering passage 98, the inverse world tree appears as the ("cosmogonic") Tamaric date palm tree, i.e. as the tree of the zodiac and 36 just (or deans) of the ten sephiroth, who walk the 32 ways of Wisdom. As we can see both the 2x36+2x32 interpretation of passage 95 and the 2x(36+32) interpretation of passage 98, together with the oneness of the union, leads to the number 137. Considering the Latin and Greek "syncretistic" background, the last two letters of Lamed and Nun also "indicate" the 50+30=80 number, as the Latin numbering gives the 80 as the sum total of 50 and 30. The letter of the 80 in Hebrew is the Pe-Fe (**פ**=80), and so replacing Lamed-Nun with it, we can obtain the nameYophiel from the letters. It of course corresponds to the LVI AFI **אפי לוי** phrase as well, which refers to a person of Levite order. On the basis of their attributes present equally in the context and gematria, the words of tree and angel,

expression of the introduced sephirotic Eucharist, the Gimel-Chet letter-pair. Together with the Inverse World Tree and its 12, 36 (32) structure (2x36+2x32+1=137) - in §95 - "*this cosmogony and cosmology, based on language mysticism betray their relationship with astrological ideals. From them, direct paths lead to the magical conception of the creative and miraculous power of letters and words"* (Scholem [20]).

[15] The detail of the Midrash text in Hebrew : **כי השחית כל בשר רבי *לוליאני* בר *שבדין* בשם רבי יצחק אמר** furthermore **רבי *לוליאני* בר *שבראי* בשם "ובשתים יעופף"נבראו מלאכים שנאמר ועוף יעופף על הארץ וכתיב ר'**

the LVI MLAK **מלאך לוי** composition of 137 could also prevail. Namely Yophiel, the archangel of grammar and philology is personified as a Levite or a "high priest" angel of the spatial-temporal world (as in the Eleazar fragments- MLAK KHN (–**מלך כהן**) in the given person belonging to Gens Iulia as "son of Tiberius", symbolically in an Augustian monarch. In addition to Tabri, the feasibility of the interpretation of Taburia (**טבוריה**), which is of course the Hebrew equivalent of the word Tiberias, might verify the hidden meaning of the philologist Levite. 'The son of Tiberias' phrase may likewise refer to the ancient scholars, as to the great philologist, Aron ben Moshe ben Asher of Tiberias, who introduced vowel pointing and who died at the end of the 10th century. In general of course it may allude to a language scholar. Applying the letter "He" from Tiberia the Hebrew word LVIH (**לויה**) could be interpreted, meaning Levite order and crown equally, which is always translated in the LXX as **Στεφανος** (Stephanos). Another version present in Midrash, the bar Tabrin **בר טנרין,** may allude to the son of Tiberinus Alban king, i.e. a person belonging to Gens Iulia, who himself is symbolically an Alban king, who is a living Augustus and his name might mean the crown, i. e. Stephanus. Through the Scythian Dardanian king, the inherency link to the Roman Dardanian house, i.e. the Gens Iulia was a motif of central importance in king Saint Stephen's (with Alba headquarters indeed) genealogical mythology, as is notable in several of our papers [14, 28, 29]. In this way a great philologist, a live Augustus, an Alban king belonging to Gens Iulia, whose name is crown or Stephanus, in whom Yophiel archangel's spirit functions, clearly on the basis of the depiction method of the Casula and the Pala d'Oro, could be nobody else than the great saint king, namely St. Stephan of Hungary. Naturally, the primary name of Iulianus could not have been left in the crafting of the creative deformation, because in this way the genuine quotation, according to its role, would not have conveyed any additional meaning, i.e; such a peculiar information dispatch that might draw our attention to the uncommonly numerous meaning content of the name in the Judaic and synchretistic/multilingual (Greek-Latin) tradition. However, in addition to the world tree, the other concealed creative deformation, the alteration of the name, ensures a perfect possibility for the interpretation of the substituted primary name by the unexpected impact, as well. The Levitas ben Tabrus (**לויטס בן טברוס**) the *substitute name (with a strong creative deformation)* on the one hand signifies the name hidden in Luliani, i.e. the Levite hidden in Luliani or more exactly the tree of the Levite, which grounds the substitute name too; and on the other hand it might allude to the angelic Levite, that is, to the one below Emperor Tiberius, or in other words, to the protomartyr St. Stephen and also to the world tree or the cross growing out from the centre of the world or from the omphalos of God.[16]. As we can see the LVI AILN phrase from the word

[16] The Hebrew anagram of the Levite tree from the name Luliani makes directly feasible such an anagram interpretation of the whole name, which corresponds to the saying gained by the powerful creative deformation of the genuine Midrash text about the tree planted by God. The (V)LVLIANI BR TBRAI (**ולוליאני בר טבראי**) anagram of the primal name is (V)IRA LVI AILN BTB(V)R (**וירא**

Luliani alludes to the tree of the 36 just men of the 10 sephiroth. This tree is called Kol (KL **כל**) in Bahir, as the completeness of the 10 sephiroth. So considering additionally the Hebrew letter of Yud (I=10), this might lead to the phrase ANI LVI KLIL, which could be read as "I am the Levite Stephanus". Evidently, given the name Luliani of the numeric value of 137, replacing the letter Nun of 50 with the word Kol we even "directly" come to the phrase KLIL LVI A' (**לוי כליל א**=137), which exactly corresponds to the well-known Latin medieval phrase of "Stephanus primus diaconus". According to the tradition deriving from Empress Helena, the *Kelil (***כליל***)* here was the Hebrew name of the Protomartyr[17].

In this way from the primal and the creatively deformed name combination, considering also the context of Bahir which here can be read exactly about the inverse world tree and angels, we might draw an unequivocal conclusion regarding the hypothetic author of the opus. All this is verified by the clearly interpretable inverse world tree pictures of the analyzed 137 entities, seen on the Hungarian Holy Crown, on the Coronation Mantle, and also on the incarnation picture of the Hortus as "primordial models", which represent a strong correlation to the sephirotic model of the inverse world tree of the Bahir. The numeric value of the name *Levitas ben Tabrus* yields the number 444, i.e. the value of the letter Daleth (**דלית**=444), indicating the number 4, also appearing in Bahir as the lingual and letter symbol of kingship and its equivalent female crown, the Atara in verse 27. Thus, the name of the Rabbi, which is likewise an allusion to the name Stephan, could be found in Daleth and in Atara, i.e. Stephanus[18].

לוי אילן בטבר). The latter means that the Levite, i. e. the substitute Greek-Latinized Levitas saw or will see the tree growing from the omphalos of God. The Hebrew TBR or TBVR, likewise the Greek omphalos means naval or centre. In the same way the LVITS BN TBRVS = **בן טברוס לויטס**phrase could be rewritten in the form of the anagram of LVITS NS BTBVR**לויטס נס בטבור**. It is well established that the above mentioned IRA LVI AILN BTBVR anagram is derived from the primal name. The two words following the Levitas in the anagram indicate the tree, symbolically the cross growing out from the omphalos or the centre of the world. Notably, it is about the inverse tree, where NS (**נס**) is the Hebrew word for the "tree" of Moses, the pre-figuration of the cross in the Bible, where the prophet lays the pre-figuration of Christ, the bronze snake that conquered death. In its Greek and Latin translation, the "sign" symbolizes jointly the cross that is based on the omphalos of the world (see for example the T maps) and its sign. Therefore, on the basis of Tibur, the Hebrew word for omphalos in both cases refers to the inverse tree growing out from the omphalos of God or from the centre of the world.

17 In verse 23, the KL TLVI BV (**כל תלוי בו**) phrase (everything depends on him only) in addition to the anagram interpretation of LVIT KL, as „crown of wholeness", **(לויט כל)** and TV KLIL (**תו כליל**-the sign of the crown, the sign of Stephanus) might also allude to the phrase of LVITN BV (**לויתן בו**). Thus, this celestial tree seems to outreach Leviathan in this symbolism. Here we considered the phrase. Thus, it is about the world's central tree. The same could be interpreted at the phrase NS BTBVR, where the central Mosaic, the Messianic cross with the snake is the pre-figuration of Christ with the caught Leviathan snake. It is supported by the traditional interpretation, where the Hebrew word for snake has the same numeric value as the word messiah. In both cases, the world tree could be related to the sign of the cross and the catching of the "Leviathan snake".

18 As we have shown elsewhere the Daleth is the symbol of the Tamaric date palm, representing the tree of life, too and the group of David, Christ and Tamar [28]. Considering the presence of the

On the basis of the above "analysis" the possibly most simple 'summary' seems to be the following. The name LVLIANI (**לוליאני**=137) can be interpreted, in addition to its compounds of Levi and the Hebrew word tree, as ANI LVLI (**אני לולי**), i.e. 'Ego Iulius' in Latin, meaning 'I am Julius'. The significance of this interpretation is that it divides the 137 into the composition of 61+71, which corresponds to the double genealogy number of Christ's incarnation, with which we dealt in great detail in the first two parts of our paper. Thus, in this case we may assume that the person in question is a monarch (obviously a Messianic, i.e. Christian, monarch) belonging to Gens Iulia, in whom Christ incarnates mentally and spiritually. On the other hand, the Latin reading of the transformed name of Luliani into the Hebrew Levitas (**לויטס**), as Levitis in addition to the Levites, may mean not only the word Levita, but also the Levita order, as well. This is an axiomatic interpretation, since the name Luliani itself means a Hebrew variation of a Latin name of Greek mediation. In this way, the Hebraic LVITS (**לויטס**) coming from the Latin-Greek can be interpreted in a reverse direction in Latin. Completing the circle of interpretation, however, the Levita order in Hebrew is LVIH (**לויה**), with the Greek translation of **Στεφανος** in the LXX, i.e. of Stephanus in Latin. Thus, the given lingual and religious "synchretistic" circle self-evidently conveys a message about a Julius, or Julianus Levita Stephanus Augustian monarch (i.e. Augustus), in whom the Messiah is being incarnated in the hidden meaning system of the text.This important "identification" will be discussed in section 8 as well.

6.2 On the Names of God Consisting of 72 (137=72+65) Letters

The mystical name of God of 72 (105+32=137) letters[19] of 12 words or "names" (tribes) constituting the High priest's crown is derived from the triple–Tetragrammaton in the Priestly Blessing (Num 6.24-6.26 in Bahir: §107, 111 and 127) by permutation of the four letters[20]. From the Hebrew expression of "H'

names Levi and Chanina in the text the LVI ET'RH ChNVN (**לוי עטרה חנון** = 444), illetve LVITA STFNVS ChNINH (**לויטא סטפנוס חנינה** = 444) phrases, where both the chanun and chanina could correspond to Clemens, Clementia in Latin. In both cases they evince about the name Levita Stephanus Clemens in Latin and his kingship in exactly such pairs like Stephanus and Clemens could be seen next to each other on the Coronation Mantle. The Divina Clementia is the attribute of Augustus dignitary, so the name Chanina (Clementia) can be linked to the name Iulianus ("Augustus") in a natural way from the point of view of the "meaning".

19 The crown of the so called manifested God's name, i.e. the Explicit Name of God, especially of the Divine names consisting of 72 and 42 letters, can be traced back to the Antique mystic Judaist tradition, the formation and history of which G. Scholem elucidated in several of his works [19-21]. The Explicit Name of God in Bahir was dicussed in detail in another of our papers [32].

20 The Explicit God's Name in the Bahir based on the 137 letters and signs (132+5 letters and/or signs) of the words of verses Num 6.23-6.27. These are the direct words of God to specify how Aaron or the actual high priest ("his son") has to bless the people of Israel. These very five

FNIV ALIK" (**ה פניו אליך**) here (Num 6:25) we can clearly obtain (priest-angel) Yophiel Kohen (IVFIAL KHN= **יופיאל-כהן**=137). This derivation of the name of the priest-angel Yophiel (as the "personification" of the number 137) and his partly "hidden" identification with the crown of God's Name is explicitly stated in the Eleazar's fragment where Yophiel is still the Atarah too, i.e. Στεφανος in Greek, and Stephanus in Latin.

Here in the given context, the anagram of the first two and the fifth words are directly related to the name of the opus's author. The anagram of the first word AHTzYTzHRVN (**אהציצהרון**) is evidently the VHTzYTz AHRN (**והציץ אהרן**), i.e. Aaron's tzitz, the pontifical crown, that is –in our context- Levite Stephanus in the broader sense of the Latin translation. The letter sequence of the second word is AKLITHRVN (**אכליתהרון**); its anagram is KTR IVLANH (**כתר יולאנה**) i.e. the "corona (keter) Iuliana", so it is about the crown of the Gens Iulia. In another version the anagram is LVI KTR NAH (**לוי כתר נאה**), so it is about the crown of the beautiful Levite, or about "the crown beautiful Levite", which could again mean the phrase Levite Stephanus (beautiful, with an angelic face). Finally the fifth word, VTzFTzFS'YTRVN (**וצפצפסיתרון**), might lead to the phrase TzFYRVT (or VTzFYRT) TzFNVS' **צפירות צפנוס** the Crown of Sephanus or Crowns of Sephanus in absolute coherency to the allegoric picture of the Admonitions (see Iz 28.5 and the Admonitions). According to another version it is about S'FYRVT TzFNVTz (**ספירות צפנוצ**)[21]. Using the Latinized Grecian interpretations, it might mean the Sephiroth of ***Sephanus***, i.e. Sephanus rex's crown of decimal sephiroth, his kingship of the 10 (the central concept of the Eleazar fragments is the kingship of the 10 or the kingship of the 10s (**מלכות עשיריות**) [4], thus completing in this way the triad of the names of Sephanus rex (Levite), Stephanus and Clemens identified in the portrayal system of the Coronation Mantle as a ternary unity. Actually, the "kingship of the Tens" is a possible translation of "Regnum Ungarorum". The **9**th prophet, Sephania, is the symbol or the "personification" of the letter Teth, the concealed and revealed, or the concealer and declarer, similarly to the letter Teth, which is concealed, which is not revealed in the Ten Commandments, in the Law of the Torah, but in the Bahir's context, it manifests Grace as the receiving womb [27, 32]. From the pair of Tzade (Tzadik) and Pe (Phe) the given Divine name in the 5th God's name or word, which we identified with the crown of **Sephanus,** in the Bahir's context (§61) is clearly the hidden, but

passages are organised by 4 Setumot, **סתומה** (closed portion) and a Petuha, **פתוחה** (open portion – see these paragraph breaks in Leningrad Codex cca 1008) consisting of a unified system (these five signs can be comprehended as five letters, out of which the first four is the letter Samekh, and the last one is a Pe. Thus, this division of five consists of 137 letters).

21 The first and the third name discussed here is essentially the same in all the known versions of the Bahir. (The letter Shin instead of the Samech does not change the interpretation). The letter Lamed in the second name is also definite here (as in Kaplan's and Margalioth's etc versions [2, 16]) because the crown's name (except the letter Teth, similarly to the Decalogue) should contain all (Hebrew) letters and this name is the only possible place for the letter Lamed which does not occur in the other eleven names.

the dominant presence of the Hebrew name Sephania, links closely with the 36 just men[22].

This motif of **Sephanus** and Sephania can be found in and on the Coronation Mantle and the Admonitions. On the Coronation Mantle, only the names Sephania (9^{th}) and Hosea (1^{st}) cannot be observed out of the 16 prophets. The restoration of this strong creative deformation occurs via representing Sephania of the feminine side of the Robe with **Sephanus rex**, visible on the masculine side (see e.g. Corona Sephania – Crown of **Sephanus**). The name of the prophet Hosea can be seen in the inscription of "A STEPHANO", exactly in the blank spot of the inscription, under the figure of the anonymous prophet. The anagram of A Stephano is N(OMEN) HOSEA P(ROPHE)TA, i.e. in this way the king represents Sephania as Sephanus, and prophet Hosea as Stephanus. Thus, one of them is the personification of the revelation (with its "sum" of 1+9=10!), while the other can be viewed as the symbol of similar meaning as the release from captivity. This motif occurs in the Admonitions, as well, where the first caput (passage) is *"Inimicus et ultor*", the Latin expression of Satan from the famous commentary of Sophonias, i.e. Sephania, and in the 10^{th} Caput, where the famous quotation of Hosea, the *"misericordia volo"* can be found. Thus, the two prophets, both on the Robe and in the Admonitions, equally personify mercy and judgement, respectively. Hoseas' name, "God is the Liberation", in hermeneutics alludes to the revelation, in other words, to the liberation of the eternal concealed (and hidden) meaning. Thus, the King also represents the revelation of the Divine mystical knowledge.

The exceptionally specific feature of the letters of the three words in the crown of God's name consisting probably only of 105 (Kaplan) or 104 (Margalioth) letters altogether (considering only 72 letters out of them as "chosen" by the ancient interpretation) evidently suggests the anagrams above. According to the text, the heart (in Hebrew) with its number 32 relates to the 105 letters to ensure (probably) the number archetype of 137 of the God's name crown [32]. This high-priestly

22 As a result of the identification of the letters Yud, Nun and He (this latter is its counterpart, as it is the 9^{th} in reverse order, in the Hebrew Alphabet) with the letter Tzadik in passage 61. The linking word is the AF (**אפ**), i.e. the letter Pe (Fe) in reverse order. In addition, the letter, or the Tzadik is of high importance in the Kabbala. Its other name is Yesod with the numerical value of 80, which is the number of letter Pe-Fe. (This can be verified in the line next to the passage with the mention of the TzVFIM (**צופים**), that is the visionaries, alluding to the issue that in the multilingual cross-correspondence the name Sephanus can mean visionary, as well). Thus, the letter pair in the Divine Name, in addition to the name Sephanus, also signifies the name Sephania, and in this way manifests the letter Teth, or in other words here also the sign of grace. The Hebrew TzFNYH (**צפניה**) itself in this context can be interpreted in a way, that is the first letter is the Tzadik, while the meaning of the other letters are the Lord's face or faces (FNY H'). Since in Greek the Lord's faces, the Prosopa (Προσωπα), is the word for the 36 deans, as well, (see Ameisenova [1]). In this way, the name Sephania also means the redemption of the Lord's 36 deans in the form of the 36 true men. (We can observe King Solomon's close relationship with the 36 deans [31]).

crown of letters was given by the angel (**מסמריה**) Messamariah (almost surely another name for Yophiel) to the "prophet angel" Elijah (in Christian view St John the Baptist) to ascend into the heaven from the top of Mount Carmel according to the Bahir. Archangel Yophiel in its more or less hidden temura (anagram) interpretations could be detected at several significant spots in the text of the Bahir in addition to the ones already mentioned. Here, the Speaker of the crown's name is Rabbi Ahilai. The vowel points of this mystical name is given by three names, and one of these is Yaphoel. Thus "Ahilai-Yaphoel" (**אהילאי יפועל**) allows for the anagram "Hailai-Yophiel" (**העלאי יופיאל**), i.e. the "Majestic Yophiel". Due to the particular "probabilistic distribution" of the letters of the "names", the above anagrams can derive only and exclusively from these "names".

According to the Christian tradition Yophiel is the leader of the 36 deans as a cherub angel. It is the exact way in which we meet him in the Book of Bahir, where he is the leader of the cherubs guarding the 32 ways of the Garden of Eden. In this way he appears (in a hidden way) in passages 92 and 98. Tamar, the date palm tree, appears as the tree of Life, or the World tree, alluding to Gen.3:24, the guarding of the tree of Eden. The Lulav, the 36 just men are the offshoots of Tamar, who walk the path of wisdom, and in our case, in passage 99, the 32 ways of Eden guarded by the cherubs. Considering the Tamaric twins, the germination of the Tamaric offshoots, as we can see, leads to the number 137, alluding to the cherub angel Yophiel. In the next passage Salamon's prayer to the heavens pertains to the lower 7 attributes of the sephirotic system, which are impersonated by the cherub angels here in the given context. It also proves the relationship, already discussed in detail, between Yophiel and King Solomon. The notion of the 36 deans or just men, according to which the 4 chief deans or chief just in the centre of the 32 are the 4 cherubim of Ezekiel's vision, was a generally accepted schema of medieval Judaism demonstrated and analysed by Amaisenova in several medieval pictures [1]. Archangel Yophiel could also be considered as the embodied symbolic figure of the acausal background intelligence discussed in the described scriptures. It seems the authors viewed him in this way quite consciously in the hermeneutic conceptual circle of the given era. Thus, this symbolic depiction is likely to precede the notion of Maimonides, being already considered as "modern", with the angel being interpreted as the Active Intelligence.

6.3 Context, Symbolism and the Meaning System (a Detailed Analysis)

In and on the Bahir, Hortus, the Pala d'oro and the Royal Mirror, King Solomon appears in a quite similar archetypal image before us. On one hand, he is the Lord, the allegoric embodiment of Christ of the Christian perception; on the other hand, he embodies the current eternal Roman monarch, too. On the Pala d'Oro he appears with an angelic face and an angelic arch of triumph as the conciliatory of

archangels Michael and Gabriel, speaking with the quotation of the Proverbs to the "Roman royal son" as the builder of Sophia's house. Here the Roman royal's bride is Irene i.e. the "Peace". It is in this way that the interpretation of him as the king to whom the peace belongs, the "symbol" of the Church, is fulfilled symbolically. Otherwise he advances before us as the monarch of Rome in Byzantine Caesarean attire [14]. Thus, each and every detail of the mythologem of the Book of Bahir is fulfilled. He is partly the Lord, and at the same time the temporal king, whose bride is Peace (or the Church; see in the next section the notion of Knesset Israel-§66). And yet, Sophia, in the sense of the double Sekhinah principle as the text reads, is his mother, his daughter and his sister at the same time, representing the whole Sephirot system. King Solomon on the Holy Crown, as we discussed in detail, appears in Emperor Constantine's image between the archangels Michael and Gabriel, while the Godmother picture related to the two archangels also impersonates Sophia.

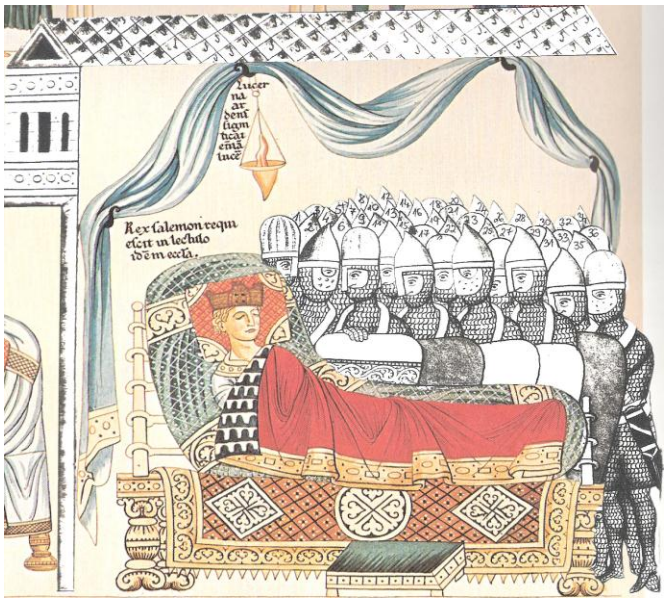

Figure 6

King Solomon's rebirth as Christ in his bed, i.e. in Ecclesia, watched by the 12 zodiacs (representing 12 heads of tribes or the 12 apostles) and the 36 deans (just men) - "*60 mighty men"* [7]

In the Royal Mirror King Solomon is the eternal father and the eternal son, impersonating the Lord, at the same time he is the eternal temporal Roman monarch, as well. As in Caput 6, he steps out before us as the member of Gens Iulia, who liberates Rome [26, 28]. The expression "Libera" alludes to the double mother image of the Eleusinian Mysteries in full agreement with the famous Saint Paul allegory [28]. Naturally the awarded first liberator is Emperor Constantine. He again appears anew as King Solomon in Caput 9, who catches a glimpse of

Cora, i.e. Libera and prays to God to send him Sophia. At the end of the Caput he, the king Solomonic, is to perfect his career with Peace, i.e. Irene. (According to the fatherly imperative) The joint interpretation of the temporal Roman monarch as King Solomon and Emperor Constantine is completed [26, 28].

In the pictures of the Hortus, King Solomon is portrayed on the one hand as Christ, and on the other hand as a Roman monarch, receiving the high priests of the church. Sleeping in his bed, cum pace somniae (requies pacifica veri Salemonis), which is the symbol of the Church, he was reborn, as in Fig. 6. In all four cases, the presence of the 12 chieftains or apostles, or the 36 just men or deans, is dominant in the depiction meanings system of these great works [7]. Returning to the two passages of the Bahir (21-22 and 65), highlighted from the language mystic point of view, the royal Roman name, and the allusion to a hypothetic Roman king called Levite Stephanus concealed in it, alludes to the hidden mystical "identification" of the Roman monarch and the Lord. In passage 65, the expression of intention of Sophia and the Peace (Shalom) to marry King Solomon, with its expressively Latinate semantic modification [20] hypostatizes the identity of the Roman monarch and King Solomon, representing the Lord, found in the hidden meaning system, in an almost complete consonance with the identical or allegoric pictures briefly outlined above. The mentioning of Solomon in passages 64 and 65 in Song of Songs, in the given context, gives an unequivocal allusion to verse 3:11, in which his mother (Sophia) crowns King Solomon on the day of his wedding. The Bahir says: "*Solomon had married (carried) God's name"* and furthermore *"God said to him, since your name is like the name of My Glory I will let you marry my daughter."* (**ושמך כשם כבודי אשיא שלמה נושא שמו-בתי והא נשואה**). The Hebrew one is the Latin semiotic modification of the marry (nassa), and therefore it requires the Latin interpretation of the wedding of Solomon in the given hermeneutical circle.[23] Considering the incest feature of the wedding (the interpretation of mother, daughter and sister as bride) which can also be found in passage 3, naturally we will think of Pope St. Gregory the Great's interpretation of verse 3:11, that it is the Mother of the God (who is also daughter of God and in this way also sister of Christ) who crowns the Son of the God with her womb, while the wedding of Christ and the Ecclesia takes place. Concerning the wedding, the continuation of the text of Bahir reveals that Shekina (as the "daughter of God") is the Knesseth Israel, fitting precisely to the notion of the Church in the given proto-Kabbalistic interpretation. The comparison to passage 3 about King Solomon's wedding of incest feature shows that it is given in the correct form (**מלך שהשיא את בתו לבנו**), fitting to the Hebrew grammar, and in this way it confirms the conscious application of the Latin semantic

[23] *"This is a play on words. At first it is said that "Solomon bore (nassa') the name of God". The Hebrew word for marry is the hiph'il form of the same root. The pun is not, however, based upon an authentic usage of the expression "nassa 'ath ha –shem", which in reality means pronounced the name. The semantic modification suggests the influence of a Romance language (Scholem 1987, footnote 189* [20]*)".*

modification in passage 65. Thus, it proves the fact of concealing the meaning in the mystic pun and in the application of the applied lingual deformation. The Latin interpretation of Solomon in the hidden layer of the meaning system naturally alludes to the Roman monarch supervising the Church of the Holy Roman Empire, whose prototype is naturally Emperor Constantine the Great. As we have mentioned, the same double Solomon-Roman interpretation we can precisely see on the Holy Crown and the Pala d'Oro, as well as in the interpretation of the Hortus. In the case of the latter with the difference of King Solomon's rebirth in the womb of the Virgin as Christ of the Church, alluding to the interpretation of Pope St. Gregory the Great, as well.

6.4 Symbolism and the Meaning System of the 3-4 Transfomation

6.4.1 General Description

In Bahir, the "Divine (sephirotic) inverse tree" passage and the hypostatized concealed name by conscious and unequivocal editing is to be found between the mystic sephirotic interpretation of the third and fourth Hebrew letters, the Gimel and Daleth. Beyond the importance of these two letters, the location of the idea of God's sephirotic World Tree and the name of the author between the numbers three and four show the well-known mystic (viewed as "objective") ambivalence as a conscious composition of variation feature. The ambivalence symbolises the objective archetypal transformation, where, as we shall see, the "sephirotic transformation" is the theurgical task of the divine king (or Messianic king). To execute the analysis, we will need to quote the relevant passage of the Bahir, where the translation was made by modifying Kaplan's text [2] and taking into account Scholem's German translation [22]:

19. ***Why is Gimel third? It has three parts, teaching us that it bestows (gomel) kindness. But did Rabbi Akiba not say that Gimel has three parts because it bestows, grows, and sustains. It is thus written (Genesis 21:8), "The lad grew and was bestowed." He said: He says the same as I do. He grew (augmented) and bestowed kindness by his guest (or dweller) to his people and the faith was with him (guest)[24]. 20. And why is there a tail at the bottom of the Gimel? He said: The Gimel has a head on top, and is like a channel. Just like a channel, the Gimel draws from above through its head, and disperses through its tail. This is the Gimel. 21***. *Rabbi Yochanan said: The angels were created on the*

[24] We would translate the person living there as guest or newcomer in the given context, not at all as a neighbour. Scholem does the same, as well. *"Er antwortete : das ist auf meine Erklarung, denn er wurde gross und erwies (nun selbst) Liebe und man wohnte bei ihm…"*) Scholem writes about it: *"Der nächste Satz ist höchst unklar",* furthermore *„Das Kind war gross und ihm Gutes getan "* (See the correlation between Clementia and bonum in the Royal Mirror).

second day. It is therefore written (Psalm 104:3), "He rafters His upper chambers with water [He makes the clouds His chariot, He walks on the wings of the wind]." It is then written (Psalm 104:4), "He makes the winds His angels, His ministers from flaming fire." [Rabbi Chaninah said: The angels were created on the fifth day, as it is written (Genesis 1:20), …"With two wings did they fly."] Rabbi Levitas (Levatas) ben Tavrus (instead of Luliani bar Tabri!) said: All agree, even Rabbi Yochanan, that the water already existed [on the first day]. But it was on the second day that "He raftered His upper chambers with water." [At that time He also created] the one who "makes the clouds his chariot," and the one who" walks on the wings of the wind." But His messengers were not created until the fifth day. ***22****. All agree that none were created on the first day. It should therefore not be said that Michael drew out the heaven at the south, and Gabriel drew it out at the north, while God arranged things in the middle. It is thus written (Is44,24)"I am God, I make all, I stretch out the heavens alone, the earth is spread out before Me. [Even though we read the verse "from Me" (May-iti), it can also be read] Mi iti –"Who was with Me?* ***I am the One who planted this tree in order that all the world should delight in it. And in it, I spread All. I called it All because all depend on it, all emanate from it, and all need it. To it they look, for it they wait, and from it, souls fly in joy. Alone was I when I made it. Let no angel rise above it and say, "I was before you." I was also alone when I spread out My earth, in which I planted and rooted this tree. I made them rejoice together, and I rejoiced in them. "Who was with Me?" To whom have I revealed this mystery?***

We shell quote, skipping the following short two passages explaining the above mentioned point, the Kabbalist interpretation of the letter Daleth and the previous important passages of Bahir:

25.*Rabbi Berachiah said: What is the meaning of the verse (Genesis 1:3), and God said, 'Let there be light,' and there was light"? Why does the verse not say,"And it was so"? What is this like? A king had a beautiful object. He put it away until he had a place for it, and then he put it there. It is therefore written, "Let there be light, and there was light." This indicates that it already (***כבר***) existed.* ***26.*** *Rabbi Amorai said: What is the meaning of the verse (Exodus 15:3). "God is a man (Ish AIS* ***איש****) of war"? Mar Rachumai bar Kibi (* ***מר רחומאי בר כיבי***[25]*) said to him: Great master, do not ask about something that is so simple. Listen to me and I will advise you. He said to him: What is this like? A king had a number of beautiful dwellings, and he gave each one a name. One was better than the other. He said: "I will give my son this dwelling whose name is Alef. This one whose name is Yud is also good, as is this one whose name is Shin." What did he do then? He gathered all three together, and out of them a single name and a single house. He said: How long will you continue to conceal your meaning? The*

[25] Perhaps it hides the following anagram: **רבי אורחים כברים** i.e. the master (tutor) of the guest Kabars..

other replied: My son, Alef is the head. Yud is second to it. Shin includes all the world. Why does Shin include all the world? Because with it one writes an answer. (T'shuvah). ***27.*** *The students asked him: What is the letter* **Daleth***? He replied: What is this like? Ten kings were in a certain place. All of them were wealthy, but one was not quite as wealthy as the others. Even though he is still very wealthy, he is poor (Dal) in relation to the others.* ***28.*** *They said to him: What is the letter Heh? He grew angry and said: Did I not teach you not to ask about a later thing and then about an earlier thing? They said: But Heh comes after [Daleth]. He replied: The order should be Gimel Heh. Why is it Gimel Daleth? Because it must be Dalet Heh. He said to them: Gimel is in the place of Daleth, on its head it is in the place of Heh. Daleth with its tail is in place of the Heh.*

The 25 § deals with the famous creation of constriction (which appears here for the first time, counting out the allusion located in the first line of the book), with one of the most important ideas of the opus. According to Scholem, this first step of the creation is related to the mystical etymology of the Hebrew word of the light AVR (**אור**). In this case, the ancient light is contained in the primordial "ether" whose name in Hebrew is AVIR (**אויר**). Thus, this ether contains the ancient light (**אור**) together with the letter Yud (**י**) as a sign of the denary sephirot through a formless primordial point characterizing the state before the Creation (consequently the manifestation of the light means at the same time the manifestation of the Ten Sephirot as well in the act of the Creation)[26]. The AVIR naturally means the "air" and plays a crucial role in the proto-Kaballistic bread-Eucharist too in §184 (see f32]).

Figure 7
The transformation of the letter Gimel (=3), into Dalet (=4) and He (=5=4+1 as a quincunx) according to Kaplan [2]

Concerning the 26 and 27 §, it is obvious from the context, that it is about the third and tenth Sephirah of the Sephirotic system, since the number four is the letter Daleth (in passage 27), and the tenth Sephirah is the kingdom, the crown

26 *"… durch eine Etymologie gewann man die sprachmystische Unterlage für diese Ansicht:* **אויר** *(Aether) enthalt das Wort* **אור** *in dem sich also das mystische Jod (*י*), der gestaltlose Urpunkt, aus dem Aether Gottes löste, entstand aktuell das Licht."* (Scholem [22]) *„A close look at §.25 in the Bahir will also reveal a clear allusion to the (self-constriction) Tzim-tzum* (of the Creation myth*). Rabbi Berachiah says that the Light was like a „beautiful object" for which the King had no place. It is explicitly stated that this light had existed earlier, but that there was no place in which to put it. Only after a „place" was provided could the light be revealed."* (Kaplan [2])

(Atara=Stefanos) or the queen (or the princess, as the bride) who "invites" all the Sephiroth. The letter Gimel, as is stated in the next passage, is the third sephira, which substitutes the letter He standing on the third place of the ten Sephirot consisting of God's name (YHVH). The second letter, He, is substituted by the letter Daleth in passage 28 (see Fig. 7). The sum of the HGIML HDLIT (the Gimel the Daleth **הגימל הדלית = ת** or X +137) gives the symbol of redemption (Tav, Thau) and the number 137, while Thau can allude to the value of 137 of the Hebrew word for crucifixion (**צליבה**=137). The third letter of the Tetragram (YHVH), the Vav, is the symbol of the inner 6 sephirot as is well-known. Prior to the Gimel discussed in passages 18 and 20, it is said that the letter Beth derives from the Alef and unity. From a certain point of view. the rendering of the ten Sephiroth Alef-Beth, Gimel, Vav, Dalet represents the ten Sephirot with four entities in the same way as it is done with God's name (we have seen that the entire name conceals in itself the first Sephirah, the letter Alef, which is here the function of the letter Beth). So the placing between the numbers three and four, or the number-archetypal transformation of the letters 3-4, shows the union of the whole Sephirotic system in a quaternal Hieros Gamos, or if we want, in a Jungian marriage quaternio [11]. It is naturally in complete consonance with the Mary Prophetissa axiom of Jung frequently quoted and in each of his works, namely that from one there will be two, from two there will be three and from three there will be the fourth as a unit. It also corresponds to quincunx geometrically. In our case the marriage quaternion consists of the letter Beth, the letter Gimel, the letter Vav and the letter Daleth. From a different point of view, the trio of the first three letters together with the fourth concealing the inner 6 Sephiroth along with the inverse tree between the third and fourth, fits exactly to the Assumption of the Holy Virgin, or the symbolic picture of the crowning of the Trinity, in precisely the same way as interpreted by Jung [10, 11]. It is made unequivocal later in passages 29 and 30 by the interpretation of the letter Vav.

Jung recognises ingeniously the function of the Tifereth, as the Son and the Holy Spirit together, symbolising the inner 6 Sephiroth in the centre, which is identified with the Arikh Anpin in the marriage quaternion by the later Kabbalah [21]. The Tifereth here symbolises not only the union of Sophia and the Lord with the function of Christ and the Holy Spririt, or the wedding of the Lamb and the Heavenly Jerusalem, but within the latter Hierosgammos it verifies the temporal aspect in addition to the pleromatic one, in so far as the wedding of Christ and the Church, or the wedding of the kingdom by the Holy Spirit, incarnates the new king in its church, or kingdom. The given passages of Bahir are meant to express it precisely. The Daleth with the number of 444 and the special name of Levitas ben Tavrus (as the creative deformation of Luliani of 137), with the provision of number 444, symbolises the new king to be born in its church and kingdom. All is ensured by the unity of the "trifold quaternion" (444 in the denary system): the Daleth, "in which" the "Roman king" is Christ incarnated (of course David and

Solomon, as well, as we can see in the contemporary crowning ordos[27]). Here it reads about the inverse tree of Levitas ben Tavrus, its root is the letter Gimel, followed by the seventh attribute of the tree, as the 10th Sephirah). In Daleth as the incarnation of the six inner Sephirot the king himself gets crowned in his kingdom. (2x444!, the number of the name of Jesus in Greek.)

So in this way, passages 19 and 20, which deal with the letter Gimel and mystic interpretation of the number 3, introduce the theory of the inverse tree, together with the aforementioned hidden name of its author. The number archetypes and the number systems are very important here, as well, as the particularly honoured mediator-mediumship (see Scholem) of the letter Gimel in passage 19 is connected to the number pair of 3-8, which is here the symbol of Sephirotic "Eucharist", as the abbreviation of Gomel or Gmiluth Chessed (**גמילות חסד** =561!). This expression is equivalent to the Thanksgiving, as it is reflected in the Latin action gratiarum, as well, which is the Latin translation for the Eucharist in the New Testament. The author binds this Gimel-Chet (**3=ג 8=ח**) letter pair, i.e. the Thanksgiving of Gomel-Chessed, to the Abrahamic supper organised on the occasion of Isaac's separation. In passage 135 of Bahir it can be considered as the establishment of Abraham at the oak wood of Mamre, for the "Holy Trinity" of the Christian interpretation. A mutual basis and ancient image can be found for the Abrahamic and Dominical (Sephirotic) Eucharist, or for the Last Supper. Assuredly, it is not a coincidence that in "Sermon on Law and Grace" by Ilarion in Kiev (approximately 1040), which was definitely written on the inspiration of the Royal Mirror by Saint Stephanus, the renowned Abrahamic supper (on the occasion of Isaac's separation) is the symbol of the Eucharist, the Last Supper. Thus, the 3-8 couple of letters introduces "forcibly" the (only probably) 3-8 verse of the Beresit Rabba, containing the name of Luliani bar Tabri of the value of 561 (**לוליאני בר טבריא**=561), which is substituted here by the name of Levitas ben Tavrus of the value of 444. Additionally to the 3-8 couples' (leastways synchronistic) isomorphism, as we have seen, the numeric value of the name of Luliani is 137, in close connection to the number 444. Seeing it from this point of view, the choosing of the name Levitas ben Tavrus is not arbitrary, as the value of the Hebrew name of primordial Latin-Greek nature is 561, which has a Roman value of DLXI. If we have them correspond to the Hebrew letters, taking into consideration, that the X is the old Hebrew letter Tav, we obtain the Hebrew expressions DLTI or DLIT (**דלית**). Having the value of 444, this alludes to the denary Sephirotic system, and to the letter Daleth. We can perceive the formation of the number and letter isomorphism of quasi-poetic nature as a variation artefact being seemingly fairly modern. In passage 19, the poetic expression "GVDL VGVML ChS'D" (**גודל וגומל חסד**) exerted for the letter Gimel unfolds the enhancing and distributing of the grace, obviously for the people of the author of

[27] see e.g. Gerics J., and Ladányi E.: "The Idea of King-St Stephen of Hungary- Europe", Levéltári Szemle, 54, No. 2, 2004, pp. 3-14, Budapest

the Bahir by the "guest dynasty". On one hand, as we have seen, it is the ancient image of the Eucharist, since the Gimel, as the third Sephirah, is no other than Sophia and the "Intelligence" (Binah) as Mother. In this way this Eucharist takes place in his temple by the Abrahamic establishment, which is natural as well, as He (Abraham) is the next, i.e. the fourth, the impersonator of the Chesed's sephira in Bahir. Consequently, the guests, i.e. the dynastic guests (the Gens Iulia), ensure the enhancement of the grace at the kingdom. It is expressed in exactly this way in the chapter about the "Guests" in the Royal Mirror. We can see, related to the letter Gimel, that the guests, the newcomers, mediate the Eucharist and the good given by God for their people. We noted that this is about the noteworthy/honoured role of the dynasties (Gens Iulia and the House of David) assumed in the hidden meaning system in the Messianic Rome [26, 28]. The noteworthy word in the Hebrew text, in addition to the producing of Gimel-Gomel, is the Gadol (Godal!), i.e. the *augmentation*. It appears accurately like this in relation to the dignity of the Church and the role of the king in the Royal Mirror, as well. "Ac per hoc fili mi florente studio debes invigilare in sancta ecclessia de die in diem ut potius *augmentum* capiat." "Unde quidem in primis reges *augusti* dicebantur quia *augebant* ecclessiam." The same can be read in the chapter about the guests (De detentione et nutrimento hospitum), where the guests adorn the kingdom. If he destroys what the father king established and dissipates what he collected (the collected guests), it will cause maximum damage to the kingdom, *"quod ne fiat tuum qottidie* ***auge*** *regnum ut tua* ***corona*** *ab hominibus habeatur* ***augusta****".*

6.4.2 An Application: On the King (3) and His People (4)

In the so-called text of the 3-4 transformation section of the Bahir, however, we may assume the "presence" of not only the name of the supposed royal author, but as well of the people of the king's new Rome – hidden as a consequence of our hypothesis. It is made possible by the following particular coherencies and creative deformations. In passage **25** of decisive significance, depicting the creation, Rabbi Berekah (BRKIH - **ברכיה**) speaks. In the next passage hypothesising God's becoming human, Rabbi Amorai (AMVRAI - **אמוראי**) talks. As we have seen, passage 25 is about the ancient light, which can be found in the ancient ether of Avir (AVIR - **אויר**) with the concealment of the letter Yud (**י**), i.e. the 10 Sephiroth, which emanates out of this amorphous ancient spot together with the manifestation of the light as the act of creation. It is said about the Hebrew word for light, the AVR (**אור**), that it has already been created, where the passage ends with the word "already" KBR (**כבר**). For the mystic interpreter, the former AVR can be pronounced as AVaR, while the KBR can also be pronounced as KaBaR or KaVaR. If we have a look at the two adjacent names, we can see that the first one can be written in the form of HKBRI (**הכברי**), and the second one as AVARIM (**אוארים**). The first name according to our hypothesis can be pronounced as HaKaBaRI, and the second name as Avarim. As we can see, it can be a mystic

etymological hypothesis, or word game (pun), that from the ancient light the genesis, which can mean the first and second genesis, can be analogous with the allegoric picture of a "third genesis", or namely, with the foundation of the new Rome and new Christian Israel of the united peoples of the Avars and Kabars[28]. In this case, the act of creation obviously means that the "ancient existence", quasi ancient substratum (ancient ether) of the given peoples is the "AVIR KBR" (**אויר כבר**), i.e. "which has already been" in existence. Thus, these peoples had already been living together in an amorphous denary system, signified by the number of the letter Yud and its amorphous ancient point. Additionally, this "AVIR KBR" can be written by contracting the letters Alef (**א**) and Vav (**ו**) into Zain (**ז**) as BR I' KZR (**בר י כזר**); i.e. it is about the "Antique" Khazars' son or sons, consisting of ten tribes (in fact). The "genesis" of constriction ("exile") can be identified here with the emergence of the Avars and Kabars and the new decimal ("created") kingship resulting from the constriction. To make the hypothesis "highly" possible, let us have a look how Rabbi Mar Rachumai bar Kibi (**מר רחומאי בר כיבי**) explains the Ex.15:3 to Rabbi Amorai in passage 25. According to Scholem the "expression" of the name yielded by a powerful creative deformation, is unsurpassed and unprecedented[29]. But the anagram it may yield is meaningful. The Hebrew name may yield this anagram: ChBR I' AVRIM KBRIM (**חבר י**[30] **אורים כברים**). Thus, the previous Hebrew expression means the decimal alliance of the Avars and Kabars for the mystic interpreter. In the line following Mar Rachumai bar Kibi, we likewise meet a very special Aramaic sentence that all we have to understand is a "simple thing" hiding within itself the name "MLK LVLIANI "(**מלך לוליאני**)[31]; in other words returning to the hidden name of Luliani in passage 21, the solution is none other than a Rex Iulianus, whose new Rome seems to consists of the decimal league or alliance of the Avars and Kabars. Like Iulianus, the Roman king of passage 21 draws the Latin and the Greek into unity with the ("Western") Dardanian dynasty, so here the Kabars correspond to the Greek and the Avars to the Latin, while the Scythian ("Eastern") Dardanian dynasty mediates between them, or ensures their unity [14, 26, 28]. As we have presented earlier in detail, the monarch of Gens Iulia (Dardania) evolves symbiosis with Solomon, i.e. with the kingdom of David's House. In this way on the basis of the imperatives of John's Apocalypse only the representation of the

---

28 It entirely corresponds to the X. century "name-representations" of the 7 Magyar and 3 Kabar tribes of the "Denary Hungarians" as ***Avari*** *("Magyars")* in Latin (see e.g. in Fulda Almanac: (894): »Avari, qui dicuntur ungari«) and Kabars in Greek (see Const. Porphyr. : ***Καβαροι***).

29 "*The book is identified as it were as a Merkabah text, yet its two principal speakers (Rabbi Amorai and Rachumai) are teachers whose names are obviously fictitious"(Scholem [20]).*

30 The "Chabar" (**חבר**) can be translated as the "federation" of the House of Judah and Joseph in Ezekiel 37,16/17 which is cited in Bahir's 109§!!

31 After the Aram "simple thing" (**מילתא דפשיטא**) the anagram of "LK SME LI VAMLKINK" (**לך שמע לי ואמלכינך**) is "KSMLK EMK LVLIANI" (**כשמלך עמך לוליאני**), i.e. **"it is simple one: when the king of your people is Julianus"**). An anagram (**דלית אם פשיטא**) of the „simple thing" hints at the Dalet (27. §) and means**:"It is obviously the Kingdom of the Mother**". ("*Daleth,…usually said to represent Malkuth-Kingship"* – Kaplan [2])

lost ten tribes is needed for the completeness of the united new Messianic Rome-Israel (where the unity of the House of David, Joseph and Levi is isomorphic to the above two "trinities"). It can be found at the end of passage 26, where AYS signifies the three sons, the three houses or the three crowns [32], of which the first is the Alef (Avar), the second is the Yud (Iulianus), and the third is the letter Sin (Kabar), which according to the text includes the world in itself. In Hebrew SIN KLVL KL HEVLM (**שין כלול כל העולם**). The anagram of the text is KLVL HKLIL SMEVN (**כלול הכליל שמעון**), i.e. it includes in itself Symeon's crown, as well, about which it is said that they are to convert or to gain absolution. This latter one here, the (other Messianic) house of Joseph[32] symbolized by Symeon, may mean the conversion of the ten lost tribes into the Christian faith[33]. The hypothesis of this previous anagram is also definitely reinforced by the quite special, inappropriate text of a creatively deformed nature of passage 195. To the question about the guiltiness of the just men and their punishment (which is related to the reincarnation) even Rabbi Symeon gives the answer that nobody is to be punished for their sin committed below the age of 20. That is not the point is the answer in return. The Hebrew text of this statement occurring in Talmud and in other old scriptures of Judaism, as well, can be interpreted in the Bahir that Rabbi Symeon claims he is not amongst the convicted at the celestial court (in the Tribunal on high, but amongst the tens' sons (MBN ESIRIM – **מבן עשירים**), the praiseworthy is **Symeon** himself (by anagram formation). Here we utilised that the word 20 (twenty, i.e. the mystical letter Kaph **כ**=20) can be translated for the mystic interpreter as the plural of ten. This has likewise happened in passage 164, where we can read about the houses, the "ten weak ones" [2]. Its Hebrew spelling is identical to the previous word also meaning 20, i.e. ESIRIM (**עשרים**). This peculiar Hebrew text continued as ESIRIM (**עשירים**), and from here we obtain the HLL HSMEVN (**הלל השמעון**) expression, i.e. the praised up, who is **Symeon** (from the sons of the tens).

In this way the coherency with passage 26 is very tight, since once more Rabbi Symeon claims that obviously Symeon is not amongst the convicted at the celestial court, but on account of his return and conversion to Christian faith, from

[32] In the Schechter text of 10th century according to the prevailing "myth" the Judaized Khazaria might have originated from Symeon's tribe. So he is the representative of the 10 lost tribes (see in the Schechter text, Golb, N., Pritsak, O.: Khazarian Hebrew Documents of the Tenth Century. Ithaca and London 1983). See a similar symbolic interpretation for the distinguished representation of Apostle Sym(e)on in Pala d'oro [14].

[33] This tradition among the old Hungarians (or Kabars) is strongly confirmed by the chronicles from the second half of the 10th century: *"Ungaros dentique notum est huie famae assentari velle, qui et iactant, se a ludeis originem ducere."* (Hariger: Gesta episcoporum Tungrensium et Leodensium). On the basis of the discussed hermeneutical context and the similar parts of the Royal Mirror the Gnostic or proto-Kabbalistic cult of the denary divine attributes in the court of St Stephen's father is supported by the chronicles *"Hic Deo omnipotenti variisque deorum inlusionibus impolans, cum ab antistite suo ob hoc accusaretur, divitem se et ad haec facienda satis potentem affirmavit"* (Thietmar:Chronicon. VIII. 3)

the sons of the tens, Symeon is the one who is praised (by the heavens). The whole presented train of thought displays an extraordinary match with the appropriate text sections of the Royal Mirror (mostly the 6th and 8th Caput), and with the peculiar depiction system of the Pala d'Oro. Levita Stephanus Iulian king builds his new Rome on the alliance of the Greek and Latin, on the new decimal alliance of Kabars and Avars. His dynasty, in turn, along with the western and eastern Dardanian dynasties of divine origin, unites the Messianic houses of David's son, Joseph's son and Levi's son, thus ensuring the especially rich and seemingly whole genealogical myth for his royal house reigning in the new Rome and the new Messianic Israel [14, 26, 28].

On the basis of footnote 31, we may summarize the "true meaning" of the dialogue: "Rabbi of the Avars" said: What is the meaning of the verse (Exodus 15:3). "The Lord is a man (AIS **איש**) of war"? "Rabbi of the league of the Avars and Kabars" (or "Rabbi of the Kabars, the guests" – **רבי אורחים כברים**) said to him: Great master, do not ask about something that is so simple when the king of your people is Julianus (gens Dardania). The answer is in the one Son, the unified Royal houses and the unified crowns according to the "meaning" of the above three letters. The term of "unified crown", in Hebrew Atarah Echod (**עטרה אחד**), can be translated into Greek and Latin as Stephanus primus (rex Ungarorum) closing the hidden meaning-system of the section for the 3-4 transformation with the union of the "Ten Kings" (as "regnum Ungarorum" i.e. the Latin form for the "Ten tribes" in old Turkish) in the 27.§. (see [14, 30, 32])

7 The 3-4 Transformation in the Royal Mirror and in the Bahir (Comparative Analyses)

We have shown so far the central importance of the 3-4 transformation along with the number 137 in close correlation with the Sephirotic inverse World tree. We have presented that the letter-or word-mystic Sephirotic representations are isomorphic to the representations of the inverse World tree "model". A particular dymanic theurgic system was identified behind them. The number 137, as we could see in Bahir, is related to the name LVLIANI (**לוליאני**=137), i.e. to Julianus, keeping in the background, but having a cardinal importance. The name can be interpreted, in addition to its compounds of Levi and the Hebrew word tree, as ANI LVLI (**אני לולי**), i.e. "Ego Iulius" in Latin, meaning I am Julius. The significance of this interpretation is that it divides the 137 into the composition of 61+71, which corresponds to the double genealogy number of Christ's incarnation, with which we dealt in great detail in the first two parts of our paper. Thus, in this case we may assume that the person in question is a monarch belonging to Gens Iula and obviously a Messianic, i.e. Christian, monarch, in whom Christ incarnates mentally and spiritually. As we could see, the number

three, the letter Gimel represents the Holy Trinity, the Eucharist, while the number of the Hebrew phrase of the Eucharist is the same as the numerical value of the rabbi's name, called Iulianus; in other words he represents the letter Gimel, or the trinity in the given context. His name's transformation leads to the number 4, the letter Dalet, while the LVLIANI, i.e. the name Julianuus, becomes Levi, or Levitas, the "name" Levites. This, in the given context, bears that hidden meaning that it is about a rex Saccerdos. In addition to the number 137, which is the symbolic number through the Hebrew word of wheel, Ophen (137=**אופן**), and of the word Atara, crown; translating the Atara into Greek leads us to the name Stephanos. On the other hand, as we have discussed, the Latin reading of the Hebrew Levitas, and taking Levitis in addition to the Levites, can mean not only the word Levita, but the Levita order, as well. This (as we have discussed earlier) is an axiomatic interpretation, since the name Luliani itself means a Hebrew variation of a Latin name of Greek mediation. In this way the Hebraic LVITS (**לויטס**) coming from the Latin-Greek can be interpreted in a reverse direction in Latin. Completing the circle of interpretation, meanwhile, the Levita order in Hebrew is LVIH (**לויה**), with the Greek translation of **Στεφανος** in the LXX, i.e. of Stephanus in Latin. Thus, the given lingual and religious "synchretistic" circle self-evidently conveys a message, about a Julius, or about a Julianus Levita Stephanus Augustian monarch, in whom the Messiah is incarnated in the hidden meaning system of the text. The 3-4 transformation is naturally the symbol of the incarnation of the 10 Sephirot, which is in accordance with the crowning of Maria, i.e. with the renowned 3+1, or the 3-4 transformation symbolism, signifying the divine incarnation.

The same can be observed in the Constantine picture (on the Holy Crown), analysed in the first part of this paper. He (as king Solomon and archangel Yophiel), as we could see – according to their particular way of portrayal – forms a trinity with the Archangels Michael and Gabriel, since the two archangels belong to the God Mother according to the traditional depiction; thus mirror-symmetrically the 3+1, or the 1+3 structure, suggests a 3-4 transformation, as well. The number of 61 ornamental elements of the two archangels Efod-rim, together with the emperor's similar number of 76 decorating entities, can be in this way interpreted as the name LVLIANI (ANI IVLI), i.e. as the eternal Julianus, who frees the church and maintains and supervises the free church, the Libera, and who is at the same time a Davidic and Salamonian reigning high priest, symbolically an eternal king belonging to the Levita order (filius regis et semper rex). Our previous hypothesis is assured by the symbolism of 137 and, in addition to the heart, the fact that in the much analysed order of the white pearl depiction, the 137th, the only wholly singular element on the elbow of the emperor, can be seen constructed into a spiral pattern (see Fig. 7 in part I). The word for helix or spiral in Hebrew is LVLINI (**לולינ**), with the numerical value of 136, and it differs only in the Hebrew letter of Alef (A=**א**), with the numerical value of 1, from the name LVLIANI (**לוליאנ**). In this way, in this unique portrayal system the white pearl of the tangential spiral signifies the number 137, twice as much, and thus

signifies twice the 76+71 composition, and does so with the name LVLIANI, i.e. with the name Julianus, in almost complete accordance with the meaning system in Bahir, summarized above[34].

Since in the Royal Mirror David and King Solomon are rex Augustus, who is attributed to the Corona Augusta and are symbolically members of Aeneades, i.e. the Gens Iulia, the question arises, are we able to catch the 3-4 transformation with the number 137 in the text of the Royal Mirror? We can see that the interpretability of Caput 6 makes it possible to interpret[35] the Hebrew IVLH HLVI LVIH (**יולה הלוי לויה**) temura, i.e. an anagram consisting of identical letters, which may equally mean the Gens Iulia, being a Levita and the name Stephanus, ensuring in this way the presence of the name of Iulius Levita Stephanus in the meaning background of the text, which is reinforced by the Corona Augusta, i.e. in Grecian-Latin the Augustus Stephanus[36].

In our other paper [26, 28], we analysed in detail in the Royal Mirror the numeric system of the Capitulatio, its system of 36 and 32, and its allusion of 137; or from the number 284 of the 10 chapter titles, through the word of Atara (**עטרה**=284), we came to a conclusion of the name Stephanus and the crown, in a close correlation

---

34 On the Holy Crown, if we have a look at the pictures of Emperor Constantine and king Geobitzas, considering them to belong together, we could see the powerful similarity of the pair of Kings Solomon and David of the Pala d'Oro. Thus, on the Holy Crown, and on the Pala d'Oro King David fits to the king's picture; i.e. on the Holy Crown, the king's picture signifies the Davidic fatherhood, as Constantine signifies the Solomonian "princedom" as the son of King. It is reinforced by our observation that the 14 letters of the inscription at the right of the Geobitzas enamel can be divided into a group of 6 (2x3) and two groups of 4, representing in this way the Hebrew name of David (4+6+4 = **דוד**). We have already discussed in detail the "representations" of the emperor's picture by Salamon and Yophiel. Interestingly, the pattern of the heart of 36 and the Labarum of 10 makes it possible to interpret the Hebrew word LVIT by transcribing the tau into tav, with the translation of Stephanos in the LXX. Thus, the theoretic generator of the Crown represents the relationship between the father of Saint Stephen and his son with the pair of David and Solomon. It exactly corresponds to the allegories of the legend about Saint Stephan (and of his Royal Mirror [28]), where his father appears as David and in his dream the angelic messenger of the birth of his son (as we have already demonstrated) is most probably Yophiel. In this way, Saint Stephan corresponds to the church builder King Solomon, while in his mother's dream the messenger of his birth is Levita Stephanus.

35 The name of St Stephen's maternal grandfather was Rex Iulus and his residence's name was Alba Iulia!

36 In this chapter of the Royal Mirror (on guests and newcomers) the word of the newcomers *("in adventitiis"*) raises the hypothesis of the allusion to the Hebrew word "HGRIM" which can be read, as "the newcomers" ("advena" in Latin), who are mentioned in the Torah together with the Levites. As has been well-known for a long time, in the Middle Ages, one of the Hebrew names of Hungaria was Hagar, most probably on the basis of (the people from Bible) Hagarim's (**הגרים**) Aramaic translation of Hungri (**הונדראי**), i.e. Hungaria (**הונגריא**) if we want (Samuel Kohn: Hebrew sources to hystory of Hungary-1881). In this way the Levite order, the Levite woman, as on the basis of the interpretative of Maria and the Hebrew name of the country together with the allusion to the Gens Iulia, seems that the author coded Levita Iulianus Stephanus with concise language mystic resources as "rex Hungariae" (or "rex Ungarorum"), Augustus of the kingdom of Maria (regnum Mariae).

with the 10 Sephiroth. The **42** words themselves are a symbol of the lineage, i.e. of the incarnation from Abraham to Christ by Saint Matthew. The distinctive system of the letters D and C in the Royal Mirror, however, proposes the presence of **3-4** transformation interpretation of Latin letters of the 3-4 transformation, since the initials of the first three words of the Royal Mirror *("Cvm Cvncta Dei")* compose the CCD letter-triad (C[3 is 1=A], C[3 is 2=B], D[3=C is D=4] i.e. ABC[3]-D[4] - see footnote 37). All these may mean that the third letter of the Latin alphabet, the C, as the substitute of the Gamma, or the Gimel, contains the first and second letters A and B corresponding to the Alfa and Beta (Alef and Bet, respectively). It shows the significance of the letter D starting the titles, that the first title, the first line, (in Hebrew the first line of the Psalm is the Dalet) is given in two ways, with the words 'observantia' and 'observanda', which also shows the priority of the letter D. In a similar way, the word 'nutrimento', we believe, is consciously given (in the text), with productive deformation in the incorrect form of 'nutrimendo' deviating from the "Content"(Caputilatio).

Thus, focused on the letter D, we obtain a 10+8+1 composition, to which the letter D may also contribute (additionally), highlighting the letter T (i.e. the cross) in the word 'nutrimendo'. The numeric value of 72 or 76 "generated by the letter D" may allude to "mercy" or "clemency" (72=**חסד**), or to the incarnation lineage of Maria (76) using the "additional D (=4)". The Graeco-Latin number interpretation of the "D" leads to the number 504, which is the number of the Greek word Discus (δισκος=504) and the Hebrew LVIT ChN (**לויתחן**=504), from the cited Proverbs. 1:9 and 4:9 below, which could mean "the grace of Stephen". Thus we get the structure of the Holy Crown, which is reinforced by the 10+8+1 arranging of the 10 chapters with a particular code system, which we discussed in detail in our aforementioned paper [28]. In the equivalency of 'observantia' and 'observanda', in the "TID", ordering the capital Latin T can be equally interpreted as the letters 'Teth' and 'Thav'. The letter Yod (**י**=10) corresponds to the I, so here for the third time, it renders the 10+9+X structure. This structure, as we will discuss later, may carry the hidden meaning of '*alive is the Lord, the Christ'*, since the numerical value of the word 'alive' from the expression of "*the Lord, the Christ*" appearing in the Bible over and over again, is 18 (**חי**); meanwhile, assigning the number 1 to the Hebrew Alef, we can partly draw conclusions that "the Lord is One", and we are also drawn to the Tetragammaton on the basis of the interpretation of the Bahir. Now let us consider the structure and letters of „Caputilatio":

*D*e o**b**serv**a**n*d*(ti)**a** c**a**tholi**ca**(e) fi*d*e(i).

*D*e **c**ontinen*d*o e**cc**lesi**a**sti**c**o st**a**tu.

*D*e impen*d*en*d*o honore pontifi**c**um.

*D*e honore prin**c**ipum et militum.

*D*e o**b**serv**a**tione iu*d*i**c**ii et p**a**tienti**a**e.

*D*e *d*etentione et nutrimento hospitum.

*D*e m**a**gnitu*d*ine **c**onsilii

*D*e exe**c**utione filiorum.

*D*e o**b**serv**a**tione or**a**tionis.

*D*e piet**a**te et miseri**c**or*d*i**a**, **c**eterisque virtuti**b**us.

(where **a**[1]-14, **b**[2]-4, **c**[3]-13, *d[4]*-19 and (1x14+2x4+3x13) +4x19=**61+76=137**)

After all, it seems right to determine the number of the alphabetical letters consisting of the "first part" of the 3-4 transformation, and of the letter D in the Capitulatio, evidently bearing in mind the *observanda* variation. Then it yields 50 letters, where the sum of the ABC letters is altogether 31 (A-14, B-4, C-13), i.e. the value of the shorter Hebrew name of God, the AL (**אל**). Thus taking this together with the aforementioned 18+1 (=19) composition of the D, we can make out the *"Alive God is One"* expression. If on the basis of their given order in the Latin alphabet, we assign to the letter A the number 1, to the B the number 2, to the C the number 3, and to the D the number 4, then the sum total of the ABC is 61 (14x1+4x2+13x3=61). Meanwhile, the 19 letter D shows the number 76 (19x4=76), or in other words, we we also get to the 76+61 composition of the incarnation number of 137, in the framework of the 3-4 transformation, and furthermore to the name LVLIANI (LVLI **לולי**=76+ANI **אני** =61), that is to the name Iulianus or Julius with the Stephanus of the Atara of the 284 letters. In this way, it is about king Julianus Levita Stephanus, i.e. about the symbolism of the Messiah incarnated by the crown[37]. As we also consider the Dominican allusion signified by the 'nutrimento', through the number 137, then we may interpret the meaning as the acceptance of the Christ in the given hermeneutic circle.

Considering the hypothetical D and "T" letters of 'nutrimend(t)o, it is about 51 letters in the 3-4 transformation. This is the numerical value of the Hebrew word LVIH (51=**לויה**), which means Levita-order, Levita woman and Crown/ Thus, with Grecian Latin it can lead to the deduction of the name of Levita Stephanus. This Hebrew word for the crown appears twice in the Bible, in verses 1:9 or 4:9 of the Proverbs (**לוית חן**). Meanwhile in the Preamble of the Royal Mirror, the author quotes verses 1:8 and 4:10 jointly, which are in correlation with each other by

[37] Consequently, the "letter-triad of "CCD" and the first three words *"Cvm Cvncta Dei"* in the Royal Mirror, adequately symbolize the 3-4 transformation because of the alternative reading (using the sing. fem. abbl. of "cvncta" instead of the "neut. plur. acc..") "with (or in) the wholness of God" can mean, here, that the Trinity (through the Holy Ghost –"C") is in the "Fourth" ("D"), i.e. in the Mother of God, symbolizing the "incarnatio continua". It is "manifested" through the 61+76 =137 structure of the incarnation (as "Julianus Stephanus") in the above discussed letter-symbolism of the "Capitulatio".

analogy, along with the related next (1:9) and previous verses (4:9), as a result most likely of a conscious "planning" (in that era the verses were not numbered!):

1.8: Hear, my son, the instruction of thy father, and reject not the rules of thy mother. **9** For thou shalt receive for thine vertex (*"crown"*) a **crown** of graces, and a chain of gold round thy neck. **4,9**: that it may give unto thy head a **crown** of graces, and may cover thee with a **crown** of delight. **10** Hear, *my* son, and receive my words; ***and the years of thy life shall be increased, that the resources of thy life may be many.***

[1,8]ακουε υιε παιδειαν πατροσ σου και μη απωση θεσμουσ μητροσ σου [9]στε φανον *γαρ χαριτων δεξη ση* **κορυφη** *και κλοιον χρυσεον περι σω τραχηλω* **[4 9]** *ινα δω τη ση κεφαλη* **στεφανον** *χαριτων* **στεφανω** *δε τρυφησ υπερασπιση σου* **[10]** *ακουε υιε και δεξαι εμουσ λογουσ* **και πληθυνθησεται ετη ζωησ σο υ ινα σοι γενωνται πολλαι οδοι βιου.**

As we can see above in the quite short text resulting in this way, in which we marked bold the frame-like quoted lines, the word crown appears three- or four times, **Στεφανος** corresponding to Stephanus three times and the Greek word **Κορυφη** one time, and the crown can be found likewise amongst its meanings. (In the English translations of the LXX the word korufe is sometimes translated as crown). Here we can consider the translation of korufe evidently as crown, since in verse 4:9 the same crown of clemency is given for the head, where the head, i.e. the word **Κεφαλη,** can be read. Though in both cases in the original Hebrew the word rash (**ראש**) is used, it can be significant to distinguish the korufe from kefale. The language formula obtained in this way can also signify the 3+1 transformation on the basis of the word of 3, Stephanos, and of the 1, Korufe. Considering the meaning, we can distinguish three crowns, since the crown of the clemency or grace occurs two times; so in this way the crown of korufe, or the crown of clemency, and the crown of joy or beauty can make up a triple unity. This is established by the fact that in the Greek text the crown of the clemency is given to the "crown of the head's crown", i.e. to the lower crown. Then, later, the crown of the clemency is covered by the crown of joy (**τρυφης**) and beauty (Tifereth - **עטרת תפארת**). It corresponds exactly to the triple structure of the Holy Crown, with the feminine crown of the head's crown, since the word korufe is "female", while the crown of clemency on the Holy Crown is from the 72 letters (mercy, clemency) indeed, its masculine crown, since the word Stephanos is male. The consolidation of the "*misericordia"* (**חסד** =72) and the "*iudicium"* (**דין** =64) in the 5th caput of the Royal Mirror is the *"corona decora",* which corresponds to the crown of the Tifereth (beauty), where in the Kabbalah they exactly consolidate the Chessed (misericordia) and the Din (iudicium). In the Holy Crown, X (the slanted cross) may correspond to the Tifereth between the 72 (Chessed) and the 64 (Din). The X, as Christogram signifies the Lord, and in this way, on the basis of the *"Christus ...decor angelorum et hominum"* [7], may allude to its being and function of

"Decor"[38]. Thus, the Lord covering the crown with the slanted cross may correspond to the crown of the joy and beauty. There may also arise another "natural" interpretation of the trinity of the crown. According to this, if we again concentrate on the meanings of the words, then the crown of Stephanus of the original Hebrew Atara would be the lower queenly crown in accordance to the spirit of the proto-Kabbalah in Bahir, while the crown of the high priest (the apostolic one) would be evidently the crown corresponding to the word LVIH (**לויה לויה**). The korufe in this case could be the crown of the upper most uniting enamel picture (Pantocrator), meaning the crown of the head (with the slanted cross), interpretation of which is reinforced by the fact that the Lord is portrayed with a black pointed beard, alluding in this way to the word korufe, as well. Because the "mystical equation" "H Κορθφη"=1106="Αστερισκος" the higher crown can be concerned as an "Asterisk-crown" which is really valid for the Holy Crown too. All of these are amplified by the hidden symbolism of the several-times-mentioned triad crown-setup (10+8+1, 10=Deka) "AChD" (**אחד**) in the Royal Mirror, similarly to the triad crown of the Bahir (kingship, priesthood, Torah) in the 152 §.[39] Just as in the text of the Royal Mirror it reads that all which is sanctified in the text constitutes the eternal and temporal crown, so the above interpretation is also justified here. Interestingly, the appearance of the words zoe (ζωη) and bio (βιο) in the Greek text, which do not occur in the Hebrew and Latin texts normally, anticipates the interpretation of the eternal (undestructible) and the everyday, i.e. the finite living crown and the kingdom (regnum).

---

38 This unified crown could be in Araboth (§153) obviously Yophiel (see Araboth and Yophiel above). The consolidation or reconciliation of *"iudicium vs misericordia"* by the "*corona decora*" is a pattern which corresponds to the "idea of Yophiel-Dina" as well. Namely, as we have seen, the number of the name Yophiel (in Latin, e.g. Decor Dei) is 137, where the number of Dina (65) is completed to 137 by the number of 72, which is the number of Chessed, i.e. in Latin misericordia, while the Dina means iudicium.

39 As we have seen, the interpretation of number 137 with the participation of "72+1+64" ("Mercy"-"One"- "Justice" or "Strength") "naturally" represents the 3-4 transformations, where the "complete unity" of 137 is the "Crown" as the fourth. Similarly, the participation of the angelic name of Yophiel as "IV-FI-AL" (**יו פי אל**) with the unification of the two names of God through Yophiel's pronunciation (Hebrew FI--**פי** means mouth), who is the transformer, the transformation and the transformed as well, into the Atara, i.e. the Crown as the fourth. This symbolic formulation can be recognized by the representation of the "three popes" between the two deacons, Stephanus and Lavrencius, on the Royal Robe. Thus, the three Popes are between the two "Crowns" (see Laurea as wreath or crown), where obviously one is "Greek" ("Stephanos') and the other (Lavrencius) is "Latin". The name of Clemens harmonizes with "Mercy" (**חסד**=72) and Cornelius (from the Cornua) to "Strength" or "Justice" (**דין**=64), while Sixtvs (with the anagram X(P)ISTVS, corresponds to the reconciliation of the above two in the centre as one (**א**=1). The 137 days between the two "Crowns", i.e. the feast days of Stephanus and Lavrencius (Lavrentius), symbolically show their unity in the unified "Latin-Greek Holy Crown" with the slanted cross as the symbol of unity. It is worth nothing that, in our hermeneutical context, the 3-4 transformation plays a crucial role in Pauli's dreams on the Pointy beard along with the "three Popes with their united House for Pauli" (see [17, 31]).

Returning to the ABC D 3-4 transformation, the above-mentioned examples reinforce the LVIH (**לויה**=51) interpretation of the number 51 and its allusion to Levita Stephanus. Whereas the LVIH can mean the Levita woman along with the words Levita order and the crown, who is par excellence the Virgin Mary (Aaron's sister through the denominator Mary, as well), we can talk about the Levita Stephanus, or the crown of the Virgin Mary. Since the number 76+61 of the 50 letters makes possible the interpretation of the Luliani-Iulianus the number 51 therefore can also allude to the several-times-mentioned triple temura of HLVI IVLH LVIH (**הלוי יולה לויה**), which through the Greek may mean the Levita Iulius Stephanus. Further, through the interpretation of the Levite woman (**לויה**), we might also find allusion to the Virgin Mary, as well, in the frame of the given crown-symbolism, such is the interpretative potential of the 3-4 transformation[40].

8 Model of Hermeneutics: "Name-Numbers" and Meaning Transformations

Based on our preparations, explanations, assumptions (using a circular but not linear way of the "explicatio continua" according to Jung's "hermeneutical circumambulatio") and the "principle of the un-detached observer" we are attempting to enter that world of hermeneutics and imagination in which the authors "could see" and "form" the hidden meaning system of the analysed text.

First of all, we attempt to summarise the numeric structure:

GIML (3) – GMILVT ChS'D – 561 - **גימל - גמילות חסד**

(DLT) (4) – DLIT - 444 - **דלית - דלת**

The above number formation, that is the 561-444 number-pair, expresses symbolically the Gimel and Dalet, i.e. the transformation between 3 and 4, as the author identifies the letter Gimel with the expression of the "Abrahamic Eucharist" (see Ilarion Zakon i blagodat'). On one hand, it is about the Abrahamic banquet (a large impressive meal) in the quotation of passage 19 of Bahir; on the other hand, in passage 135, the "Gmilut Chessed", is about the "thanksgiving" (**גומל חסד למלאכים**) for the "three angels" (**ג מלאכים**), i.e. about the foundation of "Cabbalistic Eucharist" [2].

However, the name Luliani bar Tabri has the numeric value of 561, while the Levitas ben Tabrus (or Levatas ben Tavrus) is 444. So the name transformation

[40] The interpretation of Luliani can reinforce the possible anagram interpretation of the heading of the first chapter, the name Dardanus, because the Gens Dardania is identical with the "Iulianus-ness", or the Gens Iulia: "*(Ego) Dardanvs Beo E Catholica Fide"* (I, Dardanus make others happy (flourish) via the Catholic faith).

expresses exactly the Thanksgiving (Eucharist) offered to the three angels (the Cabbalistic upper Triad or the Holy Trinity), i.e. to God, for what as a reciprocation; as we saw with the interpretation of the letter Gimel, God maintains, renders and flourishes the Church, the kingdom, which is symbolised, as we saw, by the letter Daleth. On the basis of transformation, the person with two names becomes "one", who in the original name appeared as a monarch, while in the new name he appears in front of us as the high priest of his church and kingdom. Since "bar Tabri", i.e. the "son of Tiberius", corresponds to Augustus in the given hermeneutic circle, it is about a rex Augustus, belonging to Gens Iulia, who is a Levite as well. The Luliani-Levitas transformation, however, can be comprehended as one single person and name. This is so because of the numeric value of the Luliani is 137, which is the numeric value of the Hebrew Ophen (wheel, 137=**אופן**), which is the archetype of the Atara i.e. the crown (see [3]), so the person can be shortened as "Levi(tas) Atara". However on the basis of the "Hebrew-Greek-Latin name ensemble" it can be translated into Greek as Λευιτας Στεφανος, and into Latin as Levita Stephanus (while the numeric archetype of Atara is naturally 137). Furthermore, when LVITS (**לויטס**) is transferred from Latin and from Greek into Hebrew, the transformation of Julianus transferred from Latin into Hebrew can also be the Hebrew transferred form of the Latin Levitis, corresponding to the Hebrew word LVIH (**לויה**) (levita order), which is translated as Στεφανος in the LXX. On the basis of this train of thoughts, the authors could "interpret" the monarch Iulianus Levitas Stephanus Augustus (rex) in the name transformation of the given hermeneutic circle. Here we took into consideration the Roman numerals of the 561 and the word Daleth (**דלית**) of 444 formed by Hebrew transcription from its letters (DLXI), as the synchronistic "soundness" of the name transformation. The name Rabbi Chanina found in this section of the Midrash (but omitted in between the two quoted sections of Bahir), can be suited very well to the name Clemens, or the expression of Divina Clementia (the omission may be an indication to the hidden tracking of Clemens with the confirmation of the "original converting by Clement"). Completing the previous name with the latter one, we obtain the name: Iulianus Levita Stephanus Augustus, reigning by the grace of God (Divina Clementia). The name formed this way fits exactly to the name Iuliana (Aeneades) Corona-Crown (Στεφανος) Augusta hidden in Royal Mirror (Caput 6), or to the naming of the king, where the denominator, according to the Hartwick Legend, Levita Beatus Stephanus *("…ornatus Levitici…")* from the word Levites.

Conclusion

We have shown the directing and controlling central role of the general physical and psychic world views, concealing the dynamic isomorphic meaning systems, related to Saint Stephen (Sephanus Rex, according to its own self-naming on the Coronation Mantle), found in works 1000 years old, the number archetype of 137, as well as, the 137-type "fine structures" within the decimal Sephirotic world "controlling system" of the pleroma (the hypothesised informational cosmos as a

"transcendent cyber space"). Following the comparison of the representations (pre-figurations of the dynamic models) of the demonstrated and analysed differing ontical layers and background languages, taking into view of other paper of ours dealing with cosmogonic language mystic representations [28], we can determine that the authors (considering the assumed Khazar sources) devoted the hypothesised proto-Kabbalah to the common background language of the four religious courses, with the hidden and concealing (Sephanus) saint king himself as the probable interpreter. Thus, the four religious courses could be equated to the "Lord's four background languages" [25], placing however into its centre a background language (considered in general as a mapping of system and control problems), the proto-Cabbala, or its concealed meaning system, in tight relation with the numeric archetype of 137 and the 137-type of "fine structures" in order to express God's glory, many times in a hidden way, in accordance with the customs of the era[41].

Our European life nowadays is facing similar intellectual and ideological conflicts, and attempts to seek solutions. The most significant task of our near future seems to be the creative re-vitalisation and peaceful co-existence of the different religious courses (and world-views) in a broader sense with a (depth-psychological) background language, resting on traditions, but containing the modern "scientific approaches", as well. Without it, a peaceful, flourishing European life, resembling to the one in Saint Stephen's court with the peaceful co-existence of the four religious courses, as the continuation of the Khazar traditions, cannot be imagined. The prophetic anticipations of the mediator background languages, resting partly on religious, and partly on "scientific" layers, as we have seen, sprout from Jung and Pauli's co-operation" on the number archetypes and especially on the number 137. This revolutionized (reinterpreting) path of the ancient mystic traditions opens for walking along in the hope of

[41] In the Bahir and the Royal Mirror too, the main forms of the allegoric depiction of the Sephirotic system are the characteristic representations corresponding to the four ontic layers (See even Scholem [20]). The mental layer (the Logos) can be taken granted with the letter- and word-mystic representations (for example the words' peculiar letter compositions or the Decalogue itself in 124 §, while the physical and the vegetal description is ensured by the parts of the human body and the live inverse world tree. In the sephirotic representation of the spiritual-human layer each of the Sephiroth are personified by the patriarchs. The transcendent ontic layer is usually represented by the 10 angels or the kings. In the centre we can hypothesize the Sephirotic crown-representation corresponding maybe to the symbolism of the mandala. The classification is of course relative and view-dependent. From the perspective of the 4+1 background language, the angels and the kings may correspond to the mythological and religious background language, i.e. the mental layer, while the letter- and the abstract language-mystic representation can rather be understood as the abstract hermeneutical background language corresponding to the transcendent layer. The anatomic and the vegetal representation may correspond to the "physical" background language, while the interpretation of the patriarchs corresponds well to the psychological background language. The crown representation is, par excellence, the pre-image of the system and control background language.

carrying on of mankind's individuation process,[42] notably the expanding, widening of the reflective human consciousness.

References

[1] Ameisenow, Z.: Animal-headed Gods, Evangelists, Saints and Righteous Men. Warburg Institute, London, 1948, pp. 21-44

[2] The Book Bahir. (ed. A. Kaplan) Samuel Weiser, INC., York Beach, Maine, 1989

[3] Dan, J.: 'The Emergence of Mystical Prayer', Studies in Jewish Mysticism, Proceedings of Regional Conferences held at the University of California, Los Angeles, and McGill University, eds. Joseph Dan and Frank Talmage, Cambridge Mass: Association for Jewish Studies 1982, pp. 85-120

[4] Dan, J. : תרות **הסוד של חסידי אשכנז ירושלים. 8691,** pp. 119-122

[5] Gaster, M.: „Hebrew Visions of Hell and Paradise," in the Journal of The Royal Asiatic Society, London, 1893

[6] Gnutova, S., Ruzsa Gy., Zotova, E.: Prayers Locked in Bronze - Russian Metal Icons. Museum of Applied Arts. Budapest, 2005

[7] Green, R. (ed.): Herrad of Hohenbourg: Hortus Deliciarum, (Commentary and Reconstruction) I-II London, 1979

[8] Hahnloser, R - Polacco, R.: Una nuova lettura della Pala d'oro.Canal & Stamperia. Venezia, 1994

[9] Idel, M.: Kabbala New Perspectives. Yale Univ. Press, 1988

[10] Jung, C. G.: Psychologie und Alchemy. Walter Verlag, Olten (1972)

[11] Jung, C. G: Mysterium Conjunctionis. Princeton Univ. Press 1977

[12] Jung, C. G.: Collected Works, Bolingen, Vols. 8, 9, 11, 12, 14. Princeton University Press (1973)

[13] Jung, C. G. (ed. G. Adler, A Jaffe) Letters I-II. Princeton Univ. Press (1973)

[14] Kóczy, T. L, Várlaki, M. P.: Structural and Hermeneutical Comparison of the Holy Crown of Hungary with the Pala d'oro of Venice, Symp. on the 1010 anniversary of St Stephen's Coronation and 600 anniversary of the Foundation of the Óbuda University", pp. 19-86, Budapest, 2012 (in Hungarian)

[15] Lawrence, R. M. The Magic of the Horse-Shoe, With Other Folk-Lore Notes, (1898)

[16] Margalioth.:(The Book Bahir), **ספר הבהיר מרגליות מוסד הרב קוק, ירושלים**

[17] Meier, C. (ed.): Atom and Archetype: The Pauli/Jung Letters, 1932-1958. Routledge, London (2002)

[18] Pauli, W. (eds. Enz, C., Meyenn, K. V.): Writings on Physics and Philosophy. Springer (1994)

[42] See A. Jaffé: Was C. G. Jung a mystic?, Daimon, 1989

[19] Ricoeur, P.: Structure et herméneutique. In: Le Conflit des Interprétations, pp. 31-63, Seuil (1969)

[20] Scholem, G.: Origins of the Kabbalah. Princeton Univ. Press, 1990

[21] Scholem, G.: Major Trends in Jewish Mysticism, Schoken, New York, 1983

[22] Scholem, G.: Das Buch Bahir, Verlag von W. Drugulin, Leipzig, 1923

[23] Tóth E., Szelényi K.: The Holy Crown of Hungary, Budapest, 2002 (in English)

[24] Várlaki, P., Kóczy, L.: A Comparative Study of Pictures from Pala d'oro in St. Mark Catherdral of Venice and from the Holy Crown of Hungary. In: Proc. of Intl. Conference on Genealogy and Heraldry. Hungary (2006) pp. 131-171 (In Hungarian)

[25] Várlaki, P., Nádai, L., Bokor, J.: Number Archetypes and "Background" Control Theory Concerning the Fine Structure Constant. Acta Polytechnica 5 pp. 71-104 (2008)

[26] Várlaki P., Kóczy L T. Genealogical Myth and Allegory in the Pala d'Oro of Venice and Saint Stephen's Royal Mirror. Internat. Conf. of the Hungarian Heraldic and Genealogical Society, pp. 89-124 (In Hungarian)

[27] Varlaki, P., Rudas, I.: Twin Concept of Fine Structure Constantas the 'Self Number-Archetype'in perspective of the Pauli-Jung Correspondence. Part I. Observation, Identification and Interpretation, and Part II. Cognition, Imagination and Background Process, Acta Polytechnica Hungarica, 2009, No. 2, pp. 77-108 and pp. 109-137

[28] Várlaki P, Bokor J.: Number Archetypes, Symbolic Coding Letters and "Background Communication Theory" in Saint Stephen's Royal Mirror. In: IEEE 7th International Conference on Computational Cybernetics, Palma de Mallorca, 2009, pp. 201-211

[29] Várlaki, P., Rudas, I., Kóczy, L.:Historical Origin of the Fine Structure Constant. Part I. St Stephen's Crowning Achievement, Acta Polytechnica Hungarica, Vol. 7, No. 1, pp. 119-157

[30] Várlaki, P., Rudas, I.: Comparative Structural and Hermeneutical Analysis of the Hungarian Coronation Robe (Casula), Symp. on the 1010 anniversary of St Stephen's Coronation and 600 anniversary of the Foundation of the Óbuda University", pp. 87-152, Budapest, 2012 (in Hungarian)

[29] Várlaki, P., Rudas, I., Kóczy, L.: Historical Origin of the Fine Structure Constant. Part II. Subtilis Structurae Constans Inversae Arboris Dei, Acta Polytechnica Hungarica, Vol. 8, No. 2, 2011, pp. 161-196 [30]

[31] Várlaki, P., Rudas, I., Kóczy, L.:Historical Origin of the Fine Structure Constant. Part III: Pauli with Jung Retro-cognizes St. Stephen's Crowning Achievement, Acta Polytechnica Hungarica, Vol. 8, No. 6, 2011., pp. 43-78

[32] Várlaki, M. P., Rudas, I. J., and Kiss, G.: Structural and Meaning Identification of the „Explicit God's Name" of Number Archetype 137 in the Book Bahir comparing with the „Fine Structure" of the Holy Crown and the Royal Robe of Hungary*, Proc. of Workshop on Computational Intelligence, In Honor of L. T. Kóczy on his 60th birthday,* Óbuda University, Budapest, 2012

Double Layer Tensegrity Grids

Tatiana Olejnikova

Department of Applied Mathematics, Civil Engineering Faculty
Technical University of Košice
Vysokoškolská 4, 042 00 Košice, Slovakia
e-mail: tatiana.olejnikova@tuke.sk

Abstract: This paper describes the geometry of a double layer tensegrity grids assembled of three or four strut prismatic cells. The elementary cells are self-equilibrated and so is their assembly. The paper shows the creation of a planar grids composed of elementary equilibrium and grids with single or double curvatures composed of modified equlibrium shapes.

Keywords: tensegrity system; compression; tension; equilibrium; prismatic cell; grid structures

1 Introduction

A tensegrity structure is a class of tension structures consisting of tensile members and compressive members. In civil engineering, the light-weight characteristic of tensegrity is recognized as a significant advantage for space structures over conventional structural systems. According to the definition given by Fuller (1975), a tensegrity structure is a jointed structure consisting of continuous tensile members (cables) and discontinuous compressive members (struts).

A tensegrity system is established when a set of discontinuous compression components interacts with a set of continuous tensile components to define a stable volume in space. However, it needs to be slightly modified, taking into account the following factors: the components in compression are included inside the set of components in tension, and the stability of the system is self-equilibrium stability.

There are three types of tensegrity systems: tensegrity grids, tensegrity frameworks and tensegrity domes. This article describes the geometric relations of tensegrity grids assembled of prismatic cells. There are three orbits of members: horizontal cables, vertical cables and struts. Each node is connected by two horizontal cables lying in a horizontal plane, one vertical cable and one strut. The

vertical cables and struts connect nodes in different horizontal planes. The members in each orbit are of equal length. The necessarily even number of nodes characterises the case of tensegrity systems. If "*n*" is this number, and if attention is paid to the spatial case, the minimal value of *n* is 6.

2 Geometry of the Prismatic Three-Strut Tensegrity Grids

The geometry of a spatial reticulate system is completely defined by its relational structure and by the knowledge of the coordinates $x(k)$, $y(k)$, $z(k)$, $k = 1,\ldots,n$, for its "*n*" nodes in reference to a chosen axis system. It is necessary for all internal elements (struts) to have the same length "*s*" and for the external elements (cables) to have the same length "*c*".

If the length of the struts is insufficient, the set of envelope elements will not have a definite shape (the system is then kinematically indeterminate). A first geometry is defined as a triangular prism (Fig. 1). This system is unstable, and another shape can be defined (Fig. 2) by relative rotation of the two triangles of cables in the parallel planes.

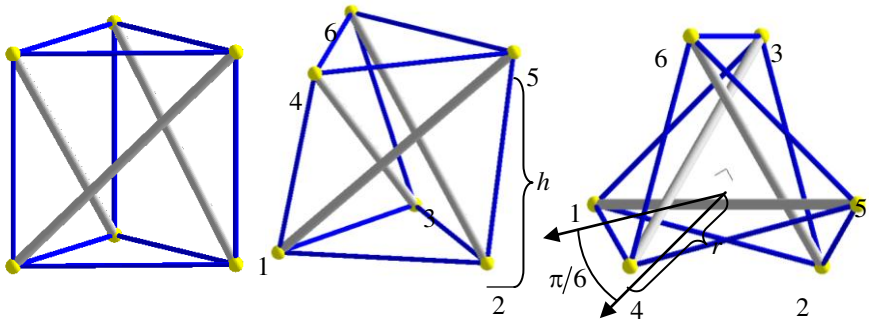

Figure 1
Triangular prism

Figure 2
Equilibrium, axonometric and top view

For a given value of the strut length, the totality of the cable net takes a singularly definite shape, which will be referred to as "null self-stress equilibrium geometry". The geometric distance between the nodes corresponds strictly to the length of manufactured elements. Two geometrical ranges can be identified. If the relationship between the lengths of the struts and cables is ratio $s/c = \sqrt{2} = 1{,}467$ and the relative rotation between triangles is $\pi/6$. When the parameter r is specified, then the length of the struts is $s = r\sqrt{3+2\sqrt{3}}$, the length of the all cables is $c = r\sqrt{3}$ and the height of the equilibrium is $h = r\sqrt{1+\sqrt{3}}$.

2.1 Bi-Dimensional Assemblies

This section describes examples of bi-dimensional assemblies. Several junction modes can be used: node on node, node on cable, cable on cable.

In type a) in Figure 3, the junction is operated with a single vertical (bracing) cable: each of two ends of the strut lies in different horizontal planes, and it will be used in a plane configuration leading to a double layer grid, in types b) and c), the junction is operated with horizontal cables.

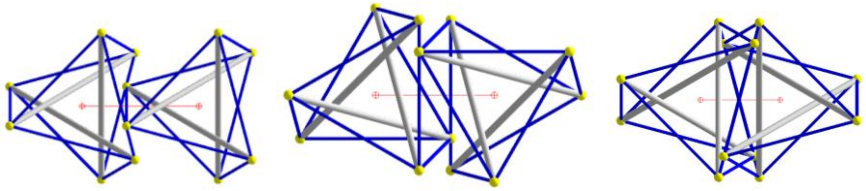

a) Junction: node on vertical cable

b) Junction: node on horizontal cable

c)

Figure 3
Junction modes "node on cable"

A planar double layer tensegrity grid (Fig. 5) is created by using three-struts cells via a node on cable junction of type a) (Fig. 4).

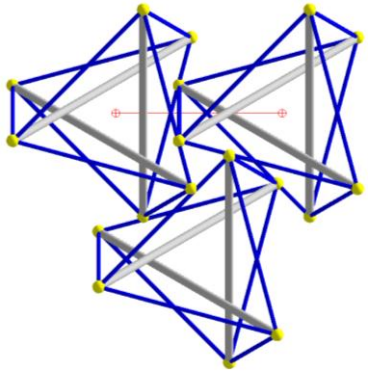

Figure 4
Three cells junction in mode "node on vertical cable" of type a)

The node coordinates $x(\mathrm{k}), y(\mathrm{k}), z(\mathrm{k})$ of one cell in the planar grid are in (1):

$$x(\mathrm{k}) = k_0\ r\cos\varphi(\mathrm{k}),\ y(\mathrm{k}) = k_0\ r\sin\varphi(\mathrm{k}),\ z(\mathrm{k}) = h_1$$

$$\text{for } \mathrm{k} = 1,2,3 \quad \varphi(\mathrm{k}) = -\frac{\pi}{12} + (\mathrm{k}-1)\frac{2\pi}{3},\ h_1 = 0 \tag{1}$$

$$\text{for } \mathrm{k} = 4,5,6 \quad \varphi(\mathrm{k}) = \frac{\pi}{12} + (\mathrm{k}-4)\frac{2\pi}{3},\ h_1 = h = r\sqrt{1+\sqrt{3}}$$

where the parameter $k_0 = 1$, r is a radius of a triangle created by the three horizontal cables in the cell, h is a height of the cell (Fig. 2).

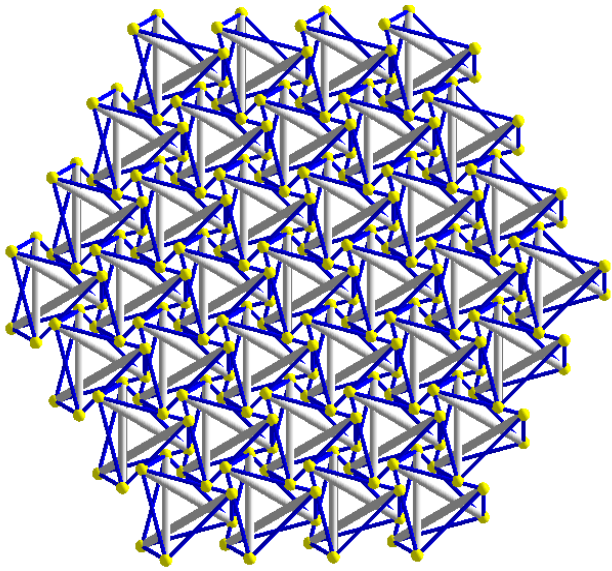

Figure 5
Planar double layer tensegrity grid by three-struts cells

The node coordinates $x_1(\mathrm{i},\mathrm{j},\mathrm{k}), y_1(\mathrm{i},\mathrm{j},\mathrm{k}), z_1(\mathrm{i},\mathrm{j},\mathrm{k})$ of all cells in the planar grid displayed in Figure 5 are

$$x_1(\mathrm{i},\mathrm{j},\mathrm{k}) = x(\mathrm{k}) + d_x(\mathrm{j}),\ y_1(\mathrm{i},\mathrm{j},\mathrm{k}) = y(\mathrm{k}) + d_y(\mathrm{j}),\ z_1(\mathrm{i},\mathrm{j},\mathrm{k}) = z(\mathrm{k}) \tag{2}$$

$$d_x(\mathrm{j}) = v_x(\mathrm{i})\cos(\frac{\mathrm{j}\pi}{3}) - v_y(\mathrm{i})\sin(\frac{\mathrm{j}\pi}{3}),\ d_y(\mathrm{j}) = v_x(\mathrm{i})\sin(\frac{\mathrm{j}\pi}{3}) + v_y(\mathrm{i})\cos(\frac{\mathrm{j}\pi}{3}) \tag{3}$$

where $\mathrm{i} = 1,\ldots,6, \mathrm{j} = 1,\ldots,6, \mathrm{k} = 1,\ldots,6$, coordinates $x(\mathrm{k}), y(\mathrm{k}), z(\mathrm{k})$ are expressed in (1), and

$$\begin{aligned} &v_1 = \frac{3r}{2}, v_2 = \frac{\sqrt{3}r}{4},\ v_x(1) = v_y(1) = 0, v_x(2) = v_1, v_y(2) = v_2, \\ &v_x(3) = \frac{5}{4}v_1, v_y(3) = \frac{9}{2}v_2, v_x(4) = 2v_1, v_y(4) = 2v_2, v_x(5) = 3v_1, \\ &v_y(5) = 3v_2, v_x(6) = \frac{9}{4}v_1, v_y(6) = \frac{11}{2}v_2, v_x(7) = \frac{3}{2}v_1, v_y(7) = 8v_2. \end{aligned} \tag{4}$$

By maintaining the principle of elementary self-stressed cells, it is possible to modify the equilibrium shape so as to generate a double curvature system and spherical surface with a radius R. The elementary cell must be modified by the

parameter k_0 in the equations (1) of the node coordinates of the upper triangles, for $\mathrm{k}=4,5,6$, $\mathrm{i}=1,\ldots,6$, $\mathrm{j}=1,\ldots,6$.

The transformation equations of the node coordinates of the lower layer of the planar grid to the spherical surface with a radius R and centre $S(0,0,-R)$ for $\mathrm{k}=1,2,3$, $\mathrm{i}=1,\ldots,6$, $\mathrm{j}=1,\ldots,6$ and parameter $k_0=1$ in equations (1) are:

$$\begin{aligned} &P(x_1(\mathrm{i},\mathrm{j},\mathrm{k}), y_1(\mathrm{i},\mathrm{j},\mathrm{k}), z_1(\mathrm{i},\mathrm{j},\mathrm{k})) \rightarrow P'(x'(\mathrm{i},\mathrm{j},\mathrm{k}), y'(\mathrm{i},\mathrm{j},\mathrm{k}), z'(\mathrm{i},\mathrm{j},\mathrm{k})) \\ &x'(\mathrm{i},\mathrm{j},\mathrm{k}) = R\ \cos\ u(\mathrm{i},\mathrm{j},\mathrm{k})\cos v(\mathrm{i},\mathrm{j},\mathrm{k}) \\ &y'(\mathrm{i},\mathrm{j},\mathrm{k}) = R\ \cos u(\mathrm{i},\mathrm{j},\mathrm{k})\sin v(\mathrm{i},\mathrm{j},\mathrm{k}) \\ &z'(\mathrm{i},\mathrm{j},\mathrm{k}) = R\ \sin u(\mathrm{i},\mathrm{j},\mathrm{k}) - R \end{aligned} \tag{5}$$

where

$$\begin{aligned} &u(\mathrm{i},\mathrm{j},\mathrm{k}) = \frac{\pi}{2} - \frac{d(\mathrm{i},\mathrm{j},\mathrm{k})}{R}, d(\mathrm{i},\mathrm{j},\mathrm{k}) = \sqrt{x_1^2(\mathrm{i},\mathrm{j},\mathrm{k}) + y_1^2(\mathrm{i},\mathrm{j},\mathrm{k})}, \\ &v(\mathrm{i},\mathrm{j},\mathrm{k}) = \mathrm{sgn}\ y_1(\mathrm{i},\mathrm{j},\mathrm{k})\ \arccos\ \frac{x_1(\mathrm{i},\mathrm{j},\mathrm{k})}{d(\mathrm{i},\mathrm{j},\mathrm{k})} \end{aligned} \tag{6}$$

coordinates $x_1(\mathrm{i},\mathrm{j},\mathrm{k}), y_1(\mathrm{i},\mathrm{j},\mathrm{k})$ are expressed in equations (2). The transformation equations of the node coordinates of the upper layer of the planar grid to the spherical surface with a radius $R+h$ and a centre $S(0,0,-R)$ for $\mathrm{k}=4,5,6$ and parameter $k_0 = \frac{R+h}{R}$ in equations (1) are

$$\begin{aligned} &x'(\mathrm{i},\mathrm{j},\mathrm{k}) = (R+h)\ \cos u(\mathrm{i},\mathrm{j},\mathrm{k})\cos v(\mathrm{i},\mathrm{j},\mathrm{k}) \\ &y'(\mathrm{i},\mathrm{j},\mathrm{k}) = (R+h)\ \cos u(\mathrm{i},\mathrm{j},\mathrm{k})\ \sin v(\mathrm{i},\mathrm{j},\mathrm{k}) \\ &z'(\mathrm{i},\mathrm{j},\mathrm{k}) = (R+h)\ \sin u(\mathrm{i},\mathrm{j},\mathrm{k}) - R \end{aligned} \tag{7}$$

where

$$\begin{aligned} &d(\mathrm{i},\mathrm{j},\mathrm{k}) = \sqrt{x_1^2(\mathrm{i},\mathrm{j},\mathrm{k}) + y_1^2(\mathrm{i},\mathrm{j},\mathrm{k})},\ u(\mathrm{i},\mathrm{j},\mathrm{k}) = \frac{\pi}{2} - \frac{d(\mathrm{i},\mathrm{j},\mathrm{k})}{R+h}, \\ &v(\mathrm{i},\mathrm{j},\mathrm{k}) = \mathrm{sgn}\ y_1(\mathrm{i},\mathrm{j},\mathrm{k})\ \arccos\ \frac{x_1(\mathrm{i},\mathrm{j},\mathrm{k})}{d(\mathrm{i},\mathrm{j},\mathrm{k})} \end{aligned} \tag{8}$$

Figure 6 shows the grid composed of three-strut cells transformed to the spherical surface. Figure 7 illustrates the transformation of the point $P(\mathrm{k})$ to the point $P(\mathrm{i},\mathrm{j},\mathrm{k})$, both located in the tangent plane of the spherical surface and its transformation to the point $P'(\mathrm{i},\mathrm{j},\mathrm{k})$ located on the spherical surface. Figure 8 displays a determination of the parameter $d(\mathrm{i},\mathrm{j},\mathrm{k})$ and angles $u(\mathrm{i},\mathrm{j},\mathrm{k})$ and $v(\mathrm{i},\mathrm{j},\mathrm{k})$, which are used in equations (8).

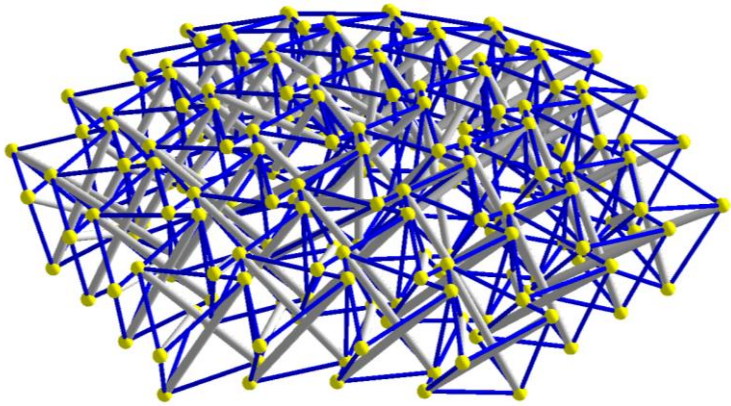

Figure 6
Double curvature tensegrity grid system

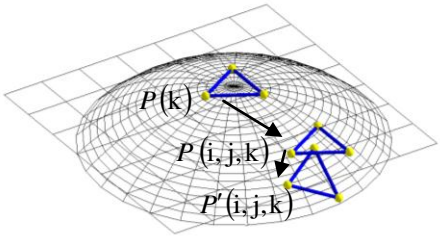

Figure 7
Transform.: $P(\mathrm{k}) \rightarrow P(\mathrm{i,j,k}) \rightarrow P'(\mathrm{i,j,k})$

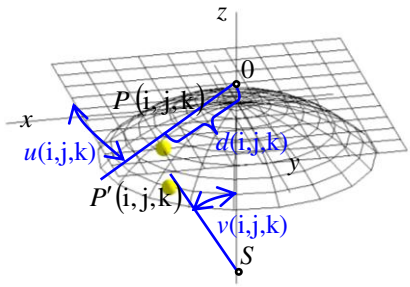

Figure 8
Determination of d(i,j,k),u(i,j,k),v(i,j,k)

In Figure 9 are displayed the nodes and cables of the triangles of the bottom layer on the spherical surface. Figure 10 displays the triangles of the bottom layer of the tensegrity grid located on the tangent plane of the spherical surface, and in Figure 11 are these triangles placed on the spherical surface together with a spherical surface.

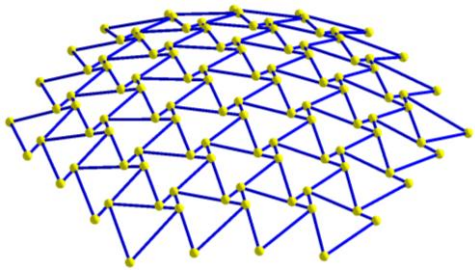

Figure 9
Nodes and cables of the bottom layer of the spherical grid

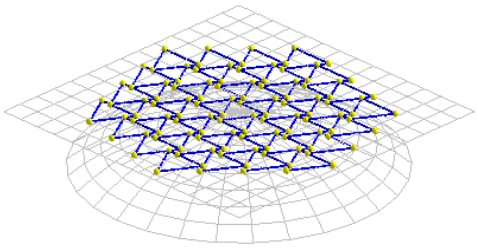

Figure 10
Triangles on the tangent plane

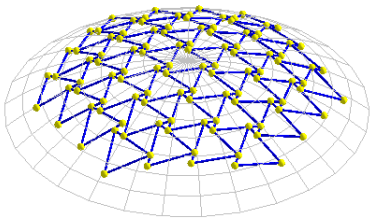

Figure 11
Triangles on the sphere

3 Geometry of the Prismatic Four-Strut Tensegrity Grids

Geometry of the four-strut cell is dependent upon only one parameter a (Fig. 11). When the topology is defined, then the geometry is qualified by the whole set of coordinates, which is closely related to the self-stress equilibrium. When the parameter a is specified, then the length of the struts is $s = a\sqrt{20/3}$, the length of the cables of the bottom layer is $c_1 = a\sqrt{2}$, length of the cables of the upper layer is $c_2 = 2a$ and the height of the equilibrium is $h = a\sqrt{5/3}$.

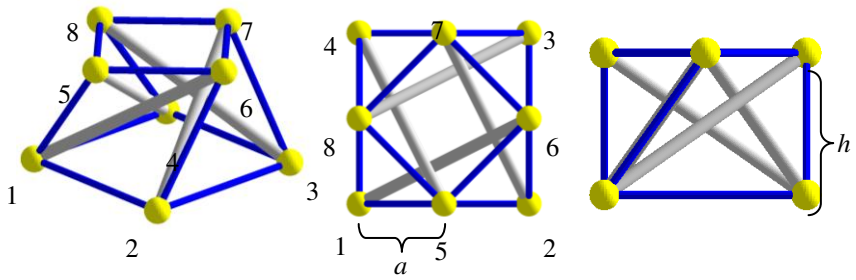

Figure 11
Axonometric, top view and frontal view of the 4-strut cell

Planar double layer tensegrity grid is created by using of four-struts cells by node on node junction. The node coordinates $P(\mathrm{k}) = (x(\mathrm{k}), y(\mathrm{k}), z(\mathrm{k}))$ for $\mathrm{k} = 1,2,3,4$ and $\mathrm{k} = 5,6,7,8$ of one cell in the planar grid are expressed in equations (9)

$$\text{for } k = 1,2,3,4 \text{ and } \varphi(k) = (k-1)\frac{\pi}{2} + \frac{\pi}{4},\ z(k) = 0,$$
$$P(k) = (x(k), y(k), z(k)) = \left(\sqrt{2}a\cos\varphi(k) + a,\ \sqrt{2}a\sin\varphi(k) + a,\ z(k)\right)$$
$$\text{for } k = 5,6,7,8 \text{ and } \varphi(k) = (k-4)\frac{\pi}{2},\ z(k) = a\sqrt{\frac{1}{2} + \sqrt{2}} \tag{9}$$
$$P(k) = (x(k), y(k), z(k)) = (a\cos\varphi(k) + a,\ a\sin\varphi(k) + a,\ z(k))$$

where parameters a, h are illustrated in Figure 11. A planar double layer tensegrity grid is created by using 3×3 four-struts cells by node on node junction. The coordinates of the nodes in the planar grid for $i = 1,\ldots,3,\ j = 1,\ldots,3, k = 1,\ldots,8$ are in equations (10)

$$x(i,j,k) = x(k) + 2a(i-1),$$
$$y(i,j,k) = y(k) + 2a(j-1), \tag{10}$$
$$z(i,j,k) = z(k),$$

where $x(k), y(k), z(k)$ are coordinates of the nodes of one cell expressed in (9). Figure 12 shows the planar double layer grid composed of 9 four-strut cells (top view and frontal view).

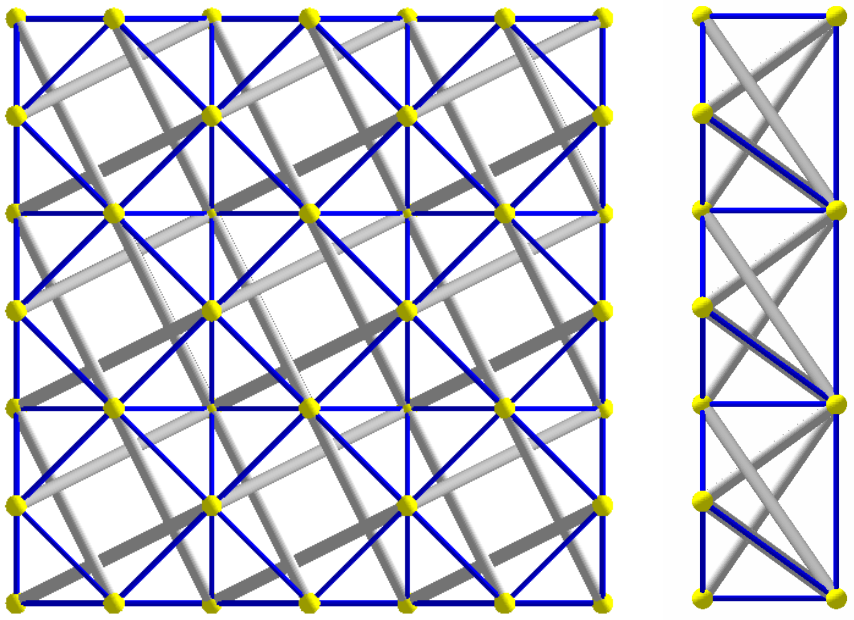

Figure 12
Top and frontal view of the planar double layer tensegrity grid of 3×3 cells

By maintaining the principle of elementary self-stressed cells it is possible to modify the equilibrium shape so as to generate a single curvature tensegrity grid system (on the cylindrical surface). Then the node coordinates are expressed in transformation equations (11), where the nodes located in the plane are transformated to the nodes located on the cylindrical surfaces with radii R and $R+h$, $P(\mathrm{k}) \rightarrow P(\mathrm{i},\mathrm{j},\mathrm{k})$, $\mathrm{i}=1,\ldots,7$, $\mathrm{j}=1,\ldots,7$

$$\begin{aligned} x(\mathrm{i},\mathrm{j},\mathrm{k}) &= x(\mathrm{k})\cos\alpha_{\mathrm{i}} - (z(\mathrm{k})+R)\sin\alpha_{\mathrm{i}}, \\ y(\mathrm{i},\mathrm{j},\mathrm{k}) &= y(\mathrm{k}) + 2a(\mathrm{j}-1), \\ z(\mathrm{i},\mathrm{j},\mathrm{k}) &= x(\mathrm{k})\sin\alpha_{\mathrm{i}} + (z(\mathrm{k})+R)\cos\alpha_{\mathrm{i}} - R, \end{aligned} \tag{11}$$

where parameter a for nodes $P(\mathrm{k})$, for $\mathrm{k}=6,8$ in (10) is modified on $b=a(1+h/R)$ illustrated in Figure 14, parameter $\alpha_{\mathrm{i}} = -6\alpha + (\mathrm{i}-1)\,2\alpha$, where $\alpha = \arctan(a/R)$, R is radius of the curvature of the single curvature system.

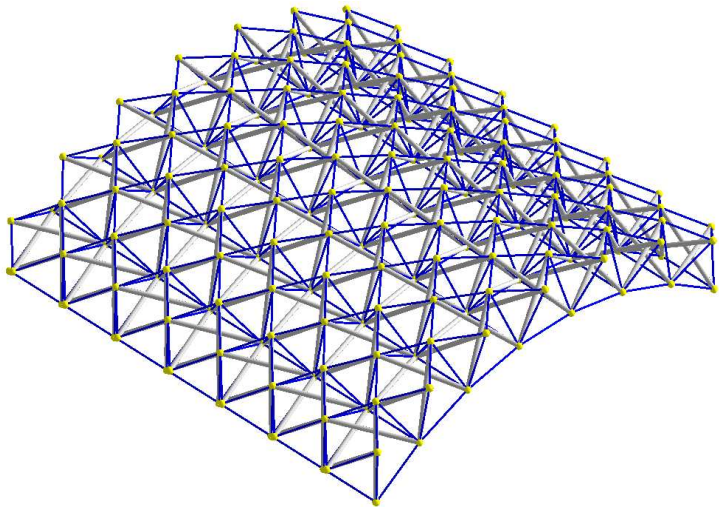

Figure 13
Single curvature double layer tensegrity grid of 7×7 four-strut cells

In Figure 14 is displayed a 1× modified four-strut cell and in Figure 15 a 2× modified one. Figure 13 displays a single curvature double layer tensegrity grid containing 7×7 1× modified four-strut cells.

The node coordinates of the grid with double curvature (created surface with two curvatures R_1 and R_2) are

$$\begin{aligned} x'(\mathrm{i},\mathrm{j},\mathrm{k}) &= x(\mathrm{k})\cos\alpha_{\mathrm{i}} - (z(\mathrm{k})+R_{\mathrm{l}})\sin\alpha_{\mathrm{i}}, \\ y'(\mathrm{i},\mathrm{j},\mathrm{k}) &= y(\mathrm{k}), \\ z'(\mathrm{i},\mathrm{j},\mathrm{k}) &= x(\mathrm{k})\sin\alpha_{\mathrm{i}} + (z(\mathrm{k})+R_{\mathrm{l}})\cos\alpha - R_{\mathrm{l}}, \end{aligned} \tag{12}$$

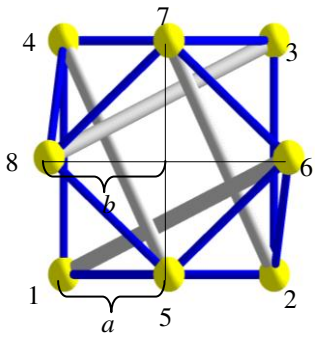

Figure 14
1× modified four-strut cell

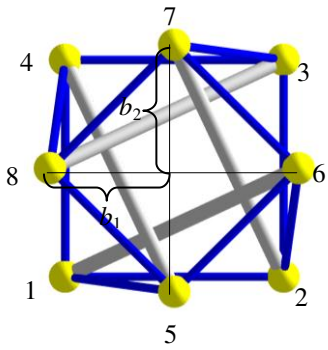

Figure 15
2× modified four-strut cell

$$
\begin{aligned}
x(\mathrm{i},\mathrm{j},\mathrm{k}) &= x'(\mathrm{i},\mathrm{j},\mathrm{k}) \\
y(\mathrm{i},\mathrm{j},\mathrm{k}) &= y'(\mathrm{i},\mathrm{j},\mathrm{k})\cos\beta_{\mathrm{j}} - \left(z'(\mathrm{i},\mathrm{j},\mathrm{k}) + R_2\right)\sin\beta_{\mathrm{j}}, \\
z(\mathrm{i},\mathrm{j},\mathrm{k}) &= y'(\mathrm{i},\mathrm{j},\mathrm{k})\sin\beta_{\mathrm{j}} + \left(z'(\mathrm{i},\mathrm{j},\mathrm{k}) + R_2\right)\cos\beta_{\mathrm{j}} - R_2,
\end{aligned}
\tag{13}
$$

where parameter a for nodes $P(\mathrm{k})$, if $\mathrm{k}=6,8$ in (10) is modified on $b_1 = a\left(1+h/R_1\right)$, and for nodes $P(\mathrm{k})$, if $\mathrm{k}=5,7$ on $b_2 = a\left(1+h/R_2\right)$, $\alpha = \arctan\left(a/r_1\right)$, $\beta = \arctan\left(a/r_2\right)$, $\alpha_{\mathrm{i}} = -6\alpha + (\mathrm{i}-1)\,2\alpha$, $\beta_{\mathrm{i}} = -6\beta + (\mathrm{j}-1)\,2\beta$, where $r_1 = \mathrm{sgn}_1 R_1$ and $r_2 = \mathrm{sgn}_2 R_2$ are the radii of the curvatures of the double curvature system with its orientation determined by the parameter $\mathrm{sgn}_{1,2} = \pm 1$.

In Figure 16 is displayed a double curvature double layer tensegrity grid containing 7×7 2× modified four-strut cells, where the radii of curvature are the same size and the same orientation $r_1 = r_2$. This grid has the form of a spherical surface.

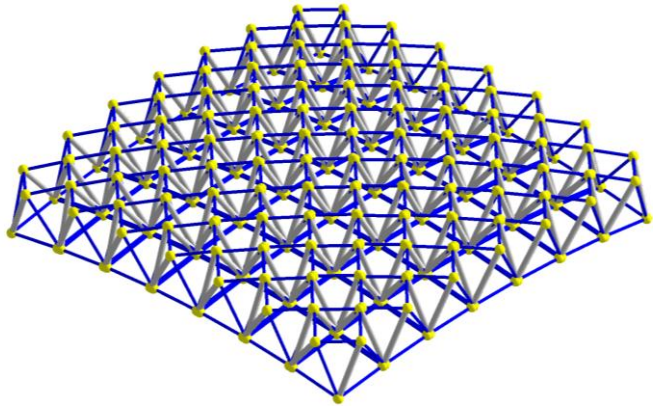

Figure 16
Double curvature double layer tensegrity grid 7×7, $r_1 = r_2$

In Figure 17 the tensegrity grid with the same radii but with opposite orientation $r_1 = -r_2$ has the form of the translational surface created by the translation of the circle with radius R_1 along the circle with radius R_2. In Figure 18 the tensegrity grid with different radii and opposite orientation $r_1 = -4\,r_2$ has the form of the translational surface created by the translation of the circle with radius R_1 along the circle with radius R_2.

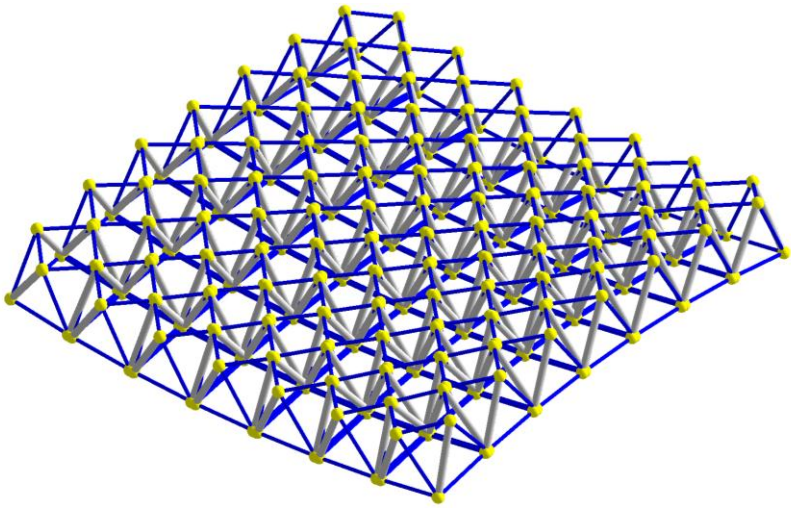

Figure 17
Double curvature double layer tensegrity grid with radii $r_1 = -r_2$

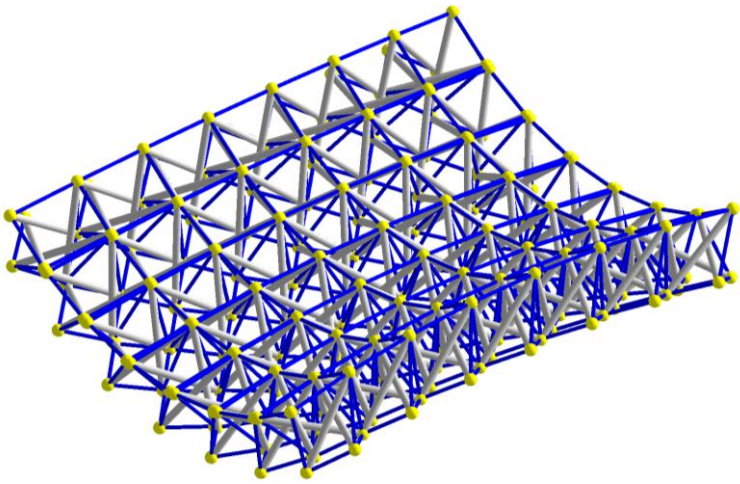

Figure 18
Double curvature double layer tensegrity grid with radii $r_1 = -4\,r_2$

Conclusions

This paper aimed to provide some examples of planar or non-planar prismatic tensegrity grid systems. Some are only geometrical studies without equilibrium considerations. It is not easy to define tensegrity systems. It could be claimed that everything in the universe is tensegrity with properties related to the continuum of tensioned components. Tensegrity structures are the most recent addition to the array of systems available to designers. The concept itself is about eighty years old and it came not from within the construction industry but from the world of arts. Although its basic building blocks are very simple – a compression element and a tension element – the manner in which they are assembled in a complete, stable system is by no means obvious.

The idea was adopted into architecture in 1960 when Maciej Gintowt and Maciej Krasiński, architects of Spodek, a venue in Katowice in Poland, designed it as one of the first major structures to employ the principle of tensegrity. The roof uses an inclined surface held in check by a system of cables holding up its circumference. Another example of a practical implementation of the tensegrity system is Seoul Olympic Gymnastics Arena designed by David Geiger in 1980 for the 1988 Summer Olympics. The Georgia Dome, which was built for the 1996 Summer Olympics, is a large tensegrity structure of similar design to the aforementioned Gymnastics Hall.

Acknowledgement

This work was supported by the Slovak Grant Agency of Ministry of Education of the Slovak Republic within the project VEGA No. 1/0321/12 "Theoretical and experimental analysis of adaptive cable and tensegrity systems under static and dynamic stress considering the effect of wind and seismic".

References

[1] Olejíková T.: Geometry of Tensegrity Systems, Proceedings of Scientific Works „Innovative Approach to Modeling of Intelligent Construction Components in Building 2010", Košice, 2010, pp. 98-104

[2] Motro R.: Tensegrity. Structural Systems for the Future. Kogan Page Limited, London and Sterling, 2003 http://www.google.com/books?hl=sk&lr=&id=0n0K6-zOB0sC&oi=fnd&pg=PR7&dq=Tensegrity:+Structural+Systems+for+the+Future&ots=85AsVSIo_l&sig=amBKpKIADyZVPlpc0vVQ03g0OUI#v=onepage&q&f=false

[3] Burkhardt R. W.: A Practical Guide to Tensegrity. Cambridge, USA, 2008, MA 02142-0021 http://www.angelfire.com/ma4/bob_wb/tenseg.pdf

[4] Kmeť S., Platko P., Mojdis M.: Design and Analysis of Tensegrity Systems, The International Journal "Transport & Logistics", Vol. 18, 2010, pp. 42-49

The Efficiency Rate of a Steam-Water Injector

Masa Bukurov, Sinisa Bikic, Miljana Prica

University of Novi Sad, Faculty of Technical Sciences
Trg Dositeja Obradovica 6, 21000 Novi Sad
mbukurov@uns.ac.rs, bika@uns.ac.rs, miljana@uns.ac.rs

Abstract: This paper analyses the influence of relevant parameters on the efficiency rate of a supersonic injector and its parts. Forced condensation in the injector is achieved by the mixing of cold water and steam with the goal of getting higher pressures of hot water (6-12 bar) with an outlet temperature of 70-80 °C to enable distant transportation of hot water and heating. Although the energy potential of pressure is not significant compared to inlet energy of steam, it is of importance since it represents the potential to realize external work. The complex flow process through the mixing chamber, the most important part of the injector, is presented with a diagram of forced condensation energy change, flow and geometry changes of the mixing chamber and the distribution of the relevant forces on the borders of the mixing chamber. It is shown that higher efficiency rates are achieved if condensation is speeded up by the reduced mixing of cold water and steam. Analyses are done according to analytical laws and experimental investigations of a steam-water injector prototype, with the data enclosed. The efficiency rates of the mixing chamber ranges from 60 to 85%, depending upon the following: the injection coefficient, the inlet pressures and the temperatures of the cold water and steam (and the desired outlet hot water temperature and pressure). Investigations are mostly directed to the particular needs of energy and process devices and the significance of the Mach number was not especially emphasized in them.

Keywords: steam-water injector; efficiency rate; supersonic steam-water injector; forced condensation

1 Introduction

The main purpose of the considered steam-water injector is to substitute the pump and heat exchanger, which is a great challenge for numerous applications [1, 2]. The relatively cheap acquisition of a steam boiler with low-demanded performances eliminates the need for electric energy supply and makes possible the autonomy of certain process. The remaining important question is if it is possible to get low outlet temperature and relatively high pressure (6-12 bar, $\dot{m}_w / \dot{m}_s < 5$) with a steam-water injector.

Due to very high velocities of steam (v_s) at the outlet of Laval nozzle of about 600-800 m/s, velocities of mixture through mixing chamber ($v_{mix\ mc}$) are also high, so the whole flow process of mixing and condensation happens very fast. It is of importance that the transition from supersonic into subsonic flow is realized in vicinity of the throat of mixing chamber, which, as a matter of fact, occurs no matter if all steam is condensed or water is completely mixed with condensate. This fact, experimentally confirmed, indicates that the homogeneity of flow field and uniform mixing are not necessary in order to achieve the transition from supersonic into subsonic flow at the end of mixing chamber or near to it.

Sound velocity (c), i.e. the Mach number (M), is the main criterion for such a complex and quick energy flow process through mixing chamber, which is in accordance with dynamic equation of compressible flow without losses in which balance of flow is reached by equilibrium of only inertial and elastic (compressible) forces. Isentropic-polytrophic changes of flow parameters in the transition zone ($M \approx 1$), shown in diagram in Fig. 1 [3, 4], are valid also for the flow in vicinity of the mixing chamber throat. Smooth transition - without shocks - from supersonic into subsonic flow is achieved also during experimental investigations.

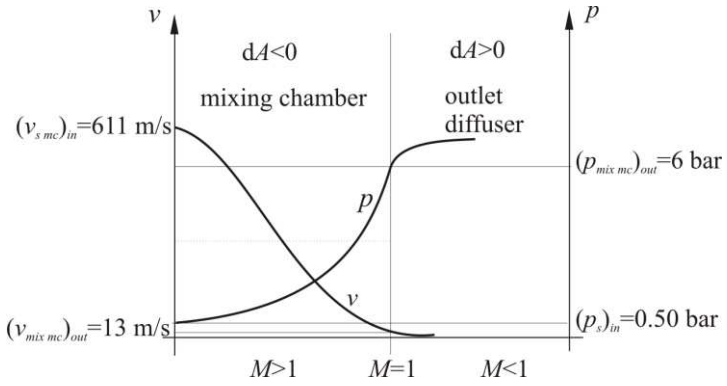

Figure 1

Steam-water mixture polytrophic changes of pressure (p) and velocity (v) through mixing chamber for supersonic transition as a function of Mach number (M) and cross-section change dA

The energy diagram, which is very important for the physical representation and analysis of flow, can be gained indirectly in this case, thanks to the energy diagram of forced condensation. The modified Mollier's diagram of forced condensation, connected with longitudinal geometry change (change of the cross section) of the mixing chamber, accurately presents energy changes along mixing chamber (p, t, h).

The application of reliable momentum equation, which is valid without any limitations for flow process in the mixing chamber, gives data about the pressure change in it, depending on the inlet and outlet parameters.

The efficiency rate of the steam-water injector η_{inj} is presented with:

$$\eta_{inj} = \eta_{L+cw\,nozz} \cdot \eta_{mc} \cdot \eta_d \tag{1}$$

where

$\eta_{L+cw\,nozz}$ – is the efficiency rate of the Laval nozzle and the cold water nozzle

η_{mc} – is the efficiency rate of the mixing chamber

η_d – is the efficiency rate of the outlet diffuser.

The efficiency rate of the Laval nozzle for steam and outlet diffuser for hot water are well known. The efficiency rate of the mixing chamber is determined according to the known energy characteristics of: cold water at disposal $(p, t)_{cw}$, steam at disposal $(p, t)_s$ and the desired characteristics of the hot water (mixture) in the throat of mixing chamber $(p, t)_{mix}$.

2 Results and Disussion

2.1 Flow Model in Mixing Chamber

The mixing chamber, which is 10 cm long, is fictively divided into 10 sections, each 1 cm long. The inlet cross section is 4.2 cm in diameter, and the outlet is 1 cm. The changeable orifice inlet of cold water can be regulated in a range from 0.5 to 3 mm (Fig. 2).

The assumption is that forced condensation in the mixing chamber forms following the flow model (Figs. 3, 4 and 5):

- Cold water gradually mixes with steam and condenses, and during this process, it is constantly in contact with mixing chamber walls, with no steam present. The velocity of water part, which mixes (v_{wm}) and is heated, increases until it has reached the velocity of steam and condensate. From that point forward, their velocities are the same (v_{mix}). The rest of water (v_{wrest}), which is located along chamber walls, accelerates from inlet velocity ($(v_w)_{mc\ in}$) gradually to mixture velocity at the outlet of mixing chamber $(v_{mix})_{mc\ out}$. The temperature of both these parts of water is almost the same and increases almost linearly through whole chamber.
- Steam mixes with certain parts of the water for mixing and condensates uniformly along the mixing chamber. Steam fulfills a larger part of mixing chamber. It is present in the throat and after mixing chamber throat (referent point). Steam is dominant at about 80 mm length from inlet section of chamber. In this region are valid compressible flow laws with

parameters of wet steam shown in Fig. 5. The velocity of the steam (v_s) suddenly decreases from inlet velocity from Laval nozzle (($v_L)_{in}$=611 m/s) to outlet velocity from mixing chamber (($v_{mc})_{out}$=13 m/s). In the vicinity of the mixing chamber throat, the velocities of steam (v_s) and mixture (v_{mix}) are equal.

- The velocity profiles in certain sections of mixing chamber show a tendency to equalize velocities of all components in the vicinity of the mixing chamber throat.

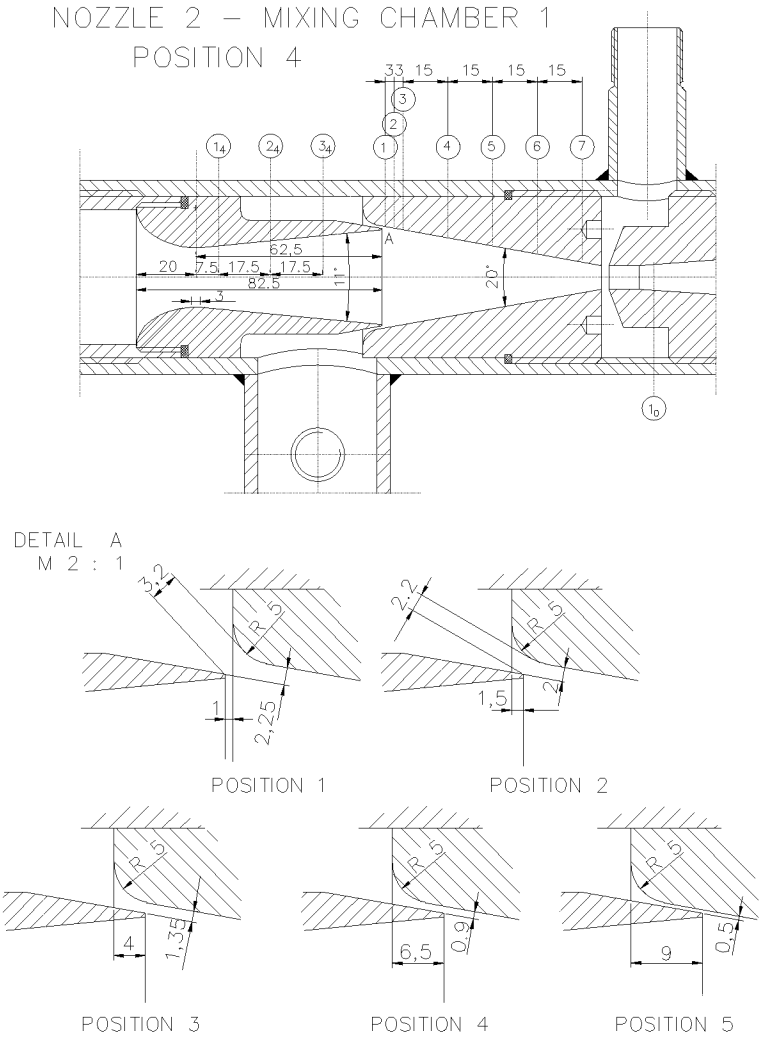

Figure 2
Configuration of cold water nozzles orifices

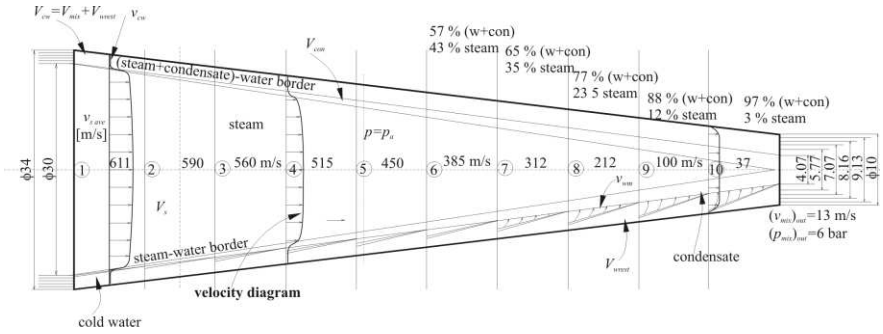

Figure 3
Flow model of forced condensation in mixing chamber

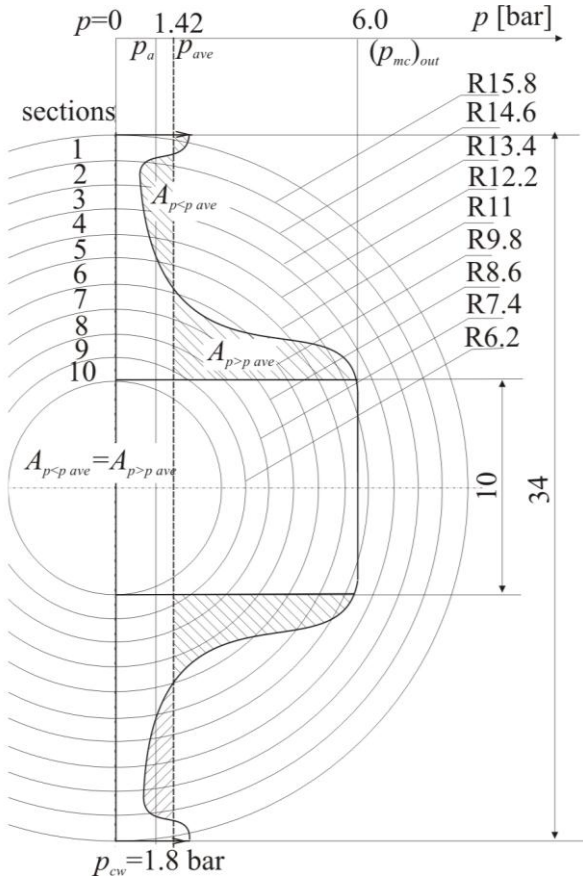

Figure 4
Pressure distribution along mixing chamber walls

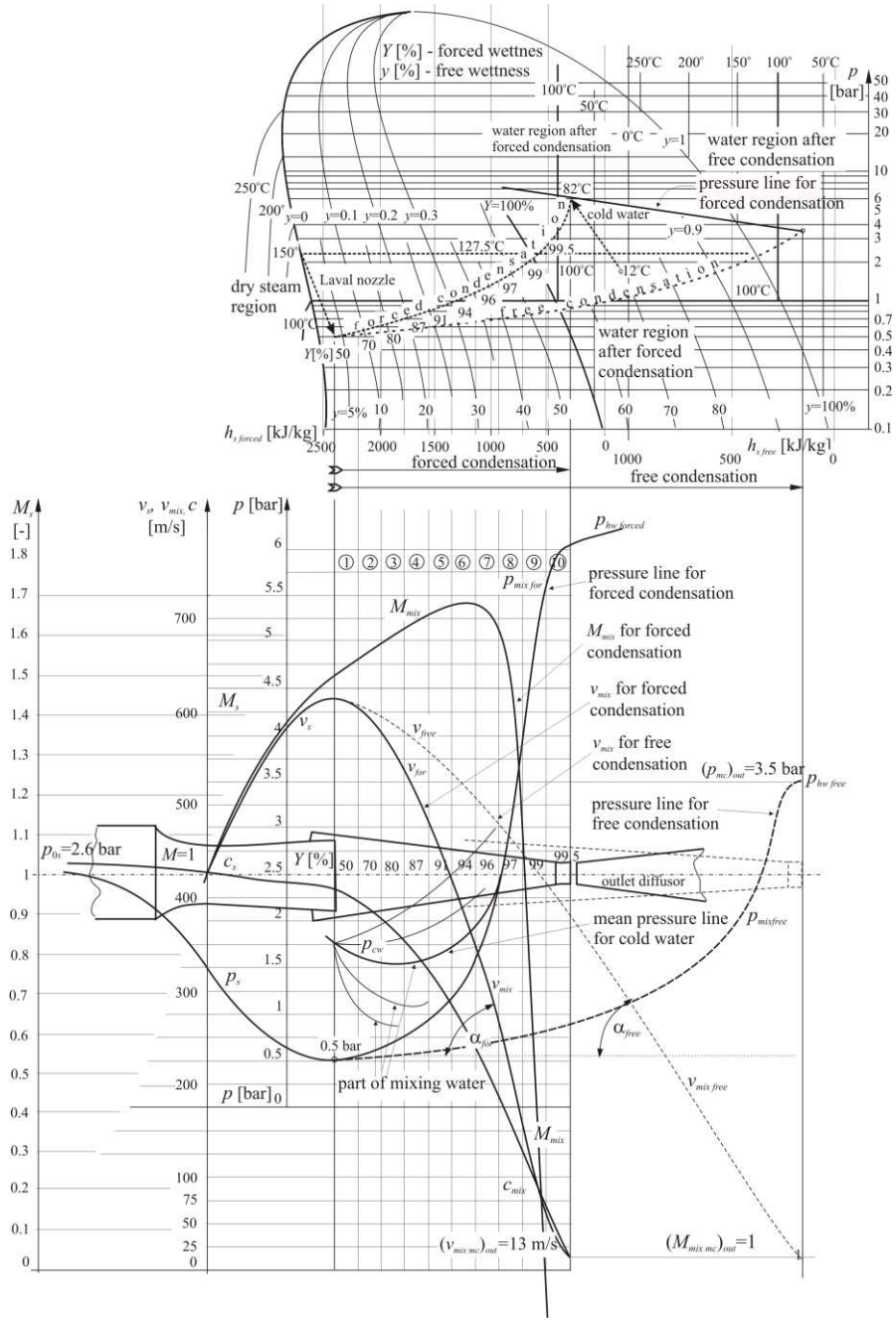

Figure 5

Diagram of Mach number, pressure, velocity, temperature and density for forced condensation

The condensation core's forming rate is greater under forced condensation according to Deich and Filipov [5]. The condensate has significantly lower velocity compared to surrounding steam due to the density difference ($\rho_w/\rho_{s\,ave}$=500).

The pressure diagram of steam and mixture contains points of inlet pressure of steam, the average pressure of mixture (gained from momentum equation) and the outlet pressure of the mixture – hot water ($(p_{mix})_{out}$) (Fig. 1). An abrupt mixture pressure rise happens in the immediate vicinity of the mixing chamber throat, i.e. where M=1, according to diagrams given in Fig. 1. and Fig. 5. Experiments [3, 4] confirm that the pressure change through mixing chamber is stationary, stable and smooth, without visible and sensed shocks and disturbances. The pressure diagram (Fig. 4) shows the pressure at the inner side of mixing chamber wall. Each circle in Fig. 4 corresponds to a certain section (Fig. 3) for which pressure is demanded.

2.1.1 Losses in Mixing Chamber

The efficiency rate of the mixing chamber depends on different kinds of losses:

- loss due to friction on the chamber walls;
- loss due to local drags, oblique and normal shock waves of different origin, and intermolecular reactions (friction of water, steam and condensate);
- local losses of cold water and steam at the entrance into the mixing chamber and mixture at the outlet of the mixing chamber.

Friction losses on the inner side of conical wrap of the mixing chamber are manifested as a pressure drop which is present in whole flow cross section [6]. This downstream pressure drop diminishes outlet pressure in the mixing chamber throat. Water heat increases due to friction cannot be transformed into pressure energy because of its low energy potential. Losses due to friction on the chamber walls are not small compared to the pressure rise along the chamber. If the average velocity of the rest of the water, near to conical wrap, is v_{wrest}=10 m/s, the pressure drop through mixing chamber is about Δp=3000 Pa, which is 0.5 % compared to the outlet pressure of 6 bar. If the average velocity is 20 m/s, the pressure drop through the mixing chamber due to friction would be 12,000 Pa, which is, compared to outlet pressure of 6 bar, 2%. Because of this, it is important to disable greater velocities of water layer, which is desired to be in constant connection with walls of mixing chamber.

The internal energy of steam consists of intermolecular and intramolecular interactions, as well as the energy of random molecular movements, which depends on temperature. If there are no chemical reactions in the fluid, all changes in internal energy are due to thermal changes in the fluid, i.e. due to changes in the kinetic energy of molecular movement and the molecular interaction. Since in the larger part of mixing chamber there is steam, which can be considered as ideal gas in that part, its internal energy depends only on the starting and end temperatures.

Losses due to local changes of stream flow, as well as the occurrence of waves of different origin, can be considered as irreversible, compared to the pressure drop decrease which appears no matter where the local resistance takes place. Partial heat increase, which occurs downstream from these disturbances, cannot diminish the downstream pressure drop either. Normal stationary shock waves cannot be transmitted or occur in mixing chamber because of the suppressed effect of the inlet cold water.

Losses due to friction and mixing of the steam, water and condensate are hard to estimate, but they can be diminished if continuity in changes of temperature, steam and velocity of all mixture components are reached. Continuity means uniform:

- pressure rise of: steam, condensate, water and mixture,
- velocity drop of: steam, condensate and mixture,
- water temperature increase.

Continuity in velocity distribution through a cross section of the mixing chamber along its whole length, along with maintaining steady water film along chamber walls, probably presents optimal flow model.

Mechanical efficiency rate of mixing chamber of water-water injector, which takes into account the friction of the mixing water, as well as the friction of the water and the walls of the mixing chamber, according to Menegay [7], is 25% for a relative chamber wall roughness of 0.03. If this value is taken for the steam-water injector, with assumption that condensate is a drive fluid and cold water is sucked one, there would appear difference in their kinetic energies at the entrance and exit of mixing chamber of about 2 kW. The efficiency rate of the mixing chamber would change by about 0.5%.

Muffling of the supersonic flow, according to its nature, leads to a muffling of flow anomalies and disturbances. It is known in the transportation of mixtures that the flow of the mixture calms the whole one-phase fluid flow, which indicates that both flows are compatible and collectively characteristics of joint model provides a stable flow.

The reduction of losses in the muffled stream of supersonic mixture increases flow stability, which can be maintained in moderately non-stationary conditions. If increased disturbances result in the impossibility of maintaining a stable operation, these disturbances are source of losses which influence the energy efficiency of the process.

The estimation of pressure drop due to other mentioned resistances demands much more information of an experimental nature.

2.2 Supersonic Flow through Steam-Water Injector

The graphically presented distributions of the Mach number (M), pressure (p), and the velocities of steam and mixture (v_s, v_{mix}) are products of laboratory research [3, 4]. Credible pressure lines are those through Laval nozzle and outlet diffuser. The pressure gradient through mixing chamber is positive, with a steep inflection in front of the throat of the mixing chamber. The main results of the supersonic flow through the steam-water injector are presented in Fig. 5.

The discontinuity of pressure due to appearance of shockwaves at the exit of Laval nozzle, as well as in the mixing chamber, is not registered during the proper working of the device. Stable work requires a smooth pressure line throughout the injector, without shockwaves in any part of injector.

The relation between pressure and Mach number could be recognized in already existing law of compressible flow:

$$\frac{p_0}{p} = \left(1 + \frac{\kappa - 1}{2} M^2\right)^{\frac{\kappa}{\kappa - 1}} \tag{2}$$

where coefficient (κ-1)/2 and exponent κ/(κ-1) should be exchanged with variable and independent coefficients (κ-1)/2=m and κ/(κ-1)=n. It is assumed that in the throat of the mixing chamber prevails almost total pressure, due to the low velocities in the throat.

Deich and Filipov [5] gave the values for κ depending on wetness (y). If an assumption is made that the wetness during forced condensation (Y) is equivalent to the wetness during free condensation (y), according to eq. (2) total pressures may be calculated in the throat of mixing chamber.

Calculated values of mixing chamber outlet pressure from eq. (2) partly can be identified with polytrophic change in the mixing chamber.

The representative parameters of the conducted experimental research are:

- mass flow rate: steam $\dot{m}_s = 0.17$ kg/s , cold water $\dot{m}_w = 0.85$ kg/s ,
- dryness rate at: entrance into injector x=1, exit from Laval nozzle x=0.95,
- cross section: in front of injector ϕ40, exit of mixing chamber ϕ10, exit of diffuser ϕ25,
- velocities: cold water at the entrance of mixing chamber 4.1 m/s, steam at the entrance of mixing chamber 611 m/s, mixture in the throat of mixing chamber 13 m/s, mixture at the exit of diffuser 2.1 m/s,
- pressure of: steam in front of Laval nozzle $p_{0s} = 2.6$ bar , cold water at the entrance into mixing chamber p_{cw}=1.8 bar, mixture (hot water) at the exit of mixing chamber p_{mix}=6.0 bar, hot water at the exit of diffuser 6.66 bar,

- temperature of: cold water t_{cw}=12 °C, steam at the entrance of injector t_s=127.5 °C, mixture at the exit of injector t_{mix}=82 °C,
- enthalpy of: steam (total) in front of injector h_0=2718 J/kgK, at the entrance of mixing chamber h=2530 kJ/kgK (0.5 bar, 0.33 kg/m^3).

The maximal pressure of hot water is achieved by a rise in outlet downstream pressure (back pressure), which represents a hot water pipeline pressure drop. The steam-water injector acts like a volumetric pump since the flow rate is not dependent upon the variation in outlet pressures.

During experimental research were obtained:

- stable flow for:

  - l_{mc}=100 mm and d_0=10 mm

- unstable flow with shocks and vibrations and flow rate decrease for:

  - l_{mc}=80 mm (for d_0=10 mm and d_0=8 mm)

  - l_{mc}=100 mm and d_0=8 mm.

In Fig. 5 is also given the comparative diagram for forced and free condensation (p, v).

2.3 Effect of Energy Transformation in Mixing Chamber

2.3.1 Water Velocity Distribution in the Mixing Chamber

The velocity distribution of the main water flows in the mixing chamber could substantially contribute to determining the complex process properties: mixing, condensation, heat transfer and losses.

Analyses of the flow through the mixing chamber, which are based on present knowledge about the process, show that basic losses through the mixing chamber are connected to losses due to inter-phases mixing and friction, and to the friction of the water (and maybe steam) and the walls of chamber.

Local losses at the entrance of the mixing chamber form a useful initial weak oblique shock of pressure, which is changed into a continual pressure wave and culminates at the entrance of the sonic flow region, in front of the chamber throat. The formation of condensation sources probably influences the pressure wave shape by changing frequencies, but it is neglected in this case.

It is reasonable to expect that the water heats, mixes with steam and condensates within optimal energy conditions. It seems that for the rest of water the following stands:

- heating is homogenous from inlet (12 °C) to outlet (82 °C) temperature, which agrees with experimental investigation of Malibashev [9];
- velocity increases from inlet (4.1 m/s) to outlet velocity (13 m/s);
- pressure grows from inlet (p_{cw}=1.8 bar, p_s=0.5 bar) to outlet (p_{mix}=6.0 bar).

2.3.2 Energy Transformation

The energy equation, which comprises kinetic, pressure and heat energy, is clearly presented through injector efficiency analyses.

The efficiency rate of the injector is defined as the ratio between the energy of outlet hot water and the sum of the energies of the steam and cold water at the entrance of the mixing chamber. It is accepted that all energies are useful: heat energy (q [J/kg]), kinetic energy ($v^2/2$ [m^2/s^2]) and pressure energy (p/ρ [m^2/s^2]). Kinetic and pressure energy have the same dimensions as heat energy (J/kg or m^2/s^2).

The sum of heat and pressure energies is enthalpy (h). The basic inlet energy is gained from steam, which is being condensed. Heat energy of about 2200 kJ/kg is mostly at disposal, and it is latent heat released from the steam during condensation.

All three kinds of energies are present during the forced mixing of cold water and steam through the injector, but with huge differences in energy content. Heat and pressure energy of steam are present in tens and hundreds of kJ, water pressure energy from 0.1 to 1 kJ/kg, and kinetic energy of steam during supersonic flow reaches several hundreds of kJ, while kinetic energy of water during standard flow does not exceed 0.05 kJ.

This means that in order to reach relatively high pressure of water, high heat energy of steam is not essential, since there is 2200 kJ/kg. (E.g. in order to increase pressure of 1 kg of water from 0 to 50 bar, 5 kJ is needed.) Water heating and cooling needs about 4.2 kJ/kgK of heat energy, which is a main energy requirement in comparison with medium kinetic and pressure energies.

Since flow processes are conducted continuously, each kind of energy (q, p/ρ, $v^2/2$, [kJ/kg]) is multiplied with mass flow rate [kg/s] and become power in kW. Therefore, energy efficiency is presented in the relation between exit and inlet powers (kW_{out}/kW_{in}).

The injector is designed according to its application. The investigated steam-water injector is used for heating, distant transportation and warm water distribution for different users. These applications require:

- outlet water which is not too hot (70-80 °C) due to diminishing heat losses along the way;

- outlet water pressure which is high enough to conquer hydraulic losses (6-8 bar);
- the inlet water temperature should be about 70 °C, lower than steam condensation temperature, in order to successfully conduct condensation process;
- the inlet water pressure depends on characteristics of the water sources. It can be atmospheric pressure, but if it is available, water under pressure can be used as well; in that way, the efficiency rate is increased and a higher pressure of warm water is more likely;
- inlet steam pressure can be low, which allows for using less quality steam (p_m=1,5-2 bar).

2.4 Efficiency Rate Definitions

Efficiency rates can be defined in different ways, with respect to the basic postulate that the efficiency rate is a relation between useful (or needed) and engaged. The terms "useful" and "needed" could be applied to numerous variables: energy (power, work), bulk (mass, volume), flow surfaces, pressures or their differences (inlet, outlet), concentrations, granulometric fractions, etc.

The definitions which describe process quality or quality of one of its segment are: universal efficiency rate, thermodynamic efficiency rate, kinetic energy efficiency rate, efficiency rate of mixing, etc.

Natural - free condensation of steam (static conditions) is conducted under constant pressure and almost constant temperature in the whole two-phase area. Numerous pressure diagrams through cylindrical, and sometimes conical mixing chambers, accept this law for flow processes too.

Water velocity at the inlet section of the mixing chamber $(v_{cw})_{mc\ in}$ and mixture velocity in the mixing chamber's throat $(v_{mix})_{mc\ out}$ are assumed according to the energy diagram.

Since the difference of latent heat of evaporation $\Delta\lambda$, for pressures ranges from 1 to 10 bar is only 3.5%, it can be considered that pressure and temperature do not influence the heat exchange between water and steam in the two-phase region.

The efficiency rate of the mixing chamber η_{mc} is:

$$\eta_{mc} = \frac{\left(h_{mix} + \frac{1}{2}v_{mix}^2\right)_{mc\ out} \dot{m}_{mix}}{\left[\left(h_s + \frac{1}{2}v_s^2\right)_{L\ out} \dot{m}_s + \left(h_{cw} + \frac{1}{2}v_{cw}^2\right)_{mc\ in} \dot{m}_{cw}\right]} \tag{3}$$

The efficiency rate which is used for heat pumps is validated with one of the following pressure increase efficiency rates ($(\eta_{cw})_p$, $(\eta_s)_p$):

$$\left(\eta_{cw}\right)_p = \frac{p_{mix}}{p_{cw}};\ \left(\eta_s\right)_p = \frac{p_{mix}}{p_s} \tag{4}$$

The commonly used efficiency rate η_p for small injection coefficients $u_{cw\ p}$<3 ($u_{cw\,p} = \dot{m}_{cw}/\dot{m}_s$) is given as following:

$$\eta_p = \frac{p_{mix} - p_s}{p_s - p_{cw}} \tag{5}$$

where:

p_{mix}, p_{cw} and p_s are the pressures of mixture, water and steam [Pa].

For higher injection coefficients the next relation is valid:

$$\eta_p = \frac{p_{mix} - p_{cw}}{p_s - p_{cw}} \tag{6}$$

For both relations, the denominator is the same and can be considered as engaged pressure.

2.5 Efficiency Rate of Laval Nozzle η_l

In the ideal case, the flow through the nozzle and diffuser is isentropic. But in the actual case, friction exists and affects in following ways:

- reduces the enthalpy drop and the final velocity of steam
- increases the final dryness fraction and specific volume of the fluid
- decreases the mass flow rate.

The efficiency of the nozzle depends upon:

- the material it is made of and its smoothness,
- the size, shape and angle of the nozzle divergence,
- the nature of fluid flowing and its state,
- the fluid velocity and the turbulence in nozzle flow.

The efficiency rate of the Laval nozzle for superheated and wet steam flow is determined by many experimental results with satisfying accuracy. So far, the transformation of friction through the Laval nozzle into thermal energy is not explained enough. The nature of energy loss in the case of a normal shockwave in the diffuser of the Laval nozzle can be explained. The inlet parameters of the steam in the mixing chamber can be determined if the efficiency rate of the Laval nozzle is known.

The efficiency rate of the Laval nozzle is based on knowing the investigated features of the convergent nozzle, whose efficiency rate is dominant in the equation for η_L.

The complete diagram of the efficiency rate of Laval nozzle η_L is shown in Fig. 6 with three curves: real nozzle (with friction) η_L, theoretical η_{Lth} and with post expansion η_{Le}.

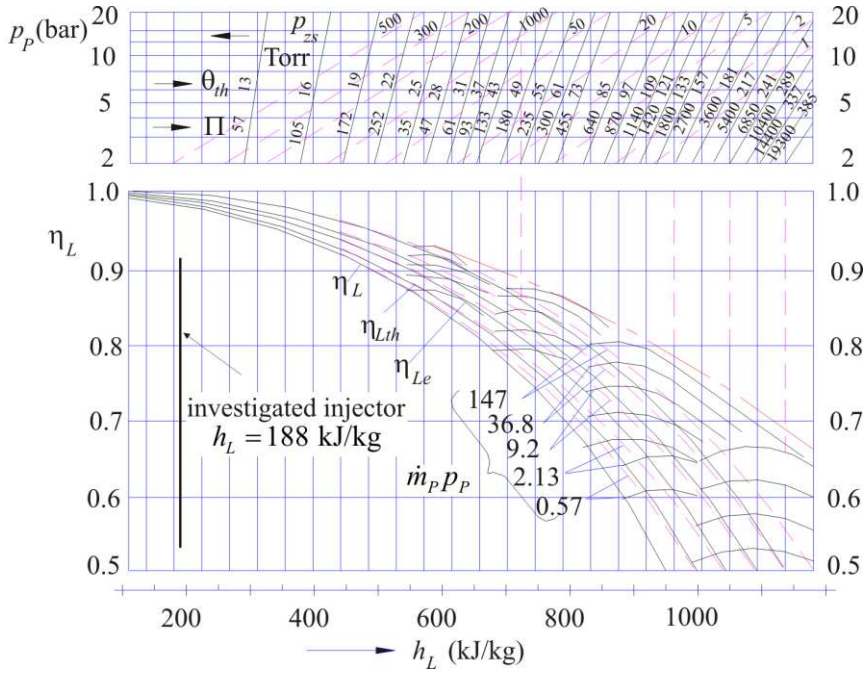

Figure 6

Efficiency rates of Laval nozzles for smooth surfaces and shock less processes ($p_s\,\dot{m}_s\,[\mathrm{bar}\cdot\mathrm{kg/s}]$; $\Delta h_L = h_{Lin} - h_{Lout}$) according to Hess [4]

The efficiency rates' theoretical curves of the Laval nozzle with post expansion η_{Le}=f(h_L) are parallel and with one maximal value. Only experiments can show the magnitude of post expansion in order to achieve the maximal efficiency rate for the given Laval nozzle.

Each of the curves is given for the certain value of the Reynolds number or characteristics of flow $\dot{m}_s p_s$. Divergent section is with central angle of 10-20°. In this range of angles, the change in efficiency rate is within tolerable limits. During the flow of steam through the Laval nozzle, the boundary layer is turbulent.

In the representative case, where $\dot{m}_s = 0.17$ kg/s, p_{0s} =2.6 bar, h_0=2718 kJ/kg, $(h_0)_{L\ out}$=2530 kJ/kg, Δh_L=188 kJ/kg and $\dot{m}_s p_{0s} = 0,442$;

- the efficiency rate of the Laval for all kind of energies is η_L=0.98.
- the power loss through Laval nozzle is 0.17·188·0.02=0.64 kW.
- The steam power at the outlet of the Laval nozzle is 2718·0.17-0.64=461.42 kW, where
  - kinetic power is ((611^2/2)·0.17)/1000=31.73 kW
  - enthalpy power (thermal and pressure power) is 2530.0.17=430.1 kW.

The outlet pressure should not be too low compared to the nozzle throat pressure, in order to eliminate the possibility of a shock wave forming in the supersonic nozzle section, which does not contribute to the proper operation of the injector. The outlet pressure from the Laval nozzle should be about 0.4-0.5 bar (absolute pressure), which allows for the usage of low-pressure steam in suction of cold water on atmospheric pressure.

2.6 Overall Efficiency Rate of Laval and Cold Water Nozzle

According to [10], the efficiency rate for designed cold water nozzle for lost kinetic energy (without thermal energy) is estimated as η_{cw}=0.90.

For outlet water velocity of a nozzle of 4.1 m/s:

- the intake kinetic power of the cold water is (4.1^2/2)·0.85=7.144 kW,
- the lost kinetic power through the cold water nozzle is 7.144·0.1=0.714 kW
- the kinetic power at the inlet of the mixing chamber is 7.14·0.90=6.43 kW
- the efficiency rate of the cold water nozzle, which refers to all kind of energies, is (42.738+7.14·0.9+0.153)/(42.738+7.144+0.153) =49.317/50.035=0.986.

The power loss through the Laval nozzle is 0.64 kW, and for the cold water nozzle it is 0.714 kW.

The total steam power at the entrance of the injector (462.06 kW), and cold water (50.035 kW) is 512.09 kW.

The total power of steam and cold water at the inlet of the mixing chamber with embraced losses is:

512.09-0.714-0.64=510.74 kW.

Overall efficiency rate of Laval and cold water nozzle is

$\eta_{L+cwnozz}$=510.74/512.09=0.99.

2.7 Efficiency Rate of Outlet Diffusor

The efficiency rate of the outlet diffuser is discussed according to several assumptions:

- The diffuser is filled with an homogeneous stream of hot water without steam bubbles;
- The heat losses are neglected;
- Condensation is completely finished in the throat of mixing chamber.

With assumption that velocity profile uniformly decreases through diffuser cross section, the efficiency rate (without thermal energy) – cold η_{dc} is:

$$\eta_{dc} = \frac{\left(p_{out} - p_{in}\right)_d}{\frac{1}{2}\rho\left(v_{in}^2 - v_{out}^2\right)_d} = \frac{\left(p_{out} - p_{in}\right)_d}{\frac{1}{2}\rho\left(v_{in}\right)_d^2\left[1-\left(\frac{A_{in}}{A_{out}}\right)_d^2\right]} \tag{7}$$

The outlet diffuser is designed with diameters ratio 1:3 (10:30) and half angle α=6°; for which is, according to [10] efficiency rate η_{dc}=0.95. The efficiency rate of the outlet diffuser of 0.95 refers to the lost kinetic energy of 5%. For η_{dc}=0.95 and an inlet velocity of 13 m/s and an outlet velocity of 2.1 m/s, the lost power is $P_{lost} = \left(v_{in}^2 - v_{out}^2\right)\dot{m}_{mix}\left(1-\eta_{dc}\right)/2 = 0{,}0042$ kW. From this it follows that the efficiency rate of outlet diffuser is η_d=1.

According to equation (7), which is in accordance with experimental results, the absolute pressure of the hot water at the outlet of the diffuser is:

$(p_d)_{out}$=6.66 bar

2.8 Efficiency Rates of Mixing Chamber (η_{Mc}) and Injector (η_{Inj})

According to known characteristics of hot water at the outlet of the diffuser, as well as the diffuser's efficiency rate, the parameters in the throat of the mixing chamber are: $p_{mc\ out}$=6.0 bar, $v_{mc\ out}$=13 m/s, $t_{mc\ out}$=82 °C, and $\dot{m}_{mc\,out} = 1.02$ kg/s. Steam is completely condensed at the outlet of the mixing chamber.

Hot water power at the outlet of the mixing chamber is:

$(82 \cdot 4.19 + 132 \cdot 0.5 + 0.6) \cdot 1.02 = 437.25$ kW.

Power at the inlet of the mixing chamber is 510.74 kW.

The efficiency rate of the mixing chamber is

$\eta_{mc} = 437.25/510.74 = 0.856$.

The efficiency of the whole injector is given by eq. (1):

$$\eta_{inj} = \eta_{L+cwnozz} \cdot \eta_{mc} \cdot \eta_d = 0.99 \cdot 0.856 \cdot 1.0 = 0.847 .$$

The small difference in the efficiency rates of the mixing chamber and the whole injector is a result of the small powers that are spent in: the Laval nozzle, the cold water nozzle and the outlet diffuser. The efficiency rate of the Laval nozzle is the relation between the total energies at its outlet and inlet section, while in the case of the cold water nozzle and the outlet diffuser, losses are connected only to the change of kinetic energy, which is several times smaller than total power that is being transmitted through them.

The mixing chamber efficiency rate cannot be determined without knowing the flow-phases and energy transformation through them. Without any doubt, part of the pressure increase is fulfilled due to the kinetic energy of the steam which enters into mixing chamber.

The basic question without proper answer is whether it is possible to control and manage the process of complex changes through the mixing chamber or whether the process depends, to the greatest extent, on the thermo dynamical nature of the free condensation of steam. No matter the answer to this unanswered question, the efficiency rate of the mixing chamber can be determined for some assumed cases. The flow through injector is characterized by complex processes of steam, condensate, cold and hot water inter reactions.

Conclusions

In addition to the known and frequent transformation of thermal into kinetic energy, the transformation of steam thermal energy into pressure energy of a mixture in a supersonic stream, which is possible by condensation, using latent heat, was also confirmed.

During experimental investigation, the stable work of a steam-water injector (without pulsations and shocks) was established. In order to reach stable work, it is necessary that the flow process through all parts of the injector is in balance. This means: The sound velocity of steam in the throat of Laval nozzle and supersonic velocity are reached at its outlet; and supersonic compressible flow prevails through the mixing chamber and subsonic flow of hot water prevails through the outlet diffuser of steam-water injector.

The flow through the Laval nozzle depends on the geometry of the nozzle and the inlet state of the steam. The parameters at the outlet section of the Laval nozzle are dictated by the steam. The inlet cold water pressure can vary depending on the water source.

During the proper operation of the steam-water injector, water does not evaporate in the mixing chamber; otherwise it would be noticed by unsteady effects. The steady range of the steam-water injector operation depends on a limited coefficient of injection.

The inlet section of the mixing chamber is filled with cold water (orifice with small thickness), i.e. mixture of steam and cold water (Y=0.5). In the greater part of mixing chamber is a two phased region, which is completely condensed in the vicinity of the mixing chamber throat. Supersonic flow exists in the whole mixing chamber; at the beginning, the average velocities of steam are high, and in the vicinity of the throat, the velocity of the mixture are considerably lower. At the entrance of mixing chamber, the Mach number is greater than unity, M>1, because of the expansion of the steam through the Laval nozzle, and in the environment of the throat M≈1, because of very low sound velocities in the very wet steam.

In the throat of the mixing chamber, changes in the flow parameters without shocks are with high gradients and pretty independent of the size and changes of the Mach number through the mixing chamber.

In this paper is presented the recommended velocity distribution of the active and inert components of cold water. It is impossible to determine losses in the mixing chamber without knowing the velocity distribution of the water that is actively and directly mixed with steam (v_{wmix}) and of the water which flows further on and continuously, partially and actively mixes with steam (v_{wrest}). The efficiency rate of the injector device shows that major losses happen in the mixing chamber. The losses are the immediate consequences of considerable friction between the steam, condensate, and active and rest (inert) water. It seems that the mixing chamber walls cause the most significant loss, which means that the better velocity profile is the one with higher gradient in the zone of intensive steam and water mixing.

Forced condensation, compared to free condensation, increases the mixing chamber outlet pressure of hot water. The supersonic mixing chamber is actually a diffuser through which pressure rises downstream. Pressure rise during supersonic flow has the same nature as flow through diffuser in subsonic flow.

The average pressure in the mixing chamber, gained from momentum equation, enables a more accurate determination of the pressure distribution through the mixing chamber. In this way the determined average pressure agrees with the actual pressure.

Acknowledgement

This work was supported by Serbian Ministry of Science in the framework of the project 31058.

Appendix

Nomenclature

A	[cm^2]	cross section area
c	[m/s]	sound velocity
d	[m]	diameter
h	[J/kg]	enthalpy
l	[m]	length

M	[-]	Mach number
m	[-]	coefficient
$\dot{m}$	[kg/s]	mass flow rate
n	[-]	coefficient
P	[W]	power
p	[Pa]	pressure
Q	[m^3/s]	flow rate
q	[J/kg]	heat energy
T	[K]	temperature
t	[°C]	temperature
u	[-]	injection coefficient
V	[m^3]	volume
v	[m/s]	velocity
X	[%]	dryness during forced condensation
x	[%]	dryness during free condensation
Y	[%]	wetness during forced condensation
y	[%]	wetness during free condensation
α	[°]	half angle of diffuser
η	[-]	efficiency rate
κ	[-]	isentropic exponent
λ	[J/kg]	latent heat
ρ	[kg/m^3]	density

Subscripts

0	total
a	atmospheric
ave	average
c	cold
con	condensed
cw	cold water
d	diffuser
hw	hot water
i	section number (*i*=1,2,...10)
in	inlet
inj	injector
L	Laval nozzle
Le	Laval nozzle with post expansion
l	losses
lost	lost
m	manometric,
mc	mixing chamber
mix	mixture
nozz	nozzle
out	outlet
s	steam

th throat
w water
wm water for mixing
wrest the rest of water

References

[1] H. El-Dessouky, H. Ettouney, I. Alatiqi, G. Al-Nuwaibit, Evaluation of Steam Jet Ejectors, Chemical Engineering and Processing 41, pp. 551-561, 2002

[2] M. Trela, R. Kwidzinski, D. Butrymowicz, J. Karwacki, Energy Analysis of Two-Phase Steam–Water Injector, Applied Thermal Engineering 30, pp. 340-346, 2010

[3] M. Bukurov, Research on Supersonic Steam-Water Injectors Characteristics (in Serbian) Doctor Thesis, Faculty of Technical Sciences, Novi Sad, Serbia, 2004

[4] M. Bukurov, S. Tasin, S. Bikić, Modified Diagram for Steam-Water Injector Mixing Chamber, Annals of the Faculty of Engineering Hunedoara - Journal of Engineering, Fascicule 4, No. VII, pp. 75-82, ISSN 1584-2665, 2009

[5] M. E. Deich, G. A. Filipov, Gas Dynamics of Two-Phase Flow (in Russian) Energy, Moscow, Russia, 1968

[6] Y. Yamazaki, T. Nakayama, T. Narabayashi, H. Kobayashi, T. Shakouchi, Effect of Surface Roughness on Jet Pump Performance, JSME International Journal, Series B, Vol. 49, No. 4, pp. 928-932, 2006 [7] P. Menegay, A Computational Model for Two-Phase Flow, Dissertation, State University, Virginia, 1997

[8] F. Hess, The Efficiency of Motive Nozzles in Steam-Jet Pumps, Proceedings of 1st Symposium on Jet Pumps and Ejectors and Gas Lift Techniques, D1-11, BHRA, UK, 1973

[9] S. K. Malibashev, Experimental Investigation of Transparent Models of Steam-Water Injector with a Convergent Nozzle, Atomic Energy, Vol. 90, No. 6, pp. 469-474, 2001

[10] Fluid Flow Data Book, General Electric Company Corporate Research and Development, NY, 1973

Method of Data Center Classifications

Krisztián Kósi

Óbuda University, Bécsi út 96/B, H-1034 Budapest, Hungary
kosi.krisztian@phd.uni-obuda.hu

Abstract: This paper is about the Classification of big data centers, based on top500.org's data. The classification begins with data weighting and Multidimensional Scaling. Multidimensional Scaling produces 3D data. The clustering method, K-means, helps to classify the data. Nine different groups of data centers have been identified with appropriate parameters.

Keywords: Multidimensional Scaling; MDS; K-means; C-means; Clustering; Petri Net; Classical Multidimensional Scaling; CMDS

1 Introduction

Two methods were used in this classification. The first is Multidimensional Scaling, also known as MDS. Multidimensional Scaling was developed originally by John W. Sammon Jr. in 1969 [1]. Many another variants have been developed; the most common ones are Classical Multidimensional Scaling (CMDS), and Non-Metric Multidimensional Scaling. In this paper CMDS was used for problem solution. Classical Multidimensional Scaling allows many fine tuning and it is good enough for that method. Multidimensional Scaling can be used to reduce multidimensional problems into two or three dimensions [2].

Multidimensional Scaling has a wide spectrum of applications, such as Agricultural Economics [3], biology [4] Wireless Sensor Network Localization [5], Social Network Analysis [6], and Psychophysics [7].

One of the most popular clustering algorithms is K-means, also known as C-means. K-means has many implementations. Some of the most interesting implementations are High Parallel Implementation [8], Recovery for Burst-Mode Optical Receivers [9], and Clustering over a Peer-to-Peer Network [10].

2 The Main Algorithm

The algorithm consists of three main steps. (Fig. 1) The first major step is data preparation for MDS [13]. The second one is the execution of MDS, which creates a two or three dimensional point cloud. The last step is clustering with K-means. The algorithm is very flexible; it has the possibility to change or tune its various parts.

Figure 1
The main algorithm

In the overall look, the algorithm is sequential, but some steps may have parallel implementation. The most convenient implementation can be done by the use of R. R is a free statistic environment [12], and most of the MDS methods and a lot of clustering algorithms are implemented in R. It can be used simply as a function call.

3 Data Preparation

The first step is the preparation part. This part is about putting the data into a starting matrix and creating a distance matrix from it. This part is one of the most flexible parts. There are possibilities for weighting the problems and determining which attributes are more significant than the others. For distance definition, a wide assortment of various norms is available.

The starting matrix must contain measurable values. Classical Multidimensional Scaling works just on numbers. In the matrix, the row index denotes the number of the appropriate element, while in the columns the attributes are numbered (Table 1).

The next step is optional. Weights can be applied to the starting matrix with the following tensor (1), where $g_{ii} > 0$ is the weight and i represents the number of the appropriate attribute. This tensor recreates the matrix, which is more suitable for the problem. Expression (1) describes the square of the distance between elements *i* and *j*.

Table 1
Start Table

	Attr. 1	Attr. 2	Attr. 3	…	Attr. n
1	$x_1^{(1)}$	$x_1^{(2)}$	$x_1^{(3)}$	…	$x_1^{(n)}$
2	$x_2^{(1)}$	$x_2^{(2)}$	$x_2^{(3)}$	…	$x_2^{(n)}$
3	$x_3^{(1)}$	$x_3^{(2)}$	$x_3^{(3)}$	…	$x_3^{(n)}$
4	$x_4^{(1)}$	$x_4^{(2)}$	$x_4^{(3)}$	…	$x_4^{(n)}$
5	$x_5^{(1)}$	$x_5^{(2)}$	$x_5^{(3)}$	…	$x_5^{(n)}$
⋮	⋮	⋮	⋮	⋱	⋮
m	$x_m^{(1)}$	$x_m^{(2)}$	$x_m^{(3)}$	…	$x_m^{(n)}$

$$\left[\underline{x_i} - \underline{x_j}\right]^T \begin{bmatrix} g_{11} & 0 & 0 & \cdots & 0 \\ 0 & g_{22} & 0 & \cdots & 0 \\ 0 & 0 & g_{33} & \cdots & 0 \\ \vdots & \vdots & \vdots & \ddots & \vdots \\ 0 & 0 & 0 & \cdots & g_{nn} \end{bmatrix} \left[\underline{x_i} - \underline{x_j}\right] \tag{1}$$

CMDS needs a rectangular, symmetric distance matrix, the main diagonals of which are zeros. Because the distant matrix is symmetric, the upper part can be filled in with zeros too. Computing the distance matrix means getting the norms of the difference of elements (2). The results have to be placed into the distance matrix.

For this purpose, an arbitrary norm can be applied.

$$\delta_{ij} = \left\| x_i - x_j \right\| \tag{2}$$

$$\underline{\underline{\delta}} = \begin{bmatrix} 0 & 0 & 0 & 0 & 0 & \cdots \\ \delta_{12} & 0 & 0 & 0 & 0 & \cdots \\ \delta_{13} & \delta_{23} & 0 & 0 & 0 & \cdots \\ \delta_{14} & \delta_{24} & \delta_{34} & 0 & 0 & \cdots \\ \delta_{15} & \delta_{25} & \delta_{35} & \delta_{45} & 0 & \cdots \\ \vdots & \vdots & \vdots & \vdots & \ddots & \cdots \end{bmatrix} \tag{3}$$

4 Multidimensional Scaling

The Multidimensional Scaling part reduces the multidimensional problem into a two or three dimensional one, which can be visualized.

CMDS is satisfactory for this purpose because the distant matrix is rectangular and symmetric.

The first step is to choose a vector $\underline{a}$ (4), where I is the dimension where the problem will be scaled.

Usually $\underline{a}$ will be two or three dimensional.

$$a_1, a_2, \dots, a_I \in \mathbb{R}^n \tag{4}$$

The norm of the difference between the elements of $\underline{a}$ has to be approximately equal to the distance (5).

$$\left\| \underline{a_i} - \underline{a_j} \right\| \approx \delta_{ij} \tag{5}$$

Vector $\underline{a}$ has to be chosen to minimize the following expression (6).

$$\min_{a_1 \dots a_I} \sum_{i<j} \left(\|a_i - a_j\| - \delta_{ij} \right)^2 \tag{6}$$

After the minimization, $\underline{a}$ will represent the problem in the selected dimension.

The upper part of the matrix is not necessary in R. In the literature, various *measures of goodness* are applied for assessing the result of a fitting. The so called Shepard plot describes the distances versus the dissimilarities in a 2D diagram [13]. If the individual data fit well to the $y=x$ line with little standard deviation, the fitting is good. If the points scatter too much around the line, the fitting is not too good. In the software package R that was applied for the calculations, the CMDS function used the best fitting algorithm, and no goodness measures were available as a default. For the purposes of this research, the default option was quite satisfactory.

The idea behind Multidimensional Scaling originally was the distance between two cities that is measurable with a ruler on the map. The main problem was how to recreate the map from the distance data. A popular example is flight paths between large cities in the USA.

5 Clustering

The clustering part is to decide which elements are in the same group. One of the most popular clustering methods is the K-means. The following Petri Net is about the base of the K-means clustering algorithm Fig. 5.

In an intuitive way, the clustering method creates groups around a set of points. Each group has a center point. A point belongs to a particular group if it is closer to the center point of this group than to the center points of the other groups.

The points created by MDS in the selected dimension are denoted as $(x_1, x_2, \dots, x_n)$ (7).

$$D = (x_1, x_2, \dots, x_n) \in \mathbb{R}^d \tag{7}$$

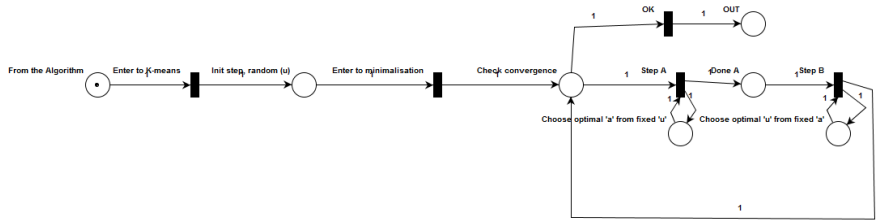

Figure 5
K-means described by a Petri Net

Each group has a center denoted by μ (8).

In the K-means algorithm, we need to know how many groups we have. It can be estimated from the figure of the finished Multidimensional Scaling.

$$(\mu_1, \mu_2, \dots, \mu_K) \in \mathbb{R}^d \tag{8}$$

Let us use the matrix a_{ij} of size $n \times K$ for describing the grouping of the individual elements. Let $a_{ij} = 1$ if elements x_i is in the group j, otherwise $a_{ij} = 0$ (10). Let $\mathcal{L}$ be defined by the following expression (9).

$$\mathcal{L} = \sum_{j=1}^{K} \sum_{i=1}^{n} a_{ij} \left\| x_i - \mu_j \right\|^2 \tag{9}$$

$$a_{ij} = \begin{cases} 1 \; x_i \; is \; assigned \; to \; j \\ 0 \; otherwise \end{cases} \tag{10}$$

$\mathcal{L}$ must be minimized under the following constraints: each element must belong to only one of the groups, i.e. for each j $\sum_{i=1}^{n} a_{ij}$. Furthermore each element must belong to one of the groups.

The minimization of $\mathcal{L}$ cannot be solved in closed form. There are many ways to solve this problem, but one of the good ways is to solve it with iteration.

Iteration steps:

0. Initialization: choose random centers.
a. choose optimal points to fixed centers.
b. choose optimal centers to fixed points.

Repeat ”a” and ”b” steps until convergence.

If the groups remain invariant, the algorithm can be stopped.

There are exact forms for the individual steps.

This minimization algorithm does not always work. However, in most of the practical cases it works perfectly.

Step ”a” can be computed with the following expression (11).

$$a_{ij} = \begin{cases} 1 \; if \; j = argmin_i \left\| x_i - \mu_j \right\|^2 \\ 0 \; otherwise \end{cases} \tag{11}$$

If a point can belong to more than one group according to (11), some arbitrary choice must be done.

Step ”b” can be computed with the following expression (12). n_j is the number of points in the cluster (13).

$$\mu_j = \frac{1}{n_j}\sum_{i:x_i is\ assigned\ to\ j} x_i \tag{12}$$

$$n_j = \sum_{i=1}^{n} a_{ij} \tag{13}$$

6 The Particular Data under Consideration

The starting data is from top500.org [14]. The attributes chosen from the list that was released in November, 2011 are: Year, Total Cores, Accelerator Cores, Rmax, Rpeak, Efficiency, Processor Speed, and Core per Socket. Rmax and Rpeak are performance values from the LINPACK benchmark in TFlops. The Rmax is the maximal performance that LINPACK achieved; Rpeak is a theoretical peak value.

Due to the fact that the order of magnitudes of the original data in the above specified fields roughly corresponded to the significance of the appropriate attributes, no special weighting technique has been applied. That is, $g_{ii} = 1$ was used in the main diagonal elements of the matrix in (1).

For describing the distances at the starting point, Euclidean metrics was chosen because it is independent of the direction.

The second step is scaling the data. The distance has been transformed by the logarithm function (14). In the logarithmic function, the very short distances come loose, and the very far distances come closer (14). In this manner, more compact and distinguishable structures can be obtained.

$$\log(1 + distance^{\alpha}), where\ (0 < \alpha < 1) \tag{14}$$

7 The Results by CMDS Using All Attributes

After applying the Multidimensional scaling for the all dataset, we obtained Fig. 6.

In Fig. 6 two well-defined big groups having internal fine structure can be revealed. To find the parameter according to which the whole set is split into these groups, one of the attributes can be neglected in MDS. This investigation can be done quite systematically. It was found that the attribute "Accelerator Cores" caused this splitting. According to Fig. 7, by neglecting this attribute, only one big group can be obtained (of course, with internal fine structure).

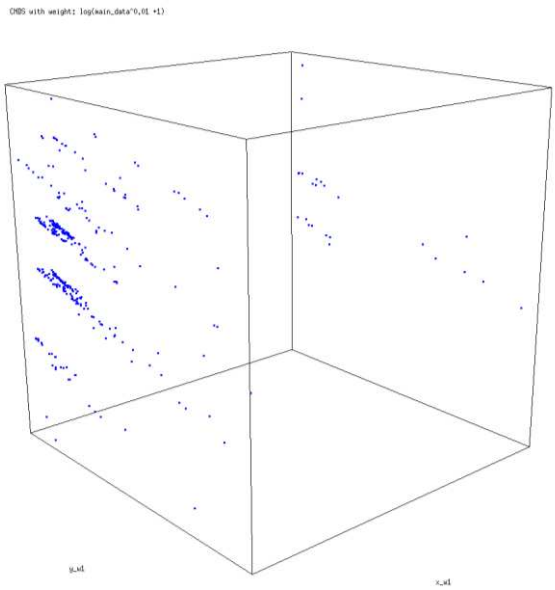

Figure 6
CMDS with $\log(1 + data^{\alpha})$ scaling

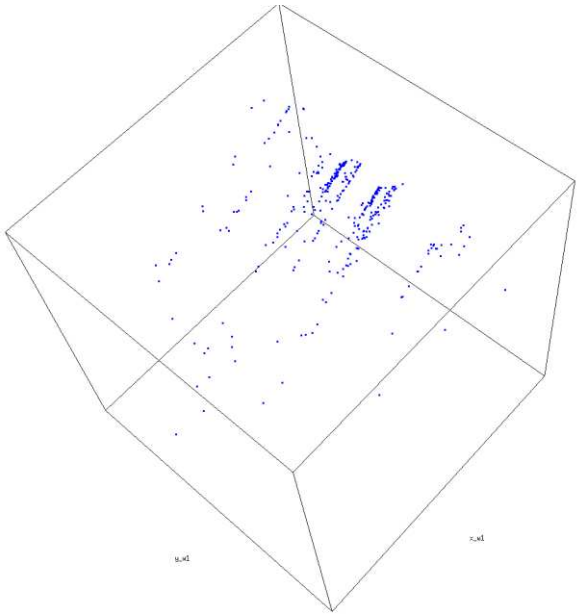

Figure 7
Without Accelerator Cores attribute, CMDS applied with $\log(1 + data^{\alpha})$ scaling

8 Classification of the Fiber Structure

In the first group, the significant splitting attribute was Rmax (Fig. 8). Dropping two other attributes ("Rpeak" and "Total Cores") caused a less significant reduction in the structure (Figs. 9, 10).

The same method was applied for the investigation of the other seven main groups with the results as follows:

The second group's main attribute is the Efficiency; the side attributes are Rmax and Rpeak.

The third group's main attribute is the Efficiency too, but the side attribute is Processor Speed.

The fourth group's main attribute is the Rpeak; the side attributes are Total Cores and Rmax.

The fifth group's main attribute is the Year; the side attributes are Core per Socket, Processor speed, Efficiency.

The sixth group's main attribute is the Processor speed, and the side attribute is Rmax.

The seventh group's main attribute is the Total Cores, and the side attributes are Rmax and Rpeak

The eighth group's main attribute is the Total Cores.

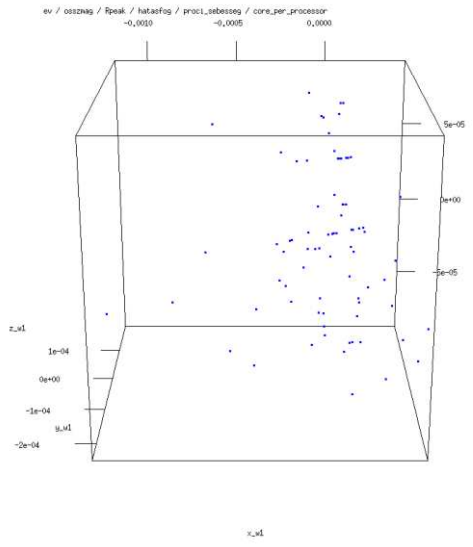

Figure 8
First group, Rmax

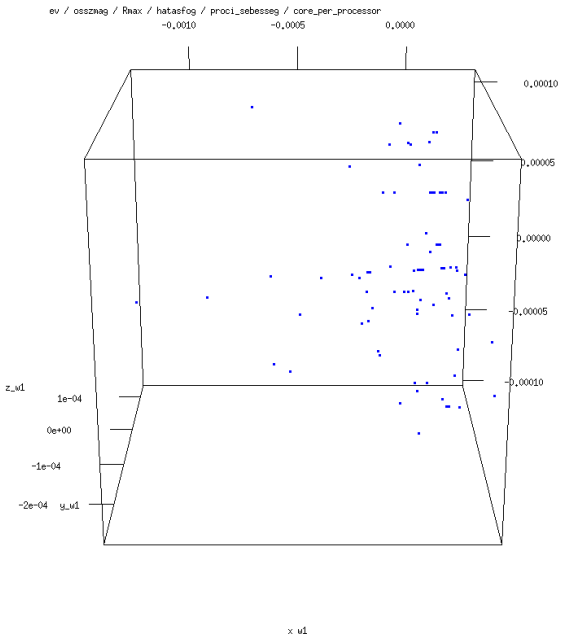

Figure 9
First group, Rpeak

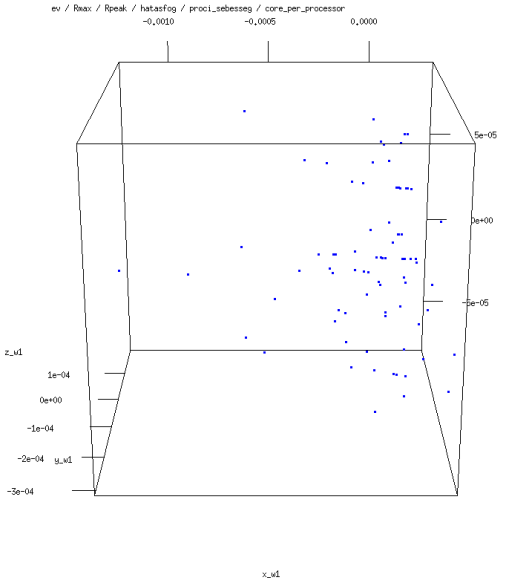

Figure 10
First group, Total Cores

9 The Software Environment

R is a software environment for statistic computing [15], which is Open Source and free, available under GPL. The R is another implementation of S language and environment, which originally was developed by Bell Laboratories [15]. In these investigations, for this reason an implementation of R was used on a laptop with a Linux system. In this manner no extra programming activity was needed for the investigations. After specifying the initial matrix, the necessary computations were automatically executed, and appropriate figures were immediately displayed.

Conclusions

The combination of MDS and C-means clustering is a useful tool of classification for measurable multidimensional problems.

This method is very flexible. It can be fitted to real problems easily, just by fine-tuning the problem with weights, or by choosing other norms. The Clustering part is changeable. It is very easy to implement a short script in R and plot many variations. This helps to decide which modifications are the best.

This classification could help planning the computer systems of Data Centers. In future research, further attributes can be involved in the investigations. These attributes can be some service based system parameters, such as some kind of availability for software, hardware, and service. This could be service based planning, as well.

References

[1] John W. Sammon Jr., A Nonlinear Mapping for Data Structure Analysis IEEE Transactions On Computers, Vol. C-18, No. 5 (May 1969)

[2] Seung-Hee Bae, Jong Youl Choi, Judy Qiu, Geoffrey C. Fox, Dimension Reduction and Visualization of Large High-Dimensional Data via Interpolation HPDC'10, ACM 978-1-60558-942-8/10/06 (June 20-25, 2010)

[3] Douglas Barnett, Brain Blake, Bruce A. McCarl, Goal Programming via Multidimensional Scaling Applied to Senegalese Subsistence Farms American Journal of Agricultural Economics, Vol. 64, No. 4 (Nov. 1982) (pp. 720-727)

[4] Julia Handl, Douglas B. Kell, and Joshua Knowles, Multiobjective Optimization in Bioinformatics and Computational Biology IEEE/ACM TRANSACTIONS ON COMPUTATIONAL BIOLOGY AND BIOINFORMATICS, Vol. 4, No. 2 (APRIL-JUNE 2007)

[5] Frankie K. W. Chan and H. C. So, Efficient Weighted Multidimensional Scaling for Wireless Sensor Network Localization IEEE TRANSACTIONS ON SIGNAL PROCESSING, Vol. 57, No. 11 (NOVEMBER 2009)

[6] Purnamrita Sarkar, Andrew W. Moore, Dynamic Social Network Analysis using Latent Space Models SIGKDD Explorations, Vol. 7, No. 2

[7] James A. Ferwerda, Psychophysics 101 SIGGRAPH 2008 Courses Program (2008)

[8] Vance Faber, John Feo, Pak Chung Wong, Yousu Chen, A Highly Parallel Implementation of K-Means for Multithreaded ArchitectureHPC '11 Proceedings of the 19th High Performance Computing Symposia (2011)

[9] Tong Zhao, Arye Nehorai, Boaz Porat, K-Means Clustering-based Data Detection and Symbol-Timing Recovery for Burst-Mode Optical Receiver IEEE TRANSACTIONS ON COMMUNICATIONS, Vol. 54, No. 8 (AUGUST 2006)

[10] Souptik Datta, Chris R. Giannella, and Hillol Kargupta, Approximate Distributed K-Means Clustering over a Peer-to-Peer Network IEEE TRANSACTIONS ON KNOWLEDGE AND DATA ENGINEERING, Vol. 21, No. 10 (OCTOBER 2009)

[11] Forrest W. Young, Multidimensional Scaling Kotz-Johnson (Ed.) Encyclopedia of Statistical Sciences, Vol. 5 (1985)

[12] http://www.r-project.org (2011 Dec.)

[13] R. Shepard, The Analysis of Proximities: Multidimensional Scaling with an Unknown Distance Function, I, II, Psyhometrika, 27, 219-246, 1962

[14] http://top500.org (2012 April)

[15] The R Development Core Team, R: A Language and Environment for Statistical Computing: Reference Index, ISBN 3-900051-07-0 (2011- 09-30)

A Connected Dominating Set Based on Connectivity and Energy in Mobile Ad Hoc Networks

Ali Kies, Zoulikha Mekkakia Maaza, Redouane Belbachir

Department of Data Processing
University of Sciences and the Technology of Oran
BP 1505 El M'Naouar, Oran, Algeria
kies_ali@yahoo.fr, mekkakia@univ-usto.dz, belbachir_red@yahoo.fr

Abstract. A connected dominating set (CDS) has been proposed as a virtual backbone for routing in wireless ad hoc networks. Ad hoc networks offer new routing paradigms. Therefore, the routing operation needs a broadcast algorithm. Broadcasting in an ad hoc network is still an open issue. The main focus here will be on optimizing the energy and the bandwidth utilization for packet diffusion.

In this paper, we describe the Connected Dominating Set-Energy Protocol (CDSEP) for mobile ad hoc networks to optimize broadcast in the network. The key concept used in this protocol is a new distributed algorithm which computes the connected dominating set (CDS) based on node energy and node connectivity. In the CDSEP protocol, the CDS nodes are selected to forward broadcast packets during the flooding process, and the information flooded in the network through these CDS is also about the CDS. Thus, a second optimization is achieved by minimizing the contents of the control packets flooded in the network. Hence, only a small subset of links with the nodes is declared instead of all the links and the nodes. Our simulation experiment results demonstrate that the CDSEP responds well to scaling in terms of broadcast control packet and energy consumption.

Keywords: ad hoc; self-organization; CDS; energy; routing

1 Introduction

An Ad hoc mobile network is a set of mobile nodes which are dynamically and arbitrarily scattered in a manner where the interconnection between the nodes can change constantly. An ad hoc mobile network can be modeled by a graph $G = (V, E)$ [1]. V represents all nodes and E models the connections set that exists between these nodes. If $e = (u, v) \in E$, this means nodes u and v are able to communicate directly at that moment.

In most cases, the node destination is not in the transmission range of the node source, which implies that data exchange between two nodes (source, destination) may be carried out by intermediate nodes. The management of this routing of data implies the establishment of certain architecture, and one must take account of the mobility of the nodes and fickleness of the physical medium. An ad hoc mobile network must be self-organized to convey the traffic from one point to another.

The self-organization of an ad hoc network allows the creation of a different view of topology radio called virtual topology. This introduces one or more hierarchy levels and facilitates the establishment of the services necessary to the expected network operation, such as the routing [2].

Several techniques have been proposed to optimize flooding with neighborhood knowledge. Link state routing protocols usually provide this information. It is usually obtained by regularly emitting so-called Hello packets containing lists of neighbors.

From a graph theory point of view, the set of nodes that will retransmit a given broadcast packet must form a connected dominating set (CDS).

If V^- is the node set of the CDS, the formal definition is:

$$\forall u \in V, \exists v \in V^- / v \in N(u), \forall (u,v) \in V^{-2}, \exists e = route_{u \to w} / \forall w \in e,\ w \in V^- \quad (1)$$

In equation (1), V represents all nodes and V^- represents CDS nodes. $N(u)$ is the neighbor set of u.

A connected dominating set is a set of nodes such that any node in the network is a neighbor of some element of the set. It is connected if the sub-graph formed by this set is connected. The connected dominating set property insures that all nodes will receive the packet.

The CDS forwarding rule is that a node retransmits if it has not already received the packet and it is in the connected dominating set.

Moreover, the selection of the connected dominating set must be distributed. Based on neighborhood knowledge, a node must decide whether or not it is in the dominating set. A CDS is a good candidate of a virtual backbone for wireless networks, because any non-CDS node in the network has 1-hop distance from a CDS node. With the help of the CDS, routing is easier and can adapt quickly to network topology changes.

Routing protocols are used with the aim of discovering the route which exists between the nodes. The principal goal of such a routing protocol is the establishment of the routes which are correct and effective between any pair of nodes, which ensures the exchange of messages in a continuous way.

Ad hoc routing protocols can be classified into three categories: proactive protocols, reactive protocols and hybrid protocols [1].

Proactive (table-driven) routing protocols maintain up-to-date routes between all nodes in the network. This requires each node to maintain some kind of routing table to store routing information. The ability of the protocol to provide routes to mobile nodes depends on the consistency of the routing tables. Therefore, a node noticing a change in network topology must propagate the updated routing information to all other nodes.

In the reactive routing protocol case, when a node wants to communicate with another node, it initiates a specific route discovery process to obtain a valid route. Hybrid protocols use both proactive and reactive routing protocols. Other types which are based on geographical position are detailed in [3].

2 Related Works

Three types of virtual topologies are defined: CDS (Connected Dominating Set) allows for the collection of the data traffic and forms a network backbone [2]. Cauterization allows for the partition of the network into zones. The third type integrates CDS and clusters.

The first type is based on the construction of a connected dominating set (CDS) as a virtual backbone to convey information in a mobile network.

[4] proposes a localized algorithm for constructing a CDS. The first step of this algorithm is to mark the nodes having at least two neighbors not directly connected as dominant nodes (become node in the CDS). Applying two dominating reducing rules can reduce some redundant nodes in the CDS. In Rule 1, a marked node can unmark itself if another marked node covers it. In Rule 2, a marked node can unmark it, if covered by two other directly connected marked neighbors. Node A is covered by node B, which means all A's neighbors are a subset of B's neighbors. Each node learns its neighbor information and status (mark or unmark) before the next reducing process, through broadcasting Hello messages. So it imposes a significant communication overhead, and energy consumption is high. To reduce communication overhead, the algorithm [5] presents new rules or extended rules to select/reduce the connected set of dominant nodes. In order to prolong the lifespan of each node, the extended rules are based on two approaches, the approach *Node-Degree-Based Rules* and *Energy-level-Based Rules*. Also [6] proposes an improved algorithm [4], in which nodes are assumed to have a record key (degree, x, y), and where x and y are location coordinates. This record is used to apply rules 1 and 2, in which they define that a node can unmark itself if it is covered by one or two connected neighbors, no matter whether they are marked or not. [6] proposes the creation of a source oriented CDS in order to optimize the diffusion of information. The authors of [7] and [8] propose an iterative exploration starting from a leader in the network to allow the building and interconnecting tree. The approach is based on DS

(Dominating Set) construction and its interconnection. A node has one of four following states: initial state, dominating (CDS member), dominated (neighbor of a dominant) and active (in election). An active node that has the highest weight among its active neighbors becomes dominant, and its neighbors become dominated. The weight for the election can take the degree value, node identifier and energy level. There exist other algorithms based on the same approach without the use of a leader, as described in [9]. In [10] they use the concept of multi point relays. The idea of multipoint relays (MPR) is to use the knowledge of two-hop to optimize local broadcast. Thus, each nodes elects a multipoint relays set among its neighbors, allowing it to attain all nodes at two hops. The more formal definition is:

$$\forall u\ M(u) \in N(u),\ N2(u) \in N(M)\ (with\ N(M) = \bigcup_{m \grave{\alpha} M} N(m)) \quad (2)$$

Where *u* is a node, *M(u) is* a multipoint relay set of *u*, *N(u)* is a neighbor set of *u* and *N2 (u)* is a two-hop neighbors set of *u.* Only the multipoint relay of *u* retransmits a message from *u*.

Among the routing protocols based on virtual topology, we note Optimized Link State Routing (OLSR) based on the concept of multipoint relay (MPR) [11] and Ad hoc On-demand Distance Vector (AODV) based on CDS [1].

The second type is based on the cluster concept. A cluster is a set of remote limited nodes.

In [12], the node that has the smallest identifier among all its neighbors is elected as the cluster-head. The cluster is formed by the cluster-head and all its neighbors. In [13] this is reversed; the node whose identifier is the highest among all its neighbors becomes the cluster-head. In [14], the election of cluster-heads is based on the degree of connectivity (the neighbor's number of nodes) instead of the identities of the nodes. In [15], the weight is defined as the speed of each node. [16] presents a clustering algorithm. This algorithm involves three steps. Group formation involves two tests: test1 on signal strength, and test2 on mobility, with each one a cluster-head for the management of the cluster and overall cluster-head for network management. The cluster-head is the node with the minimal average distance between it and the other nodes of the group. Overall cluster-head is the node that has the maximum of the cluster-head in its field of coverage. This election is made by using the GPS. There exist routing protocols based on this type; we cite the Cluster Based Routing Protocol (CBRP) [17], the zone routing protocol (ZRP) [18] and the Clusterpow protocol [19]. The Clusterpow protocol uses the power of transmission to build the clustering.

Among the algorithms of the third type, [20] presents a distributed algorithm for constructing a CDS in the form of a K-CDS: the distance between a node and the CDS. The construction and interconnection stages are inspired from [7] and [8].The presence of a leader is obligatory in a hybrid network; the access point (AP) may play the role of natural leader [2].If instead there exists no Access Point,

it is necessary to elect a node using the algorithm described in [21]. The clusters election is done only by nodes which are members of CDS. A dominant node that has the highest weight among all its neighbors at K-cluster and K-CDS, where K is a distance, without cluster-head amounts to the cluster-head. The author of [22] proposes Virtual Structure Routing (VSR) based on the previous virtual topology [20]. In [23], the principle of the algorithm is summarized as follows: Initially, each node in the network selects its preferred node as the diffusion node, the node that ensures a better diffusion in two hops. Then, the diffusion node having an average of choice higher than that of its neighbors is declared as the cluster-head. The average of choice is the ratio of dominant nodes which are neighbors to a node and choose the same node as diffusion node divided by number of node's neighbors. Ordinary nodes are always attached to their node of diffusion. These nodes have a null average of choice. A forest is then built by connecting the cluster-heads, the secondary cluster-heads (members of the CDS, but which are not cluster-heads) and ordinary nodes. Afterwards, the algorithm constructs the routing table within the cluster to provide an appropriate structure for each tree. The latter is located only at the cluster-heads.

3 CDSEP Algorithm

The desired functions of our virtual topology are:

- Leveraging heterogeneity involving more actively the strong nodes in terms of energy,
- Optimizing the flooding in order to prevent the formation of a broadcast storm,
- Creating a logical cutting near to a physical division allowing locating and addressing the nodes.

Naturally, this structure must follow the following properties: strength, persistence, distributive, scalability and low traffic control.

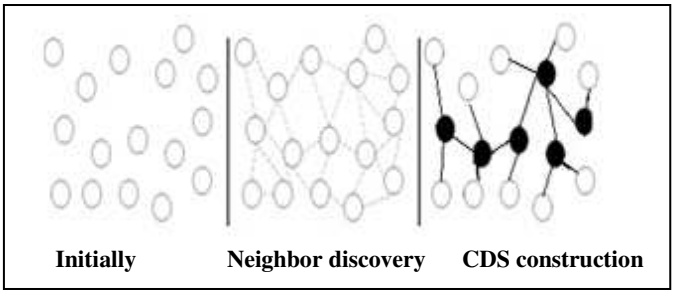

Figure 1
The construction of virtual topology

Fig. 1 presents an overview of our virtual topology. Nodes initiate a neighbor discovery to discover their neighboring radios. From this neighborhood radio, the CDS is built by electing the dominants and interconnecting them to form a CDS.

For this, we proposed a new distributed algorithm for construction but also maintenance events. The CDSEP algorithm goes through via two stages:

- Creating Dominant nodes (DNs), i.e. CDS nodes via the Hello messages,
- Interconnecting the dominant nodes (DNs) via the IM (Interconnection Message).

3.1 Virtual Topology Based on Connectivity and Energy

The idea of the CDSEP algorithm is to minimize flooding of broadcast messages in the network by reducing duplicate retransmissions. Each node in the network selects a node in its neighborhood which may retransmit its packets. This node is called a dominant node (DN), i.e. a node in the CDS. The DN set creates the virtual topology named the CDSE in the network. Node neighbors which are not CDSE nodes receive and process broadcast messages but do not retransmit broadcast messages received from the node. Each node selects its DN among its one hop neighbors. This DN has the maximum of Selection Parameter (SP).

3.1.1 Selection Parameter

The selection parameter (SP) is a parameter which enters decision making to build our virtual topology based on CDS and Energy named CDSE (CDS-Energy). For this, we must study all possible values of this parameter. The selection parameter is calculated from two parameters, a parameter related to the node energy and the other related to the network called the connectivity, i.e. the degree of node in the network, by the following equation (3):

$$SP_i(t) = E_i(t) * log\left(C_i(t)\right) \Big/ 1000 \tag{3}$$

$SP_i(t)$:Selection parameter of node *i* at time *t*,

$E_i(t)$:Energy of node *i* at time *t* in Joule,

$C_i(t)$:Degree of node *i* at time *t*.

Table 1 shows the different states of selection parameter, and shows six cases of the Selection Parameter. In case 1, node *i* has a value of SP null because node *i* has a value of energy null. In case 2, node *i* has value of Connectivity null, so this node is located in the border of the network. Therefore, this node does not participate in the construction of the CDS (not a candidate to be a CDS node).

Table 1
Different states of SP

	E(j)	*C*	*SP*
1	$if\ E_i = 0$	$\forall C_i$	$SP_i = 0$
2	$\forall E_i$	$If\ C_i = 1$	$SP_i = 0$
3	$if\ E_i = E_j$	$and\ C_i = C_j$	$SP_i = SP_j$
4	$if\ E_i > E_j$	$and\ C_i \geq C_j$	$SP_i > SP_j$
5	$if\ E_i \geq E_j$	$and\ C_i > C_j$	$SP_i > SP_j$
6	$if\ E_i \neq E_j$	$and\ C_i \neq C_j$	$SP_i \neq SP_j$

Fig. 2 shows this case: node 1 has a value of SP_1 (SP of node 1) equals zero because this node has a connectivity value C_1=1 (connectivity of node 1 equals 1), i.e. has a neighbor; and the other node 2 has C_2=3 and E_2=2000 (energy of node 2 equals 2000), and when we apply the equation (3) it gives SP_2 =0, 95 as the Table 2 shows.

For the third case, when the energy and connectivity of node *i* and node *j* are equal, the SP of node *i* and node *j* are also equal.

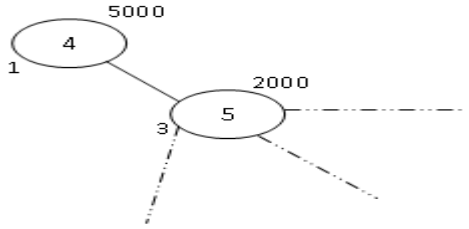

Figure 2
Example with two nodes

Table 2
Values of SP

Node	*E(j)*	*C*	*SP*
4	5000	1	0.00
5	2000	3	0.95

To illustrate case 4 and case 5, we use Fig. 3 and Table3. We note that SP_{24} equals 3.01, superior to SP_4 equal 2.41 because E_{24}>E_4 and C_{24} = C_4.

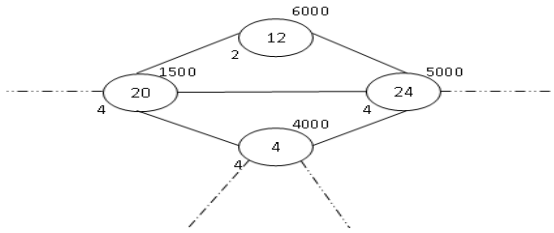

Figure 3
Example with 4 nodes

Table 3
SP Values

Node	*E(j)*	*C*	*SP*
20	1500	4	0.90
24	5000	4	3.01
4	4000	4	2 .41
12	6000	2	1.81

Also, we have a good example to illustrate case 6, when $E_i > E_j$ and $C_i < C_j$. In Fig. 3, node 12 has E_{12}= 6000 and C_{12}= 2, and node 4 has C_{12}=4 and E_{12} =4000, which implies SP_4=2, 41 > SP_{12}=1, 81, as Table 3 shows.

The formula can provide a significant value, taking into account the difference between the two parameters energy and connectivity. So, this formula gives a fair value without neglecting any parameter.

The Dominant Node (DN) of node n is denoted DN (n). Each node maintains information about DN.

The DN is recomputed when a change in the SP of a neighborhood is detected or a new neighbor with a SP max is added; a node obtains this information from the periodic Hello messages received from the neighbors.

3.1.2 Process Hello Messages

Each node broadcasts Hello messages containing information about its neighbors and their link status. The link status can be "CDSE" or "S". S is a link of type Symmetric and indicates that the link has been verified to be bidirectional. "CDSE" indicates that a node is selected by the sender as a DN and it is a link of type Symmetric.

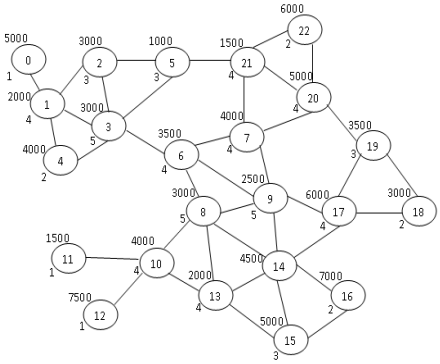

Figure 4
Neighbor discovery

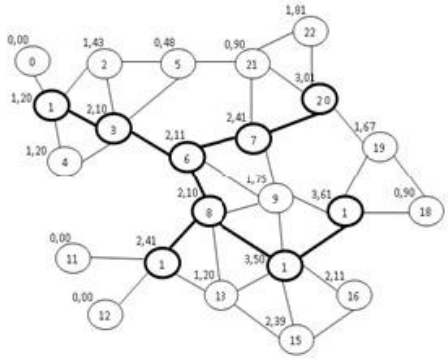

Figure 5
CDSE

In Fig. 4, nodes initiate a neighbor discovery to discover their neighbor. From this neighborhood, the virtual topology is built in a distributed manner. Electing dominants and interconnecting them to form a connected virtual topology, i.e. connected dominating set-Energy (CDSE), as Fig. 5 shows.

A Hello message contains:

- SP value of sender node,
- A neighbor list, with type of link.

After receiving a Hello message, each node maintains a Neighbor table in which it records the information about its neighbors, its SP, the status of the link with this neighbor, a list of two hop neighbors that this one hop neighbor gives access to, and an associated holding time. The holding time is the lifetime of the neighbor table entry. The information is recorded in the Neighbor table as a neighbor entry, with the field names as shown in Table4:

Table 4
The neighbor table entry

Address of neighbor	SP of neighbor	Link status	2 hop list	Holding time

Based on the information obtained from the Hello messages, each node constructs its CDSE table. In the CDSE table, a node registers the addresses of those one-hop neighbor nodes, and the latter selects the node as a DN.

The CDSE table entry may have the following format in Table 5:

Table 5
The CDSE table entry

Node address	Holding Time

3.2 Interconnecting Dominant Nodes (DNs)

In order to interconnect the CDSE nodes, each dominant node (DN) broadcasts specific messages called Interconnection Messages (IM). IM messages are forwarded to all nodes of the network, an advantage specific to CDSE nodes. The CDSEP protocol enables a better scalability in the distribution of topology information.

An IM message is sent by a node in the network to declare its CDSE table, i.e. the addresses of those one hop neighbor nodes which have selected the node as a DN. The information diffused in the network by these IM messages will help each node to compute its topology table. The topology table gives a global overview of the virtual topology CDSE. A node which nobody has selected as a DN cannot generate any IM messages. To reduce the problems of broadcast, each node transmits and retransmits the IM message only if it belongs to the CDSE nodes. The node belongs to the CDSE nodes if in the neighbor table of this node exists the link of type "CDSE". When a change to the CDSE table is detected, an IM message should be transmitted.

Each node in the network maintains a Topology table in which it records the information about the virtual topology of the network as obtained from the IM messages. A node records information about the DNs of other nodes in the network in its topology table as a topology table entry, which may have the following format, as Table6 shows:

Table 6
The topology table entry

Node address	Dominant Node address	Holding time

4 Results

The main purpose of these simulations in NS2 (Network Simulator) is to analyze the behavior of our CDSEP algorithm in various scenarios.

We present simulations that illustrate the results of the CDSEP. We evaluated the CDSEP algorithm with the mobility and density parameter.

Table 7
Simulation parameters

Parameter	Value
Number of nodes	20 – 200
Time of simulation	200 s
radio propagation	250 m
Mobility	10 m/s
Degree	Between [1,10]

Interval Hello message	2 s
Interval IM message	5 s

The first aspect we notice is the CDSE size (the number of dominants nodes according to the network size). In Fig. 6, we notice a decrease in the number of dominant nodes in CDSE. This number increased from 7 to 43, in the case when we increase the network topology size from 20 to 200 nodes, but not exceeding 22% of dominant nodes overall network nodes. On the other hand, in OLSR this rate reaches 77% MPR number, by applying the equation (6) as Fig. 7 shows.

Such that:

$$Dominant\ \ rate\ \ = \frac{dominant\ \ nodes}{network\ \ size} \tag{6}$$

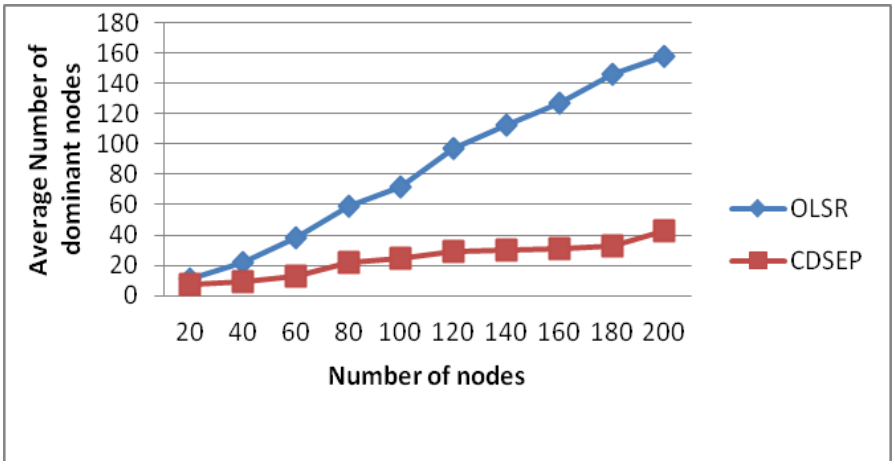

Figure 6
Average number of dominant nodes in CDSE (CDSEP) and in MPR (OLSR)

The same comments apply to Fig. 8, which shows the stability of dominant rate about 22% for CDSEP and 77% for OLSR, in all scenarios from 20to200 nodes.

Consequently, the CDSEP protocol adapts well with high density networks. A reduced number of dominant nodes optimize the diffusion in the network.

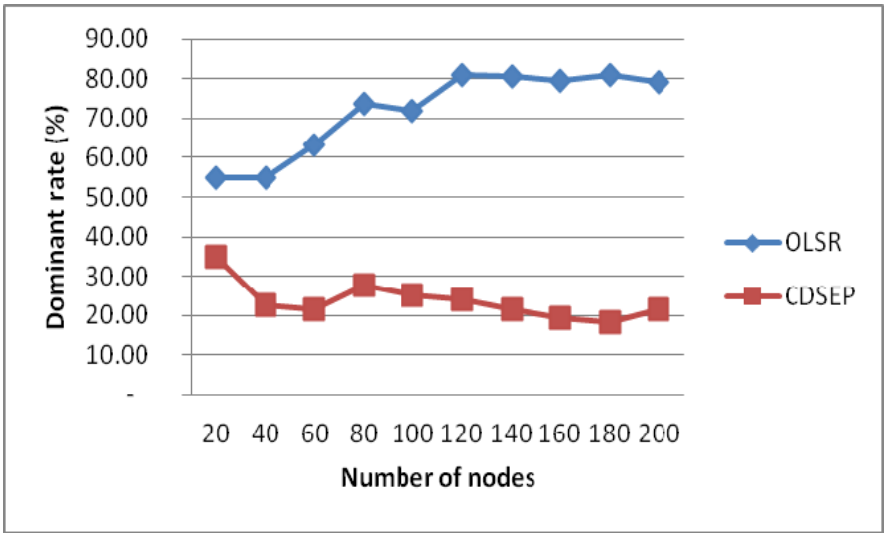

Figure 7
Rate of dominant nodes

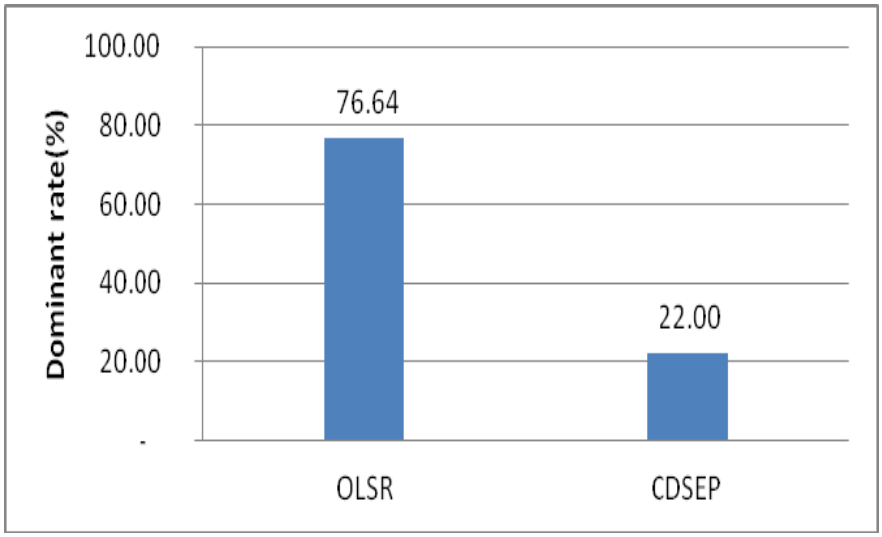

Figure 8
Dominant rates of CDSE and MPR

We notice in Fig. 9, the CDSEP reduced the number of control packets generated in the network over OLSR.

When the number of nodes increases, the number of OLSR control packets increases. Consequently, the control traffic decreases in CDSEP, inducing a reduction of energy consumption in the network as Fig. 10 shows.

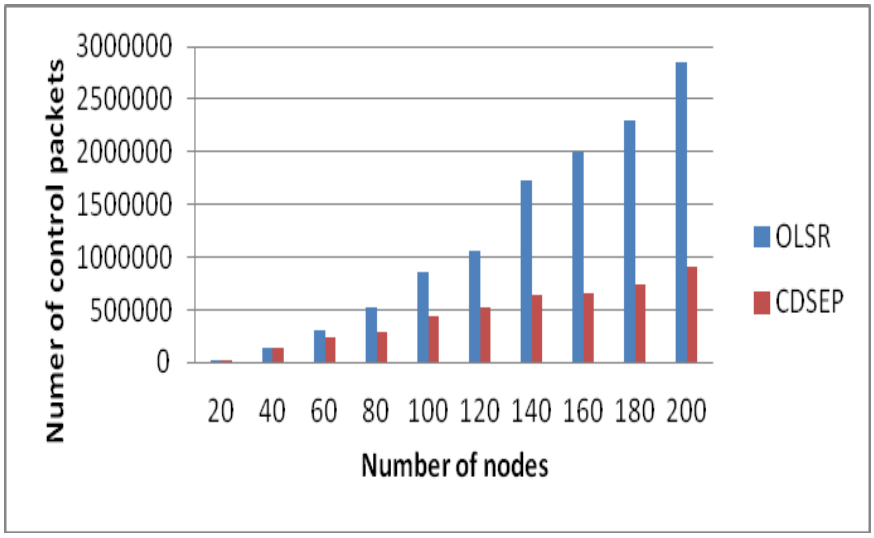

Figure 9
Number of control packets

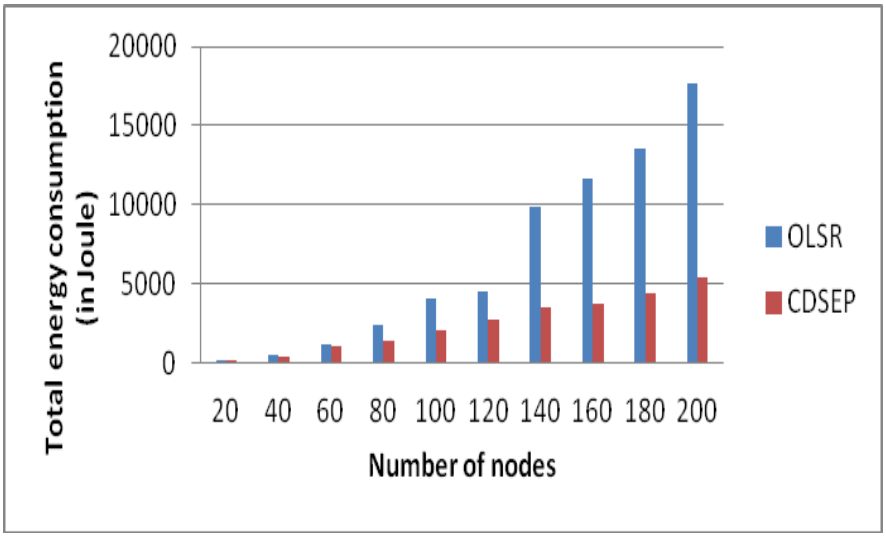

Figure 10
Energy consumption

Finally, Fig. 11 shows the rate in terms of control packets and the energy consumed between OLSR and CDSEP, the rate of control packet is calculated using the equation (7):

$$Control\ \ packet\ \ rate = \frac{number\ \ of\ \ OLSR\ \ control\ \ parquets}{number\ \ of\ \ CDSE\ \ control\ \ parquets} \tag{7}$$

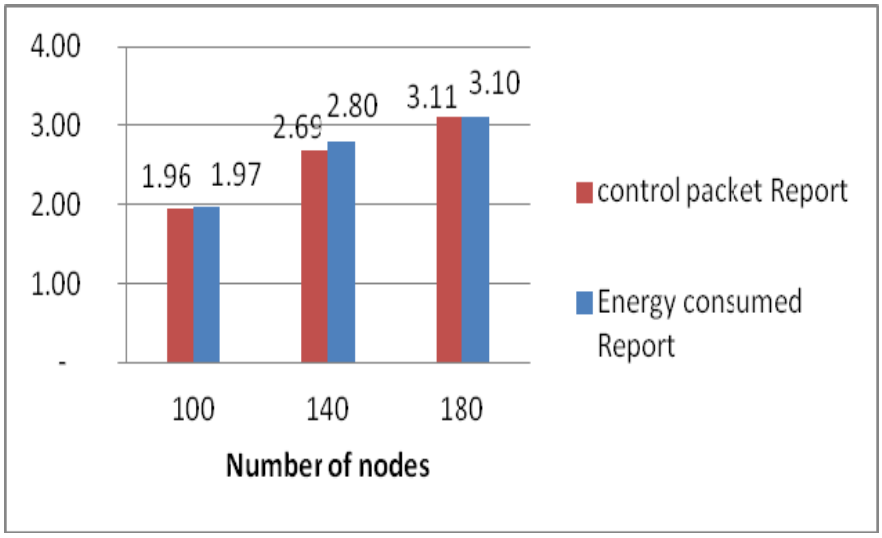

Figure 11
Control packet and energy consumed report

And for consumption energy by applying equation (8):

$$Energy\ \ consumption\ \ rate = \frac{energy\ \ consumed\ \ in\ \ OLSR}{energy\ \ consumed\ \ in\ \ CDSE} \tag{8}$$

We note that the CDSEP is 3times better for a topology of 180 nodes than the OLSR in terms of the diffusion control packet and energy consumption. As an example, in the OLSR, each node in a topology of 180 nodes consumes an average of 0.38 joules per second, compared to the CDSEP, which consumes 0.12 joules per second.

Conclusion

In this paper, we proposed a distributed algorithm for computing a connected dominating set based on the degree and energy of the node. This information can be contained in hello packets that nodes periodically broadcast to their neighbors. The CDSE nodes should be responsible for broadcasting packets of other nodes in addition to its own packets, and their energy consumption is high. So it is desirable in selecting nodes for CDSE that we consider the residual energy in the node.

Our contribution, the CDSEP, allows for building a virtual topology based on connectivity and energy. This topology reacts well to scaling, i.e. the rate of control packet to build and interconnect and it is scalable to optimize energy consumption in the network. This structure also allows the participation of the strongest nodes in terms of energy, which permits a longer life of the virtual topology and also permits the building of a connected dominating set, because the dominant nodes are chosen according to the connectivity parameter.

This study laid the foundation for proposing a new routing protocol, and that is the subject of our next work.

Acknowledgments

This work is part of the CAPRAH project 08/U311/4966, supported by the Algerian Ministry of Higher Education and Scientific Research.

References

[1] S. K. Sarkar, T. G. Basavaraju, C. Puttamadappa: Ad Hoc Mobile Wireless Networks, Principles, Protocoles, and Application. Taylor edition (2008)

[2] P. Santi," Topology Control in Wireless Ad Hoc and Sensor Networks," Wiley edition (2005)

[3] M. L. M. Kiah, L. K. Qabajeh and M. M. Qabajeh: Unicast Position-based Routing Protocols for Ad-Hoc Networks. Acta Polytechnica Hungarica, Vol. 7, No. 5, 2010

[4] J. Wu, H. Li: On Calculating Connected Dominating Set for Efficient Routing in Ad Hoc Wireless Networks. In Proc. of the 3rd Int'l Workshop on Discrete Algorithms and Methods for Mobile Computing and Communication (1999)

[5] H. Li, J.Wu: Dominating-Set-based Routing in Ad Hoc Wireless Networks. In Proc. of International Workshop on Discrete Algorithms and Methods for Mobile Computing and Communications(DIAL'M) USA, August (1999)

[6] I. Stojmenovic, M. Seddigh, J. Zunic: Dominating Sets and Neighbor Elimination-based Broadcasting Algorithms in Wireless Networks. IEEE Transactions on Parallel and Distributed Systems, January (2002)

[7] B. Liang, Z. J. Haas: Virtual Backbone Generation and Maintenance in Ad Hoc Network Mobility Management. In Proc. of INFOCOM, March (2000)

[8] X. Cheng, D. Du: Virtual Backbone-based Routing in Multihop Ad Hoc Wireless Networks. Technical Report 02-002, University of Minnesota, Minnesota, USA, January (2002)

[9] B. Ryu, J. Erickson, J. Smallcomb, S. Dao: Virtual Wire for Managing Virtual Dynamic Backbone in Wireless Ad Hoc Networks. In Proc. of International Workshop on Discrete Algorithms and Methods for Mobile Computing and Communications (DIAL'M), Seattle, USA, August (1999)

[10] T. Clausen, P. Jacquet, A. Laouiti, P. Muhlethaler, A. Qayyum and L. Viennot: Optimized Link State Routing for Ad hoc Networks, IEEE INMIC, Pakistan (2001)

[11] P. Jaquet, P. Muhlethaler, A. Qayyum: Optimized Link State Routing (olsr) Protocol. Internet Draft, draft-ietf-manet-olsr-01.txt, February (2000)

[12] A. Ephremides, J. Wieselthier, D. Baker: A Design Concept For Reliable Mobile Radio Network With Frenquency Hopping Signaling. Procedings of the IEEE, Vol. 75, No. 1, January (1987)

[13] B. Haggar: Self-Stabilizing Clustering Algorithm for Ad Hoc Networks. Wireless and Mobile Communications, 2009. ICWMC '09. Fifth International Conference, Cannes, La Bocca (2009)

[14] H. Taniguchi, M. Inoue, T. Masuzawa, H. Fujiwara: Clustering Algorithms in Ad Hoc Networks. Electronics and Communications in Japan (2005)

[15] S. Basagni: Distributed Clustering Ad Hoc Networks. In Proceedings of the IEEE International Symposium on Parallel Architectures, Algorithms, and Networks (I-SPAN) (1999)

[16] N. Benaouda, HervéGuyennet, Ahmed Hammad and M. Mostefai: A New Two Level Hierarchy Structuring for node Partitionning in Ad Hoc Networks. In Proceedings of *ACM Symposium on Applied Computing, SAC'10,* Zurich, Switzerland, pp. 719-726, March (2010)

[17] M. Jiang, J. Li, Y. C. Tay: Cluster-based Routing Protocol (CBRP). Internet Draft, draft-ietf-manet-cbrp-spec-01.txt, 14 August (1999)

[18] J. Haas, R. Pearlman: The Zone Routing Protocol (ZRP) for Ad Hoc Networks. Internet Draft, draft-haas-zone-routing-protocol-00.txt, November (1997)

[19] P. Santi: Topology Control in Wireless Ad Hoc and Sensor Networks. Wiley edition (2005)

[20] F. Theoleyre and F. Valois: A Virtual Structure for Mobility Management in Hybrid Networks. In Wireless Communications and Networking Conference (WCNC) IEEE, Vol. 5, pp. 1035-1040, Atlanta, USA, March (2004)

[21] N. Malpani, J. L. Welch, N. Vaidya: Leader Election Algorithms for Mobile Ad Hoc Networks. In International Workshop on Discrete Algorithms and Methods for Mobile Computing and Communications (DIALM), USA, August (2000)

[22] F. Theoleyre and F. Valois: Virtual Structure Routing in Ad Hoc Networks. In International Conference in Communications (ICC), IEEE, Vol. 2, pp. 3078-3082, Seoul, Korea, May (2005)

[23] K. Drira, H. Khedouci, N. Tabbane:Virtual Dynamic Topology for Routing in Mobile Ad Hoc Networks. Proceedings of the International Conference on Late Advances in Networks (ICLAN'2006) pp. 129-134, Paris France (2006)

Fast Fourier Transform in Papermaking and Printing: Two Application Examples

Aleš Hladnik[1], Tadeja Muck[1], Maja Stanić[2], Marjeta Černič[3]

[1] University of Ljubljana, Faculty of Natural Sciences and Engineering, Department of Textiles, Snežniška 5, 1000 Ljubljana, Slovenia
ales.hladnik@ntf.uni-lj.si, tadeja.muck@ntf.uni-lj.si

[2] Kenniscentrum Papier en Karton, Ijsselburcht 3, 6825 Arnhem, Netherlands
m.stanic@kcpk.nl

[3] Pulp and Paper Institute, Bogišićeva 8, 1000 Ljubljana, Slovenia
meta.cernic@gmail.com

Abstract: The Fast Fourier transform was applied to demonstrate how to solve two related technological problems in the fields of papermaking and printing using ImageJ, a public domain Java image processing program. By converting a digital image of a multifunctional office paper surface from the spatial- into the frequency domain followed by an appropriate filtering, it was possible to identify and separate two different types of patterns – non-periodic structures such as formation, and periodic structures such as fabric marks. In addition, the moiré pattern, a negative phenomenon often occurring in printing, was eliminated to a large extent. The method proved to be a valuable tool in investigating and quantifying various paper and print quality-related phenomena.

Keywords: image processing; Fast Fourier transform; fabric marks; paper formation; print quality; moiré

1 Introduction

With the rapid increase in computer processing power and data storage capacities, accompanied by a constant decrease in hardware and software prices, complex scientific and engineering problems can now be solved in a very short time period using a typical personal computer. Fourier transform is a mathematical tool frequently used in a number of technical fields, as diverse as applied mechanics, biomedical engineering [2], image- and sound compression, NMR and MR imaging and partial differential equation solving [3].

In our study, a Fast Fourier transform was implemented as an advanced digital image processing operation used for analyzing two related technical applications:

first, the separation of two types of patterns that are generated during an industrial paper making process – paper formation and fabric (cloth) marks – and second, the moiré phenomenon, which often occurs in printing. The focus of this article is on demonstrating the applicability of FFT in two real-world situations rather than on going into details of its technical implementation.

2 Fourier Transform

According to Fourier's theorem, any continuous periodic signal (function) can be represented as the sum of properly chosen sinusoidal waves, i.e. by a series of sine and cosine terms with appropriate frequency, amplitude, and phase [15]:

$$g(x) = \sum_{k=0}^{\infty} [A_k \cos(k\omega_0 x) + B_k \sin(k\omega_0 x) \tag{1}$$

where the constants Ak and Bk denote the Fourier coefficients of the function g(x), from which they can be derived in a process referred to as Fourier analysis [4]. For non-periodic functions, a modified version of Eq. (1) – a Fourier integral – applies:

$$g(x) = \int_0^{\infty} A_\omega \cos(\omega x) + B_\omega \sin(\omega x)\, d\omega \tag{2}$$

where Aω and Bω denote the weights for the corresponding cosine and sine functions with the continuous frequency ω. The weights can be computed as follows:

$$A_\omega = A(\omega) = \frac{1}{\pi} \int_{-\infty}^{\infty} g(x) \cdot \cos(\omega x)\, dx \tag{3}$$

$$B_\omega = B(\omega) = \frac{1}{\pi} \int_{-\infty}^{\infty} g(x) \cdot \sin(\omega x)\, dx \tag{4}$$

The original signal *g(x)* is uniquely represented by the correspondent coefficient functions $A(\omega)$ and $B(\omega)$, which hold the continuous distribution – a spectrum – of frequency components contained in the original signal. In the Fourier transform (FT), both the original signal and its spectrum are treated as complex-valued functions yielding the following well-known expression for the continuous Fourier spectrum $G(\omega)$:

$$G(\omega) = \frac{1}{\sqrt{2\pi}} \int_{-\infty}^{\infty} g(x) \cdot [\cos(\omega x) - i \cdot \sin(\omega x)] dx = \frac{1}{\sqrt{2\pi}} \int_{-\infty}^{\infty} g(x) \cdot e^{-i\omega x} dx \tag{5}$$

While the (forward) FT shown in Eq. (5) enables the computation of $G(\omega)$ from $g(x)$, the inverse (backward) FT makes it possible to reconstruct $g(x)$ from $G(\omega)$:

$$g(x) = \frac{1}{\sqrt{2\pi}} \int_{-\infty}^{\infty} G(\omega) \cdot [\cos(\omega x) + i \cdot \sin(\omega x)] d\omega = \frac{1}{\sqrt{2\pi}} \int_{-\infty}^{\infty} G(\omega) \cdot e^{i\omega x} d\omega \quad (6)$$

The original function "signal space" (domain) and its "frequency space" representation – the spectrum produced by the FT – are two alternative and interchangeable mathematical representations of the same function.

Since digital computers can only process discrete signals, a continuous function should first be converted into a discrete one through sampling. Then the discrete FT (DFT) can be used with the forward transform defined for a discrete signal $g(u)$ of length M ($u = 0 \ldots M\text{-}1$) as:

$$G(m) = \frac{1}{\sqrt{M}} \sum_{u=0}^{M-1} g(u) \cdot \left[\cos\left(2\pi \frac{mu}{M} \right) - i \cdot \sin\left(2\pi \frac{mu}{M} \right) \right]$$

$$= \frac{1}{\sqrt{M}} \sum_{u=0}^{M-1} g(u) \cdot e^{-i2\pi(mu/M)} \qquad \text{for } 0 \le m < M \quad (7)$$

and the inverse transform (DFT^{-1}) as:

$$g(u) = \frac{1}{\sqrt{M}} \sum_{m=0}^{M-1} G(m) \cdot \left[\cos\left(2\pi \frac{mu}{M} \right) + i \cdot \sin\left(2\pi \frac{mu}{M} \right) \right]$$

$$= \frac{1}{\sqrt{M}} \sum_{m=0}^{M-1} G(m) \cdot e^{i2\pi(mu/M)} \qquad \text{for } 0 \le u < M \quad (8)$$

The Fast Fourier transform (FFT) is one of the most efficient algorithms for implementing, i.e. computing, the DFT and its inverse. Its main advantage over other approaches lies in its speed, since the required computation time can be reduced by several orders of magnitude. The mathematical details of this complex procedure can be found elsewhere; see, e.g. [13] or the original article by Cooley and Tukey [6].

When DFT is applied to a digital image, its spatial information is expressed as frequency and phase data. The frequency component can be displayed via the power spectrum, as shown in the Experimental part.

Various types of filtering, such as low-, high- or band-pass, can be performed on the Fourier transformed image via its multiplication by the appropriate filter function. This operation is identical to convolution in the spatial domain, but is often faster and more suitable for some applications.

3 Paper Formation and Periodic Marks

The modern industrial paper manufacturing process on a paper or board machine consists of a number of consecutive technological stages, such as sheet forming, dewatering, wet pressing, drying, roll calendering, coating, and others. Each of these operations has a distinctive and profound effect on the final paper sheet bulk and surface properties. For instance, when a soft, wet paper passes a nip between a pair of press section rolls designed to remove water mechanically and to smooth and compress the sheet, it is exposed to the pressures ranging from 400-8500 N/cm [5].

At various paper machine locations – the forming screen, wet press and drying section – a sheet of paper comes into a direct contact with synthetic cloth (fabric, felt). Depending on the paper grade and exerted pressure, the surface structure – e.g. a weaving pattern – of the fabric material can leave more or less noticeable periodic, regular markings in the paper surface and consequently can adversely affect its appearance. In addition, due to the quasi-random process of the cellulose fibres' distribution, which takes place during the paper forming stage, the paper sheet is also inevitably characterized by having a non-uniform, irregular structure of fibres and other paper ingredients, resulting in a cloudy visual appearance, known as (uneven) formation or cloudiness. Either or both of these two phenomena, if too pronounced, can severely degrade the end product quality.

In the past, the detection, separation and quantification of these two types of structures in paper proved to be a difficult task. Easy access to PC-based image processing and analysis systems, however, has made it possible to successfully investigate these and other issues related to paper science and technology. Our approach is based on the work done by dr. I'Anson from UMIST [8], [9] who had already implemented FFT in the 1990s to solve numerous real-world, paper quality related problems.

4 Moiré in Printing

The moiré effect is a visual perception that occurs when viewing a set of lines or dots that is superimposed on another set of lines or dots, where the sets differ in relative size, angle, or spacing. The moiré phenomenon has been known for a long time. It was already used by the Chinese in ancient times for creating an effect of dynamic patterns in silk cloth. However, modern scientific research into the moiré phenomenon and its application started only in the second half of the 19th century. The first significant steps in the introduction of the Fourier theory to the study of the moiré phenomenon can be traced back to the 1960s and 1970s [1].

The moiré possesses an enormous magnification power – in some cases a million times or more – and provides an extremely sensitive means of visually detecting minute differences in almost identical repeating figures. Because of this property, the moiré phenomenon has useful applications in areas such as crystallography to check crystal defects, for measuring refractive index, in electrophoresis, for testing diffraction gratings and lenses [10], [12], [17], [18]. The only requirement for a moiré pattern is that the interacting figures with two or more periodic structures and with some sort of solid and open regions are superimposed. The solid regions can have different shapes, such as straight, curved or wiggly lines, or dots, ellipses etc. This may happen in two ways; if two periodic structures have close but different periods superimposed in parallel or if two structures have an identical period intersected at a small angle. The result of the periodic interaction is that a visible regular pattern is clearly observed at the intersection, although it does not appear in the original structures.

A moiré can produce interesting and beautiful geometric patterns, but it always degrades the quality and resolution of graphic images. It is the most noticeable spatial domain problem in color printing. Two possible reasons for a moiré pattern appearing in printing are:

- The superposition of halftone screens of different primary colors (C, M, Y and K).

- If the original image is already half-toned or contains some other periodic fine details, an unwanted pattern may appear as an interference between the original screen ruling and the printed halftone frequency.

The moiré effect can be observed in one-color printing, but it is more problematic in color printing, where color line screens are needed. This kind of interaction not only gives texture differences but also color differences [7]. The knowledge of understanding the natural causes of moiré patterns will make it possible to avoid or minimize their adverse effects on color printing. Literature cites three approaches to the moiré treatment: a simple qualitative measure, a geometric model and a complete Fourier spectral analysis [11].

5 Experimental

In our study FFT was applied using ImageJ [14], a public domain Java image processing program developed by Wayne Rasband at the U.S. National Institutes of Health (NIH). To separate paper formation from its periodic marks, the following consecutive image processing operations were performed:

1. Image acquisition and preprocessing

Two 80 g/m^2 multifunctional office papers Navigator Universal – No. 1 (see Figure 1) and No. 2 (see Figure 2) – were scanned using a Hewlett-Packard

ScanJet G4010 flat-bed scanner in transmission mode at 200 dpi, and the acquired RGB color images (65 x 65 mm = 512 x 512 pxl) were converted to 8-bit grayscale images and saved as uncompressed TIFF files. The contrast of the images was improved by performing an automatic contrast adjustment ("histogram stretching") operation so that the available range of 256 values was fully covered.

2. Transforming grayscale images from spatial to frequency domain using FFT and displaying its power spectrum

Power spectrum displays squared amplitudes of the frequency spectrum in a 2D map (see e.g. Figure 1c and Figure 2b) having a distinct pattern, typically symmetrical about the origin [16]. Here lower frequencies lie closer to the origin and higher ones closer to the edges of the image.

3. Creating and applying appropriate filters (masks) using information from the power spectrum

Filters that were either transparent (white; pixel value = 255) or nontransparent (black; pixel value = 0) in the appropriate frequency range were designed and subsequently applied to passing through either exclusively regular (high frequencies) or solely irregular (low frequencies) image structures. After performing the inverse DFT, only selected frequencies appeared in the image.

The moiré removal principle was demonstrated using a color printed sample produced with a four-color offset printing machine, a Heidelberg SM 52 (screen frequency 70 lines/cm). A moiré pattern occurred because the order of the four printing forms was deliberately altered. The color cyan was printed with a printing plate prepared on a yellow color separation. Magenta was printed with a printing plate for cyan and yellow with a printing plate for magenta color. The printed sample (paper Biogloss 135 g/m^2, A3 format) was scanned with Hewlett-Packard Photosmart C6280 in the normal reflection mode with a resolution of 150 dpi, and the resulting image was saved in an uncompressed TIFF format. The image was further processed as discussed below.

6 Results and Discussion

6.1 Separation of Paper Formation and Periodic Marks

The results of image processing operations are depicted in Figure 1. Figure 1a shows the original grayscale image of the paper sample No. 1, (b) is its contrast-enhanced version to increase the visibility of regular structures, while (c) shows the enlarged central part (200 x 200 pxl) of the power spectrum image having

several sharp peaks positioned in a regular pattern around the central white blob. Note that the brightness was reduced to enable better visualisation of the peaks. By drawing two vertically placed white circles (2r = 4 pxl) using the ImageJ drawing tool at the appropriate locations on the power spectrum image (d) and transforming the frequency domain image back to the spatial domain, horizontal periodic marks become visible (g). In a similar manner, the horizontal white circles (e) produce an image with distinctive vertical stripes (h). The combined effect of a four-circles' filter (f) on visualizing both the horizontal and vertical marks is shown in (i). Note that in the output images (see, e.g. (g), (h), (i)) apart from this high-frequency image information corresponding to the periodic, regular structures, such as wire and/or felt marks, also a substantial amount of non-periodic, irregular structures stemming mainly from paper formation is present.

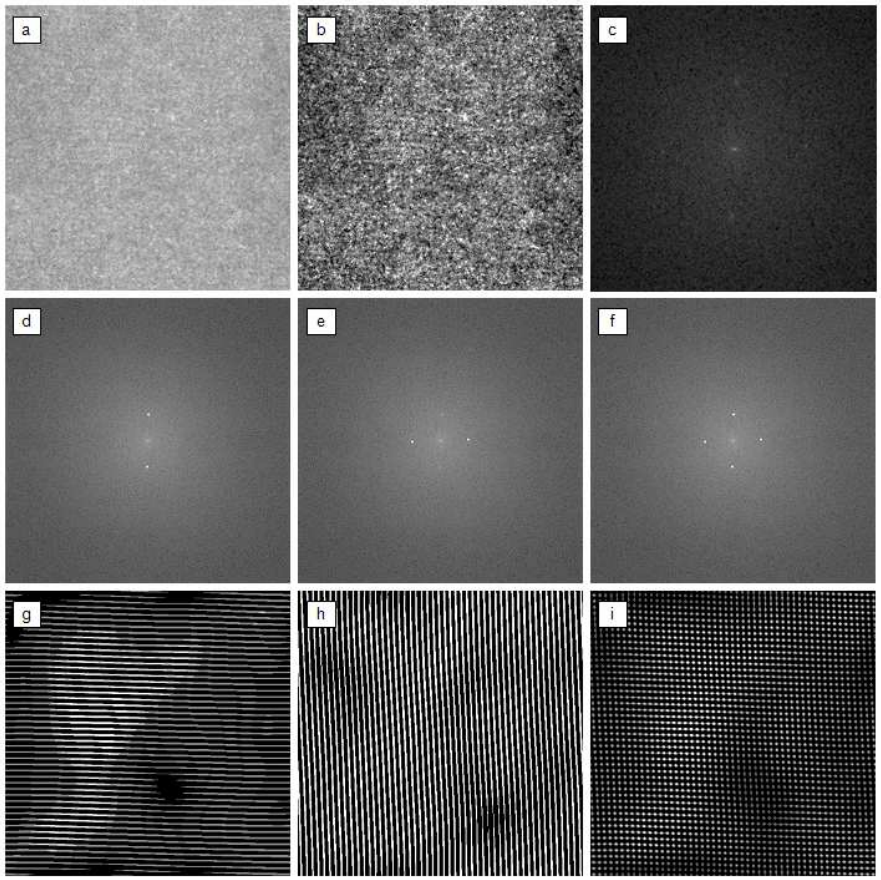

Figure 1

Results of implementing FFT and subsequent filtering on office paper No. 1. See text for details.

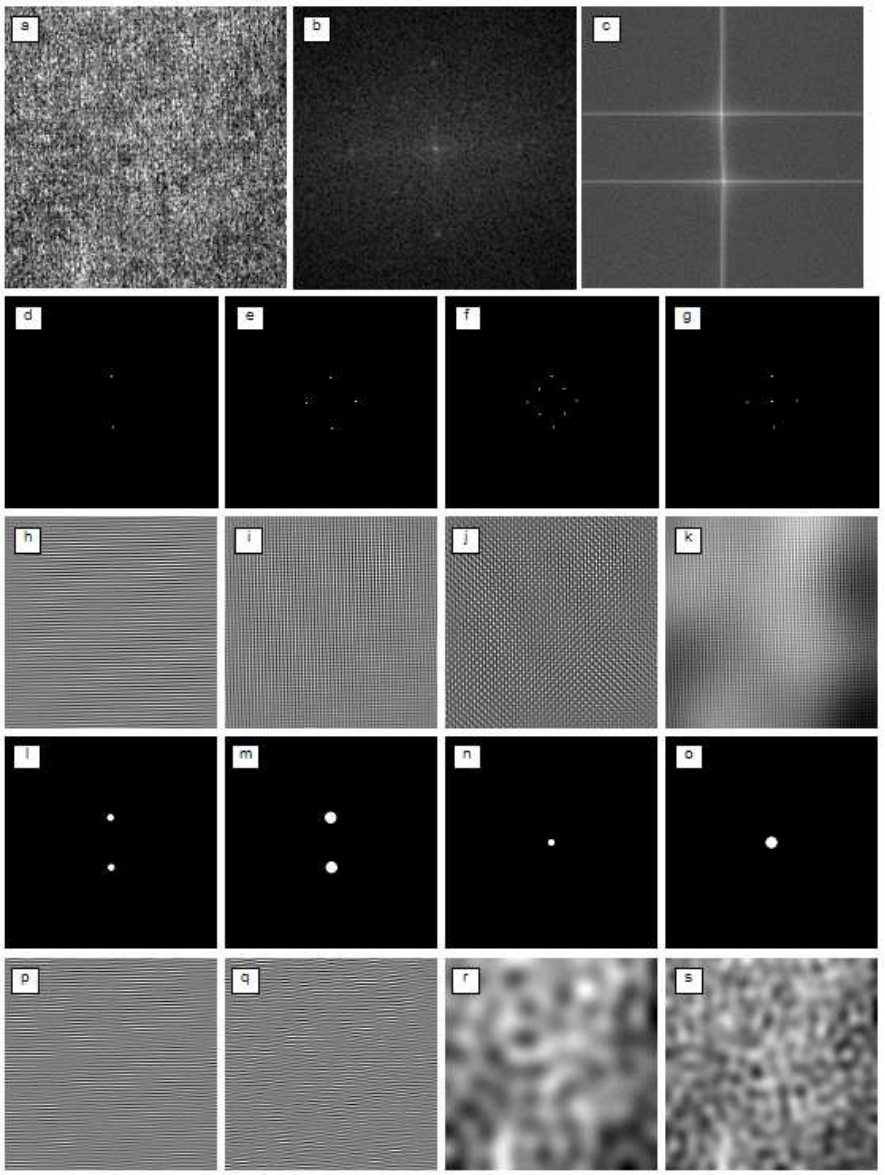

Figure 2
Results of implementing FFT and subsequent filtering on office paper No. 2. See text for details.

Alternatively, one can design circular filters from scratch using the amplitude and frequency information from the power spectrum and perform filtering of the image using these ideal low- or high-pass filters. Black filter pixels block corresponding spatial frequencies while white pixels cause respective frequencies

to pass without attenuation (see also discussion on the moiré pattern removal, below). The filter should be symmetric with respect to the center, so that no artefacts are generated.

Figure 2 presents the results of adopting this approach. The paper sample No. 2 was, after scanning and performing contrast adjustment, (a) FFT transformed – (b) again displays only the enlarged central part of the power spectrum image – and filtered. The effects of applying filters consisting of white circles that varied in position, number and size are shown. Filtering using vertical and horizontal circles (d), (e) results in emphasizing horizontal and vertical lines (h), (i), respectively, as already seen in Figure 1. Since due to the black background of the filter masks no other frequencies are allowed to pass through, results here are much better, i.e., the paper formation-related structures have been almost entirely eliminated. Note that applying FFT on one of the resulting images – e.g. (h) – reveals the exact location of the corresponding white filter circles – as shown in (c). An increase in the size of the two vertical circles – from 4 (d) to 16 (l) to 28 (m) pixels – has a consequence of producing images with progressively less articulated horizontal stripes – see (h), (p) and (q). A closer inspection of the image power spectrum (b) reveals four additional high-frequency structures, so the corresponding symmetrical filter mask with eight circles (f), when applied to the image, leads to (j), displaying another two diagonal (top-left to bottom right and top-right to bottom-left) regular marks. In practice, information about the directionality, i.e. the angle, periodicity and other characteristics of these structures, can be very valuable to both the paper maker and the fabric manufacturer when examining problems that might occur during the paper or wire/felt production. In particular, the geometrical arrangement of peaks in the power spectrum image, such as Figure 1c or Figure 2b, can serve as a kind of fingerprint that is characteristic for each paper machine-paper grade combination; thus a paper mill operator can, especially when having access to an actual piece of cloth from various paper machine sections, unambiguously determine whether the paper marks are caused by a forming wire, a press felt cloth or a dryer fabric [8].

If even a very small number of low spatial frequencies corresponding to the central white blob are allowed to pass through (g), a clearly visible irregular pattern typical of paper formation appears (k). By increasing the central white circle size from 4 (g) to 16 (n) and 28 pixels (o), a progressively more detailed structure of formation becomes evident – see (k), (r), (s).

6.2 Moiré Pattern Removal

First the moiré-containing grayscale image (Figure 3a) was opened in ImageJ. Then a part of the image where only the moiré pattern – without any other disturbing image details, i.e. irregular structures – was selected (b), isolated and saved as a TIFF file. An ImageJ FFT plugin converted this image from a spatial into a frequency domain, generating its power spectrum image (c).

Similarly to the above discussed problem of separating the paper formation from the regular markings, the power – FFT – spectrum of the moiré-containing image also shows several white spots (Figure 3c), producing, however, a considerably more complex pattern. Again, the exact location of the white peaks is the key that enables one to determine what sort of variation is present in the original image. White dots in the centre of the power spectrum image correspond to non-periodic structures, while white regions located towards the edges of the FFT image are related to periodic structures.

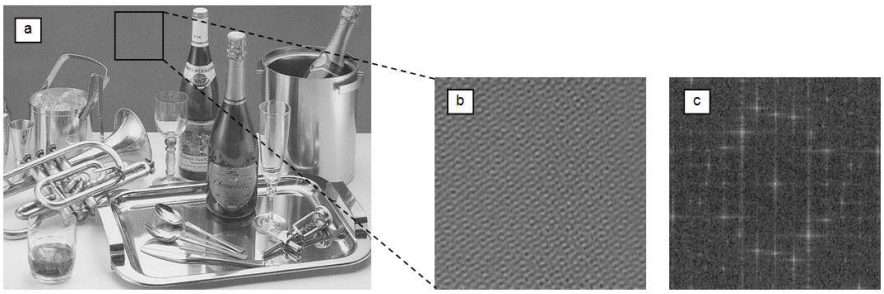

Figure 3
Original image (a), part of the image background with moiré pattern (b) and its power spectrum (c).

Using this information, a bilevel filter (mask) shown in Figure 4a and its inverted version, in Figure 4c, were designed. Note that both are characterized by having either a white or a black central circle. As was already seen in the previous example, due to this circle, the moiré pattern could be neither completely isolated and displayed (b) nor removed (d) in the resulting spatial domain images. In the case of (b), apart from the high frequency (moiré) structures, some low frequency information, corresponding to the picture scene, was also allowed to pass through. In the case of (d), on the other hand, not only were the majority of high frequencies suppressed by the black filter regions (crosses and dots), but also the image details themselves were somewhat blocked by the central black spot, resulting in a washed-out, low contrast image.

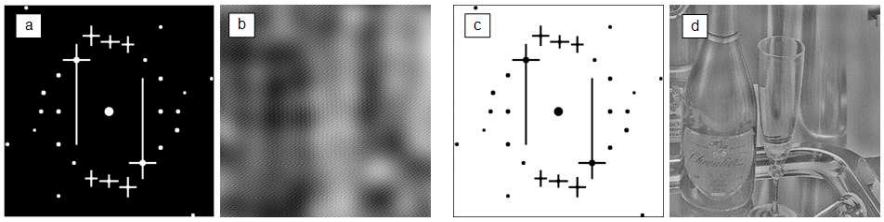

Figure 4
High frequency-passing (a) and -blocking (c) filters with a central circle and the resulting spatial domain images (b, d)

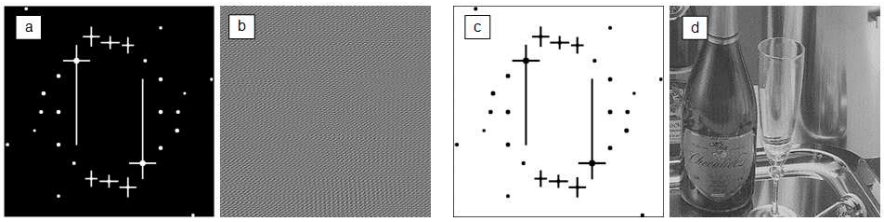

Figure 5
High frequency-passing (a) and -blocking (c) filters without a central circle and the resulting spatial domain images (b, d)

On the other hand, when the created filters did not contain the central circular masking regions, see Figures 5a and 5c, the results of applying these images to the original one (Figure 3a) were much better. In the case of using the filter that preserves exclusively high-frequency information (a), only the moiré pattern was visible (b), while when adopting the filter that attenuates or stops all high-frequency features in the original image (c), the result was a clear, almost moiré-free picture (d).

Conclusions

As the two presented examples demonstrate, FFT is a useful technique for transforming images into the frequency domain where appropriate either low-pass or high-pass filtering can be carried out. This enables on to make changes to the original images that would be very difficult to perform in the spatial domain using convolution operations. The clear separation of the two distinctive types of patterns present in a paper or board – non-periodic structures such as formation and periodic structures such as fabric marks – and a more detailed characterization of the latter, such as identification of the marks' angle, periodicity and origin, can be made using a standard PC with open-source image processing software.

A moiré pattern, a negative phenomenon often occurring in printing, was also successfully eliminated using FFT. Conventional, spatial filtering-based methods for dealing with moiré – e.g. the Gaussian blur – act on the image as a whole, resulting in a decrease in sharpness, and they are in general also less successful in removing a moiré pattern.

References

[1] Amidror I., *The Theory of the Moire Phenomenon, Computational Imaging and Vision*, Kluwer Academic Publishers, Netherlands, 2000, p. 474

[2] Benyó, B., *Acta Polytechn. Hung.,* 4(4): 66 (2007)

[3] Brigham E. O., *The fast Fourier Transform and its Applications,* Englewood Cliffs, N. J.: Prentice Hall, 1988, p. 2

[4] Burger W. and Burge M. J., *Digital Image Processing, An Algorithmic Introduction using Java*, Springer, New York, 2008, p. 318

[5] Biermann C. J., *Handbook of Pulping and Papermaking,* 2nd ed., Elsevier, 1996, p. 237

[6] Cooley, J. W. and Tukey, J. W., *Math. Comput.,* 19: 297-301(1965)

[7] Hains, C. M., *Digital Halftoning,* Tutorial notes, IS&T/SID 4th Color Imaging Conference, 1996

[8] I'Anson, S. J., *Tappi J.,* 78(3): 113(1995)

[9] I'Anson, S. J., *Tappi J.,* 78(7): 97(1995)

[10] Kafri O. and Glatt I., *The Physics of Moire Metrology,* John Wiley & Sons, New York, 1990, p. 1-l7

[11] Kang H. R., *Digital Color Halftoning,* SPIE/IEEE Series on Imaging Science & Engineering, New York, 1999, p. 509

[12] Nishijima, Y. and Oster, G., *J. Opt. Soc. Am.,* 54: 1-4(1964)

[13] Press W. H., Teukolsky S. A., Wetterling W. T., Flannery B. P., *Numerical Recipes – The Art of Scientific Computing,* 3rd ed., Cambridge University Press, 2007, p. 608

[14] Rasband, W. S., *ImageJ,* U. S. National Institutes of Health, Bethesda, Maryland, USA, 1997-2009, Website: http://rsb.info.nih.gov/ij/, Accessed: June 2011

[15] Smith S. W., *Chapter 8: The Discrete Fourier Transform. The Scientist and Engineer's Guide to Digital Signal Processing,* 2nd ed., San Diego, Calif.: California Technical Publishing, 1999, Website: http://www.dspguide.com/ch8.htm, Accessed: June 2011

[16] Spring, K. R. et al. (1998-2009): *Molecular Expressions: Optical Microscopy Primer – Digital image processing: Fourier Transform filtering techniques*, Website: http://micro.magnet.fsu.edu/primer/java/digitalimaging/processing/fouriertransform/, Accessed: June 2011

[17] Takasaki, H., *Appl. Opt.,* 9: 1467-1472 (1970)

[18] Theocaris P. S., *Moire Fringes in Strain Analysis,* Elsevier, 1969, p. 426

Assessment of the Nanohardness of a-SiC: H Film by Cyclic Nanoindentation

Daniel Tischler[*], Marie Válová[*], Ivo Štěpánek[**]

* CTU in Prague, Faculty of Mechanical Engineering, 167 06, Prague, Czech Republic, E-mail: daniel.tischler@fs.cvut.cz, marie.valova@fs.cvut.cz

** University of West Bohemia, Veleslavinova 11, 301 14 Plzen, Czech Republic, E-mail: ivo.stepanek@volny.cz

Abstract: Due to very little depth of indent, the cyclic nanoindentation test is used for nondestructive testing of thin films of amorphous hydrogenated silicon carbide (a-SiC: H). We prepared the films, containing various volumes of hexamethyldisiloxane (0.6 g/h and 1 g/h), onto stainless steel substrates by Plasma Enhanced Chemical Vapor Deposition technique. In this paper, the mechanical properties, especially nanohardness, are assessed by the cyclic nanoindentation test. We found out that higher volumes of vapors of Hexamethyldisiloxane cause increases in the nanohardness and thickness of the prepared film.

Keywords: cyclic nanoindentation; a-SiC: H thin film; hexamethyldisiloxane; PECVD

1 Introduction

Amorphous hydrogenated silicon carbide (a-SiC: H) coatings of a thickness of a few micrometers have been applied onto optoelectronic, photovoltaic [1] and dielectric diffusion barriers, and at present time they are a promising possibility for tribological applications in the mechanical and aeronautical industries [2].

The cyclic nanoindentation test is a very useful tool for measuring and evaluating nanohardness. The cyclic nanoindentation measurement is an advanced technique which derived from the nanoindentation technique. Due to the small mass of load used (e.g. 0.1 mN), which resulted in a very thin layer of the indent (about 1 μm), the cyclic nanoindentation test can be categorized as a nondestructive test. The little load of the indenter and progressive loading (and unloading) has the following advantages; the ratio of the depth of the indent to the depth of the thin layer is easy to maintain, and it is possible to study both the running of multilayer, sandwich and gradient systems and the running of degradation process from a deep profile. The measurement can be taken in a very small area. The

measurement can be taken directly on the thin layer-substrate systems. The changes in characteristic in the substrate interface can be evaluated. The hardness can be measured during the load and unload directly. The plastic and elastic deformation ratio can be determined. The correlation between the applied load and the depth of the indent is investigated by the measurement of the hardness. During the measurement, the depth of the indent is monitored at the load and unloads. From the so-called indentation curve, the correlation between the load and the depth of the indent, the hardness and other mechanical values can be obtained (e.g. Young's module, fracture toughness of brittle materials), as well as can be information about the plastic and elastic deformation ratio, etc. from the whole load cycle. Most frequently the Vickers sharp diamond quadrilateral pyramid or the Berkovich trilateral pyramid is used as an indentor for the hardness evaluation. Both the plastic and elastic deformations originate during the indentation of the indenter into the substrate. Only the nonreversible plastic deformations are preserved after unloading, so the plastic and elastic deformations can be distinguished [3].

In the experimental study, amorphous hydrogenated silicon carbide coatings (a-SiC:H) were prepared using the PECVD technique throughout the decomposition of hexamethyldisiloxane, which was diluted by a mixture containing vapors of argon (Ar) and methane (CH_4). The effect of hexamethyldisiloxane volume on the mechanical parameters of the deposited films is investigated and discussed. A comparative study has been carried out with the cyclic nanoindentation test under the same measurement conditions.

2 Experimental

2.1 Preparation of the Samples

Amorphous hydrogenated carbon films (a-SiC:H) were deposited onto a stainless steel substrate using plasma enhanced chemical vapor deposition (PECVD), which is described elsewhere [4] .The samples (size 20 mm in diameter × 5 mm in thickness) were polished to a surface roughness of R_a = 0.02. The samples were cleaned in an ultrasonic bath containing isopropylalkohol for 10 minutes and instantly put on an electrode of a plasma-chemical reactor. In order to remove any remaining impurities (including oxygen) and to activate the surface of the used samples, argon plasma precleaning was applied for 15 minutes (Ar: 60 sccm/min, 15 Pa). The mixture of Argon (Ar) and Methane (CH_4) was diluted by vapors of hexamethyldisiloxane in order to form a-SiC: H layers at work pressure 10 Pa in plasma immersion. Details are in table 1. The mentioned thickness was investigated after the test. The process gases as well as the vapors of

hexamethyldisiloxane were controlled by mass flow controls and the pressure was controlled using a butterfly valve. The working pressure (20 Pa) of the deposition processes was kept constant.

Table 1
Details of depositing parameters

Samples	Argon cleaning	HMDSO [g/hod]	Ar [sccm]	CH_4 [sccm]	Time [min]	Pressure [Pa]	Thickness [μm]
A	15 min	0,6	42	9	120	20	2
B	15 min	1	42	9	120	20	4,2

2.2 Nanoindentation and Cyclic Nanoindentation

The cyclic nanoindentation was derived from the conventional nanoindentation technique. In the first step, the tip is pressed into the material, resulting in indistinguishable elastic and plastic deformation. It is shown that the loading part of the curve is a combination of both elastic and plastic deformations, while the unloading curve is largely dominated by elastic deformation (Figure 1).

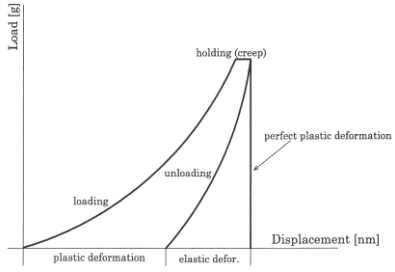

Figure 1
Nanoindentation curve

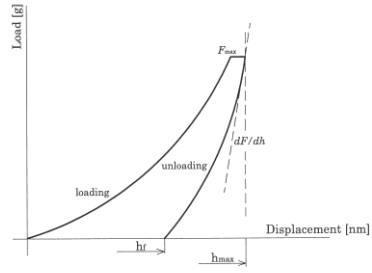

Figure 2
Nanoindentation curve. h_f = depth after unloading; h_{max} = depth at maximal load F_{max}

Then the tip is held at the maximum force, resulting in creep of the material under the tip. In the third step, the performed unloading leads to elastic recovery of the material. Usually, each indent requires 15 seconds to several minutes, representing a compromise between a desired quasi-static strain rate and the thermal drift of the instrument (possibly below 0.1 nm/second). This device is load-controlled, and linearly increasing and decreasing loading protocols were therefore applied. The loading rate corresponds to:

$$\frac{dF}{dt} = \frac{F_{\max}}{t}, \tag{1}$$

with $F_{\max}$ as the maximum load and t as the (un)loading time (Figure 2). According to the definition, the hardness is the resistance to local plastic deformation. It can be expressed as the maximum indentation loading, $F_{\max}$, divided by the projected contact area of the nanoindentation. The hardness, *H,* is determined as the ratio of the maximum load to the ("on load") contact area at maximum load:

$$H = \frac{F(h_{\max})}{A(h_{\max})}, \tag{2}$$

where $F(h_{\max})$ is the maximum load and $A(h_{\max})$ is the projected contact area as a function of the penetration depth h and can be determined according to the following form:

$$A(h) = 24{,}5.h^2, \tag{3}$$

where the constant of 24.5 was used for a perfect indenter tip. It should be noted that the results of traditional microhardness tests consider only the permanent plastic deformation. However, in nanoindentation tests, the area under the maximum indentation load may contain portions that do not show permanent plastic deformation, which Bhushan rightly called "on load", as mentioned before [5, 6]. From slope of unloaded curve, it is possible to assess stiffness, *S,* as:

$$S = \frac{dF}{dh}, \tag{4}$$

which is the gradient of changes characterizing elastic material properties [7, 8].

We investigated the roughness and thickness of the coating with the calotest method [9] and, above all, with the running of nanohardness of the prepared a-SiC: H layers. The cyclic nanoindentation measurements of the a-SiC:H coatings were carried out at room temperature using nanoindenter DUH 202 with Vickers shaped diamond tip with a load resolution of 0.1 mN. The distinguishing resolution is 0.2 nm. For these measurements mode 7 was applied, which is a unique modus for cyclic nanoindentation. The mode 7 enables the measurement of the cyclic indentation curves, gradually increasing the maximal normal load at several steps at each cycle during the time delay (1-10 s), up to the maximal normal load (Figure 3).

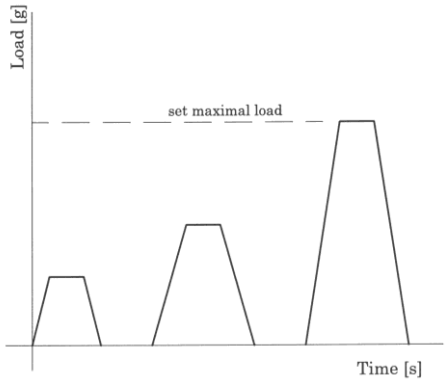

Figure 3
Gradually increasing load of cyclic test

The normal load is unloaded after each step to the pre-set minimal load. The nanohardness is evaluated during the measurement at each time delay. The mode 7 enables one to observe the plastic and elastic deformations at a particular step. Measurements were sequentially performed under maximum load of 200 g, 25 g and 5 g. Every cyclic nanoindentation test was performed in 20 cycles, with a gradually increased normal load. The first measurement was provided under the load of 10g to a maximum load of 200 g to obtain the hardness of substrate, which is influenced by deposited coating. The second measurement was provided under the load of 1.25 g to a maximum load of 25 g, for the determination of the properties of the interface of layer. Finally, the third measurement was performed under the load of 0.25 g to a maximum load of 5g to obtain the hardness of the thin film itself. The universal hardness was calculated from the load-displacement curves using an analysis programmer.

3 Results

The a-Si-C: H layers were obtained after 2 hours with the PECVD technique. From the calotest measurement was determined the thickness of coating (a) hexamethyldisiloxane (HMDSO): 0.6 g/h. 2 μm and the second coating (b) hexamethyldisiloxane: 1 g/h. 4.2 μm. The roughness of the layers was the same as of the substrates (Ra = 0,2). Cyclic nanoindentation tests were carried out by the equipment nanoindentor DUH 202 with a Vickers diamond-shaped tip. The nanoindentation measurement on all systems was performed by mode 7, which is able to register changes of surface and the deep profile of layers. Figure 4 shows the running of cyclic nanohardness of the examined layers for maximal load 200 g (Figure 4). We can see that every loading curve slightly overlapped the previous

unloading curve and was displaced slightly after each reloading cycle. In this case the influence of coating at a load of 200 g on the system has negligible significance; because the nanoindenter penetrates into greater depth than is the thickness of the film itself. So it is not possible to assess the properties of the thin films but rather the properties of the substrate, which is influenced by thin film. Evidently, the sample (a) HMDSO: 0.6 g/h compared to sample (b) HMDSO: 1 g/h has higher curves densification at a higher load, which is caused by the hardening in the deeper layers of substrate. The second sample (b) has more slopes of curves then sample (a) and therefore a higher ratio of elastic deformation than the first sample (a). Sample (b) has equal running of penetration of indenter.

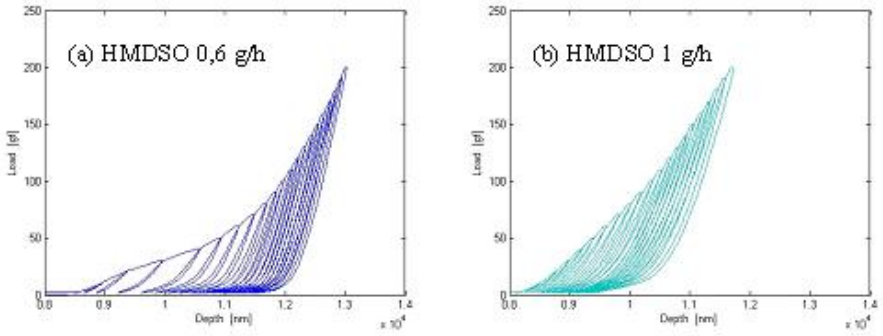

Figure 4
Records of cyclic nanoindentation test for maximal load 200 g

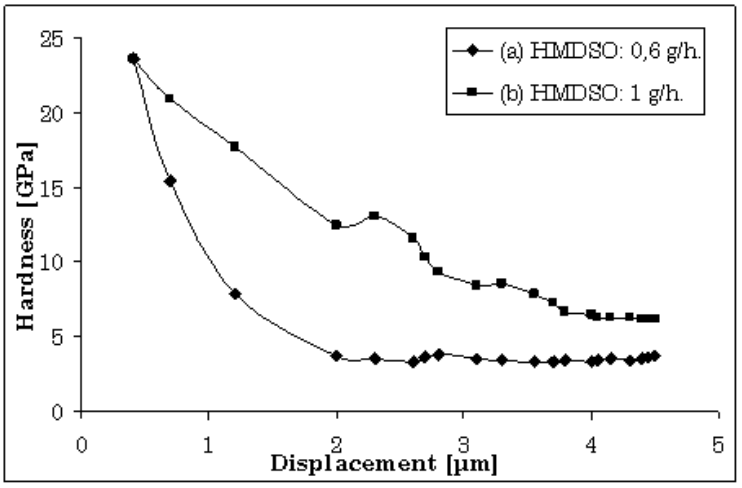

Figure 5
Record of hardness as a function of displacement. Max. load 200 g

In Figure 5 is shown the running of the universal hardness depending on displacement for a maximal loading of 200 g. In interval of displacement from 0.4 µm to 4.5 µm, the hardness for system (b) HMDSO: 1 g/h. downgrades linearly, while sample (a) HMDSO: 0.6 g/h. downgrades exponentially, which means in accord with Figure 4 that layer (a) is more ductile than the layer on the second sample (Figure 5). The hardness is from 23 GPa to 7 GPa, for system (b) and it is from 23 GPA to 4 GPa for system (a).

Figure 6 shows the load-unload curves obtained by cyclic nanoindentation for load 25 g (Figure 6). These runs of load-unload curves record the behavior of mechanical properties of interface of system substrate-coating a-SiC: H. The difference between layer (a) HMDSO: 0.6 g/h and (b) HMDSO: 1 g/h is evident.

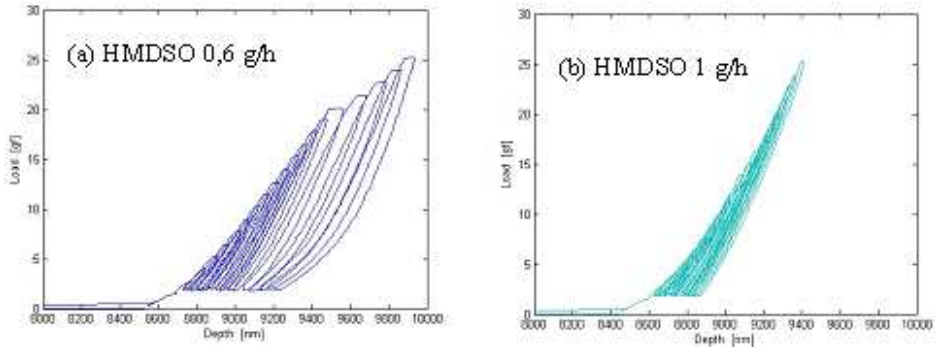

Figure 6
Records of cyclic nanoindentation test for maximal load 25 g

Layer (a) has a higher condensation of curves, due to the hardness of the surface of the thin film in the first third of the share. However, other curves are more diluted (the penetration is more rapid), which detects a break-through of the layer on the interface of the system. The running of all cyclic curves of layer (b) is similar. In Figure 7 is shown the running of the universal hardness, depending on load. During the displacement interval from 0.1 µm to 1.38 µm, the hardness for system (a) is from 38 GPa to 7 GPa, and for system (b) it is from 30 GPa to 14 GPA. The running of hardness of both curves is similar; however, the values of hardness of the layer (b) are significantly higher.

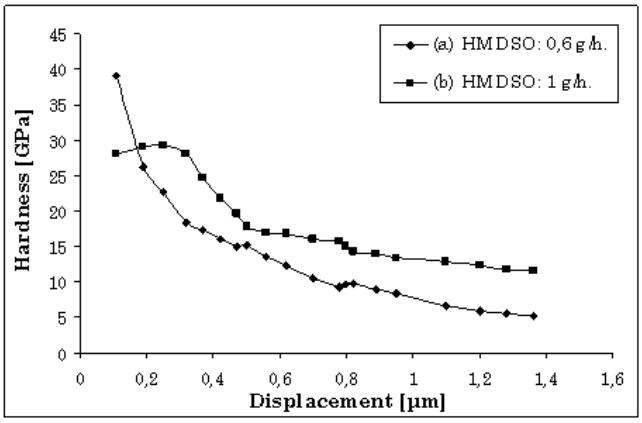

Figure 7
Record of hardness as a function of displacement. Max. load 25 g

Figure 8 records the running of the change of hardness of the a-SiC: H film itself at the maximum load of 5 g. The running of the curves of both layers is similar, because the effect of substrate is minimal, due to the little load (Figure 8).

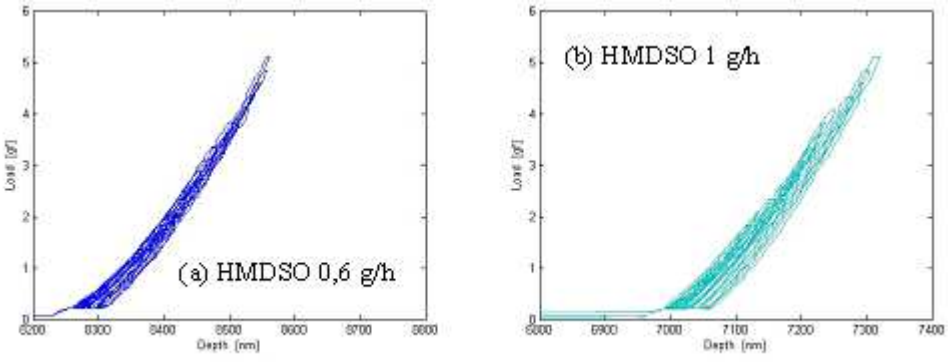

Figure 8
Record of cyclic nanoindentation test for maximal load 5 g

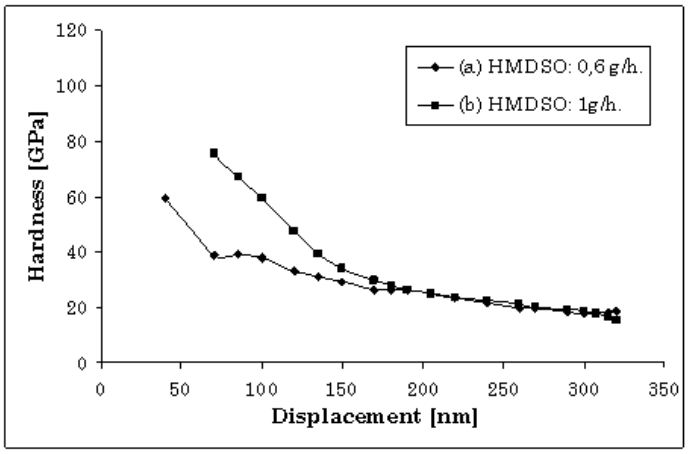

Figure 9
Record of hardness as a function of displacement. Max. load 5 g

From Figure 9 we can determine that in the displacement interval of 40 nm to 320 nm, the hardness for system (a) HMDSO: 0.6 g/h. is from 60 GPa to 20 GPa, and for system (b) HMDSO: 1 g/h., it is from 78 GPa to 20 GPA (Figure 9).

Conclusion

We achieved a-SiC:H coating on steel polished substrates under various flow of hexamethyldisiloxane. After 120 minutes, black, adherent, wear resistant and smooth coatings were obtained. The roughness of the layers was the same as for the substrates; $R_a = 0.02$. The thickness of the layer is 2 µm for system (a) and 4.2 µm for system (b). Via cyclic nanoindentation with a Vickers indenter, it was determined that the layer with flow of HMDSO - 1 g/h (system a) has higher value of hardness than the sample HMDSO – 0.6 (system b) for all loads of cyclic nanoindentation. The hardness of a single thin film is 20 GPa.

Acknowledgement

This research received support under Grant No. MSM 6840770012 of the Czech Republic Ministry of Education project “Trandisciplinary research in Biomedical Engineering II”. Authors gratefully acknowledge this support.

References

[1] A. Soum-Glaude, G.Rambaud, SE.Grillo, and L. Thomas: Investigation of the Tribological Behavior and its Relationship to the Microstructure and Mechanical Properties of a-SiC:H Films Elaborated by Low Frequency Plasma Assisted Chemical Vapor Deposition, Thin Solid Films 519 (2010) pp. 1266-1271

[2] M. Joinet, O. Borrod, L. Thomas, C. Picard, V. Lucas and F. Teyssandier.: Effect of Plasma Treatments on the Adhesion Properties of PACVD a-

SiC:H Coatings on TA6V Alloy, Diamond & Related Materials 16 (2007) pp. 1254-1258

[3] I. Stepanek, O. Bláhová O, M. Kolega: Tenke vrstvy – vytvareni, vlastnosti, Plzen, 1994

[4] D. Tischler, Z. Budinská, I. Stepanek: Si and Gradient Layer Formed by RF PACVD Technology, Manufacturing Engineering 10 (2011) pp. 32-35

[5] Shan, and S. K. Sitaraman. Elastic-Plastic Characterization of Thin Films Using Nanoindentation Technique. Thin Solid Films 437 (2003) pp. 176-181

[6] B. Bhushan, Springer Handbook of Nanotechnology, Springer, 2004, p.677

[7] M. A. Ekwinska, Z. Rymuza, New Approach to Estimate Nanowear Test Results through Nanoindentation Test. Microelectronic Engineering 87 (2010) pp. 1404-1409

[8] W. Jiang, J. Su, X. Feng. Effect of Surface Roughness on Nanoindenation Test of Thin Films. Engineering Fracture Mechanics 75 (2008) pp. 4965-4972

[9] D. Lusk, M. Gore, W. Boardman. Thick DLC Films Deposited by PECVD on the Internal Surface of Cylindrical Substrates. Diamond and Related Materials 17 (2008) pp. 1613-1621

A Comparison of Constructive Heuristics with the Objective of Minimizing Makespan in the Flow-Shop Scheduling Problem

Pavol Semančo and Vladimír Modrák

Faculty of Manufacturing Technologies with seat in Prešov, TUKE, Bayerova 1, 08001 Prešov, Slovakia, pavol.semanco@tuke.sk, vladimir.modrak@tuke.sk

Abstract: We propose a constructive heuristic approach for the solution of the permutation flow-shop problem. The objective function of all algorithms is the minimization of the makespan. Our approach employs Johnson's rule to give a good initial solution for the improvement heuristic, also known as metaheuristics. The proposed heuristic algorithm, named MOD, is tested against four other heuristics that are well-known from the open literature, namely, NEH, Palmer's Slope Index, CDS and Gupta's algorithm. The computational experiment itself contains 120 benchmark problem data sets proposed by Taillard. We compare our results to the solutions represented by NEH outputs. The computational experiment shows that the proposed algorithm is a feasible alternative for practical application when solving n-job and m-machine in flow-shop scheduling problems to give relatively good solutions in a short-time interval.

Keywords: heuristic algorithm; NEH; Palmer's Slope Index; CDS; Gupta's algorithm; benchmark problem; flow shop

1 Introduction

Many manufacturing industries meet with the problem of how to effectively commit resources between varieties of possible orders in the current competitive environment. The searching for an optimal allocation of resources to performing a set of jobs within each work order is the main role of scheduling, which has become a necessity decision-making process in manufacturing. The main problems in scheduling of jobs in manufacturing are, according to Wight [24], "priorities" and "capacity". Hejazi and Saghafian [4] characterize the scheduling problem as an effort "to specify the order and timing of the processing of the jobs on machines, with an objective or objectives."

In this paper, we focus on an environment where all jobs have to follow the same route in the same order and where machines are assumed to be set up in a series,

which is also referred to as a flow shop. We consider general flow-shop scheduling with unlimited intermediate storage, where it is not allowed to sequence changes between machines. In this flow shop, referred to as permutation flow shop, the same job sequence of jobs is maintained throughout.

Although we limited our attention to only permutation schedules with constant setup times that are included in processing times and to availability of all jobs at zero time, these kinds of algorithms can be used to improve logistic chains of container transport as well [16].

The general flow-shop problem with a makespan (Cmax) objective can be denoted as an n/m/F/Cmax that involves n jobs where each requiring operations on m machines, in the same job sequence. The solution of such problem is represented by the optimal job sequence that produces the smallest makespan, assuming no preemption of jobs. The general flow-shop problem is also assumed as NP-hard for m>2.

We propose a constructive heuristic approach, based on application of Johnson's algorithm for the solution of the NP-hard flow-shop problem. Our approach uses a pair-splitting strategy to create a two-machine problem. We provide empirical results for Taillard's problem, instances demonstrating the efficacy of the approach in finding a good initial speed.

Common algorithms to solve NP-hard problems are heuristics giving solutions that do not necessarily have to be close to the optimum. However, they give good initial solutions in a reasonable time. Based on the literature, there are two well-known types of heuristics: constructive and improvement heuristics. The constructive heuristic starts without a schedule or job sequence and adds one job at a time. The most popular constructive heuristics are CDS [1] and NEH [11]. Improvement heuristics use as a initial position a schedule, mostly represented by the result of constructive heuristic, and they try to find a better "similar" schedule, referred to as improved solution. These iterative approaches, referred to as meta-heuristic approaches, are inherently local search techniques, such as, for example, tabu search (TS), simulated annealing (SA), genetic algorithms (GA), etc.

We test our approach on a dataset including 120 benchmark problems of Taillard [20]. We compare the results of four constructive heuristics, namely MOD, CDS, Gupta's algorithm and Palmer's slope index algorithm, with the well-known NEH algorithm set as a reference algorithm.

The next section covers a review of the relevant literature of the flow-shop scheduling heuristics. Section 3 analyzes the formal description of the MOD approach. In Section 4, we provide a discussion of computational experiment and results. Section 5 reports a summary of the paper and discusses possible future research ideas.

2 Literature Review

The scheduling literature provides a rich knowledge of the general flow-shop scheduling problem to get permutation schedules with minimal makespan. It can be stated that this is a very popular topic in scheduling circles.

Taylor [21] and Gantt [2], the inventor of well-known Gantt charts that are still accepted as important scheduling tools today, give the first scientific consideration to production scheduling. Pinedo [17] is a superior reference for all types of scheduling problems, including flow-shop environment together with tutorials, and scheduling systems. Vieira et al. [23] present a framework for rescheduling when differences between the predetermined schedule and its actual realization on the shop floor effect of disturbances in the performance of the system.

Production scheduling systems that emerged later were mostly connected to shop floor tracking systems and were dispatching rules to sequence the work [5]. Similar scheduling systems are today implemented in ERP systems that were performed in the early 1990s.

Modrak [10] discusses manufacturing execution systems (MES) with integrated scheduling systems in the role of a link interface between a business level and shop floor.

Heuristic solutions for the permutation flow-shop scheduling problem range from constructive heuristics, such as CDS and the NEH algorithm, to more complex approaches, known as meta-heuristics, namely branch and bound, tabu search, genetic algorithms and the ant colony algorithm.

Johnson [6] first presented an algorithm that can find the optimum sequencing for an n-job and 2-machine problem. The concept of a slope index as a measure to sequence jobs was firstly introduced by Page [14]. Later on, Palmer [15] adopted this idea and utilized the slope index to solve job sequencing for the m-machine flow-shop problem. Gupta [3] argued that the sequencing problem is a problem of sorting n items to minimize the makespan. He proposed alternative algorithm for calculating the slope index to schedule a sequence of jobs for more than two machines in a flow-shop scheduling problem.

Campbell et al. [1] proposed a simple heuristic extension of Johnson's algorithm to solve an m-machines flow shop problem. The extension is known in literature as the Campbell, Dudek, and Smith (CDS) heuristic.

Nawaz et al. [11] proposed the NEH algorithm, which is probably the most well-known constructive heuristic used in the general flow-shop scheduling problem. The basic idea is that a job with the largest processing time should have highest priority in the sequence. Results obtained by Kalczynski and Kamburowski [7] have also given proof that many meta-heuristic algorithms are not better than the simple NEH heuristic. The proof is also supported by famous "No Free Lunch"

(NFL) theorem, which points out that all algorithms equal to the randomly blind search if no problem information is known [25]. The solution quality greatly depends on the technique selection, which does not necessarily need to perform as well on other types of problem instances if it fits a specific type of problem instances.

The most emphasized names among the contributors of meta-heuristic approaches are as follows: Ogbu and Smith [13] with their simulated annealing approach; Nowicki and Smutnicki [12], who implemented tabu search to solve the flow-shop scheduling problem; And Reeves and Yamada [18], who applied the genetic algorithm for PFSP. The new accession to the family of meta-heuristic scheduling algorithms is a water-flow like algorithm [22]. The Hybrid algorithm, based on the genetic algorithm, was applied in order to find optimal makespan in an n-job and m-machine flow-shop production, see [19].

In this paper, we focus on using Palmer, Gupta, CDS and NEH heuristics against MOD approach. For details on these heuristics, see [1], [3], [8], [11] and [15].

3 Constructive Heuristic MOD

In this section we formally explain the steps of the constructive heuristic approach used to obtain a good initial solution. Further details of this heuristic are referred to in [9]. The general idea is that we adopt the Johnson's rule in the last step of our proposed algorithm to get the minimum makespan. We use the difference between the sums of processing times for each machine as a pair-splitting strategy to make two groups of the matrix of n-job and m-machine. We further explain our approach mathematically.

3.1 Notation

The following notations were used:

J	set of n jobs $\{1, 2, \ldots, n\}$
M	set of m machines $\{1, 2, \ldots, m\}$
M_p	set of two pseudo machines $\{1, 2\}$
G	set of 2 clusters $\{I, II\}$
k	number of k machines
l	number of m-k machines
I	cluster of k machines
II	cluster of m-k machines

p_{ij} processing time of *i*th job on *j*th machine, $i \in J$ and $j \in M$

P_j sum of processing time of *n* jobs on *j*th machine

$\sum Pg$ total sum of processing time of *n* jobs on machines in *g*th group, $g \in G$

it well-fitting iteration number

DIF_{it} difference between groups *I* and *II*

C_{max} makespan

C_j completion time

s splitting ratio

s_{max} max splitting ratio

3.2 MOD Algorithm

Step 1: Calculate the sum of processing time

$$P_j = \sum_{i=1}^{n} p_{ij} \forall i \in J, j \in M \tag{1}$$

Step 2: Compute the total sum of the processing time for each cluster

Calculate ΣP_I , ΣP_{II} of cluster *I* and *II* as follows:

$$\sum P_I = \sum_{j=1}^{k} P_j \forall k \in I, j \in M \tag{2}$$

$$\sum P_{II} = \sum_{j=m-k}^{m} P_j \forall k \in I, j \in M \tag{3}$$

Step 3: *Compute the splitting ratio and apply the pair-splitting strategy*

Compute the splitting ratio for this iteration given by:

$$s_k = \frac{\min(\Sigma P_I ; \Sigma P_{II})}{\max(\Sigma P_I ; \Sigma P_{II})} \tag{4}$$

Apply the pair-splitting strategy:

a. If s_k is the maximum ratio so far, save the current *k* as well-fitting iteration (*it*) and the ratio as the maximum ratio (s_{max}).

b. If $k = m$ then go to *Step 5.*

c. If $s_k = 1$, go to *Step 5.*

Step 4: Next iteration

Increment k by one and go back to *Step 2*.

Step 5: Compute the completion time for each cluster and create two pseudo machines

Calculate the completion time C_j of ith job for both clusters according to following formulas ($k = it$):

a. Cluster *I*:

$$C_j = k \cdot p_{1j} + (k-1) \cdot p_{2j} + \ldots + p_k \tag{5}$$

b. Cluster *II*:

$$C_j = l \cdot p_{1j} + (l-1) \cdot p_{2j} + \ldots + p_l \tag{6}$$

Tabulate these values into two rows to get two pseudo machines (M_{p1}, M_{p2}).

Step 6: Apply Johnson's rule on the two pseudo machines

Apply Johnson's rule on the two pseudo machines of n jobs to get the job sequence.

Step 7: Display the solution

The C_{max} of particular job sequence from *Step 6* is the solution.

3.3 Pair-Splitting Strategy and Parameters

In Step 3 of Section 3.2, there are two splitting parameters, namely the splitting ratio (s) and well-fitting iteration number. We explain each of these parameters next.

3.3.1 Splitting Ratio

The splitting ratio is one of the parameters that control the degree of similarity of two created clusters. The pair of clusters with the highest rate is used for further computation. The splitting ratio ranges from 0 to 1, where 1 indicates the same size of two clusters and vice versa.

3.3.2 Well-fitting Iteration

We also build a parameter to backtrack the best pair of clusters created from the n-job and m-machine mechanism matrix. The well-fitting iteration parameter also indicates the number of machines for the cluster *I*.

4 Computational Experiments

We ran our experiment with objective of minimizing the makespan on Taillard's benchmark problem datasets, which has 120 instances, 10 each of one particular size. Taillard's datasets range from 20 to 500 jobs and 5 to 20 machines. The outputs of the NEH algorithm were used as reference solutions for comparison purposes.

4.1 Platform and Parameters

We coded the MOD, NEH, CDS, Palmer's Slope Index and Gupta's algorithms in PHP script, running on a PC with a 3.06 GHz Intel Core and 2GB of RAM. All PHP-coded algorithms have a user-friendly interface with the possibility to select whether to run each heuristic individually or altogether. It has also an option to draw a Gantt chart with a legend.

4.2 Performance Measures

We used a relative percent deviation (RPD) and an average relative percent deviation (ARPD) as performance measures for comparing the solutions of each algorithm to the reference solutions.

The relative percent deviation and average percentage relative deviation is given by:

$$RPD_i = \frac{HS_i - RS_i}{RS_i} \cdot 100\% \tag{7}$$

$$ARPD = \frac{1}{I} \cdot \sum_{i=1}^{I} RPD_i \tag{8}$$

where: I number of problem instances,

HS_i heuristic solution of problem instance *i,*

RS_i reference solution of problem instance *i,*

RPD_i percentage relative deviation of problem instance *i.*

4.3 Results

In the computational experiment, we use the problem instances described earlier. The summary results for Taillard's 120 instances are shown in tables 1 to 4. Each of the summary tables displays the results for MOD, CDS, Gupta's algorithm,

Palmer's Slope Index and the NEH alone. The computational experiment takes the performance indicators of the algorithms to be the solution quality (C_{max}) and runtime (CPU). Tables 1 to 3 show the computational results of makespans and RPDs for each algorithm and for each problem instance.

Table 1

Makespans and RPDs for Taillard's 20-job and 50-job benchmark-problem datasets

Problem instance	NEH (Reference makespan)	MOD		CDS		Gupta		Palmer	
		C_{max}	RPD	C_{max}	RPD	C_{max}	RPD	C_{max}	RPD
20x5									
1	1299	1322	1.8	1436	10.5	1400	7.8	1384	6.5
2	1365	1433	5.0	1424	4.3	1380	1.1	1439	5.4
3	1132	1136	0.4	1255	10.9	1247	10.2	1162	2.7
4	1329	1475	11.0	1485	11.7	1554	16.9	1420	6.8
5	1305	1355	3.8	1367	4.8	1370	5.0	1360	4.2
6	1251	1299	3.8	1387	10.9	1333	6.6	1344	7.4
7	1251	1366	9.2	1403	12.2	1390	11.1	1400	11.9
8	1215	1312	8.0	1395	14.8	1410	16.0	1290	6.2
9	1284	1371	6.8	1360	5.9	1444	12.5	1426	11.1
10	1127	1235	9.6	1196	6.1	1194	5.9	1229	9.1
20x10									
1	1681	1789	6.4	1833	9.0	2027	20.6	1790	6.5
2	1766	1802	2.0	2021	14.4	1960	11.0	1948	10.3
3	1562	1621	3.8	1819	16.5	1780	14.0	1729	10.7
4	1416	1575	11.2	1700	20.1	1730	22.2	1585	11.9
5	1502	1714	14.1	1781	18.6	1878	25.0	1648	9.7
6	1456	1607	10.4	1875	28.8	1650	13.3	1527	4.9
7	1531	1650	7.8	1826	19.3	1761	15.0	1735	13.3
8	1626	1799	10.6	2056	26.4	2084	28.2	1763	8.4
9	1639	1731	5.6	1831	11.7	1837	12.1	1836	12.0
10	1656	1917	15.8	2010	21.4	2137	29.0	1898	14.6
20x20									
1	2443	2787	14.1	2808	14.9	2821	15.5	2818	15.3
2	2134	2331	9.2	2564	20.1	2586	21.2	2331	9.2
3	2414	2598	7.6	2977	23.3	2900	20.1	2678	10.9
4	2257	2541	12.6	2603	15.3	2670	18.3	2629	16.5
5	2370	2615	10.3	2733	15.3	2868	21.0	2704	14.1
6	2349	2439	3.8	2707	15.2	2722	15.9	2572	9.5
7	2383	2465	3.4	2684	12.6	2796	17.3	2456	3.1
8	2249	2467	9.7	2523	12.2	2612	16.1	2435	8.3
9	2306	2550	10.6	2617	13.5	2701	17.1	2754	19.4
10	2257	2557	13.3	2649	17.4	2690	19.2	2633	16.7
50x5									
1	2729	2839	4.03	2883	5.64	2820	3.33	2774	1.65
2	2882	3152	9.37	3032	5.20	2975	3.23	3014	4.58
3	2650	2850	7.55	3010	13.58	3071	15.89	2777	4.79
4	2782	2925	5.14	3179	14.27	3102	11.50	2860	2.80
5	2868	2882	0.49	3188	11.16	3114	8.58	2963	3.31

Table 2
Makespans and RPDs for Taillard's 50-job and 100-job benchmark-problem datasets

Problem instance	NEH (Reference makespan)	MOD		CDS		Gupta		Palmer	
		C_{max}	RPD	C_{max}	RPD	C_{max}	RPD	C_{max}	RPD
50x5									
6	2835	2959	4.37	3175	11.99	3104	9.49	3090	8.99
7	2806	3021	7.66	3005	7.09	3109	10.80	2845	1.39
8	2700	2827	4.70	3189	18.11	3091	14.48	2826	4.67
9	2606	2783	6.79	3171	21.68	3211	23.22	2733	4.87
10	2801	2827	0.93	3224	15.10	3092	10.39	2915	4.07
50x10									
1	3175	3468	9.23	3671	15.62	3672	15.65	3461	9.01
2	3073	3174	3.29	3645	18.61	3577	16.40	3313	7.81
3	2994	3191	6.58	3677	22.81	3670	22.58	3335	11.39
4	3218	3417	6.18	3707	15.20	3645	13.27	3511	9.11
5	3186	3417	7.25	3664	15.00	3499	9.82	3427	7.56
6	3148	3340	6.10	3584	13.85	3559	13.06	3318	5.40
7	3277	3539	8.00	3784	15.47	3723	13.61	3457	5.49
8	3170	3407	7.48	3744	18.11	3746	18.17	3382	6.69
9	3025	3422	13.12	3518	16.30	3561	17.72	3414	12.86
10	3267	3370	3.15	3913	19.77	3699	13.22	3404	4.19
50x20									
1	4006	4347	8.51	4759	18.80	4645	15.95	4272	6.64
2	3958	4370	10.41	4414	11.52	4354	10.01	4303	8.72
3	3866	4265	10.32	4469	15.60	4485	16.01	4210	8.90
4	3953	4360	10.30	4793	21.25	4773	20.74	4233	7.08
5	3872	4218	8.94	4642	19.89	4649	20.07	4376	13.02
6	3861	4320	11.89	4505	16.68	4714	22.09	4312	11.68
7	3927	4138	5.37	4758	21.16	4665	18.79	4306	9.65
8	3914	4295	9.73	4609	17.76	4577	16.94	4318	10.32
9	3970	4277	7.73	4465	12.47	4543	14.43	4547	14.53
10	4036	4222	4.61	4556	12.88	4488	11.20	4197	3.99
100x5									
1	5514	5929	7.53	5602	1.60	5765	4.55	5749	4.26
2	5284	5436	2.88	5669	7.29	5697	7.82	5316	0.61
3	5222	5323	1.93	5638	7.97	5531	5.92	5325	1.97
4	5023	5310	5.71	5287	5.26	5269	4.90	5049	0.52
5	5261	5424	3.10	5584	6.14	5535	5.21	5317	1.06
6	5154	5278	2.41	5203	0.95	5200	0.89	5274	2.33
7	5282	5530	4.70	5557	5.21	5434	2.88	5376	1.78
8	5140	5230	1.75	5509	7.18	5504	7.08	5263	2.39
9	5489	5538	0.89	5821	6.05	5901	7.51	5606	2.13
10	5336	5593	4.82	5740	7.57	5670	6.26	5427	1.71
100x10									
1	5897	6208	5.27	6749	14.45	6549	11.06	6161	4.48
2	5466	5745	5.10	6285	14.98	6238	14.12	5889	7.74
3	5747	6043	5.15	6648	15.68	6359	10.65	6119	6.47
4	5924	6368	7.49	6848	15.60	6908	16.61	6329	6.84
5	5672	6025	6.22	6399	12.82	6499	14.58	6070	7.02
6	5395	5852	8.47	6136	13.73	6154	14.07	5870	8.80
7	5717	6359	11.23	6417	12.24	6535	14.31	6442	12.68
8	5752	6300	9.53	6513	13.23	6425	11.70	6168	7.23
9	6016	6304	4.79	6356	5.65	6386	6.15	6081	1.08
10	5937	6287	5.90	6835	15.13	6816	14.81	6259	5.42

Table 3
Makespans and RPDs for Taillard's 100-job, 200-job and 500-job benchmark-problem datasets

Problem instance	NEH (Reference makespan)	MOD		CDS		Gupta		Palmer	
		C_{max}	RPD	C_{max}	RPD	C_{max}	RPD	C_{max}	RPD
100x20									
1	6520	7092	8.77	7584	16.32	7668	17.61	7075	8.51
2	6550	7194	9.83	7615	16.26	7600	16.03	7058	7.76
3	6621	7350	11.01	7526	13.67	7628	15.21	7181	8.46
4	6589	7226	9.67	7909	20.03	7802	18.41	7039	6.83
5	6697	7057	5.38	7681	14.69	7628	13.90	7259	8.39
6	6813	7234	6.18	7582	11.29	7832	14.96	7109	4.34
7	6578	7156	8.79	8125	23.52	7892	19.98	7279	10.66
8	6791	7425	9.34	7902	16.36	8098	19.25	7567	11.43
9	6679	7017	5.06	7668	14.81	7687	15.09	7271	8.86
10	6680	7267	8.79	7947	18.97	7557	13.13	7305	9.36
200x10									
1	10949	11631	6.23	12151	10.98	12220	11.61	11443	4.51
2	10677	11236	5.24	12088	13.22	12170	13.98	10986	2.89
3	11080	11575	4.47	12378	11.71	11948	7.83	11336	2.31
4	11057	11397	3.07	11730	6.09	11676	5.60	11265	1.88
5	10615	11202	5.53	11634	9.60	11604	9.32	11125	4.80
6	10495	11438	8.99	11854	12.95	11592	10.45	10865	3.53
7	10950	11554	5.52	12436	13.57	12055	10.09	11333	3.50
8	10834	11361	4.86	11801	8.93	12088	11.57	11275	4.07
9	10565	11230	6.29	12197	15.45	12189	15.37	11184	5.86
10	10808	11436	5.81	11758	8.79	11893	10.04	11355	5.06
200x20									
1	11638	12750	9.55	13446	15.54	13724	17.92	13042	12.06
2	11678	12494	6.99	13129	12.43	13132	12.45	12813	9.72
3	11724	12799	9.17	13578	15.81	13651	16.44	12846	9.57
4	11796	12734	7.95	13297	12.72	13608	15.36	13061	10.72
5	11670	12559	7.62	13004	11.43	13132	12.53	12827	9.91
6	11805	12491	5.81	13583	15.06	13233	12.10	12381	4.88
7	11876	12511	5.35	13110	10.39	13175	10.94	12584	5.96
8	11824	12561	6.23	13799	16.70	13929	17.80	12824	8.46
9	11801	12886	9.19	13289	12.61	13407	13.61	12523	6.12
10	11890	12862	8.17	13709	15.30	13720	15.39	12615	6.10
500x20									
1	26774	28551	6.64	30650	14.48	29851	11.49	28246	5.50
2	27215	29031	6.67	30838	13.31	29804	9.51	29439	8.17
3	26941	28432	5.53	30532	13.33	29960	11.21	28073	4.20
4	26928	28342	5.25	30208	12.18	30372	12.79	28058	4.20
5	26928	28286	5.04	29917	11.10	29540	9.70	27768	3.12
6	27047	28428	5.11	29866	10.42	29868	10.43	28516	5.43
7	26820	28116	4.83	30428	13.45	29955	11.69	27878	3.94
8	27230	28293	3.90	30073	10.44	30021	10.25	28294	3.91
9	26541	27892	5.09	29120	9.72	30065	13.28	27745	4.54
10	27103	28979	6.92	30232	11.54	30498	12.53	28313	4.46
ARPD			**6.88**		**13.54**		**13.36**		**7.10**

The final line of Table 3 gives the overall average RPD values over all problem instances.

The solutions of developed algorithm and those of CDS, Gupta's algorithm, and Palmer's Slope Index algorithm are compared with the NEH optimal solutions for problems with a size up to 20 machines and 500 jobs.

From the results we can also make the following observations. Overall, the MOD heuristic performed better than any of tested algorithms with the exception of the NEH algorithm that was used as reference heuristic for this study. MOD's average RPD for all 120 Taillard's problems came at 6.88%. The cost of computing time was insignificant, in contrast to other three tested algorithms.

For Taillard's 20-job problems, i.e., 20x5, 20x10 and 20x20 size problems, MOD found the closest match to the reference solutions for 19 of the 30 problems. The average RPD of the MOD approach for the 20-job problems came at 8.06%. Thus, MOD performed very well on the 20-job Taillard's problems. For 50-job problems, i.e., 50x5, 50x10 and 50x20 size problems, MOD's average relative percentage deviation was 6.97%, which is the smallest ARPD of all four algorithms. For the 100-job problems, MOD's varied by the overall size of the problem. The 100x5 problems were solved to within an average RPD of 3.57%, while the 100x20 problems came at an average RPD of 8.28%.

Instead of displaying the times for each problem individually, we grouped the average computational times for each size of the problem. The average computational times (CPU) are summarized for each size of the problem and depicted in Figure 1. The CPU times, as can be seen from the graph, vary by the size of the problem. For example, MOD took between 153 and 157 milliseconds for 500-job problems. CDS took from 86 to 90 milliseconds and NEH from 617248 to 640114 milliseconds for 500x20 problems.

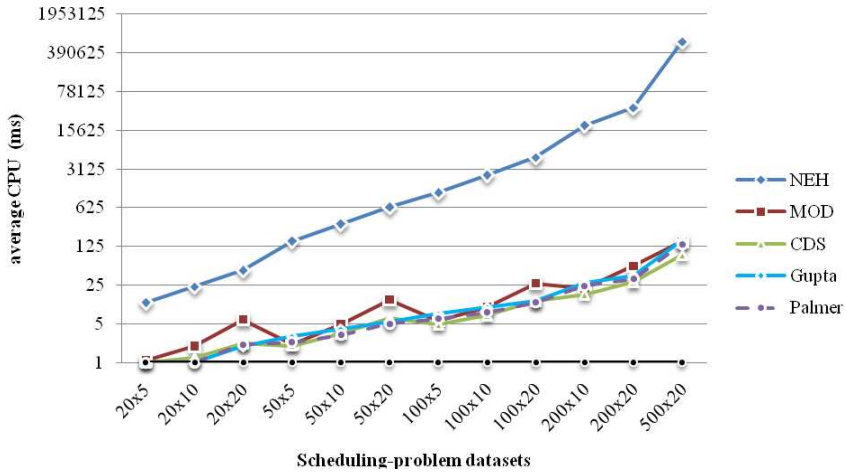

Figure 1
Average CPU times for each group of the problems

Conclusions

In the presented study, a constructive heuristic based on Johnson's rule is presented for the sequencing problem with sequence-dependent jobs, which is a quite common problem in many industries. The approach uses pair-splitting strategy and tries to find the minimal makespan. Based on the tested problems involving multiple jobs and machines, the proposed approach proved that is capable of good results. The proposed algorithm gave the best performance of all four approaches. The average RPD from the reference algorithm was 6.88% for all Taillard's problems.

The MOD approach was used to give a better solution than three other heuristics, namely Palmer, CDS and Gupta. For all three heuristics, the MOD algorithm showed significant improvements and compared well with the best-known NEH heuristic. Empirical testing on 120 benchmark problems drawn from Taillard produced some very good results.

We thus make an important contribution by proposing a new constructive heuristic for solving the permutation flow-shop scheduling problem with the objective of minimizing the makespan. The MOD algorithm finds near-optimal solutions for many benchmark problems in a reasonable time.

Future research could address this approach to more difficult flow-shop problems involving sequence-dependent setup times. Different objective functions can also be tested. Larger problems could be attempted with this approach. Future research can further try to find better pair-splitting strategies.

Acknowledgement

This work has been supported by the Grant Agency of the Ministry of Education of the Slovak Republic and Slovak Academy of Sciences (VEGA project No. 1/4153/07 "Development and application of heuristics methods and genetic algorithms for scheduling and sequencing of production flow lines").

References

[1] Campbell, H. G. et al.: A Heuristic Algorithm for The n-job, m-machine Scheduling Problem, Management Science 16, 1970, pp. 630-637

[2] Gantt, H. L.: Organizing for Work, New York: Harcourt, Brace, and Howe, 1919

[3] Gupta, J. N. D.: A Functional Heuristic Algorithm for the Flow Shop Scheduling Problem. Operational Research Quarterly 22, 1971, pp. 39-47

[4] Hejazi, S. R., and Saghafian, S.: Flowshop Scheduling Problems with Makespan Criterion: A Review, International Journal of Production Research, 43(14), 2005, pp. 2895-2929

[5] Herrmann, J. W.: Handbook of Production Scheduling, New York: Springer, 2006

[6] Johnson, S. M.: Optimal Two- and Three-Stage Production Schedules with Setup Times Included, Naval Research Logistics Quarterly 1, 1954, pp. 61-68

[7] Kalczynski, P. J. et al.: On the NEH Heuristic for Minimising the Makespan in Permutation Flowshops, The International Journal of Management Science, 35 (1), 2007, pp. 53-60

[8] Malindzak, D.: Models and Simulation in Logistics, Acta Montanistica Slovaca, 15 (1), 2010, pp. 1-3

[9] Modrak, V. et al.: Flow Shop Scheduling Algorithm to Minimize Completion Time for n-jobs m-machines Problem, Tehnicki Vjesnik, 17(3), 2010, pp. 273-278.

[10] Modrak, V. et al.: Mapping Development of MES Functionalities, Proceedings of 6th International Conference on Informatics in Control, Automation and Robotics, 2009, pp. 244-247

[11] Nawaz, M. et al.: A Heuristic Algorithm for the m-machine, n-job Flow Shop Sequencing Problem, International Journal of Management Science 11, 1983, pp. 91-95

[12] Nowicki, E. et al.: A Fast Tabu Search Algorithm for the Permutation Flow-Shop Problem, Eur. J. Oper. Res. 91, 1996, pp. 160-175

[13] Ogbu, F. A. et al.: The Application of the Simulated Annealing Algorithm to the Solution of the n/m/c Subscript Max Flowshop Problem, Computers Ops Res. 17, 1990, pp. 243-253

[14] Page, E. S.: An Approach to Scheduling of Jobs on the Machines, J. Royal Stat. Soc., 23, 1961, pp. 484-492

[15] Palmer, D. S.: Sequencing Jobs through a Multi-Stage Process in the Minimum Total Time - a Quick Method of Obtaining a Near Optimum, Operational Research Quarterly 16, 1965, pp. 101-107

[16] Pap, E. et al.: Application of Pseudo-Analysis in the Synchronization of Container Terminal Equipment Operation, Acta Polytechnica Hungarica, 8(6), 2011, pp. 5-21

[17] Pinedo, M.: Scheduling: Theory, Algorithms and Systems, New Jersey: Springer, 2008

[18] Reeves, C. R. et al.: Genetic Algorithms, Path Relinking, and Flow Shop Problem, Evolutionary Computation 6, 1998, pp. 45-60

[19] Semanco, P. et al.: Hybrid GA-based Improvement Heuristic with Makespan Criterion for Flow-Shop Scheduling Problems, Communications in Computer and Information Science, 220, 2011, pp. 11-18

[20] Taillard, E.: Benchmarks for Basic Scheduling Problems, European Journal of Operational Research 64, 1993, pp. 278-285

[21] Taylor, F. W.: Principles of Scientific Management, New York and London: Harper & brothers, 1911

[22] Tran, T. H. et al.: A Water-Flow Algorithm for Flexible Flow Shop Scheduling with Intermediate Buffers, Journal of Scheduling, 14 (5), 2010, pp. 483-500

[23] Vieira, G. E. et al.: Rescheduling Manufacturing Systems: A Framework of Strategies, Policies, and Methods, Journal of Scheduling, 6(1), 2003, pp. 35-58

[24] Wight, O. W.: Production and Inventory Management in the Computer Age, New York: Van Nostrand Reinhold Company, Inc. 1984

[25] Wolpert, D. H. et al.: No Free Lunch Theorems for Optimization, Proceedings of IEEE Trans. Evol. Comput, 1 (1), 1997, pp. 67-82

One Simple Way of Comparing the Bandwidth of a Signaling CCS No7 Channel under the Influence of Bursty and Random Errors

Dragan Mitić, Aleksandar Lebl, Žarko Markov

Institute for Telecommunications and Electronics, Iritel A.D. Belgrade
Batajnički put 23, 11080 Belgrade, Serbia
E-mail: mita@iritel.com; lebl@iritel.com; zarko.markov@iritel.com

Abstract: The bandwidth of signaling channel with bursty errors can be larger or smaller than the bandwidth of channels with random errors. In this paper, we give the answer to the question: Is it possible in an easy way to determine the relationship between the bandwidths of these two models? First, we define the method that determines the bandwidth of the signaling CCS No7 channel under the influence of random errors, and then the method that determines the bandwidth of the signaling CCS No7 channel under the influence of bursty errors. The paper also gives the procedure, which easily compares the channel bandwidth for these two types of errors.

Keywords: bandwidth of signaling CCS No7 channel; random errors; bursty errors; Jensen's inequality

1 Introduction

The bandwidth of the signaling CCS No7 (*Common Channel Signaling Number 7*) channel is inversely proportional to the time of service (processing time and waiting time, i.e. delay). This is why we can say that the bandwidth of the signaling CCS No7 channel is indirectly determined by the recommendation Q.706, [1], which determines the time delay in CCS No7 systems. Parameters: bit rate and signal propagation time on the digital channel are processed in this recommendation, and these are important parameters that characterize the digital transmission.

Parameter bit rate penetrates almost all areas of CCS No7. Its influence on the signaling characteristics of protocol MTP (*Media Transfer Protocol*) cannot be neglected. Bit rate is an unavoidable factor in the standardization of certain parts of this protocol. In this paper we will always mean a bit rate of 64 kb/s and the MTP standards related to this bit rate.

Signal propagation time through the data channel, T_p, is the time period that begins when the last bit of signaling unit leaves the data channel on the transmitting side and ends when the last bit of signaling unit leaves the data channel on the receiving side. This time depends on the distance between the points that interchange signaling information and on the digital media (Table 1/Q.706, [1]).

The importance of this parameter is primarily in the fact that it forms a new parameter called the double propagation time, T_L. In the literature [1, 2, 3] it is widely used as a constant parameter. The assigned value is T_L = 30 ms and corresponds to the longest terrestrial connections, which are about 2000 km. In this paper, it is considered that this parameter is 30 ms.

A simple method to compare the influence of *BER* (*Bit Error Rate*) on the bandwidth of the signaling CCS No7 channel under the influence of random and bursty errors is presented at the end of this paper.

2 Bandwidth of Signaling CCS No7 Channel under the Influence of Random Errors

The signaling unit's Message Signal Unit (MSU) and Link Status Signal Unit (LSSU), as well as all other signaling messages, must not be lost. Processing of the signaling channel is arranged as a waiting queuing system. The place where the messages for one channel are waiting to be sent is called the transmission and/or retransmission buffer. The signaling units are in it as long as the sending party does not receive confirmation of successful receipt of the signaling unit from the receiving side.

The main indicator of the traffic signal channel bandwidth as a waiting queuing system is the mean waiting time, which is calculated from the moment of the unit content readiness for sending until the start of sending it to the channel. This statement will be used in this paper.

The problem of bandwidth will be connected with the problem of dimensioning the signaling channel in the sense of its utilization. The signaling channel is dimensioned so that the offered traffic, a, in the normal operation of the channel do not exceed a specified maximum, a_{max}. The criterion for determining the values of a_{max} are the conditions for the operation of the signaling channel. According to the current recommendations, the value a_{max} varies between 0.2 Erl and 0.4 Erl. From Q.706 [1], we use the expression which presents the average waiting time to send the signaling message by signaling CCS No7 channel, Q_t, in the presence of uniformly (or randomly) distributed errors. In the case of error appearance, the basic error correction method and message retransmission are applied. The mentioned expression from [1] is given in the form:

$$Q_t = \frac{T_f}{2} + \frac{a}{T_m} \cdot \frac{\left(m_2 + P_{SU} \cdot T_L \cdot \left(T_L + 2 \cdot T_m\right)\right)}{2 \cdot \left(1 - a \cdot \left(1 - \frac{P_{SU} \cdot T_L}{T_m}\right)\right)} + P_{SU} \cdot T_L \tag{1}$$

where the variables are:

- Q_t – mean waiting time;
- T_f – Fill In Signal Unit (FISU) message duration;
- a – traffic of MSU units;
- T_m – mean duration of MSU message (or serialization time);
- P_{SU} – probability of incorrectly transmitting signaling unit;
- T_L – double propagation time from the sending to the receiving side;
- m_2 – the second moment of the MSU duration, ($m_2 = T_m^2 + \sigma_m^2$, where σ_m^2 is the variance of the MSU duration).

Distribution of the MSU duration and other parameters are as in the examples listed in (Model A, Table 3/Q.706, [1]).

In order to consider the error impact on the waiting time to send a signaling message by the signaling CCS No7 channel, it is necessary to calculate a function which gives the mean waiting time for sending signaling messages by the signaling channel, depending on the bit error intensity (*BER*), $Q_t = Q_t(BER)$. The connection between the probability of incorrectly transmitted signaling unit, P_{SU}, and the *BER* is given by the following expressions [3]:

$$P_{SU} = 1 - (1 - BER)^n \tag{2}$$

$$BER = 1 - (1 - P_{SU})^{1/n} \tag{3}$$

where n is the number of bits in the signaling unit. From [3] it follows that $n = 8 \cdot l_{SU}$, where l_{SU} expresses the number of octets in the signaling units.

In Eq. (1), the offered traffic of signaling units will be expressed using the effective traffic of signaling units, which is calculated according to the following expression [4, 5]:

$$a_{eff} = a \cdot \frac{1 + P_{SU} \cdot \frac{T_L}{T_m}}{1 - P_{SU}} \tag{4}$$

The effective traffic, a_{eff}, in real conditions of error existence is always greater than the offered traffic, a, because the messages are retransmitted due to the errors, and the repeated messages cause an increase in traffic on the CCS No7 channel. Ideally, when there are no transmission errors ($P_{MSU} = 0$, i.e. $BER = 0$), the effective traffic, a_{eff}, would be equal to the offered traffic, a.

The curves shown in Fig. 1 are obtained when P_{SU} is expressed by *BER*, Eq. (2) is substituted in Eqs. (1) and (4); and when the offered traffic, a, is replaced by the effective traffic a_{eff}, Eq. (4) is introduced in Eq. (1).

Parameters: a=0.2 Erl, lenght MSU 15,60 and 150 octets

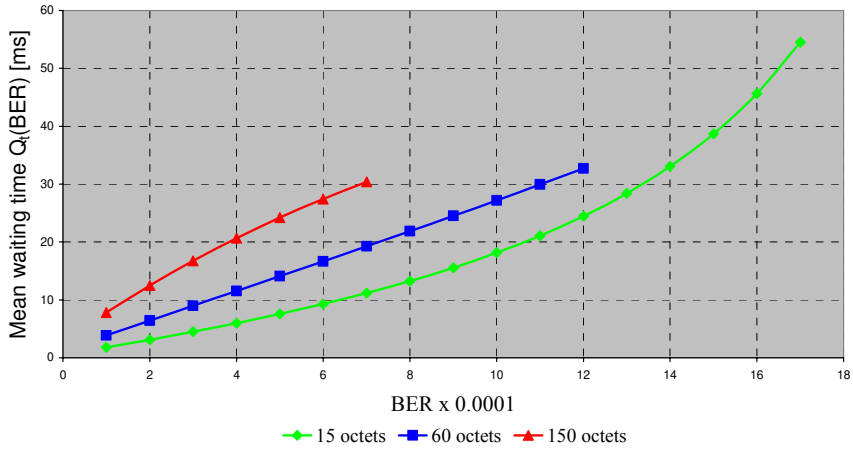

Figure 1
The average waiting time for sending MSU units, a = 0.2 Erl

Parameters: a = 0.2 Erl, length MSU 15, 60 and 150 octets

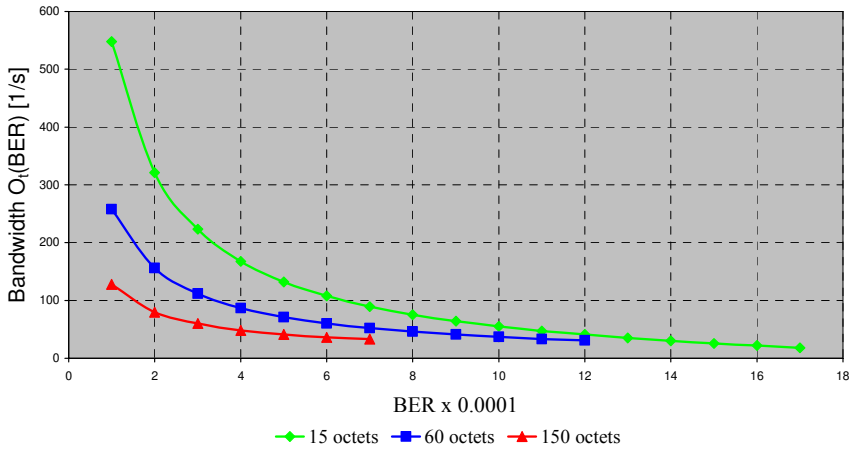

Figure 2
Bandwidth of signaling channel in the function of *BER*, a = 0.2 Erl

Bandwidth, $O_t(BER)$, of the signaling CCS No7 channel can be defined as $O_t(BER) = 1/(Q_t(BER)+T_m)$. In real situations, according to [1], the value of T_m is less than 2 ms, and thus can be neglected comparing to $Q_t(BER)$. That is why we can simplify the last expression to $O_t(BER) \approx 1/Q_t(BER)$. Upon conversion of the calculated $Q_t(BER)$ for certain values of *BER*, we get the curves presented in Fig. 2.

From Fig. 1 and Fig. 2, it can be seen that as the signaling messages become longer, the mean waiting time for the sending of messages increases, and therefore the bandwidth of the signaling CCS No7 channel decreases. In addition, the mean waiting time on MSU units for sending increases with the increase in *BER*, and thus causes a reduction in bandwidth of the signaling CCS No7 channels.

3 Determination of the Signaling Channel Bandwidth under Influence of Bursty Errors

Later in this section, special attention will be paid to the impact of bursty errors on the bandwidth of the signaling CCS No 7 channel. We will describe one simple method for determining the properties of the signaling CCS No7 channel in the case of bursty errors, which are corrected using the primary method of retransmission. This method is based on the application of Jensen's inequality, [6].

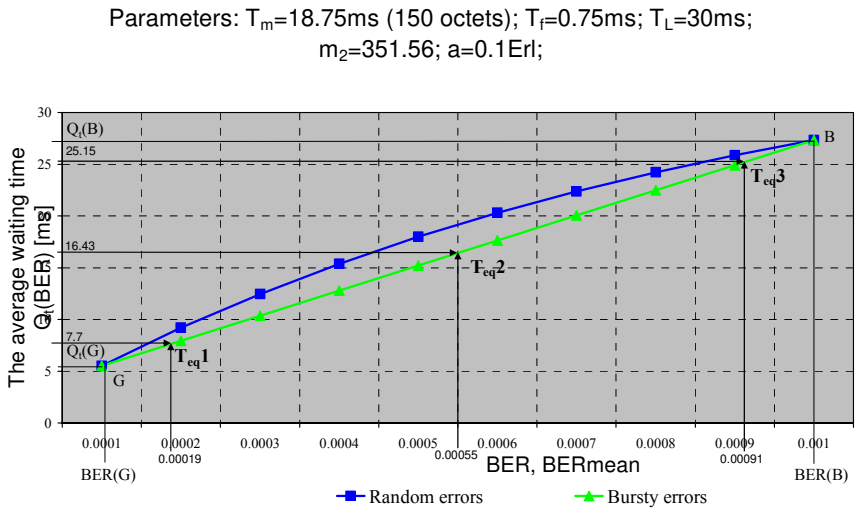

Figure 3

Average waiting time for sending signaling messages by signaling CCS No7 channel for random errors (concave curve) and for bursty errors (straight line)

Mean waiting time for sending signaling messages by the signaling channel is given as a function of traffic, $Q_t(a)$ in recommendation Q.706, (1). In order to obtain the mean waiting time for sending signaling messages by the signaling channel in function of *BER*, $Q_t(BER)$, in this section the offered traffic, a, is taken as a parameter (4), and the probability of incorrectly received message, P_{SU}, is expressed by *BER* (2). So, we obtain an expression that gives the average waiting time for sending the signaling messages by the signaling channel as a function of variable *BER*. Based on the calculated values for $Q_t(BER)$ in the function of variable *BER*, the curves in Fig. 3 and Fig. 4 are obtained.

Parameters: T_m=1.875ms (150 octets); T_f=0.75ms; T_L=30ms;
m_2=3.5156; a=0.8 Erl;

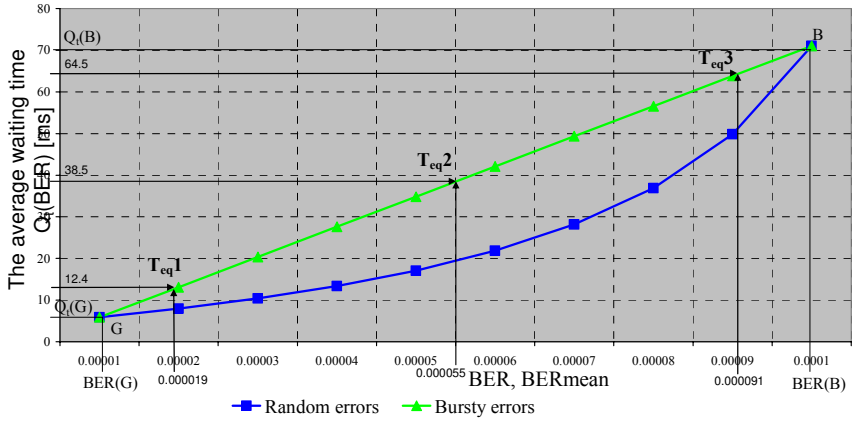

Figure 4

Average waiting time for sending signaling messages by the signaling channel for random errors (convex curve) and bursty errors (straight line)

The shape of the function $Q_t(BER)$, calculated using Eq. (1), depends on the used parameters given in Fig. 3 and Fig. 4. On the basis of the selected parameters, the curve $Q_t(BER)$ can be concave (convex upstairs) or convex (convex downstairs), and in special cases it can be approximately straight lines.

Let us now suppose that the signaling CCS No7 channel is under the influence of bursty errors, so it can be modeled using the well-known Gilbert-Elliot model. According to this model, the signaling CCS No7 channel can be found in a "good" state G or in a "bad" state B. In the graphs (Fig. 3 and Fig. 4), the left-most points are defined as states with less bit error rate *BER(G)* and marked by G, and the right-most points are defined as states with greater bit error rate *BER(B)* and marked by B [7]. It is assumed, that the signaling CCS No7 channel can be found in a state G with probabilities P_G1, P_G2 and P_G3, or in a state B with probabilities P_B1, P_B2 and P_B3, wherein always $P_Gi + P_Bi = 1$, (i = 1, 2, 3) [7]. After these

assumptions, the equivalent *BER*, BER_{eq}, and equivalent mean waiting time, Q_{eq}, can be very easily calculated, according to (5) and (6) for couples $P_G i$ and $P_B i$, (i = 1, 2, 3):

$$BER_{eq}(P_G i, P_B i) = P_G i \cdot BER(G) + P_B i \cdot BER(B) \tag{5}$$

$$Q_{eq}(P_G i, P_B i) = Q_t(G) \cdot P_G i + Q_t(B) \cdot P_B i \tag{6}$$

where:

- $Q_t(G)$ - mean waiting time for sending signaling messages in the point G;
- $Q_t(B)$ - mean waiting time for sending signaling messages in the point B;
- $BER(G)$ - intensity of bit errors at the point G;
- $BER(B)$ - intensity of bit errors at the point B.

Points $T_{eq}1$, $T_{eq}2$ and $T_{eq}3$, which are defined by the pairs $BER_{eq}1$ and $Q_{eq}1$, $BER_{eq}2$ and $Q_{eq}2$, $BER_{eq}3$ and $Q_{eq}3$, [4], are displayed in Fig. 3 and Fig. 4. If we now draw the line that connects the end points G and B (Fig. 3 and Fig. 4), we shall see that points $T_{eq}1$, $T_{eq}2$ and $T_{eq}3$ lie on the line drawn through the points G and B. Therefore, the line drawn through points G and B is the set of points that represents the mathematical expectation for the mean waiting time for sending signaling messages by the signaling channel in the case of bursty distributed errors, because for any pair of values $P_G x$ and $P_B x$, the calculated values $BER_{eq}x$, (5), $Q_{eq}x$, (6), are represented by the point $T_{eq}x$, which is situated on this line, [2].

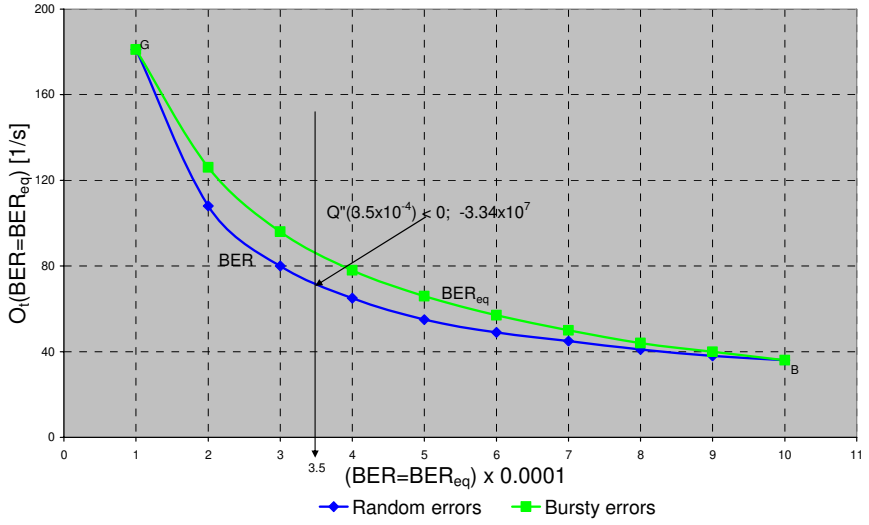

Figure 5

Bandwidth of the signaling CCS No7 channel for random and bursty errors, when the curve $Q_t(BER)$ for random errors is concave

From aforementioned, it can be concluded that if we know the curve of a mean waiting time for sending signaling messages by the signaling channel for the channel model with random errors, $Q_t(BER)$, then the graph of the mean waiting time for the channel model with bursty errors can be easily obtained as a line (chord) drawn between the end points of the curve $Q_t(BER)$ [2].

The bandwidth of the signaling CCS No7 channel that affects the random or bursty error was calculated over the function $O_t = 1/Q_t(BER)$ and $O_t = 1/Q_t(BER_{eq})$ for the two cases: for the concave curve, Fig. 5, and for the convex curve, Fig. 6.

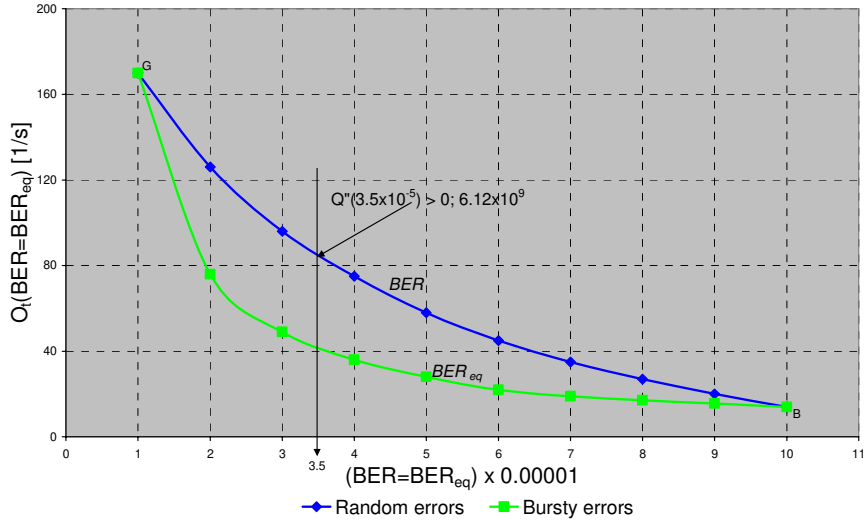

Figure 6

Bandwidth of the signaling CCS No7 channel for random and bursty errors, when the curve $Q_t(BER)$ for random errors is convex

4 A Simple Way of Comparing the Bandwidth of the Signaling CCS No7 Channel under the Influence of Bursty Errors

In the case of curve $Q_t(BER)$, which is concave/convex, Fig. 3/Fig. 4, bursty errors have less/more influence on the function of the signaling channel, because all values that represent the mathematical expectation of the waiting time for sending signaling messages over the signaling channel in the presence of bursty errors are less/greater than if errors are uniformly distributed with the same value of BER (Jensen's inequality [2]). As discussed in the previous section, based on the curve

of $Q_t(BER)$, it can be said that the bursty errors have more or less impact on the operation of the signaling channel than the random errors.

In practice, however, it is very annoying always to draw the graph of curves $Q_t(BER)$ as a function of BER for certain signaling CCS No7 channels and then to calculate the values of $Q_t(BER)$, Q_{eq} and BER_{eq}. That is why we propose a simpler method.

As was said in the introduction, the simple method for determining the impact of bursty errors on the function of the signaling CCS No7 channel starts with the calculation of the waiting time for sending a signaling message by the No7 digital signaling CCS channel, $Q_t(BER)$, in the case of a uniform distribution of errors, according to (1) from [1]. Then we calculate the second derivative of the function $Q_t(BER)$ and the second derivative values at a certain point using some mathematical programs, such as MATHEMATICA, MATLAB or any other program capable of calculating the second derivative of the function.

The calculated and obtained values of the second derivative of the function $Q_t(BER)$ can immediately provide information on whether bursty errors have more ($Q_t``(BER) > 0$) or less ($Q_t``(BER) < 0$) influence on the function of the signaling CCS No7 channel. Thus, we avoid the graphing of curves $Q_t(BER)$ as a function of BER for certain signaling CCS No7 channels and calculating the values of $Q_t(BER)$, Q_{eq} and BER_{eq}. Thus we obtain a faster and simpler method for determining the impact of bursty errors on the operation of the signaling CCS No7 channels.

Let us now choose the values for the BER to get a concave (convex) function. For $BER = 3.5 \cdot 10^{-4}$, we have the concave function and for $BER = 3.5 \cdot 10^{-5}$ we have the convex function, provided that the $BER = BER_{eq}$. The choice of values for BER is made so that the differences in the bandwidth of the signaling channels (which are under the influence of random or bursty errors) are more obvious. The figures show that in the case of concave function, the numeric value of the second derivative for $BER = 3.5 \cdot 10^{-4}$ is less than zero (Fig. 5, $Q_t''(3.5 \cdot 10^{-4}) = -3.34 \cdot 10^{7}$). Bursty errors have less impact on the function of the signaling CCS No7 channels; the bandwidth of the signaling channel is larger in the case of bursty errors. In the case of the convex function, the numeric value of the second derivative for $BER = 3.5 \cdot 10^{-5}$ is greater than zero (Fig. 6, $Q_t''(3.5 \cdot 10^{-5}) = 6.12 \cdot 10^{9}$), which means that bursty errors have a greater impact on the function of the signaling CCS No7 channels; i.e. the bandwidth of the signaling CCS No7 channel is smaller in this case.

Conclusions

In this paper the bandwidth of the signaling CCS No7 channel under the influence of random and bursty errors is considered. After all above, the following very important conclusions can now be drawn:

- The bandwidth of the signaling CCS No7 channel for the model with random errors is different from the bandwidth of the same channel under the influence of bursty errors;

- The bandwidth of the signaling CCS No7 channel with bursty errors is larger than bandwidth of the signaling CCS No7 channel with random errors if the function $Q_t(BER)$ is convex (small traffic and long MSU) and vice versa;

- The differences in bandwidth can be up to 100% (Fig. 6);

- Based on the shape of the curve of $Q_t(BER)$ and on the calculated value of the second derivative of the function $Q_t(BER)$, it can be determined whether the bursty errors have more or less impact on the bandwidth of the signaling channel than random errors, without calculating the value of the curve $O_t(BER) = 1/Q_t(BER)$.

Acknowledgement

The study was carried out within the Project TR32007: "Multiservice optical transport platform with OTN/40/100 Gbps DWDM/ROADM and Carrier Ethernet functionality". It was financed by the Ministry of Science and Technology, Republic of Serbia.

References

[1] ITU-T, Recommendation Q.706. Signalling System No 7 – Message Transfer Part Signalling Performance, 08/96

[2] Cover, T. M., Thomas, J. A.: Elements of Information Theory, John Wiley & Sons, 1991

[3] Schwartz, M.: Telecommunication Network: Protocols, Modeling, Analysis, Addison – Wesley, 1987

[4] Mitić, D.: The influence of the Bursty Errors on Digital Information and Signaling Channel Characteristics, PhD thesis, Faculty of technical sciences, University in Novi Sad, Novi Sad 2002

[5] Trenkić, M. B.: Application of Signaling CCS No 7 on Digital Channels of Lower Quality, PhD thesis, Faculty of technical sciences, University in Novi Sad, Novi Sad 1998

[6] Markov, Ž., Mitić, D.: Jensen's Inequality as a Criterion for Comparison of Bursty and Random Errors Impact, Facta Universitatis (Niš), Series: Electronics and Energetics, Vol. 13, No. 2, August 2000, pp. 213-218

[7] Mitić, D., Lebl, A., Markov, Ž.: Availability of CCS No7 Signalling Channel under Influence of Bursty and Random Errors, Przegląd Elektrotechniczny (Electrical Review), ISSN PL 0033-2097, April 2011, pp. 275-278